CRANFIELD INSTITUTE OF TECHNOLOGY

STEPHEN E. HOBBS

A QUANTITATIVE STUDY OF KITE PERFORMANCE IN NATURAL WIND WITH APPLICATION TO KITE ANEMOMETRY

Ecological Physics Research Group

PhD THESIS

CRANFIELD INSTITUTE OF TECHNOLOGY

ECOLOGICAL PHYSICS RESEARCH GROUP

PhD THESIS

Academic Year 1985-86

STEPHEN E. HOBBS

A Quantitative Study of Kite Performance in Natural Wind with application to Kite Anemometry

Supervisor: Professor G.W. Schaefer

April 1986
(Digital version: August 2005)

This thesis is submitted in fulfillment of the requirements for the degree of Doctor of Philosophy

Abstract

Although kites have been around for hundreds of years and put to many uses, there has so far been no systematic study of their performance. This research attempts to fill this need, and considers particularly the performance of kite anemometers.

An instrumented kite tether was designed and built to study kite performance. It measures line tension, inclination and azimuth at the ground, :sampling each variable at 5 or 10 Hz. The results are transmitted as a digital code and stored by microcomputer. Accurate anemometers are used simultaneously to measure the wind local to the kite, and the results are stored parallel with the tether data.

As a necessary background to the experiments and analysis, existing kite information is collated, and simple models of the kite system are presented, along with a more detailed study of the kiteline and its influence on the kite system.

A representative selection of single line kites has been flown from the tether in a variety of wind conditions. The results from these experiments are analysed to obtain general performance measurements for these kites in real, turbulent, winds.

The analysis is taken a stage further to evaluate the kites for anemometry, and to study the dynamics of the kite system. The most suitable kites for anemometry are identified, together with the wind conditions in which they may be used and the wind information available from measurements at the tether.

The study ends with a review, and a discussion of useful areas of further work.

This digital (pdf) version of the thesis was created in August 2005. The content is identical to that of the original paper copy of 1986, although the layout and pagination differs in detail. Readers should note that anemometer calibrations described in Hobbs (1994) suggest that the windspeed values given in this thesis are incorrect by a few percent: however, the general conclusions about kite performance stated in the thesis are unaffected by these changes.

Acknowledgements

It is a real pleasure to remember all those who have helped in one way or another towards the production of this thesis.

I thank my supervisor, Professor Schaefer, for the opportunity to study a subject such as kites. I have learnt much during my time at Cranfield, and not only about kites.

Ted Sills helped with the initial stages of the electronic design, and Ron Hussey did a good job building the Kite Tether Head. Without the cooperation of the farmer, Michael Nicholson, the field experiments would have been much more difficult.

Fellow students at Ecological Physics have helped in many ways, and in particular I must thank Dave and Patrick for technical help, and Jan, who was a surprisingly willing and much appreciated field assistant. Pam, Keith and Terry have played their part too.

The friends (particularly Albert, Jane, Mark, Jane and Peter) who've helped over the last few years deserve special thanks for their friendship and encouragement.

Contents

List of Tables

List of Figures

Notation

a	incidence
AR	aspect ratio
Ax	cross-sectional area
b	bridle angle
bf	bulk factor
bs	breaking strength
c	aerofoil chord
c	wave velocity
C	chord trailing edge
C_D	drag coefficient
C_L	lift coefficient
C_M	moment coefficient
C_P	centre of pressure coefficient
d	line diameter
D	drag
E	Young's modulus / elasticity
ex	maximum strain
f	kiteline windage parallel to line
F	resultant of kite reaction and weight
g	acceleration due to gravity
G	kite centre of gravity
Gf	friction couple
Gx	maximum couple
I	moment of inertia (tether arm / head)
I	second moment of area
k	kiteline elasticity
k	strut stiffness
K	bridle point

l	line length
l	tether arm length
L	lift
m	kite mass
m	line mass per unit length (also s)
m	covering mass per unit area
M	moment
n	frequency
n	kinematic viscosity
O	chord leading edge
Oab	chord axes
P	centre of pressure
q	dynamic pressure
r	kiteline windage normal to line
R	aerodynamic reaction
R	radius of curvature
Re	Reynold's number
s(x)	standard deviation (of x)
s	line mass per unit length (also m)
S	kite 1ifting area
t	non-dimensional line tension
T	kiteline tension
T_I	autocorrelation integral timescale
tmax	maximum stress
tmax	maximum strength of covering
tx	tensile strength
Tx	maximum tension
u	longitudinal wind component
v	cross-wind component
w	weight (tether arm)
w	angular velocity (tether arm)
w	vertical wind component
W	windspeed or velocity
x	coordinate along mean wind direction
X	distance upwind of mean kite position from anemometers

y	coordinate crosswind
y	radial distance from neutral axis
Y	distance crosswind of mean kite position from anemometers
z	coordinate vertical (upwards)
Z	kite height above ground
α	incidence
β	wind inclination
γ	chord inclination
ϕ	azimuth
λ	flight angle
μ	solidity ratio
ψ	angle between line element and wind
ρ	density (air or material)
θ	line inclination

Chapter 1

INTRODUCTION

Kites are an unusual and diverse area of study. Most people only know of kites from their childhood, regarding them as just another toy. But over the last few centuries, there have been many occasions when kites have been put to more "serious" purposes than play. The range of tasks is wide; from early atmospheric experiments, including perhaps the best known kite scientist, Benjamin Franklin, through kite traction and routine meteorological measurements, to present day interest, which includes sailing, anemometry, crop protection and photography, as well as a renewed interest simply for pleasure.

However, despite this broad background of applications, kites remain a minority interest, and have not established themselves as the dominant technology in any one of these areas. In several cases this is because other technologies, e.g. the aeroplane or balloon, have been developed, and are now able to offer much more than a kite can - but usually at the cost of increased complexity and expense. Kites are, of course, still able to offer much, and it may be that they turn out to be very much the appropriate technology for many applications, where their particular combination of performance and simplicity suits them ideally to the task. It is hoped that the work of this thesis will help define the potential of kites more clearly, and so point towards areas of interest where their characteristics are most relevant.

The work of this thesis is mainly concerned with kite performance measurements in natural wind. It has involved designing and building an instrumented kite tether to measure the line tension vector at the ground. A microcomputer collects and stores the information (along with detailed anemometer results) and is also used for the analysis at a later stage. All the programs for the data collection, analysis and presentation have been specially written. Lastly, the results of the analysis are used to discuss the use of kites as anemometers, and to recommend particular kites as most suitable for particular tasks.

Before going into details, the next two sections describe the background to the present work and discuss particular aspects of the subject. The review should also explain how the work here fits in with previous studies, and extends them. The

third section briefly describes the work of this thesis, showing how the ideas and research develop. This includes a brief outline of each section.

1.1 Background to the present studies

As explained above, this thesis is concerned with measurements of kite performance, and treats the kite as a scientific or technical tool. To give a useful perspective to the whole study, Table 1 lists the main recorded uses of kites as research tools. This is not meant to be a complete history, but merely lists some of the main events. Most kite hobby books include a brief history of the kite (see for example Pelham (1976) and Wiley (1984)). Probably the most authoritative history of the kite is given in Hart (1967), which traces kite history back to its origins in the Far East, and also includes a separate chapter on Meteorological Kites. Several review articles have been concerned particularly with the meteorological use of kites, for example Jenkins (1981) and chapters of Shaw (1926) and Met. Office (1961).

It can be seen that kites have a long history, and their most intensive period of development until recent years was that leading up to the invention of the aeroplane, i.e. 1885–1905. Since then, aeronautical knowledge has increased dramatically, but comparatively little work has been done to understand kites. The Royal Aircraft Establishment experiments in 1938–1942 and more recent research into the Rogallo Parawing and Jalbert's Parafoil are the main exceptions.

1.1.1 Research 1885–1905

In the period 1885–1905, kites were seen mainly as a useful aerial platform, and the main task was to develop the steadiest, most efficient design, and the most reliable system for launching and controlling them. Aerodynamics was comparatively poorly understood so that detailed fluid-dynamic studies were not made. However, the qualitative understanding was not necessarily weak; Marvin (1897) is an excellent account of the Mechanics of Kites, and indicates the level of understanding in some quarters. Hargrave's Box Kite is an important design from this period and was one of the main kites used, due to its strength and steadiness. Another important design is the Eddy bow-kite (similar to the Malay used here). These are the two designs used by the US Weather Bureau for their kite work, which continued into the 1930's. These kites were used as aerial platforms, at heights of up to several thousand feet (5 000–10 000 ft was not unusual), but as the aeroplane became more developed, it was obvious that it could extend the range of measurements quite easily, and was more convenient. Balloons too began to take over from kites since they too could carry small instrument packages, and by the end of the 1930's radiosondes were being built and used to transmit information from the sonde to the ground. Kites ceased to be used for meteorological measurements then because of the practical difficulties (and dangers) of the steel lines used (which were usually several miles

long), and the fact that balloons and aeroplanes allowed measurements to be made to greater heights more easily and conveniently. The main contributions from this period to the present work are the vast amount of practical experience gained, the new designs developed, and the first solid qualitative understanding of kite flight.

1.1.2 Royal Aircraft Establishment, 1938–1942

During the period 1938–1942 the Royal Aircraft Establishment (RAE) considered using kites for anti-aircraft barrages. A variety of kites was tested, but most work concentrated on designs similar to Cody's War Kites of around 1906. The research included wind tunnel tests, field trials and attempts at kite design and theory.

The wind tunnel tests are of most interest here. A large wind tunnel (24 ft diameter) was used for a variety of kites. Most tests used a Cody kite (either the standard with a 3 ft box (area = 9.8 m^2), or the 2 ft "storm kite" or "type A"), or one of several modifications aimed at improving performance. The other tests tried related designs and new kites designed at RAE. The results were published in a series of reports over the period 1938–1942 of which the most complete is Jackson (1942). Other reports include BA Departmental Notes - Large Wind Tunnel -numbers 17, 33, 37, 39, 42 and 43 : Naylor (1940) includes results which are used as a comparison with the Cody tested at Cranfield (see section 7.1). The kites tested were generally larger and heavier than those used at Cranfield since an important part of the study concerned strong wind performance. In strong winds the balloon barrage was unusable, and it was hoped that kites would be able to maintain an aerial barrage into such conditions.

One new design tried was a monoplane kite intended to achieve a much higher lift to drag ratio than the Codys. This is reported by Hollingdale and Richards (1939). The wind tunnel tests were generally disappointing due to the poor lateral stability and the weight of the kite. A Pterodactyl design (i.e. with one main wing swept backwards and no tail) is mentioned as "in progress", but no performance results are given. The report also considers a kite barrage more generally, including useful information concerning the frequency of surface windspeeds, and thus estimates the proportion of time for which kites may be usable. Powley and Wild (1940) continue the kite barrage study, and report that the Pterodactyl kite has been tested in a wind tunnel, achieving a lift to drag ratio of about 10. It is not considered stable enough for "free flight" (i.e. as a normal kite) but is to be used to help support the weight of balloon mooring cables. Richards and Smith (1942) describe an experimental kite barrage maintained from June 1940 to February 1941, using mainly Codys in trains. The practical experience is valuable, and they include the comment that "kites could be put to a real use for meteorological purposes especially in conditions of high wind and poor visibility, the tension in the wire giving a continuous indication of wind speed at height." Kite anemometry is not a new idea.

Independent of the RAE work, the Aerodynamics Division of the National Physical Laboratory (NPL) was working on the stability of kites and towed gliders. The

research was mainly theoretical, although some trials were made in wind tunnels, and is brought together in the report of Bryant, Brown and Sweeting (1942). A major focus of the NPL work was to consider the stability of towed gliders. The mathematics is the same as for kite stability, although assumptions such as the use of short lines are not always valid for kites. NPL also attempted to design a kite of high efficiency (i.e. a high lift to drag ratio), and one model was built. It flew successfully in a wind tunnel, but was heavy and required winds above 15 mph (6.7 ms) even to launch. It crashed during field trials. The foreword to the report comments : "The development of a satisfactory kite of high efficiency was however reckoned to be so formidable a problem that interest in the subject inevitably declined." The main contributions from this period of research are the wind tunnel results (providing a valuable reference), the documented practical experience and attempts at improved designs or modifications, and the beginnings of a study of kite stability.

1.1.3 Recent research

This section reviews post-war research into kite performance, i.e. since the late 1940's: a period which has been surprisingly fruitful for new kite designs.

Soon after the Second World War, Francis Rogallo developed his Flexible Kite, or Parawing, as the general design is known. A minimal rigid structure is used, with the kite surface able to conform to the wind. The design has been studied particularly with regard to the US space programme, who were interested in using these parawings for controlled landing of returned space capsules. In other directions, the parawing has led to the Delta kite family and the sport of Hang Gliding. Rogallo et al (I960) is the original report of this work : more recent accounts can be found in La Burthe (1979) and Sweeting (1981).

Another new kite design, the Sled, was patented in 1950 by William Allison.

In 1964, Frank Scott introduced a valuable modification by using vents in the sled's lifting surface, and it is this form which is probably most common now.

This kite has so far been restricted to mostly hobby use, and little research has taken the sled as its subject.

The third significant original design is the Parafoil, introduced by Domina Jalbert in 1964. Like Rogallo's parawing, the Parafoil was soon the subject of research since it provided an easily collapsible lifting surface. Many applications have been tried, including air dropping cargo, manned and unmanned powered flight, as well as tethered flight, i.e. use as a kite. Perhaps the most familiar use now is as the efficient and steerable rectangular parachutes used by many display teams. Two useful references are Nicolaides, Speelman and Menard (1970) and Nicolaides and Tragarz (1971). The first is a review of Parafoil applications; the second reports on Parafoil flight performance.

These three designs are the main recent developments and have spawned a wide

range of new kites. Another important new design, although one which stands by itself, is the Flexifoil -a very efficient steerable kite which has been used successfully for kite sailing. Shaw (1980) is a short report studying the aerodynamics of the Flexifoil, and includes measurements of pressure distributions.

A difficulty with collecting details of previous kite research is that many separate areas of study are involved. Since there is no continuing research programme, what research has been done tends to be linked to other areas of study, so that drawing together all the relevant information can be a rather haphazard process.

This recent work contributes some valuable aerodynamic data for the various kite types, allowing useful comparisons to be made between previous results (often from wind tunnels) and the current research (in natural wind), e.g. the Parafoil comparison of section 7.1. The level of current understanding has also helped refine kite designs, so that it is slightly less hit-and-miss (but still as much art as technology).

1.1.4 Kiteline and stability theory

In parallel with work on kites, there has been research continuing into the properties of the kiteline, and, as a natural part of this, the stability of a tethered object, i.e. kite. The introduction to section 3 (The Kiteline) gives a brief review of this work; the work of Bryant, Brown and Sweeting (1942) has already been mentioned. Perhaps the most important recent work is that of De Laurier (De Laurier, 1972a,b). Since the problem has wide applications (any tethered object in a fluid), the techniques have become fairly sophisticated. A more useful physical understanding is provided by much simpler models, as presented here in section 3.

1.1.5 Kite anemometry

Apart from the research taking kites or lines as their primary subject, there has been recent work in several areas, using kites for a specific application. The two main areas of current interest are kite anemometry and kite sailing.

Kite anemometry, which is one of the main interests of this thesis, is an area which has been developed so far largely through the TALA system (Tethered Aerodynamically Lifting Anemometer, Tala Inc., Kite Anemometers, Ringgold, VA, USA). This uses a kite as the wind sensor to measure wind velocity at altitudes of up to several hundred metres, as anticipated by Richards and Smith (1942). A number of reports have been produced using the TALA system as a tool (e.g. Daniels and Oshiro, 1982a,b; Daniels, 1982; Baker, Whitney and Hewson, 1979), and comparing it with other types of anemometer (e.g. Kunkel, 1981; Kaimal et al, 1980). Section 8 (Kite Anemometery) includes an analysis of TALA performance, as a reference for the kites tested here. The kite used for the TALA system is a plain sled with a tail, but no other designs appear to have been evaluated. Neither has a detailed study of kite response to natural wind been made. The goal of this thesis is to answer both

of these questions, so that kite anemometry is placed on a firmer footing.

1.1.6 Kite sailing

Kite sailing (or more generally, kite traction) is a recently rediscovered use of kites. Pocock (1827) gives a colourful account of his experience, mainly towing carriages on land. Other kite sailors have included Portuguese fishermen, who used kites to leave port using upper winds when the sea-level winds were too light (Lloyd and Thomas, 1978), and S.F.Cody who crossed the English Channel in 1903 using kites to tow a small dinghy (Pelham, 1976). The first recent paper on kite traction is that by Schaefer and Allsopp (1980), who describe the basic principles and provide simple estimates of performance. The potential for improved performance over conventional sails is large, as has already been demonstrated by the kite-powered boat Jacob's Ladder, which captured a world speed sailing record (C-class, 25.03 kt) in 1982. Research since 1980 has been either largely empirical (as reported by Schmidt, 1981 and Day, 1982) or purely theoretical (Wellicome and Wilkinson, 1984). The conference Windtech '85 included two other reports of recent kite traction work : Duckworth (1985) discusses a conservative use of (parachute) kites to tow oil tankers; Stewart (1985) is strong on anecdotes, but unfortunately has no firm performance measurements to offer (the inflatable kites are interesting however). The greatest opportunity for kite sailing seems to be in a sport, or perhaps rescue, application. There is a great need for thorough experiments : perhaps applying the techniques of this thesis to sea-borne experiments.

1.1.7 Other kite applications

Over the last century, kites have been put to all sorts of other tasks, apart from anemometry and sailing. Most of these use the kite as an aerial platform. Examples include insect netting at altitude (Hardy and Milne, 1938; Farrow and Dowse, 1984), aerial photography (Cochrane, n.d.; Dusariez, 1985), bird scaring (Nowell, 1984), crop spraying (New Scientist, 1978), distress beacons, radar target, and many others. There is also a significant amateur interest in kites, providing a fertile source of new ideas, designs and applications. Although many of these other uses of kites do not provide "hard" information concerning kite performance, their contribution of practical experience and understanding is very valuable. This experience is communicated through several magazines and newsletters produced regularly by the various kite clubs; for example, the magazine Kitelines (published in USA by Aeolus Press Inc. of Baltimore, MD) and the newsletter "Kite" of the English Northern Kite Group (c/o John Spendlove, 10 Higher Bank Rd, Fulwood, Preston).

This completes the review of existing kite research and knowledge. It is a very diverse field, and for many of the "other applications" it has only been possible to give a very brief indication of the work done : a fuller bibliography should be found in the examples quoted.

1.2 Why study kites ?

Kite performance may not seem the most obvious subject for a research project. However, the Ecological Physics Research Group at Cranfield Institute of Technology has an interest for two main reasons. In 1980, the paper by Schaefer and Allsopp showed that kite sailing has many potential advantages over conventional sail, but is very much an unproven technology; and secondly, there is a strong interest in insect and bird migration which is studied by various remote sensing techniques, such as infra-red and radar. The wind is obviously an important factor, and it would be a great advantage to be able to measure wind velocities at altitudes up to several hundred metres. Both these areas of research have a need which can be met by a better understanding of kite flight. The development of kite sailing needs an improved understanding of kite performance in real winds, and a kite anemometer provides a suitable method of measuring the wind profiles useful for studies of insect and bird flight. These requirements also go together quite neatly since a general study of kite performance (for kite sailing) is a necessary background to the proper development of a kite anemometer (insect flight studies). This explains the "local" motivation for the study of kites.

A more general reason for studying kites is seen in the wider context described in section 1.1. The reviews of kite anemometry (1.1.5) and kite sailing (1.1.6) point out needs for more kite research in specific areas. More generally, kite performance in itself has not been approached before using thorough experiments in the natural wind, and there has been no attempt, either, to draw the whole subject together as a single area of scientific research. It is hoped that this thesis will contribute towards all of these objectives, either directly, or by laying a firm foundation for future work.

1.3 Outline of the thesis contents

As a brief guide to what is in store and the trend of thought through the thesis, this section gives an outline of its contents.

This outline completes section 1 (Introduction) which should provide the reader with an understanding of previous work done, reasons for undertaking this research, and the approach used to carry it out. The main part of the thesis breaks down into three sections : sections 2 and 3 provide some basic, but necessary, background; sections 4 and 5 describe the experiment system; and sections 6, 7 and 8 describe and analyse results of the experiments performed.

The background provided by sections 2 and 3 is drawn from a wide range of sources, and is necessary since there is no existing literature bringing all these topics together. Current kite types and material are listed, using a kite classification devised for this thesis. Some of the kites have been designed and built at Cranfield. The next two sections explain ideas used in the thesis from the subjects of meteorology and

aerofoil theory, applying them, if appropriate, to kites. Section 2 is completed by presenting several simple theoretical models used to examine kite flight. Section 3 considers the kite line, since the limitations imposed by real lines are important for a full understanding of kite flight.

Section 4 describes all the "hardware" (the tether, anemometers, data collection and storage), including its design from the initial specification; and section 5 the "software" (the programs written for data collection, analysis and presentation).

Section 6 lists the experiments done, describes the analysis procedure, and estimates the errors involved. Sections 7 and 8 are the main analysis sections : 7 is an overview of the performance results for all the kites tested; 8 concentrates on kite anemometry, and analyses a selection of kites in more detail.

Section 9 is the conclusion, summarising the research carried out, and indicating those areas of further work which have been opened up.

Chapter 2

PRELIMINARY CONSIDERATIONS

This chapter provides a background to the work developed later in the thesis. The first section (2.1) reviews current actual kite types and the materials used in their construction, with discussion of the properties required of the various components. Since most readers may be unfamiliar with kites and their design, this section is broader in scope than the rest of the thesis, and gives examples of the influence of practical constraints on kite design. Some background is given to methods of describing the wind (2.2) and aerofoil theory (2.3), for use later in the thesis. Then some introductory theory is developed to give a general understanding of the total system comprising the kite and kiteline in the natural wind (2.4). Finally, more detailed consideration is given to a static longitudinal model of a kite and its bridling (2.5), which is used to investigate kite anemometer performance.

2.1 Current Kite Types and Materials 2.1.1 Kite types

The great variety of kite types is quickly confirmed by a visit to a kite display or examination of any of the available kite hobby books, such as Hart (1967), Pelham (1976) and Moulton (1978). Most of these kites have been developed for recreational or aesthetic reasons, although many of the more innovative designs were produced for more functional purposes.

For example, Bell's Multi-Celled Tetrahedral kite and Hargrave's Box kites were developed around the turn of the century with powered flight as one of their goals. More recently, the Rogallo wing and Jalbert's Parafoil, which have inspired many new kite designs, were developed as simple wings that could easily be collapsed for storage, since they need no rigid structural members. The introduction of these last two illustrates the importance of new materials, since it is they that have made

these new designs practical.

Figure 1 and plates 1 to 11 illustrate a variety of kite types currently available, including all those used in this thesis. It is difficult in two dimensions

to give a good impression of the shape of the kite in flight, since it often only adopts its flying form under wind pressure. This is particularly true for the "soft" kites such as the parafoil, which rely entirely on the wind pressure to maintain their shape. Many other types, for example the plane surface kites, use the wind pressure to deform them slightly to create effective keels or dihedral, giving increased stability.

Table 2 lists the main parameters for different individual kite designs, covering most of the types available. All the information has been obtained by measuring examples of each kite, with the exception of the Blue Hill Box kite, which is described in Marvin (1896, p 201). A classification system has been devised, based on kite construction, and is used to group the kite designs. The star in the column alongside the classification indicate which kites have been used in experiments here. Following this, the basic measurements are length, span, lifting area and mass, from which the remaining parameters are derived.

Many attempts have been made to classify kite types, but all have to cope with the fact that kite "species" do not have the same sort of "evolutionary" history as living organisms. In biology, species are believed to evolve one from another, with divergences along the way giving rise to new species. However, in the generation of kite "species", new types derive from combining features of any previous ones, and also from completely novel ideas, bearing no particular relation to any existing types. Thus in the development of kite types there is no natural tree structure that may be adopted for purposes of classification, and thus any classification system used will be based on somewhat arbitrary choices. With this qualification in mind, it is still useful to list categories of kites, based on their construction, which together form a basic descriptive system for current kite types. For other more specific uses it would be equally valid to develop classifications based on, for example, minimum windspeed for launch, payload lifting ability, etc. Examples are quoted for each class. These kites are described in more detail in the kite references, eg. Pelham (1976).

1) Flat-plane-surface kites

Practically any flat shape may be made to fly as a kite with a suitable bridle, although few are likely to fly well, and most may need a tail of some sort for stability. These are historically the earliest types, and still the traditional type of kite associated with China, Japan, India and the Pacific. Modern versions of the type are usually made only for decorative purposes.

Examples : Hexagon, Indian Fighter (Kiskeedee)

2) Structured-plane-surface kites

The main characteristic is that a single main surface is shaped by the structure to

give better flying characteristics than a simple flat kite. A small ventral keel may be used as part of the bridling. These are often good fliers, requiring no tail. The simpler kites tend to be light, and therefore suitable for low windspeeds, while the more complex designs are usable to quite high winds. These are predominantly more modern Western kite types, although some are very similar to traditional designs, eg. the Eddy is effectively a re-invention of the Malay.

Examples : Malay, Delta, Flare, Dunford Flying Machine

3) Box kites

Box kites are built with one or several basic box units, or cells. Almost any shape may be used for the cell, but it is usually symmetrical with 3, 4 or 6 sides. Similarly, any number of cells may be combined, but normally only two. This class traces its origin back to Lawrence Hargrave in the 1890's. The kites tend to be rather heavy, but are strong, and stable fliers, thus suitable for strong winds.

Examples : Square box (Gibson Girl), Hexagonal box

4) Complex rigid kites

These kites have a well-defined three-dimensional framework with a more complex mix of vertical and horizontal surfaces than just a simple box kite. Three sub-classes are defined to cater for the range of existing designs.

4.1) Compound kites

The elements of classes 2 and 3 may be combined in an attempt to bring together the better flying characteristics of 2 and the strength and stability of 3. This is an important class, especially for working kites designed before the advent of the soft kites described below (class 6). Applications included lifting payloads, barrages and weather kites.

Examples : Winged box, French rescue, Cody

4.2) Sculptures

This is a loose grouping of those kites which use a fully three-dimensional frame to create a good visual impact. It is necessarily a broad grouping, thanks to human ingenuity, but still reasonably identifiable. Almost by definition, such kites are for aesthetic purposes and not meant as work horses.

Examples : Prof Waldof box, Clipper kite

4.3) Aeroplane kites

These again use *a* combination of horizontal and vertical surfaces, in this case using a layout much like a normal aeroplane, with a main wing towards the front and a tailplane aft. These kites are usually intended to achieve very high lift to drag ratios, but tend not to be suitable for more general use, not being very stable in turbulence.

Examples : Bill Bigge's aeroplane kites

5) Partly-structured kites

This class includes those kites which have some rigid structural members but which also rely on the wind to achieve their full flying shape. This is a fairly modern class, the sled being invented about 1950, and includes some very good kites, which are both practical and elegant. Performances range from the light but steady sled to the highly manoeuvrable Flexifoil.

Examples : Sled, Flexifoil

6) Soft kites

Soft kites rely wholly on the wind for their shape, and so need to be well designed and built. This is a relatively modern class, needing lightweight materials. Applications include payload lifting, and tasks where the kite must be stowed very compactly, so that the lack of rigid structural members is a great advantage. A disadvantage may be the complex rigging needed to spread loads and maintain the kite's shape.

Examples : parafoil, pocket sled

7) Inflatable kites

The important feature here is the thick aerofoil dictated by the inflatable shape. Almost all other types, except some of the soft kites, have thin aerofoils. Advantages include ease of packing (no rigid structural members needed), ease of deployment (eg. compressed gas), bouyancy (on water for launching or in air for lift) and the fact that the gas pressure gives the kite some strength and form independent of wind pressure. However such kites tend to have high drag (due to the large cross-section). Other disadvantages include the need for careful design to spread loads evenly, the vulnerability to punctures, and the need to protect the material from sunlight and biodegradation.

Examples : Kytoon, Inflatakite

8) Rotor kites

This is not a large class, but potentially important. Lift is generated actively by a rotating "wing" rotor. The rotor axis may be either vertical (autogyro) or horizontal (magnus effect rotor). These kites do not tend to have high effective lift-to-drag ratios by themselves, but there is the possibility of supplying extra energy to augment the lift, or alternatively of extracting wind energy, for example by using the rotor to generate electricity (Arbouw, 1982).

Examples : Hornbeam rotor, Focke-Achgelis gyroplane

Table 2 lists sample kites, using these categories. Class 2 is well represented, probably because these kites are comparatively easy to build, and have therefore been most fully developed. Several classes are not covered by the sample, these are the

Sculptures Aeroplane Kites and Rotor Kites : these are not expected to be good general wind probes due to their rather specialised designs. Those kites used in experiments are indicated by '*'. The selection was made to be reasonably representative, with a bias towards types expected to be suitable as wind probes. The Tailed Sleds are kites already used as wind probes (the TALA system), and so are used here as a comparison.

Due to the great variety of designs, some care is needed in the definition of parameters borrowed from aeroplane theory. As far as possible, the measurements represent the kite in its flying attitude. Length (l) is measured along the kite's longitudinal axis, and the span (b) perpendicular to it. The lifting area (S) is taken to be the projected area normal to the lateral and longitudinal axes, counting double areas twice (eg. box kites). Mass (m) is measured for the kite as flown, excluding any line, but including a tail if used. The aspect ratio (AR) is a concept borrowed from standard aerofoil theory, and is not really applicable to such complex shapes as some of the compound kites (eg. winged boxes). For this reason it is only relevant to those kites with a simple planform such as a delta or parafoil, or may be specifically applied to particular parts of the kite surface (eg. the panels of a box kite). However it may be meaningful to define an effective aspect ratio for certain complex kites, deriving it experimentally from the relationship between lift and induced drag,

as discussed in section 7. For the purposes of table 2, AR is defined as (b/S). The mass loading is obtained by dividing the kite mass by its lifting area (m/S).

Solidity (u) is the ratio between the kite's mass and the mass of air in its "volume", thus $\mu = m/(\rho S)^{3/2}$. This term is involved with the kite's dynamic response and is discussed further in section 2.4. Lastly, the unit windspeed (w_0) is that windspeed at which the dynamic pressure $(0.5\rho W^2)$ is equal to the kite weight per unit area (mg/S). This gives a natural unit of windspeed, and is used in the analysis of section 2.5.

2.1.1 Materials

It is useful to compare materials commonly used in kite and kiteline construction. This information allows a more quantitative understanding to be developed, and is especially valuable for the research carried out on the kiteline.

Table 3 lists the commonly used kite materials together with their basic physical and mechanical properties. Several other materials are included for comparison. This information has been collated from a range of references, given at the foot of the table. For Tyvek, an actual sample was measured to obtain the values given. The values quoted are typical for each material, but need to be qualified before being applied to specific examples. The main points to be noted are :

1. Kite material characteristics

a) Wood

Moisture content, grain direction and natural variability are all significant. Density variations of 5-10 % are typical, due to natural variability and moisture content. For mechanical use a stable moisture content of about 12 % is ideal. The elasticity and tensile strength quoted are those along the grain. Values across the grain are lower by about an order of magnitude.

b) Natural Fibres

Moisture content and natural variability are again significant. Since these are fibres and not bulk materials, they are relatively strong. Cotton and hemp retain their full strength when wet, silk reduces to about 80 %. For long term outdoor use some protection against rotting is needed.

c) Polymers

For a given polymer, the properties depend mainly on polymer length, shape, and degree of cross-linking. These account for the variations in density (up to 5 %) and elasticity (up to a factor of 3). The tensile strength is also influenced by the material form : fibres and films tend to be relatively stronger than the bulk material. Although polymer properties depend strongly on temperature, for kite use the range of temperatures is low, and this factor is not important in practice.

d) Composites

The details of the fibre / filler mix are important. The fibres give composites their excellent mechanical properties.

e) Metals

There is little variation between samples in density or elasticity, these being bulk material properties. However, the tensile strength depends strongly on the microscopic structure of the metal, and thus on its treatment. Strength may vary by a factor of 6. Note again that fine wires (eg. piano wire) are relatively stronger.

Z. Bulk Factor (bf)

Due to the packing of fibres, the apparent density will be less than the actual density of the fibres, for all woven materials and lines. The ratio between the apparent and actual densities is the Bulk Factor. For Nylon lines the apparent density is measured at about 1000 kg m^{-3} , giving a bulk factor of about 0.85. Other lines using fibres of the same size will also have bulk factors of 0.85. The apparent density of ripstop nylon

_3 fabric is about 800 kgm , giving a bulk factor of 0.65 for the

fabric. The material properties for Tyvek have been obtained from measurements of an actual sample, and the values quoted are apparent values, unconnected for bulk factor. These are the values relevant to actual kite materials however.

Table 3 also indicates the function in kite construction normally performed by the

material (if appropriate). The following three sections apply these general material properties to a discussion of specific kite struts, coverings and lines.

2.1.2 Struts

The mechanical properties of struts are listed in table 4 for various typical strut materials. The basic physical properties are those of table 3. Then for a variety of typical cross-sections, the mass per unit length, maximum strength and couple, and stiffness are all calculated as described in Appendix A. The Maximum strength is the tension at which the strut is expected to snap. Similarly, the maximum couple is the maximum sustainable couple. The stiffness is defined as the couple per unit curvature, and is a measure of the strut's resistance to bending. Note that for aluminium, two different grades are used. 3L63 is a strengthened grade used in aircraft construction, while 3L54 is almost pure aluminium, and much "softer". In discussing these values, it is useful to have in mind the functions performed by struts.

A plane-surface kite uses struts to create a framework over which the covering is stretched. The wind pressure on the covering pulls the frame at the points where the cover is attached or supported; and in the other direction the bridle transmits the wind load to the kiteline. Extra tension in the covering will tend to compress the structure.

With wind pressure p, a kite of size L will develop forces of pL^2, and moments of order pL^3. For the kites here, p = 5..100 Pa and L = 0.5–2.O m. Thus typically forces = 1..400 N moments = 0.5..800 Nm.

Comparing these with the values of table 4, it can be seen that it is highly unlikely that the maximum tension will ever be approached. The dominant limitation is the maximum couple of the strut. There are several design techniques which tend to overcome the limitation of the comparatively small maximum couples.

Firstly, a good structured-plane-surface kite design will spread loads evenly along the struts -loads due to the wind pressure on the covering as well as the tension in the bridle. If the loads are well distributed, then not only are struts less likely to break or lighter ones may be used, but also the kite will not be so easily distorted by high wind loads. It will thus be usable over a wider range of windspeeds.

Other design techniques relate to other kite classes. Struts may be kept short, with flexible joints, so that there are no long lever arms to generate large couples. Such a kite needs to be carefully designed so that the articulated structure is adequate, ie. the bridle must be able to distribute loads. Alternatively, struts may be used only for a part of the load distribution. The partly structured kites are examples of this technique : eg. in a sled the covering itself transmits the wind loads to the bridle, the struts are merely to hold the kite open longitudinally. Developing this technique further leads to the soft kites which rely wholly on the wind for their

structure. Again, it is important to distribute the loads evenly, requiring good design and workmanship.

Another line of development to overcome large bending moments is to increase the structure's cross section. Inflatable structures resist bending moments well, and even when they do fail, it is not normally catastrophic, since the structure re-establishes itself when the load is reduced. A large effective cross-section may also be achieved by building struts into a 3-dimensional lattice, as in the box and compound kites.

Turning to strut materials, ramin is well suited to smaller kites, and aluminium tubing to the larger ones. Ramin has the advantages of being widely available in suitable knot-free lengths and a variety of sizes, is fairly strong, and is also easily worked. Tubing combines good resistance to bending moments with low weight, and is good, especially at large diameters, but cannot easily be made from ramin. Aluminium is thus used, being readily available and reasonably light. The high strength varieties (eg. 3L63) are most useful. Tubes may also be built up from fibreglass or other composites. Solid fibreglass is usually used only in small diameters, since it is relatively dense. These thin lengths of fibreglass have comparatively low stiffness, and are used where great flexibility with high strength is a positive advantage, eg. in the leading edge spar of a Flexifoil. Fibreglass may also be tapered to save weight by having the strength only where it is needed.

2.1.3 Coverings

Table 5 lists the covering materials now usually used for kites, along with their basic physical and mechanical properties. The density, elasticity and tensile strength are from table 3. Samples of each material have been measured to give the thickness (t), mass per unit area (m) and breaking strengths (bs) listed. The breaking strength is measured with a sample of known width, taking care to avoid uneven stress distributions which may cause early failure. Materials with an obvious grain or weave are tested at different orientations to the weave (parallel or 45°). An apparent density is calculated from the measurements (m/t), and the ratio of this to the true material density gives the bulk factor (bf). The bulk factor is used to estimate a calculated breaking strength (= tx.t.bf). For woven fabrics, only those fibres along the test direction are able to resist the tension, so the calculated strength is expected to be about twice the measured value.

A kite with loads well distributed is able to use lighter material than one concentrating all the forces through only a few points. Thus large parafoils use lightweight ripstop nylon, since they have many shroud lines.

Unnecessary stress concentrations are likely to be formed at points in the covering where seams do not run smoothly, and tend to weaken the whole kite. Some materials are more vulnerable to this than others : the higher the elasticity, the greater the stress for a given strain. Thus it is the inelastic materials (high elasticity) which demand the best workmanship. However inelastic materials are less

prone to distortion and so give kites a more firmly defined shape.

In practice there are several other properties of a covering which need to be considered, but which are not so easily quantified. These include porosity, uniformity, bonding techniques, abrasion resistance, as well as price and availability. The porosity and uniformity are the most important to kite physics.

The porosity will obviously have significance for the behaviour of the boundary layer, in that a small flow of air is allowed through the covering from the lower surface (high pressure) to the upper surface (low pressure). No tests related to porosity have been made here, but it is reported (eg. Moulton, 1978, p 135) to make large kites much more manageable, presumably by reducing the aerodynamic force and perhaps improving stability.

The uniformity of the material is important when the kite is heavily stressed, since any non-uniformity will give rise to uneven distortions. The resulting asymmetry makes the kite tend to fly to one side relative to the mean wind, and in stronger winds will cause it to come down. The materials most prone to this are those produced from natural fibres, eg. cotton fabric and paper, or the lightweight synthetic fabrics, eg. ripstop nylon. Dense or high quality fabrics, or the polymer films suffer less from this problem. In some kite designs, care needs to be taken to align the warp of the material along the correct direction, otherwise the kite will again distort unfavourably or asymmetrically under heavy wind loadings.

Finally, as a brief comparison, table 5 includes details of some coverings used at the turn of the century by the United States Weather Bureau (Marvin, 1896).

It can be seen that the masses are comparable with the range for modern ripstop nylon. Unfortunately the materials' strengths are not known.

2.1.4 Lines

In this section a few remarks are made on general kiteline properties, referring particularly to the actual examples used. However, the kiteline is such an important part of the whole kite system in natural wind that much fuller consideration is required : this is presented in section 3. The remarks here are limited to a discussion of material properties.

Specific examples of kitelines are detailed in table 6, with more general relationships based on these values given in figures 2a,b,c. For each line measured, the breaking strength (bs) is simply that specified for the line by the manufacturer or estimated from a knowledge of the line's material and mass per unit length. Kevlar 29 is a modern polymer with excellent mechanical properties. To retain its full strength, the Kevlar must be protected from abrasion and other damage : a polyester sheath is sometimes used. However, the weight and size of the sheath are significant relative to the core on small diameter lines. This increases the line weight and windage, making it little better than nylon in these respects. Nylon braid is readily available

in a range of sizes, and is perfectly adequate for many uses. Polyester is similar to nylon except that its elasticity is higher. Steel piano wire used to be used due to its high strength, and is included in some of the later tables and figures for comparison.

The basic measurements of table 6 are mean diameter (d), mass per unit length (m), and elasticity (k). Because of the variation between different samples, each of these parameters is subject to significant uncertainty, which is reflected in the scatter in the calculated values of the basic material properties (density, tensile strength and elasticity). It was found to be difficult to measure small line diameters -they tend to be underestimated, probably because the line is easily distorted as it is being measured. This underestimate of the diameter gives misleadingly high values for density, tensile strength and elasticity. The apparent density and tensile strength are calculated from the measured diameter, mass per unit length and quoted breaking strength, using the following relationships,

density $= m/(\pi d^2/4)$

tensile strength $= bs/(\pi d^2/4)$

The elasticity of a line is defined as the increase in tension per unit extension. Measurements show that elasticity is not always constant, but may increase with tension, especially for nylon. Figure 3 demonstrates this trend by plotting elasticity as a function of tension for the various lines tested. Both elasticity and tension are normalised by dividing by the line's breaking strength, revealing the underlying pattern to some extent. It can be seen that the lines group according to material.

The general pattern is for the elasticity to rise with tension initially, eventually reaching some constant maximum value. The initial rise is assumed to be due to progressive alignment of the fibres (and apparently molecules too for nylon, since the monofilament line shows the same effect). Once this alignment has been completed, the elasticity remains constant at a value which should be equal to the bulk material elastic modulus divided by tensile strength.

There is considerable uncertainty in the numerical values used for two reasons.

Firstly, test tensions are limited to at most half of the breaking strength, and trends have had to be extrapolated beyond this (as indicated by the broken lines —-). The extrapolation is determined by continuing the linear slope until the constant level is reached (calculated from the ratio of elasticity to tensile strength if necessary). Secondly, there is considerable variability and uncertainty in the breaking strength. Nevertheless, the data is valuable and relevant, especially since most lines will rarely exceed Z5 % of their breaking strength in use, thus remaining within the measured regions.

The relative shapes and positions of the elasticity curves give valuable information. Nylon appears to have a relatively long region of increasing elasticity, to at least 50 or 60 % of breaking strength. The relative levels of the plateaux suggests that the fibres of the braid have a higher elasticity than the nylon of the monofilament. This may easily be the case if the process of drawing out the fibres causes a large

degree of natural alignment, not present to the same degree in the much thicker monofilament.

Sheathed Kevlar's elasticity rises very steeply initially, soon reaching its constant value. Most of the initial slope is assumed to be due to the sheath, which at higher tensions plays a smaller and smaller part in the behaviour, due to its much lower tensile modulus. Bare Kevlar is not handicapped in this way, and its elasticity is constant, with a small amount of alignment allowed for at low tensions. Piano wire will have a constant elasticity : there is no scope for any alignment effects. It is not included in figure 3 since its elasticity is so much greater than for other line materials (constant at 100 times its breaking strength).

Another effect of increased line tension is a reduction in cross section (the degree of reduction is given by Poisson's ratio). This tends to reduce the apparent elasticity, by a proportion roughly equal to the extension, and thus is not responsible for the observed increase in elasticity.

Because of the variation of elasticity with tension, the values quoted in table 6 are standardised by using a least squares fit to the results of figure 3, evaluated at 10 % of the line breaking strength.

General Relationships

Table 2.1 contains typical apparent values of density, tensile strength and elasticity (bulk properties) derived from table 6 -and are thus representative over the range of breaking strengths measured.

These values are then used to derive the general relationships shown in figures 2a,b,c, using the following equations. The tensile strengths for Kevlar are based on more recent tests performed by Bridon Fibres and Plastics Ltd, which suggest that the actual breaking strength of their lines is about 20 % higher than previously quoted. The relationships are :

breaking strength, bs = Ax.tx, where Ax = ird /4

Breaking strength rather than area is taken as the independent variable since it is the most important factor determining whether a line is suitable for a given task.

diameter $d = 2bs^{1/2}/(\pi tx)^{1/2})$

mass per unit length $m = \rho Ax = bs.(\rho/tx)$

elasticity $k = EAx = (E/tx).bs$

Ax =	cross-sectional area
E =	tensile modulus
tx =	tensile strength
ρ =	density

In practice, not all these materials are suitable for use over the whole range of

Line material	Density	Modulus	Tensile strength
	kg m^{-3}	GPa	MPa
nylon, monofilament	1200	2.1	470
nylon, braided	1000	1.3 330	
polyester, braided	1300	6.3 520	
Kevlar, sheathed	1120	8	550
Kevlar, bare	1260	44 1750	
steel, piano wire	7850	210	2100

Table 2.1: Typical effective line material properties (at T = 10 % bs).

tensions up to 3000 N, and present research is limited to tensions below 1000 N. For very low tensions, monofilament nylon is all that is available. The thickest monofilament corresponds to about 500 N, and is limited by the stiffness of such large diameters making the line difficult to use. Braided nylon is produced for tensions as low as 50 N, through to several tonnes' force. Piano wire and Kevlar are not produced for loads below about 250 N; part of the reason is that being very strong materials, such lines are so fine that they become dangerous to work with, liable to cut through anything in their way when under tension.

The figures show only general relationships. Specific examples are likely to be scattered about these trends, so that is would be wrong to attempt to extract too much detail from the curves. The important information is contained in the grouping of the curves, and the relative positions of the groups. Table 3.2 in section 3.3 gives relative weights and diameters for different line materials.

Thus for a given breaking strength, bare Kevlar and piano wire have similar diameters as do (braided) nylon and sheathed Kevlar. (The curves apply only over the range of tensions used). At larger breaking strengths, sheathed Kevlar is much better than nylon, since the sheath becomes progressively less important, and the line's properties approach those of bare Kevlar, but for tensions far greater than those used here.

Considering the weight of the lines, there are three groupings. Piano wire is the heaviest, then comes a group with nylon and sheathed Kevlar, and the lightest is bare Kevlar. The relative weights are approximately 5:3:1.

Elasticity follows the basic material types, with piano wire, Kevlar and nylon with decreasing elasticity. For the figure, the elasticity at 10 % of breaking strength has been used. For braided Kevlar and nylon, the variation of elasticity with tension should also be taken into account, although this does not influence the relative performances significantly.

Practiced considerations

To complete this discussion of real kitelines, there are several other points that

should be included.

Joints and splices in lines inevitably weaken the line, although good knots / connections may retain 90% or more of the normal line strength. Some tests recorded by Marvin (Monthly Weather Review, April 1896, p.119) on knots tied in 2.8 mm line show that poor knots (double overhand and sheetbend) retain only about 70% of the line's strength, while a good knot such as the bowline can be as strong or even stronger than the line itself. The weakening effect of knots is more serious for materials with a high tensile modulus (ie. little stretch), since

a given radius of curvature will give rise to a greater stress concentration. Knotted lines of Kevlar 29 retain only about 37 % of their straight tensile strength (Du Pont, n.d.). To keep the full line strength, it is best to use single lengths, avoid chafing of the line, and use only good knots (eg. bowline) and connections which avoid small radii of curvature.

From a purely theoretical point of view, Kevlar and piano wire seem to have many advantages. However, there are two practical difficulties that can put the kite flier in serious danger. Firstly, materials which are very strong, such as Kevlar and steel, need only very fine lines for moderate loads. When under tension such lines are extremely sharp, making it difficult to handle the lines safely. For larger diameters, it is easier to take proper precautions. Secondly, a length of conductor hoisted up into the atmosphere will in certain weather conditions attract electrical discharges down the line to ground. Even in normal conditions, an electrical field exists with a gradient of about 100 V m^{-1} over open ground, so that very large voltages can easily be generated. Fortunately, the currents are very low, so that, for example, the United States Weather Bureau was able to operate regularly using steel lines without any serious risk to its personnel. However, if the air is ionised and so able to conduct more easily, for example around a thunderstorm, then lethal discharges are easily generated, and even non-conducting lines such as nylon will conduct to some extent when wet. Another danger with conducting lines in built up areas is the possibility of the line falling on overhead power lines. Modern kite fliers tend not to use piano wire (or else have short exciting lives).

2.2 Concepts from Anemometry

An important part of the background to any study of kites is an understanding of the wind. This section presents some of the concepts used to describe the wind, as they may be applicable to kites.

2.2.1 The structure of the wind

It is useful to have a physical model of the wind to describe its structure, rather than having to treat it simply as a random process. The most common model is based

on eddies, which are thought of as rotating parcels of air. In natural wind, eddies of all sizes are present, with the smaller eddies being carried within larger ones, up to the largest eddies present. This whole pattern is transported at the mean wind velocity.

Using this eddy model, the next stage is to find out the relative importance of eddies of different sizes. Ideally the wind velocity at every point in a region of space is measured, and then the wind velocity is analysed to find its spatial frequencies. In practice such measurements cannot usefully be made, and it is much easier to measure the wind velocity at a fixed point over a period of time.

These two types of measurements are related if the pattern of turbulence changes relatively slowly. The turbulence is then effectively "frozen" into the wind and carried past the anemometers at the mean wind velocity. This is Taylor's Frozen Field hypothesis, and is valid if there is little change in the wind field as it travels over the separations being studied. It provides an important link between the type of wind velocity measurements which are most easily made and the information on eddy sizes and energy content which is required.

Thus in practice, a wind component of frequency n is assumed to correspond to an eddy of size W/n, where W is the mean wind speed.

The structure of the wind changes significantly with the weather conditions. The most important factor is the stability of the atmosphere, ie. whether the temperature gradient is such that vertical air motions are encouraged or suppressed. In very stable conditions, vertical motions are suppressed, and the air is calm. This is most common early in the morning or in the evening, when the air near the ground is cool. Unstable conditions are caused by strong heating of the ground and a temperature decreasing quickly with height. In such conditions, large convective cells may form, and the wind velocity becomes very variable, with eddies up to several kilometres in size being important. Between these two cases is a neutral atmosphere when the temperature gradient is such that vertical motions are neither encouraged nor suppressed. Neutral stability is commonest in overcast conditions, or when the wind is strong enough that simple mechanical mixing of the atmosphere overcomes any temperature gradients.

2.2.2 Frequency analysis of the wind

Using the eddy model of the wind, one of the most useful ways of analysing the wind is to investigate its frequency content. The two main techniques are autocorrelations and Fourier transforms. Since measurements are almost always made at a fixed place over a period of time, the temporal frequency is used and then translated into a spatial frequency using Taylor's Frozen Field hypothesis.

Figure 4 shows a wind trace measured at a height of 22 m, when the mean windspeed was 8.5 m s^{-1}. The autocorrelation and Fourier transform have both been calculated,

and are shown in figures 5a,b and c. The autocorrelation (figure 5a) shows that after a lag of about 20 s the windspeed has become decorrelated with itself. This indicates that the largest significant structures in this example have a period of about 20 s, and thus a size of about 170 m. A related timescale is the integral timescale (T_t) given by the area under the correlation curve. The integral should be over all time, but in practice a useful estimate is obtained from twice the area on the positve side up to some suitable maximum lag. In this case, the integral timescale calculated is 19.7 s (maximum lag = 75 s), very close to the decorrelation time of 20 s. Wind readings taken at closer intervals than the decorrelation time are not independent, and thus a mean velocity over time T contains only m = T / T independent measurements. The error between this estimated mean and the "true" mean windspeed is equal to s(W) / $m^{1/2}$, where s(W) is the "true" standard deviation (ie. measured over a long period of time). Section 2.2.3 (below) extends this analysis by discussing the influence of sampling and recording times on the means and variances measured.

Figures 5b and c both present the power spectrum of the windspeed of figure 4. Figure 5b uses logarithmic axes to display the full spectrum calculated. The ordinate is the variance per unit frequency interval at frequency n (E(n)) divided by the total variance (s^2). E(n) represents the turbulent kinetic energy in the wind at frequency n, and it can be seen that most of the energy is at frequencies below 0.1 Hz. Figure 5c shows this more clearly since the ordinate is defined such that the area under the curve is proportional to the variance, and thus the turbulent kinetic energy. This Meteorological Format show clearly that in this case about 75 % of the energy is at frequencies below 0.1 Hz.

Theory predicts that for homogeneous, isotropic turbulence, in the range of frequencies between those at which turbulence is created (by obstacles etc.)

and those at which it is dissipated (by molecular scale viscosity), the energy at frequency n is proportional to $n^{-5/3}$. The power spectrum over this Inertial Subrange of frequencies is expected to follow a power law with exponent -5/3. Figure 5b includes a slope of -5/3 alongside the measured spectrum showing that for frequencies above about 0.02 Hz the energy at frequency n is consistent with this variation.

2.2.3 Finite sampling and averaging times

Frequency analysis provides an understanding of the influence of practical data sampling techniques on the data collected. Although this is applied to wind measurements here, it applies more generally to all practical data recording techniques. The main limitations of any data recording process are :

1) any individual data point will in practice be an average over some finite sampling period s, say. For the anemometers used here at sampling frequency n_0,

s = 1 / n_0

2) the length of the data record made is finite. Ideally it would extend over all time,

but real experiments can only last for a finite time T,

3) as a reading is made, it can only be recorded to a certain accuracy determined by the recording process. This is the digitisation or quantisation error. The digital anemometers used here have a resolution of 0.24 m s^{-1} on any individual reading, when operated at a sampling frequency of 10 Hz.

Of these limitations, frequency analysis allows us to discuss 1 and 2 in more detail. 3 is discussed separately in section 2.2.4 below.

Following the discussion in Pasquill (196Z), consider a sinusoidal frequency component of frequency n,

$y_n = a \sin(2\pi nt)$

Averaging this over the sampling period s gives,

$y = y_n \frac{\sin(\pi ns)}{\pi ns} = y_n \operatorname{sinc}(\pi ns)$

Thus low frequencies, n ¡¡ n_0, are measured accurately, while frequencies with n ¿¿ n_0 are strongly attenuated. The sampling frequency thus provides an upper frequency cut-off at around $n = n_0$. The half power point is at $n = 0.443\ n_0$. The variance at frequency n is reduced by a factor $\operatorname{sinc}^2(\pi ns)$, which is plotted in figure 6a.

The effect of the finite total recording time T is complementary to that of the sampling period s. If only the variance within successive periods T is known, but all information concerning any relationship between the successive periods is lost (as for the sampling period s), then the variance "lost" is given by the attenuation factor $\operatorname{sinc}^2(\pi nT)$, as above except the sampling period s has been replaced by the total recording time T. Since the recording time T is in fact the period within which information is retained, the proportion of the variance measurable is the complement of this, and is given by $1 - \operatorname{sinc}^2(\pi nT)$ and is shown in figure 6b.

The combined effect of the finite sampling frequency and recording period is thus to provide a frequency "window", with frequencies higher than n_0, and lower than 1/T effectively excluded. Figure 6c shows this sampling window, combining figures 6a and b, and is the transfer function of the recording process. The half-power points are at (n T) or (n s) = 0.443.

2.2.4 Finite measurement resolution

A quantity such as the mean wind velocity can only be measured to a certain finite accuracy. This quantisation error leaves an uncertainty in the measurement, and in subsequent analysis gives rise to extra noise on the data.

The error on any particular reading will usually be evenly distributed over a range of either O..d or -d/2..+d/2, depending on the details of the measurement process, where d is the resolution of the quantisation. This quantisation increases the vari-

ance of the data by $d^2/3$ for the single-sided error, and $d^2/6$ for the double-sided error. This error should be insignificant if the experiment has been well designed.

The effect on the mean depends on the details of the measurement technique. If all the quantisation errors are independent, then the individual quantisation variances (s^2) over the N points all add. The extra standard deviation of the mean is then approximately s / $N^{1/2}$. For the wind measurements here though, consecutive wind readings are not independent, and the error on the total is always +/- d, no matter how many points are summed. In this case the extra standard deviation is s / N, ie. decreasing in proportion to 1/N.

2.2.5 Means and variance of the wind

Although a full frequency analysis of the wind is valuable for describing its structure, for many applications, only the mean and variance are needed. These are calculated in the usual way from the relevant component of the wind, but there are a few points which may need some care.

Firstly, wind velocity is a vector and thus a mean or variance is only meaningful if related to some specific quantity relating to the wind, such as a component, the windspeed or the wind velocity itself.

Secondly, one of the main characteristics of the wind is its variability. This variability is such that even terms such as the mean need to be defined with care. The wind changes over timescales ranging from fractions of a second up to months, years, and even decades, ie. over practically the whole of the range of measuring periods available. A mean defined over one period will in general be different from one defined over a different period. Unlike some variable processes, statistical measures of the wind do not tend to asymptotic values

which can be approached arbitrarily closely simply by taking sufficiently long averages. In mathematical terms the wind velocity is a non-stationary variable.

In practice, an averaging period can usually be defined such that useful results may be obtained. For example, in this current work with kites on relatively short lines, wind velocities averaged over 5 or 10 minutes are useful since the kites' own motions are all much faster than this. Whatever the averaging period, there is almost certainly an underlying trend which has effectively been ignored. Autocorrelations are usually good indicators of this since if the underlying trend is strong they usually tend towards a non-zero value. Wind measurements on days with strong convection often show this behaviour due to large convection cells which may take many minutes to pass.

2.3 Concepts from Aerofoil Theory

Aerodynamics is a very well developed branch of science, but almost all this development has been directed towards powered aircraft. Kite aerodynamics is less well understood : partly because much less effort has been given to it, and partly because in many ways kites are more complex than aircraft. The basic ideas are still important, and are presented here along with a discussion of the ways in which kite aerodynamics needs special consideration. Many of the experiment results are analysed later using ideas of aerofoil theory.

2.3.1 Basic ideas from aerofoil theory

References such as Glauert (1959), Kuchemann (1978) and Ward-Smith (1984) discuss basic ideas of aerofoil theory in some detail. This section introduces some of these for use later in the thesis.

Mechanisms of lift and drag

The aerodynamic force on an object is usually broken into two components. The one parallel to the undisturbed airflow is called drag, and the one normal to that airflow is called lift, since it is the normal force which can be used to support the weight of an aircraft or kite against gravity. Fundamentally, aerodynamic forces are due to pressure differences, and so to support a kite against gravity and the tension in the line, the pressure against a kite's underside must be greater than that against the top surface.

Since the drag force is parallel with the undisturbed wind velocity, it corresponds to a loss of energy. Drag can be analysed into several components. Skin friction drag is the drag due to airflow over the object itself, and is energy lost to heat through the viscosity of the air around the object. Form drag is the energy lost to the wake. In practice, the airflow never joins up completely behind an object, but leaves a turbulent wake of some sort. Skin friction and form drag are minimised by using streamlined shapes which disturb the airflow as little as possible.

A third type of drag is the drag due to lift, known as induced drag, trailing vortex drag or just vortex drag. The lift generated by an aerofoil is related to a circulation of airflow around it, which increases the airspeed over the upper surface and reduces the airspeed below. It is this difference in airspeeds which generates the pressure difference and thus the lift. The circulation does not simply end at the wing tips, but continues downstream in two trailing vortices, rotating in opposite directions. The sense of rotation is such that the air between them is descending. It is the downward momentum imparted per unit time to this air between the trailing vortices which generates the lift. However, there are two losses of energy here. Firstly, energy is required to generate the trailing vortices, which are being created continuously as the air flows over the aerofoil. Secondly, the air between the vortices has acquired kinetic energy since it now has a slight downward velocity. To minimise the induced

drag per unit lift, the strength of the circulation should be reduced, and the span increased to compensate for the loss in lift per unit span. Thus wings designed to generate as little induced drag as possible at a given lift have very long spans, eg. soaring birds and sailplanes.

Boundary layer

An important concept in aerofoil theory is the boundary layer. This is the layer of air next to any surface moving through it. Because of air viscosity, the

layer of air in contact with a body must be practically stationary relative to it, with only a finite velocity gradient away from the surface. Ideally, the airflow next to the surface is simply a series of layers of air, each one gradually moving faster as the distance away from the surface increases, tending towards the speed of the undisturbed airflow. These laminar boundary layers may be very thin, and give very little drag. Often however, the boundary layer becomes turbulent and much thicker, sometimes even enclosing "bubbles" of air disconnected from the main flow. In such cases the drag can be much higher. If the boundary layer suddenly changes from one type to another then this may be reflected in abrupt changes in the lift and drag generated.

The distinction between laminar and turbulent boundary layers is important, and kites have the combination of speed and size such that they might straddle the transition. However, several features of kite design combine so that kite boundary layers are expected to be turbulent.

Interference effects

The lift and drag on individual components, independent of one another, has only been considered so far. However, any real kite or aeroplane consists of many components held together as one structure. These components influence one another, and these interference effects are often important.

There are two types of interference to consider. Firstly, at a junction between two surfaces, say, the boundary layers merge. In many cases the combination has more drag than the individual components. To minimise this extra drag it is best to avoid sharp corners, and, especially on lifting surfaces, to keep the number of junctions to a minimum. Full size aircraft are designed paying particular attention to the wing-fusalage junction for this reason, and often use fillets to smooth out otherwise sharp corners.

The second type of interference is that due to one component being in airflow distorted by another. This is particularly the case for lifting surfaces, but also applies if one component is simply in the wake of the other. For example, the lift and drag in a biplane aerofoil is redistributed by the induced flow field of the

combination, so that the upper aerofoil generates more lift and less drag while the lower one generates less lift and more drag. In practice the redistribution is nearly always detrimental for the system as a whole in that more drag is produced per

unit lift. This type of effect is bound to be significant for kites with multiple lifting surfaces, ie. any of the box or compound kites. The advantages structurally and in stability however make the aerodynamic price worth paying in many cases.

Dimensionless coefficients

By using dimensionless coefficients it is possible to study the properties of an object's shape and attitude alone, independent of size, speed and air density. The magnitude of the actual aerodynamic forces depends on the air speed and density, on the area exposed and on its shape. In order to examine the effect of the shape only, these scale effects must be removed. Using the techniques of dimensional analysis, the air density (p), speed (V) and area (S)are combined to give a natural aerodynamic unit of force,

$F = 1/2\rho V^2 S$

The factor 1/2 is introduced for consistency with Bernoulli's equation, where the dynamic pressure (q), the pressure required to bring an airflow of density ρ, speed V to rest, is given as $1/2pV^2$.

Lift (L) and drag (D) may be non dimensionalised by dividing the measured forces by this aerodynamic unit of force. The resulting non-dimensional coefficients contain information primarily about the shape and attitude of the aerofoil under consideration. The definitions used are

Lift coefficient : $C_L = L/qS$

Drag coefficient : $C_D = D/qS$

In addition to lift and drag, it is important to be able to describe the line of action of the aerodynamic force, or equivalently its moment about a specified point. The moment (M) is usually given about either the aerofoil leading edge or its quarter chord point, and the sense is chosen so that a positive moment is one

tending to increase the incidence. Since a moment has the units of a distance multiplied by a force. To non-dimensionalise it a suitable unit of distance is needed. The aerofoil chord (c) is the natural unit of distance, and the moment coefficient is defined as

Moment coefficient : $C_M = M/qSc$

The line of action of the aerodynamic reaction may be specified by the point P where it cuts the aerofoil chord. P is the centre of pressure. If OP is the distance from some origin, usually the leading edge, this is non-dimensionalised as

Centre of pressure coefficient : $C_P = OP/c$

The two coefficients are related by simple geometry involving the aerofoil's incidence (a) to the undisturbed airflow (see figure 7).

$$\begin{aligned} M &= -(L\cos a + D\sin a)PQ \\ C_M &= -(C_L\cos a + C_D\sin a)PQ/c \\ &= -(C_L\cos a + C_D\sin a)(CP - OQ)/c \\ C_P &= OQ/c - C_M/(C_L\cos a + C_D\sin a) \end{aligned}$$

The aspect ratio (AR) has already been introduced. It is a dimensionless measure of the aerofoil planform, and is involved in the relationship between induced drag and lift.

Basic relationships

Several relationships involving non-dimensional coefficients can be derived from standard aerofoil theory. All these equations are somewhat limited in their full applicability, but the trends described are generally valid over a wide range of wing planforms. As well as the terms already introduced, these relationships involve the drag coefficient at zero lift (C_{D0}), the induced drag coefficient (C_{Di}) and a dimensionless number close to one (K_v) which is a function of the lift distribution (K_v =1 for elliptical lift distributions, and > 1 otherwise).

From lifting-line theory (Glauert, 1959)

$$\begin{aligned} C_L &= (2\pi/(1+2/AR))a \\ C_D &= C_{D0} + \frac{1}{\pi AR}K_v C_L^2 \end{aligned}$$

From small aspect ratio theory (for A<2, Robinson and Lauermann, 1956)

$$\begin{aligned} C_L &= \frac{\pi}{2}ARa \\ C_{Di} &= \frac{1}{\pi AR}C_L^2 \text{(profiled wings)} \\ &= \frac{2}{\pi AR}C_L^2 \text{flat plates} \end{aligned}$$

2.3.2 Aerodynamic theory particularly relevant to Kites

Kites differ from aircraft in several important ways, and need special consideration because of this. The following paragraphs discuss the main points.

Low aspect ratio

Typical aspect ratios for kites are in the range 0.6 -4.0, whereas classical aerofoil theory is strictly applicable only to wings with aspect ratios of about 6 or more.

The effects of this difference must be considered, since the classical theory cannot be expected to apply exactly to kites.

The flow around an aerofoil of low aspect ratio is influenced strongly by the tips, so that as well as the usual chordwise circulation, there is in addition a strong flow around the lateral edges. This lateral flow gives rise to a second, non-linear, lift mechanism, with the lift related to both the incidence and the forward projected area. This second non-linear component may be more

important than the linear one for aspect ratios less than one.

Extending lifting line theory to a lifting surface theory for small aspect ratios gives the equations below. These describe the first (linear) component of lift, and are accurate for AR up to 1.0, and useful to about AR=2.

$$\begin{aligned} C_L &= k \sin^2 a \cos a \text{ with k = 1 to 2} \\ C_{Di} &= k \sin^3 a \end{aligned}$$

The lateral flow about the tips reduces the lift and lift curve slope, and delays the stall and reduces its severity. As might be expected, the detailed shape of the tips is important : round tips tend to reduce the effective aspect ratio still further, especially if the edges are also rounded. A rectangular planform with sharp edges maintains the geometric aspect ratio closest.

Low flying speeds

The typical airspeed of kites is the windspeed, while aeroplanes are usually at least an order of magnitude faster. This is significant for the types of airflow encountered, and care is needed in transferring any concepts.

To relate performance of aerofoils at different airspeeds a non dimensional parameter, the Reynolds number (Re) is used. This is the ratio between the inertial and viscous forces on the aerofoil, and is defined using a typical length scale for the aerofoil (L, usually the chord), its airspeed (V) and the air's kinematic viscosity (n = viscosity / density). For air at 10 deg C, 1 atmosphere, n = 14.3 μm^2 s^{-1}.

$Re = LV/n$

Lissaman (1983) reviews aerofoil behaviour at low Reynolds numbers. Most of the review is concerned with thick aerofoils at Reynolds numbers around 10^5, and includes discussion of the separation bubbles often formed.

Figure 8 shows typical Reynolds numbers for kites. Values range from 4x10^4 to 3x10^6. Experiments in wind tunnels have demonstrated an important change in airflow patterns around Reynolds numbers of 100 000, and kites may straddle this transition. The transition is from boundary layers which remain laminar to those which become turbulent, and is important because a laminar boundary layer is liable

to break away from the wing surface catastrophically, limiting the lift available, and generating extra drag.

However, there are two factors which operate in favour of kite aerofoils. From tests of a range of aerofoils (reported in Simons, 1978), it is found that those with sharp leading edges and thin sections tend to have transitions at low Reynolds numbers, below 40 000, and secondly that if the boundary layer is stimulated to turbulence, then this too tends to lower the critical Reynolds number, for example from 100 000 to 50 000. For kites in natural wind there is generally plenty of turbulence, including that naturally in the wind and that generated by small imperfections around the kites' leading edges. With both these factors operating, it is likely that all practical kite aerofoils will be working above their critical Reynolds number.

Wing sections and shape

The shape and sections used for kite aerofoils have several features making them different from most aircraft wings. The main features which have not already been considered are the planform, the thin aerofoils and their flexibility.

Of the common kite designs, those with vents and slots have extra flow "through" the kite, which may tend to reduce the effective aspect ratio from that expected. Some box kites and sleds have end plates to the lifting surfaces so that their effective aspect ratio may be increased. Most kites however have pointed tips, which is expected to reduce the effective aspect ratio by about 20

Figures 9a and b (from Kuchemann, 1978) show characteristics of aerofoils of different thicknesses. Thin aerofoils (curve 3) compared with thicker ones (curves 1 and 2) tend to have a gentler stall, are comparatively limited in their maximum lift coefficient and have a performance which is generally less dependent on the aerofoil shape. (The Reynolds number is well above any laminar separation problems). Curved thin aerofoils, ie. ones with camber, are able to generate more lift than flat ones, and because of the way the wind pressure billows out kite wings, this applies for most kites. Similarly, those kites with thick profiled aerofoils may be expected to operate with lift coefficients greater than one, if suitably bridled.

Potentially a very important characteristic of kite aerofoils is their flexibility. The typical kite wing is simply an area of fabric stretched over a framework of some sort. Depending on the kite design the built-in tension may be enough to hold the fabric completely taut, or leave it quite slack. The more slack the covering, the more likely it is to change shape under different pressure distributions. This aeroelasticity may lead to non-linearity in the lift curve. The changing pressure distribution may cause increasing camber with incidence so that the lift curve is much steeper initially than for a rigid wing. Work has been done on this type of behaviour for an aerofoil called the Sailwing (Ormiston, 1971). This non-linearity is investigated theoretically and experimentally, and shown, as is expected, to be strongly dependent on sail tension.

Unsteady airflows

A kite flying in natural wind is in quite a different environment to a wind tunnel.

In natural wind the instantaneous wind vector is continually changing, and the kite must respond to this. To understand kite flight the unsteady airflow patterns around the kite must be taken account of.

Wind statistics can be used to estimate typical variations in the wind as seen by the kite. Thus the typical standard deviation of the windspeed is 10 to 25 % of the mean (at heights up to 30 m), and variations in angle may be 10 to 15 degrees away from the mean. Most of this variation is on timescales greater than a few seconds.

As long as the aerofoil is operating in a linear region, the unsteady airflow is not a dominant feature, and only shows up in second order effects. However, if the aerofoil goes outside the linear range then the behaviour becomes less predictable. The stall is the major non-linear feature, and it is in this area that most work has been concentrated. It is found (eg. Ericsson and Reding, 1971; Hoerner, 1975) that an increasing incidence delays the stall to higher angles of attack, allowing the static maximum lift coefficient to be exceeded by as much as 50 %. Similarly, as the incidence is decreasing from above the stall, reattachment is delayed to a much lower angle of attack. The size and shape of this hysteresis depends on the amplitude and frequency of the variation, and the aerofoil type.

Figure 10 (from Ericsson and Reding, 1971) shows typical values of the dynamic stall overshoot as a function of non-dimensionalised pitching rate. A kite of chord 1 m pitching at 30 deg s in a wind of 5 ms has a dimensionless pitching rate of about 0.1 and is thus expected to overshoot by about 12°. These values are unlikely to be exceeded in practice, but even so the actual extra lift and hysteresis may be as much as 50 % in the most extreme cases.

For thin aerofoils there appears to be some benefit from unsteady airflows in that time-averaged lift coefficients are significantly higher than the static values. This is explained as being due to the extra energy available to the boundary layer, which presumably prevents large separation bubbles forming and destroying the lift.

2.4 Elementary Models of the Kite System

A real kite being flown in the wind is a very complicated system to analyse fully. However, aspects of the system may be understood usefully with quite simple models, and in this section, four such models are presented. They describe the kite system's dynamics, and help guide the research by identifying important features, or by explaining some of the more significant dynamic flight characteristics.

The models presented here ignore details of the kite design and only use general properties such as kite mass and area. The four models describe the

following aspects :

a) the kite's response to turbulence, based on a dimensional analysis of forces acting

on a kite,

b) the importance of various system components, using an analysis of the energy associated with each component,

c) a low pass filter effect on angle measurements due to line length,

d) a periodic response in azimuth, which affects large kites on short lines.

2.4.1 Kite response to turbulence

In a turbulent wind kites are continually buffetted by eddies of different sizes and strengths, and it is possible to estimate whether a kite tends to respond quickly to each new eddy or whether its inertia carries it through many eddies before its velocity has changed significantly.

The aerodynamic reaction acting on a kite (area - *S)* in the wind (speed = W, density = ρ) is given by

$$R = \frac{1}{2}\rho W^2 S C_R \tag{2.1}$$

C_R (the reaction coefficient) is a dimensionless coefficient with magnitude close to 1.

In turbulent winds the size of the disturbing force will be close to R, and acts to accelerate the kite mass (m). The time taken to accelerate m from rest through the kite's size (L) is

$$t_1 = \frac{2L}{W}\frac{m}{LS\rho C_R} \tag{2.2}$$

The quantity (m / LS ρ) is dimensionless and is known as the solidity ratio (μ). It is a measure of the kite's mass relative to the surrounding fluid, and allows equation *2.2* to be written

$$t_1 = \frac{2L}{W}\frac{\mu}{C_R} \tag{2.3}$$

This is the timescale for the kite's response to turbulence.

The timescale for the fastest eddies (t_2) is obtained by dividing the kite size (L) by the windspeed (W). Eddies any smaller than L tend to be averaged over the kite surface and have little net effect.

$$t_2 = \frac{L}{W} \tag{2.4}$$

The ratio between these two timescales indicates whether the kite will be sluggish (dominated by its inertia) or responsive (reacting to all eddies down to the kite size L).

$$t_1/t_2 = 2\frac{\mu}{C_R} \tag{2.5}$$

Figure 12 shows solidity ratio plotted as a function of kite size for a range of kites. The main features are,

a) for kites 0.5..1.0 m^2 in size, $\mu = 0.2..0.5$,

b) over the range covered, there seems to be a trend towards greater values of μ for small kites. A curve proportional to 1/L matches this very loosely, suggesting that kite masses may be more closely related to area (S) than volume (L^3), ie. kite masses do not increase simply as the cube of the linear dimension. This is probably due to small kites being built over-strong rather than having strength only where it is required.

c) the curve 0.3 / L may be taken as a partition between the heavy kites, such as box kites, and the lighter plane surface kites. This loosely matches the trend in solidity vs linear dimension over the range covered.

These values of solidity ratio, with reaction coefficients of 0.6 to 1.0, give estimates of the ratio of timescales close to unity. The kites tested are generally expected to be able to respond to all eddies down to the size of the kite, but not any smaller. This inertia response thus augments the averaging of eddies smaller than the kite over the kite surface.

It is likely that particularly heavy kites (perhaps built for strong winds) or kites carrying significant payloads will be influenced more strongly by their inertia, and will not respond to the smaller eddies.

2.4.2 Kite system energy analysis

Another technique for examining kite dynamics is to consider the energies involved in the various parts of the system, and to compare these with the incident flow of energy available in the wind. The idea behind this is that if any particular type of motion (referred to loosely as a 'mode') involves a large amount of energy (either kinetic or potential) then that mode will be relatively persistent, and important in the kite's overall behaviour. This analysis is simply another way of looking at the system, helping to identify the important components.

The system is specified by the kite mass (m), area (S), speed relative to the tether (V_k) and reaction coefficient (C_R), the wind speed (W) and density ρ), and the line length (l), diameter (d), inclination (θ), tension (T), mass per unit length (s) and elasticity (k). The energies of the various main components are then :

$$
\begin{aligned}
KE_{kite} &= /frac12mV_k^2 && (2.6)\\
KE_{line} &= /frac12slV_k^2/3 && (2.7)\\
PE_{line} &= /frac12kT^2 && (2.8)\\
T &= /frac12\rho W^2 SC_R \text{ approximate tension} && (2.9)
\end{aligned}
$$

The incident wind energy per unit time on the kite and line are

$$
\begin{aligned}
I_{kite} &= /frac12\rho SW^3 && (2.10)\\
I_{line} &= /frac12\rho ld\sin\theta W^3 && (2.11)
\end{aligned}
$$

Table 7 shows all these energies evaluated for eight different cases, chosen to span the range of typical kite systems. The kite speed has been set equal to W/4 and the inclination to about 53° ($\sin^{-1}$ (0.8)) as typical values.

The most striking points from the table are a) the small values of energy stored in any component relative to the wind energy incident on the kite per second, and b) of the modes available to the kite, the large amount of energy stored in the line at high tensions.

The ratio between the incident power and the energy associated with any particular mode gives an estimate of a time constant for that mode. Two time constants have been calculated in each case, one for the kite alone, and the second for the whole system. These show that the kite's own response is very fast as it is for a kite flown on a short line. However, with long lines the system's response time is much longer. This indicates that the line may be a very important part of the system, especially in situations where it stores large amounts of energy, due to some combination of high tension, low elasticity and long length. Since the line's potential energy is proportional to tension squared, and tension itself increases rapidly with windspeed, in strong winds the line's potential energy is easily the most important component.

This analysis points to the importance of the kiteline in the behaviour of the kite system, and also supports the response analysis of the previous section by suggesting that kites themselves have short response time constants.

2.4.3 Line length influence on angle measurements

A kite moving at a given speed registers a smaller angular velocity on longer lines. Therefore, limiting kite velocities to a finite value implies some sort of

filtering on the angle signals recorded. A simple model of this effect uses the assumption that the kite velocity is proportional to the kite's "error angle", where the error angle is the difference in angle between the kite's current position and its equilibrium position. In a normal turbulent wind, the equilibrium angle changes continuously with the wind direction, so the kite is always moving to adapt to the new wind direction. The assumption of strict proportionality is unlikely to be satisfied in practice, but it is valid to take the velocity rather than the acceleration as proportional to the error since the kite's response is so fast that most of its motion is spent with the velocity opposed by damping forces.

The equation describing this behaviour involves the kite angle (θ_k), wind or equilibrium angle (θ_w), line length (l) and kite velocity per unit error angle (V_0) :

$$\frac{d\theta_k}{dt} = \frac{-V_0}{l}(\theta_k - \theta_w) \tag{2.12}$$

At frequency n, the system response is given by

$$\begin{aligned} \theta_{k0} &= \frac{\theta_{w0}}{1 + int} \\ t &= \frac{2\pi l}{V_0} \end{aligned} \tag{2.13}$$

$t = 2\pi l/V_0$ is the time constant of the motion. Changes over times much greater than this are measured faithfully, while changes faster than this are attenuated :

$$\left|\frac{\theta_{k0}}{\theta_{w0}}\right|^2 = \frac{1}{1 + (nt)^2} \tag{2.14}$$

Inserting typical values of 1 = 30 m and V =10 ms^{-1} gives a time constant of about 20 s. On long lines, this attenuation will be important for all but the slowest changes in angle. Figure 13a shows the transfer function (2.14) for frequencies close to the time constant.

2.4.4 Kite azimuth dynamics and stability

Many kites on short lines exhibit a sort of pendulum motion in azimuth about the mean wind direction. This can be modelled with a simple pendulum analogy by replacing the weight of a normal pendulum with the drag acting on the kite. The model is made more complete by adding a viscous damping term given by the constant a, and allowing for a general forcing function ($D_0\psi$) which represents the

fluctuating wind direction. The kite's acceleration is included here (although not in 2.4.3) since the observed pendulum motion indicates that it is significant. In practice the pendulum acceleration is often smaller than that due to air turbulence and thus this model is only a first approximation to a real kite's motion. If the forcing function is the wind direction then $D_0\psi = D\phi_w$. Azimuth (ϕ) is given by a solution of :

$$ml\frac{d^2\phi}{dt^2} + a(mlD)^{1/2}\frac{d\phi}{dt} + D\phi = D_0\psi \tag{2.15}$$

Assuming a periodic solution at angular frequency w gives the response function

$$\frac{\phi}{\psi} = \frac{D_0/D}{1 - w^2ml/D + iwa(ml/D)^{1/2}} \tag{2.16}$$

The natural frequency (n_0) and period (t_0) are

$$\begin{aligned} n_0 &= \frac{1}{2\pi}(D/ml)^{1/2} \\ &= \frac{W}{2\pi}(C_D/2\mu lL)^{1/2} \qquad (2.17) \\ t_0 &= \frac{2\pi}{W}(2\mu lL/C_D)^{1/2} \qquad (2.18) \end{aligned}$$

The period is thus a function of windspeed (W), solidity (μ), line length (l), kite size (L) and drag coefficient (C_D). Inserting typical values (W = 7 ms^{-1} , μ = O.2, l = 30 m, L = 1 m, $C_D = 0.6$) gives a period of 4 s. In practice, the damping tends to slow the motion down, and the period is most often about twice the value estimated. Figure 13b shows the transfer function (2.19) close to the natural frequency, for several values of the damping coefficient.

$$\left|\frac{\phi}{\psi}^2\right| = \frac{(D_0/D)^2}{(1 - n^2/n_0^2)^2 + (an/n_0)^2} \tag{2.19}$$

Experiments show that large kites on short lines show this pendulum motion most strongly. Small (light ?) kites and long lines are therefore more effectively damped. Tails also increase the damping and thus improve the kite's steadiness in azimuth.

As well as describing the periodic azimuth movement, this model also suggests a basis for the observation that kites with high L/D tend to be unstable (see Bryant, Brown and Sweeting, 1940, and Schaefer and Allsopp, 1980). In this model it is the

drag which is responsible for keeping the kite steady in azimuth. However, as the kite moves away from the downwind direction, the lift may become tilted outwards, and tend to oppose the drag's restoring force. If its magnitude is much greater than the drag it will reduce, cancel, or even reverse this restoring force. Thus a kite with high L/D may tend to be unstable.

This explanation of lateral stability assumes that the lift remains more or less vertical, and so does not apply to large excursions from the mean downwind direction.

2.5 Longitudinal Kite Model

This section presents a static longitudinal model of the kite and its bridle. The model is used to investigate the relationship between the kite design, its bridle, the wind velocity and the line tension, and so models the performance of a kite anemometer.

The model is more specific than those of section 2.4 to allow more detailed study of kite performance. To keep it reasonably simple, the model is restricted to two dimensions (longitudinal motions only), is quasi-static, and ignores the effects of a finite line length (assumes constant line inclination). The characteristics of the model provide a useful comparison with the experiment results obtained later.

2.5.1 Model description

Figure 14 shows the kite model used. The information included is :

kite	coefficients of lift, drag, and centre of pressure (C_L C_D C_P)
	mass (m), lifting area (S)
	centre of gravity position (a_g b_g)
	angle of incidence (α) and chord inclination (γ)
bridle	towing point position (a_k b_k)
	or slope and intercept in chord axes
wind	speed (W), inclination (β) and density (ρ)
tension	magnitude (T) and inclination (θ)

Lengths are given in units of the kite chord, in chord axes Oab. Oa is the distance along the chord from the leading edge, Ob the distance below the chord.

For equilibrium the net force and the net moment about any point must be zero. This gives the three equations on which the model is based. Appendix B gives details of the method used to solve the model.

There are four sets of parameters -the kite, bridle, wind, and tension -any one of which may be derived in principle from the other three. Once the kite, its bridle and the wind are specified, the line tension and inclination must both take on definite

values. This is in effect what happens whenever a kite is flown. The inverse problem is to infer the wind from a knowledge of the kite, its bridle and the tension, and is essentially the function of an anemometer. This is of particular interest here.

These equations have been coded into a computer program which is used to study the model. The program is based around the four sets of parameters, and allows either the bridle, the wind or the tension to be derived from the other three. The kite model used in this implementation is a flat aerofoil of infinite aspect ratio. The coefficients of lift and drag are expressed in a simple functional form (Hoerner, 1965, page *2-6,* and 1975, page 21-1) and are illustrated in figure 15, along with the assumed centre of pressure coefficient. Compared with real kites, the flat plate has comparatively low drag, a high maximum L/D ratio, and a high maximum drag coefficient. These differences are because the model represents a flat plate of infinite aspect ratio and not a kite of finite aspect ratio, and thus the results should by treated carefully. Wind tunnel results for a Cody kite have also been used in the model, which shows encouraging agreement with the experiment results of this research.

2.5.2 Qualitative features of the model

Several features of kite design become apparent from a qualitative consideration of the model.

For static equilibrium, the tension vector must balance the resultant of the aerodynamic force on the kite and its weight. Figure 16 shows this for two different incidences. The actual forces are translated to act through a common point on the chord (K) and couples G_a and G_w introduced to maintain the original

moment balance. For equilibrium, these two couples must be equal and opposite, thus defining K. The kiteline must lie along the line of the resultant through K. From this static point of view, it is sufficient for the bridle point to lie anywhere along this resultant, although in practice some of these positions, generally those above the chord, prove to be unstable. If the reaction (R) changes negligibly with incidence and the line inclination is constant, then a slight increase in incidence moves the intersection of the kiteline with the chord (K') forward for bridle points below the chord, and backwards for bridle points above. Thus for points below the chord, a restoring couple is generated and the kite is stable, while for points above the chord the situation is unstable. In practice the resultant does change with incidence and a more complete study would take this into account. Unless the bridle point is very close to the chord, or the kite is especially heavy, these conclusions do not change.

The idea of stability has been used in the paragraph above, and should be clarified. "Stable" applied to a mechanical system means that the system tends to return to its equilibrium state when slightly disturbed from that state. The kite incidence is used here to indicate the kite's state, since given the kite, bridle and wind, the system is completely determined by the kite incidence. Any change in state is

reflected in a corresponding change in incidence. The kite is stable then if a small change in incidence generates a couple tending to oppose that change; expressed mathematically the condition for stability is

$$\frac{\partial G}{\partial \alpha} < 0$$

In general, as the kite returns to its equilibrium position it changes its pitch and inclination. This model ignores any effects of movement, although in practice the couple due to rate of change of pitch and the change in inclination may be important. This is especially true for large disturbances, which generate greater rates of change of incidence, and short lines, which give a strong linkage between the kite's tangential movement and the line inclination.

The distance from the intersection (K) of the kite line and chord to the kite centre of pressure (C) depends on the relative magnitudes of the weight and aerodynamic force. As the aerodynamic force increases, K moves closer to C

until in the limit as the weight becomes negligible, the two points coincide. The ratio of the aerodynamic force and the weight gives a non-dimensional parameter which characterises the kite solution, defining a non-dimensional kite weight (w), or equivalently a non-dimensional windspeed (u). These are given by

w = mg / qS where q is the dynamic pressure

$$u = \frac{W}{(2mg/\rho S)^{1/2}} = w^{1/2}$$

2.5.3 Kite bridling

The bridle is an important part of the kite system since it controls the kite attitude to the wind. Because of this model's limitations, the discussion is restricted to longitudinal bridling.

For equilibrium, the bridle point must lie somewhere along the resultant of the aerodynamic reaction and kite weight. In general, positions too far above the chord are unstable, and the bridle point should usually be well below the chord. However, if the bridle point (K) is below the kite's centre of gravity (G) an unstable moment is produced, which increases as the bridle point is lowered.

At low windspeeds, when the kite weight is more important, the most stable position for K may be close to the chord. To reduce unstable moments, the centre of gravity should be as low as possible. Another factor favouring stability is a centre of pressure which moves rearwards with increasing incidence.

Fortunately, this is characteristic of most aerofoils, with the centre of pressure initially well forward and then moving back as incidence increases.

Since the bridle point must lie on the line of the resultant, this line defines a bridle locus. As the incidence varies over a range of values, the bridle loci describe an envelope, within which the bridle point must lie if the kite is to achieve an angle of incidence within the chosen range. The form of the envelope changes with windspeed, as is illustrated in figure 17a, and tends to a limiting value as the weight becomes negligible. Figure 17a shows how the envelope becomes more steeply inclined and tightly defined at high windspeeds (w tends to 0). If a kite is to fly over a wide range of wind conditions with its incidence within certain limits, its bridle point must lie within the overlap between the two cases. As the windspeed increases the incidence tends to decrease.

Figure 17b shows the bridle loci required to achieve a given line inclination for the two wind conditions used in figure 17a. As expected from figure 17a, the loci are more widely spaced at the lower windspeed (w = 0.19). The tight bunching at the higher windspeed (w = 0) is probably a feature of the flat plate aerofoil which is not characteristic of general kite aerofoils. Note how a centre of pressure moving back smoothly with increasing incidence, gives improved stability and also leads to a less critical bridle adjustment, and therefore more controllable kite performance.

2.5.4 Incidence change with windspeed

Figures 18a and b show the variation of kite incidence and line inclination, and reaction coefficient with windspeed (u) for the flat plate kite model. The centre of gravity (G) and bridle point (K) are as shown (in chord axes Oab). All three curves tend to limiting values as u increases (kite weight becomes negligible). To understand a real kite, the dimensionless windspeed must be related to absolute units using the unit windspeed value for that kite, eg. as given in table 2. The model suggests that kites do not approach their limiting performance until u = 5–6. Since typical unit windspeeds are 1.4–3.0 m s^{-1} , real kites spend most of their time at flying speeds where incidence, and thus line inclination and reaction coefficient, varies strongly with windspeed. These effects should be observable in the experiments to be performed.

Figure 19 plots the relationship between incidence and inclination at constant windspeed for the same kite. In effect, a range of bridle points is used to achieve the different incidences. The two curves correspond to the two cases of figure 17, ie. dimensionless kite weights (w) of 0.19 (u=2.3) and 0 (u=infinite). Apart from the peaks at low angles of incidence, the relationship follows a straight line quite clearly. The relationship is of the form

incidence + inclination = constant

For the weightless kite the constant is 90° and for the heavy kite it is 85°. The good

linearity is because the flat plate's lift to drag ratio is very close to tan(incidence) for angles greater than about 5°. Such a close fit is not expected for more general kite aerofoils.

2.5.5 Model of a kite anemometer

For this thesis one of the most useful functions of the model is to study kite anemometers. The equations are used to calculate the wind velocity from a knowledge of the kite, its bridle, and the tension and inclination of the line. Figure 20 shows the principle of a kite anemometer in that values of line tension and inclination uniquely determine wind speed and inclination. The closeness of the contours shows how sensitive the method is to errors in any of the inputs.

Figure 20 is plotted in dimensionless units of windspeed (u) and tension. Tension is non-dimensionalised by dividing by the kite weight. Several features of the figure are significant. First, for u>2 it is possible to obtain a good estimate of the wind speed and inclination from a knowledge of the line tension and inclination, with a known kite and bridle. For u>5..6, the contours of constant u and wind inclination are practically orthogonal, and almost parallel to the line tension and inclination axes. Thus tension alone gives a good estimate of windspeed, and line inclination gives wind inclination. This independence of the two coordinates may be very useful in practice, although many kites may not often fly in winds greater than u=5. Reliable estimates of windspeed only may be obtained from the tension only down to almost the lowest flyable windspeeds, since the contours of constant u remain very closely parallel to the line inclination axis over practically the whole windspeed range.

This application of the longitudinal model suggests several points relevant to practical kite anemometers :

a) the kite should be well defined -the bridle point, aerofoil characteristics and centre of gravity should be reliable and not vary between experiments,

b) a kite with a low windspeed unit will be able to operate successfully down to lower absolute windspeeds and will also reach the operating range where the tension and inclination become independent more quickly,

c) tension alone should be a good indicator of windspeed over practically the whole of the kite's flight envelope,

d) a suitable kite will be able to measure both wind inclination and speed easily (averaged over appropriate timescales so that the results of this quasi-static model are relevant).

Chapter 3

THE KITELINE

This section gives special attention to the kiteline since it is such an important part of the whole kite system. Two reasons for this have already been indicated. In section 2.4.2 it was shown that most of the energy of the kite system is stored as potential energy of the kiteline for most conditions. The kiteline is thus expected to dominate the system's dynamics. Secondly, it is the kiteline which communicates the tension from the kite where it is produced to the ground where it is measured. For this research it is thus very important to understand the mechanisms involved, and to be able to assess any influence the line might have on the information available at the tether.

The first of these aspects is related closely to kite dynamics. These are obviously important for a kite flying in turbulent wind, but this study is mostly experimental and the theory is not taken any further. Useful references which do examine the theory of kite dynamics in more detail include DeLaurier (1972a,b). It is interesting to note that this more recent treatment approaches the problem as a line problem, with the kite simply determining the boundary conditions at the upper end of the line. Previous work, for example Bryant, Brown and Sweeting (1942) and Reid (1967), has adapted standard aircraft stability theory, allowing for the line through "cable derivatives", and assuming the line to be always in equilibrium. This quasi-static approach is valid for short lines under moderate and high tension, and simpler in that the kite is dealt with explicitly, but theories taking the line as the primary element are more generally valid and represent the physics more faithfully. So far, no full experimental study of kite dynamics has been made.

This section concentrates on the influence of the kiteline on the information available at the tether.

3.1 Forces acting on the kiteline

There are three forces which together determine the behaviour of the kiteline -its tension, the aerodynamic force, and the line's own weight. Figure 21 shows these forces : the aerodynamic force has been analysed into a friction component parallel to the line and a reaction component perpendicular to it.

Normally the tension is the largest force. It results from the restraining action of the line upon the kite, and its magnitude is thus typically close to that of the reaction force on the kite, and always acts tangentially along the line.

The aerodynamic force is usually the second most important force on the line. It is conveniently analysed into a component tangential to the line (a friction component) and one perpendicular to it (the normal component). For analysis, the line is usually treated as a series of short links, each one of which is straight, so that the aerodynamic force components act strictly parallel and perpendicular to these links. Values of these two components are given in Hoerner (1965, p 3-11). Typical Reynolds numbers for kitelines are in the range 30 to 10 , giving a reaction coefficient (based on diameter and line length) of 1.1 over most of the range, increasing to about 2.0 at the lowest Reynolds numbers (Hoerner, 1965, p 3-9). The normal reaction depends on the airflow perpendicular to the line, and acts in the plane defined by the line element and the wind direction. The tangential force along the line is much smaller than the normal reaction : the friction coefficient is about 0.02 compared to the normal reaction coefficient of 1.1. The friction force depends on the component of the airflow tangential to the line. Full analytical expressions for these two components are given in section 3.2.1.

The third force on the line is its own weight. This always acts vertically. The true density of the line may be corrected to allow for any bouyancy due to the surrounding fluid by using an apparent mass per unit length. If this is done, it should be noted that the inertial force due to acceleration still depends on the true mass.

In general, both the tension and the aerodynamic force vary continuously, so that the line is not static. However, on reasonably short lines, the line adjusts to a new equilibrium fast enough for it to be treated quasi-statically. This is discussed more fully below in the sections on line dynamics.

3.2 Static form of the line

3.2.1 Equations describing the static line profile

Appendix C gives a full derivation of the equations describing a quasi-static kiteline. For a complete dynamic analysis, these equations need extra terms describing dynamic aerodynamic factors, such as any added mass terms and forces due to flow patterns induced by the line's motion. With these qualifications in mind, the

quasi-static equation is,

$$m\ddot{\mathbf{r}} = \frac{d\mathbf{T}}{ds} + \mathbf{w} + qdC_f \cos^2\psi\mathbf{n} + qdC_r \sin^2 \mathbf{e} \tag{3.1}$$

where

C_f	=	friction coefficient
C_r	=	reaction coefficient
d	=	line diameter
$\mathbf{e}$	=	unit vector parallel to line element in plane defined by wind direction and the line element itself
m	=	mass per unit length
$\mathbf{n}$	=	unit vector along the line element
q	=	dynamic pressure
$\mathbf{r}$	=	position of the line element
s	=	distance along the line
$\mathbf{T}$	=	line tension vector
$\mathbf{w}$	=	line weight per unit length
ψ	=	angle between the wind and line element

Using inclination and azimuth angles, and cartesian axes with origin at the tether, Ox downwind and Oz vertical upwards, the vectors may be written,

$$\begin{aligned}
\mathbf{T} &= T\mathbf{n} \\
\mathbf{n} &= (\cos\theta\cos\phi, \cos\theta\sin\phi, \sin\theta) \\
\mathbf{w} &= (0, 0, -mg) \\
\mathbf{e} &= (\sin\psi, -\cot\psi\cos\theta\sin\phi, -\cot\psi\sin\phi)
\end{aligned}$$

with $\psi = \cos^{-1}(\cos\theta\cos\phi)$ and ignoring any bouyancy forces.

Equation 3.1, or an equation related to it, has been solved in various cases, using different degrees of simplification. Three broad classes of solution are available :

a) Ignoring all forces except tension and line weight. This allows a complete analytical solution to be obtained, although the omission of aerodynamic forces restricts the usefulness of these solutions significantly. See appendix C or Irvine (1981) for examples.

b) Allowing for line weight and a simplified aerodynamic force. The wind is restricted to a constant profile and the friction component may be ignored. An analytical solution may again be obtained, but its implementation is not as straightforward as a), since tables or families of non-dimensional curves are used. Examples of this technique are given by Glauert (1934), Neumark (1963) and Varma and Goela (1982).

c) A complete numerical solution. With the current availability of computers, a program to integrate equation 3.1 numerically is the most practical solution, and with suitable coding of the equations is able to accommodate all real cases. This is the technique used here, and its implementation is described in appendix C.

3.2.2 General Features of the Static Solution

The tension along the line changes in magnitude and direction due to the line weight and windage. The weight and friction cause a slight change in tension magnitude, and the weight and normal reaction give a curvature to the line. This is seen most clearly in the simple downwind case (azimuth = 0), when equation 3.1 simplifies to

$$\frac{dt}{ds} = -qdC_f f \cos^2\theta + mg\sin\theta \tag{3.2}$$

$$T\frac{d\theta}{ds} = qdC_r r \sin^2\theta + mg\cos\theta \tag{3.3}$$

The four terms on the right are the force components responsible for the tension variation (equation 3.2) and line curvature (equation 3.3). The first two terms give a small correction to the tension. Unless very long lines are used, this is unlikely to be a significant fraction of the line tension. Since $ds\sin\theta = dz$, the term involving line weight gives a change in tension $dT = mg.dz$, ie. the tension change due to line weight is the height interval multiplied by the line weight per unit length. For many lines this turns out to be the main change in tension, and friction can be ignored.

Of the second two terms, the weight is comparable with the weight component along the line, but the reaction is generally much larger than the friction, since $C_r >> C_f$. The curvature is the normal force divided by the tension, and has units of angle per unit distance. Inverting this to give a radius of curvature (distance per unit angle) gives a length scale for the line. In practice, lines much longer than anything from 5 to 50 % of this length scale will not be used -the acceptable limit depending on the task intended for the kite.

In practice, a kiteline is chosen for its breaking strength and material, and the diameter and mass per unit length are then determined by these choices. Thus the four factors determining the line forces may be taken as the wind speed and the line angle, and the line strength and material. These are now examined in turn. Table 3.1 gives values of the line forces calculated for two different line strengths and two different windspeeds. The forces are expressed in two ways : in absolute units and also as fractions of the line strength.

The following paragraphs discuss each of the four factors in turn.

line type	5 kgf nylon braid		45 kgf nylon braid	
windspeed / m s^{-1}	3	15	3	15
1. friction	0.021, 0.43	0.53, 10.8	0.057, 0.13	1.4, 1.6
2. weight, parallel	1.13 ,23	1.13, 23	9.8 ,22.1	9.8, 22.1
3. reaction	1.66 ,33.8	41.5 ,846	4.4 ,10	111 ,251
4. weight, normal	0.95 ,19.4	0.95, 19.4	8.2 ,18.6	8.2, 18.6

Table 3.1: Kiteline forces example. Force per unit length in units of (m N m^{-1}, 10^{-6} m^{-1}) for each pair (the second value of each pair is Force / bs per unit length). Inclination = 50, g = 9.81 m s^{-2}, azimuth = 0, ρ_{air} = 1.27 kg m^{-3}.

windspeed

The aerodynamic forces increase as windspeed squared. Table 3.1 shows that at low windspeeds the reaction is of the same order as the line weight, while at high windspeeds it dominates the curvature. At very high windspeeds, the friction is as important as the line weight for changes in tension.

line angle

Equations 3.2 and 3.3 show the dependence of the forces on angle for the downwind case. At small inclinations the cosine terms dominate, while at large inclinations the sine terms are most important. In cases where the azimuth is not negligible, the weight and windage may be thought of as contributing two components of curvature : the weight tending to increase the line's inclination to the vertical, and the windage tending to turn the line more oblique to the wind direction. The balance between the two varies along the line -at low inclinations weight is favoured, while for steeper lines the windage dominates, augmented by its greater magnitude in all but light wind conditions. The combined effect gives a similar curvature to the downwind case except that the line profile is now no longer planar but steepens more quickly than would be expected from simply canting the downwind curve over to one side.

breaking strength

For a given line material, the mass is proportional to the breaking strength, while the diameter varies as the square root of the strength (see 2.1.5). Thus line weight as a fraction of breaking strength is constant, but the aerodynamic forces (proportional to diameter) decrease as a fraction of breaking strength as the square root of line strength. So of two lines of the same material, the stronger line has lower curvature at the same fraction of their respective breaking strengths.

material	density	tensile strength	ρ/tx	$tx^{1/2}$	relative weight	diameter
	kg m^{-3}	MPa	μs^2 m^{-2}	μPa$^{-1/2}$		
nylon, braid	1000	330	3.03	55.0	1.00	1.00
polyester, braid	1300	520	2.50	43.9	0.83	0.80
Kevlar, bare	1250	1750	0.714	23.9	0.24	0.43
steel, piano wire	7850	2100	3.74	21.8	1.23	0.40

Table 3.2: Relative kiteline material properties .

material

Table 3.2 gives a general comparison of line materials for the line properties discussed here. The material densities and strengths are those of table 2.1 (in 2.1.5). For a given line strength, density divided by tensile strength gives a factor proportional to the line weight, and the inverse square root of tensile strength is proportional to the line diameter. The final two columns are obtained by dividing each of these factors by the corresponding value for braided nylon to give a rating relative to nylon. Figures 2a and b show related information, giving mass and diameter as a function of breaking strength for various materials.

3.2.3 Examples of Calculated Line Profiles

Figures 22 a..e show kiteline profiles under a variety of conditions. These profiles have been calculated by integrating equation 3.1 numerically. The line length increment used was 10m. A check on accuracy using a 20 m step changed the position of the upper end of a 600 m line by less than 0.04 m and shows the calculations to be sufficiently accurate. Table 8 summarises the cases run to produce figures a..e, and gives the position and inclination of the upper end of the line for each case.

The five sets of profiles illustrate the importance of different variables on the line shape. The reference condition for these comparisons is

line material	Kevlar braid
breaking strength	900 N
tension	10 % bs
wind profile	constant
windspeed at 10 m	7 m s^{-1}
tether conditions	inclination = 45°
	azimuth = 0
	x = z = 0
	line length = 600 m

Each of the first five parameters is examined in turn to produce figures 22 a..e. The base position and initial line inclination are constant throughout, and the profile is

restricted to the downwind vertical plane (Oxz). The profiles least effected by wind are those with the lowest curvature.

Each of these five sets of profiles is discussed in turn.

Windspeed

Three windspeed cases are examined : 0, 7, 15 m s^{-1}. The 0 m s^{-1} case is the line profile due to weight alone. Although the windspeed for the other two curves is in roughly equal increments, the extra curvature at 15 m s^{-1} is quite marked, showing how important windage may be. In practice, tension increases with windspeed almost as fast as windage, so that curvature increases only slowly with windspeed, unlike this example where tension is constant.

Line Material

The general relationships of 2.1.5 (and table 2.1) were used to calculate the properties of lines with a breaking strength of 900 N made from nylon, steel piano wire and Kevlar. These three lines were then compared by extrapolating under identical conditions. Cases 2, 4 and 7 of table 8 were used to make the comparison. Over the 600 m length, the curvatures were 8.0, 12.6 and 20.5 deg for Kevlar, steel and nylon respectively, giving mean radii of curvature of 4300 m, 2730 m and 1680 m. So under these conditions the length scale of a nylon line is only 39 % of that for Kevlar, and steel only 63 %. At higher windspeeds when the windage becomes more important, the percentage for nylon falls, and that for steel rises, since the diameter of a nylon line is much greater than that for Kevlar at a given strength, while piano wire and Kevlar have similar diameters.

Tension / bs

These profiles correspond to tensions of 5 and 10 % of the line's breaking strength. The curvatures are 8.0 and 16.9 deg over the 600 m, ie. very closely in inverse proportion to the tension, as expected. The discrepancy is a second order effect due to the different mean line inclinations.

Breaking Strength

Two nylon lines, with breaking strengths of 900 and 50 N are compared here. The 50 N line is vertical by 330 m, so the extrapolation is terminated at 32O m. The two mean radii of curvature are 1680 and 42O m (900 N and 50 N lines respectively), ie. in a ratio of 4.0. This is close to the expected value of 4.2 (the square root of

the ratio of line strengths), and the discrepancy is again due to second order effects such as the different mean line inclinations.

Wind Profile

The sensitivity of the line shape to the wind profile is demonstrated in figure 22 e (figure 22 f shows the three wind profiles used). Since the line shape is given by an integral of the curvature over the line length, details of the wind profile are not very important over length scales much less than the line's radius of curvature. Thus as suggested by figure 22 e, the most important factor is the mean windspeed over the line length.

3.3 Dynamics of the kiteline

Section 3.2 deals with the static profile of the kiteline. However, tension is generally not constant and it is important to understand how tension fluctuations are communicated by the line from the kite to the tether. The approach here is mainly qualitative, using simple cases to derive the quantitative results required.

Changes in tension are communicated from the kite to the tether by waves on the kiteline. For most of this discussion, the line curvature and wave amplitudes are assumed to be small, so that transverse and longitudinal waves may be treated separately. Transverse waves result from changes in the kite's tangential position, and longitudinal ones from changes in tension / radial position. On "useful" lines (ie. ones with low curvature) the assumption that the modes decouple, is perfectly valid. However, if the line has a large curvature or is subject to large amplitude motions, then the transverse and longitudinal modes couple, ie. a change in tension changes the line curvature, and vice versa. It is assumed here that second order effects due to this cross- coupling may be ignored, and that the main features of line dynamics are covered by an analysis into separate transverse and longitudinal modes.

3.3.1 Wave velocities along the kiteline

Corresponding to the transverse and longitudinal modes there are two different wave velocities, which are functions of line tension (T), elasticity (k) and mass per unit length (m).

$$\text{transverse wave velocity} \quad c_t = (T/m)^{1/2} \tag{3.4}$$

$$\text{longitudinal velocity} \quad c_l = ((k+T)/m)^{1/2} \tag{3.5}$$

Although 3.4 and 3.5 assume small disturbances from the static state, they remain valid for more general lines if T, k and m are taken only to be locally constant. Both k and m may depend on the line tension, and involve the linear strain e.

By definition

$$k = dT/(dl/l) \quad = \quad dT/de$$

If k is constant ($= k_0$) then

$$e \quad = \quad T/k_0 \tag{3.6}$$

However, for nylon lines elasticity is a function of tension, so that

$$\begin{aligned} k &= k_0 + bT \\ \text{or } k/bs &= k/bs + bT/bs \\ &= a + bT/bs \text{ as in Figure 3} \end{aligned}$$

In this case, the strain is given by

$$e \quad = \quad \ln(1 + (b/a).(T/bs))/b \tag{3.7}$$

In the limit b = 0 this reduces to (3.6). The line length and mass as a function of the values for the unstretched line (l_0, m_0) are given by,

$$m \quad = \quad m_0/(1+e) \tag{3.8}$$

$$l \quad = \quad l_0(1+e) \tag{3.9}$$

If the wave velocities are expressed in terms of speeds along the unstretched line, ie. c' = c / (1+e), then

$$c'_t \quad = \quad [T/(m_0(l+e))]^{1/2} \tag{3.10}$$

$$c'_l \quad = \quad [(k+T)/(m_0(l+e))]^{1/2} \tag{3.11}$$

In the important case k = constant, (3.11) reduces to

material	m_0/bs μm^2 s^{-2}	k_0/bs	b/a
nylon, braid	3.0	2.5	4
polyester, braid	2.5	12	0
Kevlar, bare	0.84	25	0
steel, piano wire	3.7	100	0

Table 3.3: Typical kiteline properties determining wave velocities.

$$c_l' = (k_0/m_0)^{1/2}$$

ie. the time taken for longitudinal waves to travel along a given piece of line of constant elasticity is independent of the tension. Since all signals take the same time, there is no distortion for longitudinal waves along such lines.

To calculate typical wave velocities for real materials, the following information is required:

k_0/bs (= a)
b/a
m_0/bs
and T/bs

The first two describe the line elasticity, the third gives the relative mass of the line, and the fourth is the tension. Table 3.3 presents the first three parameters for a range of possible kiteline materials. The information is drawn from figure 3 and tables 3 and 6.

Figure 23 uses the values of table 3.3 and equations 3.7, 3.10 and 3.11 to show the dependence on line tension of a) strain, and b) the wave velocities (transverse and longitudinal), for typical kiteline materials. The wave velocities are expressed in terms of the natural, unstretched, line length.

Figure 23a shows how much more stretchy a nylon line is than, for example, Kevlar. This stretchiness corresponds to a radial motion of the kite due to changing tension, and may be important enough to cause the kite to behave differently on lines of different materials. At T = bs/2, a kite on a nylon line has only about 20 % of the radial restoring force due to line elasticity compared with a Kevlar line. A kite on nylon lines offers less resistance to buffetting along the line direction, and should thus moderate the tension variations.

Figure 23b presents transverse and longitudinal wave velocities as a function of tension for various kiteline materials, expressed in terms of the natural, unstretched, line length. The longitudinal velocities are an order of magnitude higher than the transverse ones. Since Kevlar, steel and polyester have elasticities independent of tension, their longitudinal velocities are constant, whereas nylon's varies strongly.

material	transverse		longitudinal	
T / bs =	0.1	0.4	0.1	0.4
nylon, braid	180	350	1080	1450
polyester, braid	200	400	2210	2210
Kevlar, bare	340	680	5440	5440
steel, piano wire	160	330	5170	5170

Table 3.4: Kiteline wave velocites / m s^{-1} (natural line lengths), for longitudinal and transverse waves, and two values of tension normalised by line breaking strength.

material	line length / m (at T/bs = 0.1)	
	transverse, 0.4 Hz	longitudinal, 1 Hz
nylon	225	540
polyester	252	1107
Kevlar	429	2721
steel, piano wire	204	2585

Table 3.5: Line length for specified natural frequencies at tension = 10% of the line breaking strength, for transverse and longitudinal waves (of 0.4 Hz and 1 Hz respectively).

The transverse velocities vary almost exactly as the square root of tension. Generally, nylon is the slowest, due to its low elasticity, and Kevlar is the fastest since it has a high elasticity and low weight. Table 3.4 gives particular wave velocities to allow a more precise comparison.

3.3.2 Line vibrations

The kiteline may be regarded as a vibrating string for the purposes of calculating a frequency limit for information transmitted along it. If information from the kite is at frequencies well below the fundamental, then the line transmits the information without distortion.

For a line length l and wave speed c, the fundamental frequency is given by $n_0 = c/(2l)$ equivalently, the line length for a fundamental of a given frequency is $l = c/(2n_0)$.

Table 3.5 presents the line lengths at which the fundamental (natural frequency) is equal to the lower limit of the frequencies expected in the light of experiments performed. For transverse waves this is about 0.4 Hz, and for longitudinal waves about 1 Hz.

The 30 m lines used are well within these limits, and so a good frequency response is expected. The only exception is that at very low tensions, the transverse waves may become slow enough for the kite to excite the fundamental mode. If this happens, it will be obvious to an observer and the measurements should be discarded. If much

longer lines are required, Kevlar is the best material since its wave velocities are highest.

3.3.3 Signal attenuation

Real kitelines impose certain limitations on signals transmitted along the kiteline. These limitations fall into two categories -attenuation and distortion. In both cases the transverse and longitudinal signals may be considered separately.

The mechanism of signal attenuation is for energy originally in the signal pattern to be dissipated into other less ordered states. For example, if friction is present energy is dissipated as heat.

The line length over which signal attenuation becomes significant can be estimated using simple models.

Longitudinal waves

Waves may lose energy to friction, either internally in the line -as the fibres move over each other, or externally to the atmosphere -as line elements move through the air. Under reasonable tension, the fibres are firmly located and most elasticity is due to the bulk material property : friction losses here are expected to be small. Viscous losses to the air may be estimated using the expression from section 3.2 for the friction force along the line. Assuming a windspeed W along the line, and a line element velocity of $v = u\cos(2\pi nt)$, the mean rate of energy loss per unit length per unit time is

$$\begin{aligned} p &= \frac{2}{3}\rho d C_f u^3 (1 + \frac{3}{2}\left(\frac{W}{u}\right)^2) \\ p &\simeq \rho d C_f u W^2 \text{ for u}\ll\text{W} \end{aligned} \tag{3.12}$$

Most single line kites move at speeds of 20 to 30 % of the mean wind velocity, so that the second version of 3.12 is a useful approximation. A pulse of duration $1/n$ travelling along a line of length l loses energy E over the length of the line, where

$$E = p.l/n \tag{3.13}$$

Since u normally varies linearly over the length of the line (from 0 at the tether to u_0 at the kite), the mean cube velocity is $u_0^3/4$.

Substituting typical values of:

d $= 1$ mm
ρ $= 1.27$ kg m^3
u $= 1$ m s^{-1}
W $= 5$ m s^{-1}
C_f $= 0.02$

gives p = 6.5x10^4 J m^{-1} s^{-1}

A 1 mm line has a breaking strength of at least 300 N (figure 2a), and so its tension may be typically 30 N. A disturbance of u = 1 m s^{-1} at, say, 0.5 Hz has an amplitude of $1/\pi$ m, and thus an energy (force x distance) of about 10 J. Equation 3.13 gives the length over which this energy will be lost as l = En/p, which for the signal pulse considered is 7.7 km. Dissipation of longitudinal waves is not a significant problem over normal line lengths.

Transverse waves

For transverse waves, air resistance is the dominant dissipation mechanism again since internal line friction is negligible above very low tensions. At very low tensions though, there may be enough movement between fibres to lose significant amounts of energy. The energy lost to the air by motion of the line in the direction of the wind is described by an equation similar to 3.12, except that the appropriate coefficient is the normal reaction coefficient, ie. 1.1 rather than 0.02, and the relevant wind velocity is the component normal to the line element rather than tangential to it. The energies involved in the transverse modes are lower than those of the longitudinal modes, since they are generated by moving the towing point perpendicular to the tension vector. The transverse mode energy corresponds to part of the line's kinetic energy rather than its potential energy, and the kinetic energy is generally much lower than the potential energy (table 7). This, combined with the higher rate of energy loss, means that the length scale over which dissipation is significant for transverse modes may be as little as 100 m, and in strong winds and at low tensions may be down to less than 30 m. This is in fact observed at low tensions, even on such short lines.

3.3.4 Signal distortion

Three separate mechanisms of signal distortion may be identified. The first is due to the action of unsteady wind forces on the line between the kite and the tether. This adds noise to the signal received at the tether, and can only be avoided by ensuring the mean tension in the line is significantly greater than any unsteady wind forces on the line that may be generated. On short lines this is not an important problem.

A second possible cause of signal distortion is the wave velocity dependence on tension. As tension varies, different parts of the signal may travel at different speeds and lose their original relationship. In mathematical terms the behaviour is non-linear; and also non-dispersive since it is independent of frequency. The order of

signals transmitted never changes, although their spacing in time generally does.

Over short lines there is little time for this mechanism to take effect, but on long lines it may distort signals significantly, perhaps even generating shock waves. It has already been shown that lines with constant elasticity do not distort longitudinal signals, since the time taken for signals to travel from one end to the other of a given length of line is independent of the tension (equation 3.11 with k = constant). However, lines for which elasticity does vary with tension will distort signals along them.

The distortion may be visualised quite easily if the original signal as a variation of tension is instead considered as a pattern of wave velocity. Equation 3.11 specifies the form of the transformation required. This velocity signal may then be described in a coordinate system moving at the basic wave velocity (c_0): the signal amplitude (v) is the difference between the actual velocity and the basic velocity ($c - c_0$), and the abscissa is given by $X = x - c_0 t$. This transformation is described in Lighthill (1978, p 150..151). The distribution v(X) undergoes unit rate of shear, ie.

$$\frac{D}{Dt}\left(\frac{dv}{dx}\right)^{-1} = 1 \tag{3.14}$$

Thus any negative slope becomes vertical after a time $t_0 = -(dv/dX)$ and a shock wave has formed. In this time the wave has travelled distance $s_0 = c.t_0$. If the line length is less than s_0 then no shock wave forms : line lengths should be kept below this limit. Figure 24 illustrates the principle of shock wave formation for a profile v(X).

Since the relationship between c and T is known, the time variation of T at the origin may be related to the spatial variation of c.

$$\left.\frac{dv}{dx}\right|_0 = \left.\frac{dT}{ds}\right|_0 / \frac{dT}{dc} \tag{3.15}$$

$$\frac{dT}{ds} = -1/\left(c\left.\frac{dT}{dt}\right|_0\right) \tag{3.16}$$

$$s_0 = c^2/\left(\left.\frac{dT}{dt}\right|_0 \frac{dc}{dT}\right) \tag{3.17}$$

For lines such as nylon

$$
\begin{aligned}
c &= [(k+T)/(m_0(1+e))]^{1/2} \\
k &= a.bs + b.T \\
\frac{dc}{dT} &= \frac{(1+e)^3}{[(1+e)(1+b)-(1+T/k)]} 2m_0(1+e)^2 c \qquad (3.18) \\
s_0 &= \frac{2m_0c^3}{bs}.\frac{(1+e)^3}{[(1+e)(1+b)-(1+T/k)]\ \frac{d(T/bs)}{dt}\Big|_0} \qquad (3.19)
\end{aligned}
$$

For nylon at 0.1 bs this gives $s_0 = 780 \left(\frac{d(T/bs)}{dt} / \Big|_0 \right)^{-1}$ m

A change of 0.1 bs in 1 second leads to a shock wave after about 7.8 km of line. This is a comparatively fast change in tension, so that on lines even as long as 1 km, no significant longitudinal signal distortion is expected.

For transverse waves the situation is slightly more complicated since the signals travel at the transverse wave velocity, while the tension pattern, which determines the wave velocity, travels at the longitudinal wave velocity. The tension signals tend to sweep through the transverse patterns.

Consider two points on a signal waveform : point 1 takes time t_1 to travel down the line and point 2 takes time t_2. The signal is distorted if $t_1 \neq t_2$. If the difference is a significant fraction of the original time separation between points 1 and 2, then the distortion of the signal is important. For a given separation between 1 and 2, $t_1 - t_2$ depends on the line length (l) and the two mean transverse wave velocities experienced (c_1 and c_2),

i.e. $t_1 - t_2 = l(1/c_1 - 1/c_2)$

For short lines, this difference is very small, even if c_1 and c_2 differ significantly, so that only the highest frequencies of the order of $1/(t_1 - t_2)$, are affected. On long lines (which in this situation are ones over which the tension varies significantly at any one time), the mean wave velocities tend to average out fluctuations in local wave velocity, so that $t_1 - t_2$ does not increase strictly in proportion to line length. The time difference increases almost as fast as l, so the upper frequency limit decreases almost as fast as 1/l.

Eg. a nylon line of length 100 m (for a conservative order of magnitude estimate).

point 1 : T = 0.10 bs, c = 180 m s^{-1}: $t_1 = 0.555$ s
point 2 : T = 0.05 bs, c = 127 m s^{-1}: $t_2 = 0.786$ s

then $t_2 - t_1 = 0.23$ s, and frequency cut-off = 4 Hz

From measurements on 30 m lines, there is little significant kite motion at frequencies above about 0.4 Hz. The calculated cut-off frequency does not fall to 0.4 Hz until the line length is about 1000 m. Practical kitelines are well within this limit.

A third type of distortion arises if the line is significantly curved, since in this case a change in tension couples with the line deflection. This is illustrated trivially by a line under very low tension which is suddenly jerked : the line which was originally sagging under its own weight in now pulled straight. This type of distortion through cross-coupling is avoided by disregarding measurements at extremely low but highly variable tensions. In practice such occasions are obvious from watching the behaviour of the kiteline.

3.4 Summary and application of results

This discussion is primarily to understand the influence of the kiteline on the transmission of information from the kite to the tether, since in the work here, measurements are made at the tether assuming that they are usefully related to the kite's performance.

In the light of this work, it is possible to estimate limits within which the kiteline's effect on signals may be either ignored or corrected for. Generally, using a form of equation 3.1, the quasi-static effects may be calculated, and the tether measurements corrected accordingly. Similarly, the discussion of line dynamics allows estimates to be made of limits within which signal distortion is negligible. For both of these discussions, the properties of different materials have been considered, so that their relative performance may be estimated.

The experiments performed here have mostly used short lines (30 m) at tensions in the range 5..100 N. Nylon lines have been used for most experiments, and Kevlar for the others. The line used in any experiment was chosen to match the anticipated conditions, so that the average tension would be around 10 % of the line's breaking strength. Under these conditions, the line curvature is limited to at most a few degrees over its whole length, and the change in tension is less than 1 % of the mean tension. Longitudinal signals take no more than 0.03 s to travel down from the kite. Transverse signals have speeds of over 100 m s^{-1} for tensions greater than 3 % of the line strength, so that they take no more than typically 0.3 s to travel from kite to tether. Results and observations show that there is little significant transverse motion of the kite with periods less than a few seconds, and that most tension variance is over periods greater than about 1 s.

If the same information is required using lines several hundred metres long, then some care needs to be taken in selecting the kiteline. To keep the curvature low, a line with low weight and small diameter is required. Since in all but the lightest winds, line windage is more important than line weight, it is best to choose a line with a small diameter even at the expense of extra weight. Equation 3.1, or a simplified form such as equation 3.3, allows the line profile or curvature to estimated. Figures 25a to f show line curvatures expected with the lines used in the experiments here. The plots are normalised for tension equal to breaking strain. Curvature is inversely proportional to tension, so at say T = 0.1 bs it is 10 times the value for that condition

of line inclination and windspeed from the figure. These figures are useful for making quick estimates of line curvature.

Transverse waves may be used as an indicator of the line performance. Transverse wave speeds are generally an order of magnitude lower than longitudinal speeds, and are the first to be distorted by the line's limitations. If the line is fairly straight and does not appear to be imposing its own motion on the signals from the kite it is safe to assume that the tether measurements are reliable. This is useful in practice since it is relatively easy to see how the line is behaving, and to use this to ignore results taken when tether measurements do not represent kite performance well.

Chapter 4

EXPERIMENT EQUIPMENT

This section and the next describe all the equipment used for the experiments and the computer programs for handling the data. The hardware is dealt with here, and the software in section 5.

The complete experiment arrangement is shown in figure 26. The system is designed with two purposes in mind :

1. to study kite flight in the natural wind. For this an instrumented tether along with accurate measurements of the wind are required.

2. as an research tool to measure wind velocity profiles. This also needs an instrumented tether : the kite, now calibrated, is used as the wind probe.

In principle, some of the kites may carry small payloads to measure extra information. The system has been designed for this expansion, but it has not been used in this research.

Each component of the experiment system is now described in turn.

4.1 Kite Tether

The Kite Tether is designed to measure the tension and direction of the kiteline (at the ground) as well as tethering the kite. Since kite dynamics are being studied, the tether specification includes its dynamic response as well as the required ranges for tension and angles of inclination and azimuth. The tether is also designed to be an easily made practical piece of field equipment. Plate 13 is a general view of the Tether including its base and a reference load / direction used for calibration. Plate 14 is a closer view of the Tether Head Unit.

The digital resolution used is 8 bit, ie. 1 part in 256. This sets limits on the practical resolution available in angle and tension, and sources of error smaller than this are not important.

4.1.1 Mechanical design

Figure 27a shows the line tension expected as a function of kite area (S) and windspeed (W), assuming a reaction coefficient of 1.0. The highest tension expected is about 600 N (S = 4m , W = 15 m s^{-1}). The tether was designed to operate safely at loads up to 1000 N and uses a safety factor of 6, appropriate to mild unidirectional shock loading. Figure 27b shows estimated kite area and windspeed combinations which generate the maximum safe load for the tether. A lightweight arm mounted on a small turntable is used to sense line angle, and has full freedom in azimuth. In inclination it may travel from below the horizon (-30°) to almost overhead (>80°). The whole tether was designed and built as part of this research, apart from the manufacture of the Tether Head Unit, which was done by Mr. Ron Hussey of the Open University.

The Tether Head is the instrumented part of the tether. It forms a package about 0.4 m long, 0.1 m in diameter, with a lightweight arm 0.25 m long. It may be mounted on any suitable support (the present arrangement uses a pillar 40 mm square), although the Tether Base is specially designed for it. The lightweight arm pivots about a horizontal axis on the turntable to measure inclination, and the rotation of the whole turntable is measured for azimuth. This arrangement gives the line angles (inclination and azimuth) directly, and is optimised for inclination, which is the more important angle. The line from the kite leads down through the tether arm to a pulley on the tether's vertical axis. It then passes up to a frame holding the load cell where it is secured. A short length of line including the load cell is permanently attached, and runs out through the lightweight arm. The different kitelines used in experiments are fixed to the end of this line.

The second part of the tethering system is the Tether Base. This is a triangular steel frame (of side 1.8 m) with a vertical post (0.4 m high, 40 mm square) at the centre. The vertical post is supported by two struts across the triangular base. Three adjustable steel guys, running from the top of the post to the pickets holding down the corners of the triangle brace the whole structure, and allow the post to be set accurately vertical. The clamps around the outer cylinder of the Tether Head attach it to the 40 mm square vertical post. The whole structure can be dismantled easily for transportation.

4.1.2 Tension measurement

The Tether Head is designed to accommodate a small load cell. The line from the kite feeds round a pulley and then upwards along the Tether Head's vertical axis

Parameter	Value	Remarks
Maximum load	15 kgf	
Slope	20.07 ± 0.024 mV N^{-1}	15 kgf range
	77.5 ± 0.12 mV N^{-1}	4 kgf range
Slope temp. coeff.	6 x 10^{-4} K^{-1}	
Offset temp. coeff.	70 mV K^{-1}	15 kgf range
	270 mV K^{-1}	4 kgf range
	3.4 N K^{-1}	equivalent temp. coeff., both ranges
Time constant	<1.2 ms	unfiltered output, response > 140 Hz
	64 ms	2nd order filter output, n = 2.5 Hz
Thermal time constant	15 min	lagged, still air
	7 min	bare, still air

Table 4.1: Kulite load cell specification

to the load cell. The line is secured above the load cell. This ensures that tension measurements are independent of line inclination (the pulley is used to minimise friction).

Although the tether is designed for a maximum load of 100 kgf, kite loads in practice are much less than this, often only a few kgf at most. To give useful resolution at such low loads, the load cell used has a full scale of 15 kgf. This gives a digital resolution of 0.58 N for the basic load cell. The load cell used in these experiments is a prototype specially manufactured by Kulite Sensors Ltd. For greater sensitivity at low loads, an extra amplifier is used giving an effective full scale of about 4 kgf (and resolution of 0.15 N). For high loads a simple pulley arrangement doubles the full scale to 30 kgf. Careful calibration experiments were performed to check on linearity, reproducability, temperature sensitivity and frequency response. Figures 28,29 and 30 show results obtained, which are summarised in table 4.1.

Good static accuracy from the load cell is ensured by transmitting the tension faithfully to it, and by protecting it from temperature changes. The tether design achieves these by placing the load cell directly in the kiteline and by providing an insulated shield. Placing the load cell directly in the kiteline also ensures a good dynamic response. The restriction of tension frequency response is imposed by an anti-aliasing (low-pass) filter in the load cell Interface, as shown in figure 30.

The main weakness of this system is the load cell's temperature sensitivity. On sunny days the temperature changes during an experiment can cause offset drifts equivalent to several Newtons even with the insulation provided by the shield. Apart from this the tension measurements are good.

4.1.3 Angle measurements

Line angles are measured directly by servo potentiometers. One potentiometer is mounted on the Tether Head turntable to measure line inclination directly (using

the lightweight arm). A second potentiometer measures the rotation of the whole turntable to obtain azimuth.

Servo potentiometers were chosen to measure angle for several reasons. They are small precision potentiometers that may easily be configured to give an output voltage smoothly proportional to angle. The signal processing is therefore relatively simple, contributing towards overall system reliabilty. Each potentiometer has a range of 340° over which it measures angle and is mechanically able to rotate through the full 360°. Its life is rated at more than 10 million shaft rotations. Figure 31 shows the measured linearity of a potentiometer, both before and after a test run involving 1/2 million oscillations through about 100°. It can be seen that for a range of 90 or 180° it is possible to choose segments with linearities better than +/- 0.3°, and that even without this precaution, errors are unlikely to exceed 0.6° over the whole 180° interval (assuming the end points of the interval are properly calibrated). These errors are acceptable considering the required accuracy, which is about 0.5°. Anything finer than this is unlikely to be significant considering the difficulties of aligning field equipment, and the likely insignificance of such small quantities relative to wind directions varying about the mean by *20-* 30° in a few minutes.

The potentiometer measuring inclination has a range of almost 100°, giving a resolution of 0.405°. The range in azimuth is just over 180° so the resolution is 0.764°.

The static and dynamic response for angle measurements is determined predominantly by the tether mechanical design, since the potentiometers themselves have very low moments of inertia and friction torques. Possible sources of error in the design are:

a) any discrepancy between the true line angle and the position of the lightweight arm,

b) static or running friction couples about either of the axes,

c) the moments of inertia of the arm and turntable components.

Static accuracy

a) The line guide at the end of the tether arm is a hole 4 mm in diameter. The line diameter is 2 mm, thus the angular freedom is +/- 1 mm at a radius of 250 mm.

angular freedom = 1/250 = 4x10^{-4} rad = 0.23°

This is safely less than the digital resolution in either inclination (0.41°) or azimuth (0.76°).

A second source of discrepancy is the weight of the tether arm sensing the line angle. Diagram 4.la shows the principal forces, where e is the error angle at the end of the tether arm (length = 1, weight = w) with line tension T.

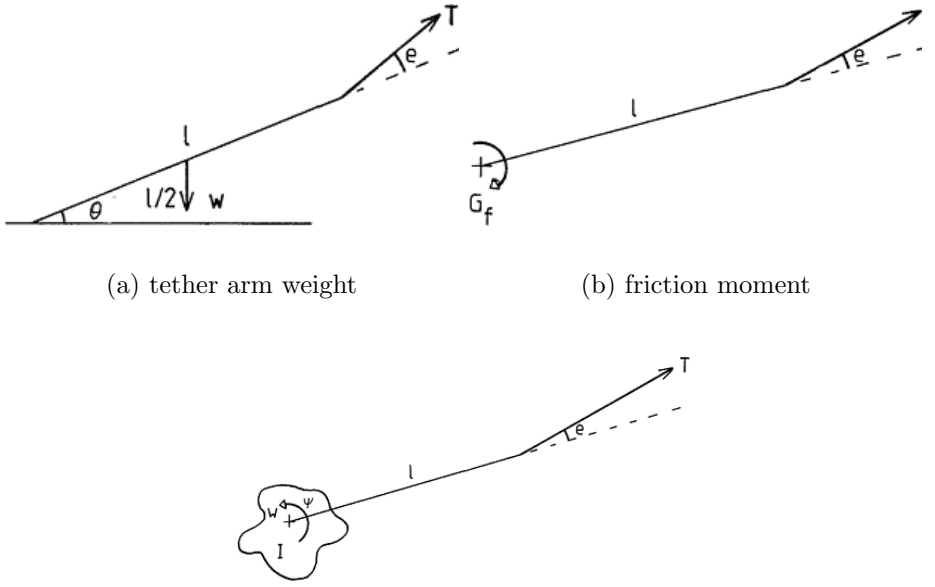

(a) tether arm weight

(b) friction moment

(c) tether head moment of inertia

Figure 4.1: Sources of Error in Tether Angle Measurements

From the balance of moments,

$$\begin{aligned} Tl \sin e &= W(l/2)\cos\theta \\ e &= W\cos\theta/(2T) \text{ (small angle approximation)} \end{aligned}$$

$$\begin{aligned} W = 20 \text{ gf } = 0.098 \text{ N}, \quad \text{so} \quad & e = 0.098\cos\theta/T \text{ rad} \\ = \quad & 5.6\cos\theta/T \text{ deg} \end{aligned}$$

Figure 32a shows the inclination reduction due to tether arm weight for a variety of inclinations. For T>14 N this error is always less than the inclination resolution.

b) Friction couples about either axis introduce a hysteresis error in measuring angles. Figure 4.1b shows the principle, with friction couple (G_f).

Balancing couples gives, $Tl \sin e = G_f$

$$Tle = G_f \text{ (small angle approximation)}$$

The error is given by $e = G_f/Tl$. The minimum usable tension if static errors are not to exceed the specified error e_0 is

$$T_0 = G_f/(le_0)$$

Inclination / °	0	30	45	60	70	75
Minimum tension / N	6.2	8.3	12	25	53	93

Table 4.2: Minimum tension for full azimuth resolution

The relevant values are:

l	0.25 m, reduced by $\cos\theta$ for azimuth
G_f	2.8 mN m (starting) - inclination
	2.1 mNm (running) -inclination
	20 mNm (starting / running) - azimuth

For satisfactory resolution in inclination and azimuth respectively:

$T > 3.5$ N	Inclination
$T > 6.2 \sec^2\theta$ N	Azimuth

Figures 32b and c show the errors in inclination and azimuth respectively as a function of tension. For azimuth, the error is given for several values of inclination. Table 4.2 gives the minimum tension needed for the azimuth error to be less than the azimuth resolution.

Good angular resolution is ensured in inclination for tensions > 4 N and in azimuth for tensions > 50 N at typical inclinations. The resolution in inclination is more important, and the design has been optimised for this.

Dynamic response

c) The Tether Head's moment of inertia opposes any change in angular velocity, and at sufficiently high accelerations results in an error between the true line angle and the angle measured. Figure 4.1c shows the elements of the system. I is the moment of inertia, e the error angle and *f the rotation angle.

$$Tl\sin e - a\frac{d\psi}{dt} = I\frac{d^2\psi}{dt^2}$$

Using the small angle approximation and assuming $e^{i\omega t}$ dependence

$$\begin{aligned} Tle &= -I\omega^2\psi + i\omega a\psi \\ e/\psi &= -\omega^2 I/Tl + i\omega a/Tl \\ &= -(\omega/\omega_0)^2 + ia'(\omega/\omega_0) \end{aligned}$$

where $\omega_0 = (Tl/I)^{1/2}$ and $a' = a/(ITl)^{1/2}$

This shows that at low frequencies the error angle is very small, but that as the angular frequency of the tension approaches w,, the error becomes significant. Experiments show that head inertia is much stronger than the viscous damping (a) at typical frequencies, ie. a is very small, and the damping term may be ignored. So the fractional error in angle is equal to the square of the ratio between the imposed frequency ω and the natural frequency ω_0.

Actual values are	inclination	l = 0.25 m, I = 0.28 gm^2
	azimuth	$l = 0.25\cos\theta$ m, $I = 0.28\cos^2\theta + 0.33$ gm^2

Figures 33a and b show the natural frequencies ($n_0 = \omega_0/2\pi$) for the tether arm in inclination and azimuth as a function of tension and line inclination. The error is negligible for $n \ll n_0$. As an example consider a kite moving with a maximum speed of 10 m s^{-1} on a 30 m line, and a natural frequency of 1 Hz (line inclination = 45°, tension = 10 N). This corresponds to a very manoeuvrable stunt kite.

angular amplitude = $1/6\pi$ rad = 3.0°
n_0 = 10 Hz, therefore expected error = 0.03°

Thus the dynamic response of the tether head to changes in line angle is perfectly adequate for measuring normal kite flight.

4.1.4 Practical calibration

Experiments have been performed to check the accuracy of the tension and angle measurements of the tether in various situations. The practical calibrations relate the tension in Newtons, or angle in radians to counts transmitted (N_t) by the Kite Tether Instrumentation. A linear relationship is used, with slopes given by

		s(slope) / %
d/dN$_t$ (tension) =	0.5795 N (15 kgf range)	0.18
	0.150 N (4 kgf range)	0.15
d/dN$_t$ (inclination) =	7.077 x 10^3 rad	0.16
d/dN$_t$ (azimuth) =	0.01333 rad	0.17

The intercepts are measured during each experiment, using a reference load and direction to which the tether is connected before and after each flying period (shown in plate 13). These reference readings also provide a check on any drift during the experiment, due perhaps to temperature fluctuations. The reference load is 9.3 +/- 0.1 N, while the angles are measured for each reference position, and are accurate to about 0.3°. These values of slopes and intercepts convert the counts transmitted to absolute units of tension or angle.

4.2 Anemometry

Two types of anemometers are used in these experiments, the 3-d Field Anemometer System using digital vane anemometers (DVAs) and the Porton anemometer and windvane. The Field Anemometer System collects the wind data used for the analysis while the Porton provides a check on the results, being an independent and straightforward measurement of the wind.

The anemometers were mounted on a 25 m tower, with the kites flown nearby. The Field Anemometer System operated two triads, one each at 10 m and 22 m, while the Porton was initially mounted at 25 m and then later at 10 m (for compatibility with other experiments).

4.2.1 3-d Field Anemometer System

A single DVA measures the wind component along its axis. In these experiments, six DVAs were used, configured as two triads. A non-orthogonal triad was used (shown in plate 12) to give more accurate measurement of the fluctuations in the wind than a standard orthogonal triad (Pinnock, 1983). The anemometer characteristics are given by a consideration of the individual DVAs and the triad geometry.

Digital Vane Anemometer

The Digital Vane Anemometer heads are manufactured by Lowne Instruments Ltd. A lightweight rotor assembly using mica vanes is mounted inside a shroud of diameter 72 mm. Opto-electronic sensors detect the speed and sense of rotation, generating six pulses per fan revolution. This corresponds to approximately one pulse per 25 mm of airflow through the fan. This pulse length and the starting velocity (ie. the airspeed at which static friction is just overcome) have been measured by calibration experiments performed at the National Maritime Institute (NMI). Using these values for the mica vanes, the wind velocity corresponding to a steady rotation rate r pulses per second is

$V = 0.0994 + 0.0243\ r\ ms^1$

The pulse rate r is determined by counting the pulses arriving in a fixed sampling period, typically 0.1 or 0.2 s, giving an average pulse rate for that period. If the pulse rate is "negative", ie. the sense of rotation corresponds to a reverse airflow, the starting velocity should be subtracted rather than added. Figure 34 shows the calibration measured at the NMI. The error is no more than 2 cms^{-1}. The instrument reading assumes the pulse rate calibration above, and the true velocity is obtained by adding the error to the instrument reading.

Cosinality

June 2005: Pinnock's cosine response calibration was flawed; see (Hobbs, 1994) for a corrected calibration.

In analysing the DVA results it is assumed that the true wind component along the vane axis is measured. This is tested by comparing the DVA reading as a function of off-axis angle with the cosine variation expected. Figure 35 presents results obtained by Pinnock (1983) showing excellent cosinality for these vanes . The error compared with a true cosine response is less than 0.01 for angles up to about 75° off-axis.

Dynamic Response

The dynamic response of an anemometer is usually characterised by a distance constant. Thus after a step change in windspeed, the anemometer error should be reduced by a factor of 1/e after one distance constant's worth of air has passed through it. The distance constant gives the approximate size of the smallest eddies which the anemometer can measure.

The distant constant for the mica DVA has been measured to be about 0.30 m (Scannell, 1983). Combining this with the cosinality discussed above, the distance constant in metres as a function of off-axis angle (t) is is 0.30 sec t. This is important for the non-orthogonal triads where each DVA is inclined by 30..40° to the mean wind, giving an effective average distance constant of 0.35..0.40 m. The full expected variation is shown in figure 36.

Triad Geometry

The triad design used is based on that of Pinnock (1983) but redesigned to place all three DVAs at the same height, and only separated laterally along an axis, which ideally is perpendicular to the mean wind. The triad is machined from metal (mostly brass) so that its geometry is stable to temperature and humidity changes, and includes reference lines to ensure correct alignment of the DVAs.

For the analysis, the DVA readings are transformed into standard axes Oxyz (with Ox along the mean wind) using a matrix transformation of the triad's three DVA readings. The DVA data are converted to windspeed values V_j, and it is on these that the matrix operates. The index j takes the values 1..3, with vane 1 on the right, vane 2 on the left and vane 3 in the centre of the triad when facing upwind.

Met Processor

This is the instrumentation unit operating the DVAs. It has been described by Bent (1982) but basically it counts the pulses received from each DVA connected

to it over a defined sampling period (100 clock cycles), and then during the next sampling period transmits those counts out along a single serial data line for storage and eventual analysis.

The features particularly relevant to this work are:

a) it may be driven by an external clock signal (a square wave input of amplitude 1 V able to supply 10 uA is sufficient),

b) there is a synchronisation facility which enables the start-up of the Met Processor to be precisely controlled.

These features allow the Met Processor to be in controlled synchronisation with the rest of the experiment equipment.

The format of the serial data stream is such that up to 12 DVA readings may be transmitted within a cycle length of 100 bits. To allow for forward or reverse DVA rotations, the DVA count is initialised to 128 and then incremented or decremented as the pulses are received, according to the sense of the DVA rotation. Thus the number transmitted (N) for any DVA is 128 plus or minus the number of pulses counted, depending on the rotation sense. These counts are transmitted as an 8 bit (1 byte) binary number (most significant bit (MSB) first). The data cycle of 100 bits consists of 12 DVA counts followed by 4 "blank" bits (held low). A 1 kHz clock gives a sampling period of 0.1 s. Figure 37 shows typical data output from the Met Processor, along with the clock used to drive it and the synchronisation signal ("sync", in three alternative phasings) which controls the Met Processor start-up. Only the last 6 channels are used, so the first 6 are blank (128 in binary). Figure 37 shows how the clock falling edge coincides with the data bit centre and so may be used to read it unambiguously.

4.2.2 Porton Anemometer

The standard Porton anemometer and windvane is also used for wind measurements. It performs two tasks, first as a check on the DVA operation, and second as a general indicator for use during experiments since it gives an immediate display of the wind speed and direction.

The Porton nominally measures the horizontal wind component, but there is also some contamination from the vertical component. The cup anemometer is accurate to about 0.2 m s^{-1} and the windvane has a resolution of 10°. The distance constant is 5 m, ie. much longer than the DVAs.

4.3 The Kite

The system is designed so that any single line kite of suitable size may be flown with it. The kite needs no special fittings or equipment, and simply uses the Tether as a tether.

Table 2 includes all the kites flown in these experiments (indicated by *). The larger ones (Cody, Flare, Parafoil) are capable of lifting small payloads (up to 500 g) which may be used to make extra measurements. In particular, the system is designed so that air temperature profiles and the kite attitude may be measured, although this has not been used for this research. A radio link would be used to transmit information from the kite to the Kite Tether Instrumentation, which includes a small radio receiver for this purpose.

4.4 Kite Tether Instrumentation

The Kite Tether Instrumentation (KTI) is the heart of the experiment system, and coordinates all the other units. It main funcion is to accept the Tether sensor inputs and convert them into a formatted serial data stream. Other functions incorporated are a radio receiver for data transmitted from the kite, and clock / timing circuits to ensure correct synchronisation of all the data generated by the system. The basic sampling frequency may be set to either 5 or 10 Hz. This was chosen so that all important kite system information could be gathered, while still being able to record data for the whole of an experment lasting about 15 minutes. Results suggest that these sampling frequencies do include the most important features of kite flight.

Figure 38 is a block diagram for the KTI. The functions of each “block” are shown more fully in figure 39.

4.4.1 General KTI features

The KTI is designed to be a practical piece of field equipment, so care has been taken to make it reasonably compact, easy to maintain and repair, and flexible in its power supply requirements. Plates 15 and 16 show front and rear views of the unit.

The unit’s mass is 2.8 kg, increased to 3.4 kg with the three interfaces used (Kulite load cell, Porton anemometer, Signal Pulse Coder). Its size is 220 x 135 x 270 mm, and is thus an easily portable unit. A power supply of 12 V, 250 mA is used (eg. car battery) although anything in the range 8..20 V is suitable, since the KTI has its own internal circuits to provide the necessary stable voltage levels.

The circuits are built on plug-in cards to simplify maintainance. The connections between cards are almost all handled through the sockets at the rear : connections

to the front panel use separate connectors at the front of the cards. Access is via the front panel which swings down allowing the cards to be removed for inspection, modification , or repair. Low-power components such as CMOS digital circuits have been used wherever possible to minimise power requirements.

Each "block" of figure 38 is now described in turn.

4.4.2 Analogue inputs

Altogether the KTI has 8 analogue signal inputs. Four of these are dedicated to the Tether sensors, and four are available for any other suitable analogue signals. The signals must be compatible with the analogue to digital converter (ADC), which takes inputs in the range 0..3 V, and samples at either 5 or 10 Hz.

A simple amplifier gives the correct full scale range, while the sampling frequency implies the need for some filtering of the signals to remove high frequencies. According to the principles of sampling theory, a signal sampled at frequency n_s must not contain any components of frequency higher than $n_s/2$ (the Nyquist frequency) if all the original information is to be preserved. If this is not the case then there is an ambiguity between the frequencies n and (N n_s + n), where N is any integer, and (since we are dealing with real variables) n may be positive or negative. All the components of frequency (N n_s + n) are mapped onto the same frequency component n by the sampling process and cannot be separated later. This is referred to as aliasing, and can only be prevented by the use of an anti-aliasing filter which removes all frequencies above the Nyquist frequency. As a precaution those signals which may contain high frequency components are filtered using an active second order filter (n_0 = 3.0 Hz). The filter's transfer function is shown in figure 40, along with an ideal anti-aliasing filter with a cut-off at 5 Hz for comparison.

There is an option to replace the data of channel 8 with a counter incrementing 1 on each data cycle. Figure 39 shows this option at A,B. If A is connected directly to B, all 8 data bytes are transmitted, otherwise channel 8 is replaced by the counter (which cycles through 0..255). The counter allows any breaks in the data flow to be detected.

Tether sensor inputs

The two potentiometers used for the angle measurements use similar amplifier circuits inside the KTI to provide the required 3 V output range. For each channel, a buffer amplifier is followed by one with preset gain and adjustable offset. The gain is fixed during initial calibration work, and remains constant throughout the experiments. The offset may be adjusted before each experiment, any variation being measured during a short period at the beginning when the tether is attached to a reference line of known tension and direction. The inclination signal goes to channel 1 and azimuth to channel 2.

The signal from the load cell is fed to channel 8 of the KTI (at present). Internally, this is connected to channel 3, and through a x4 amplifier to channel 4. This amplifier gives the load cell a more sensitive range for use at low tensions, with a full scale of about 4 kgf instead of 15 kgf.

Signal conditioners

The Kulite load cell as supplied gives an output of 1 V full scale (15 kgf). The Kulite Interface includes an amplifier to give a full scale of 3 V and an antialiasing filter to remove frequencies above about 3 Hz (figure 40).

The outputs from the Porton anemometer are not suitable for the KTI analogue inputs directly, so a small interface, the Porton Anemometer Unit Interface has been built. This contains amplifiers to adjust the gain and offset, translating the signals into the range 0..3 V. No extra filtering is required.

A third unit used in the experiments codes signal pulses into a data line. These pulses can be detected using one of the data handling programs (FLAGFIND). Labelling sections of an experiment in this way allows the data to be used much more confidently. The Porton wind direction channel is used for these pulses since the pulses cause no significant loss of information here. The Signal Pulse Generator has 6 switch positions : 1..5 correspond to 5 signal pulse levels in 0.5 V steps, and 6 allows the original data through undisturbed. These signal pulses are used to indicate the start and end of phases of the experiment, as well as special features of the flight.

Monitoring facilities

Two methods of monitoring the analogue voltages are built into the KTI. Firstly, a meter is included and may be switched to any of the eight signal channels (and a ground position to check the meter operation). Two ranges are used : 0..3 V for general monitoring and 0..30 mV to check zeros.

Secondly, all the analogue voltages are available on the KTI front panel. Channels 1..4 appear as buffered signals tapped off from the multiplexor inputs, while channels 5..8 are present since these are the signal inputs anyway.

4.4.3 Multiplexor

This is an electronically controlled switch which connects one of the eight analogue input signals, as selected by the appropriate control code, to the output. It is controlled so that all eight inputs are sampled in turn, with channel 1 being sampled twice. During the first sampling of channel 1, the part of the circuit responsible for

the data output formatting is switched instead to a null data array (all at 0 V), so that a synchronisation code is transmitted rather than a duplicate of channel 1.

The output from the multiplexor goes direct to the input of the analogue to digital converter.

4.4.4 Analogue to Digital Converter

The analogue to digital converter (ADC) takes as its input an analogue voltage in the range 0..3 V from the multiplexor output, and on receipt of a control signal generates a digital code corresponding to this signal voltage. The converter has a resolution of 8 binary bits, thus the digital output is an integer in the range 0..255, with 0 corresponding to 0 V, and 255 to the full scale of 3 V. The ADC resolution is thus 11.72 mV, ie. a change of 11.72 mV at the input will change the digital output by 1 count.

The integrated circuit chosen for this task is the RS 8703. It uses an incremental charge balancing technique, which "has inherently high accuracy,linearity and noise immunity", so that the error in the output is at most 1/2 least significant bit (LSB). CMOS technology is used to minimise power requirements. Although the conversion technique is comparatively slow, the maximum conversion time of 1.8 ms is still well within the 10 or 20 ms available, and is in fact an advantage since the signal is integrated over this time, reducing any susceptibility to noise. The precision voltage reference used is stable to better than 50 parts per million (ppm) K. A 20 K change in temperature should only alter the reference, and thus the output sensitivity, by at most 0.1 %.

The digital code is next passed to the data formatting section which turns the parallel output of the ADC into a properly formatted serial data stream.

4.4.5 Serial data formatting

The main function of this part of the KTI is to take the parallel ADC output and turn it into a formatted serial data stream. Two other functions are also performed. Firstly, as mentioned in the multiplexor description, during the first of the two samplings of channel 0, the 8 parallel digital data lines are switched to 0 V and the formatting codes altered to transmit a unique synchronisation pattern embedded in the serial data output. Secondly, a counter is incremented at the end of each data cycle and may be used to replace the digital data of input 8. If the appropriate internal connections are made to choose this option then the last tether data channel is replaced by a counter which increments by 1 each data cycle to provide a continuity check.

A standard integrated circuit is used to transform the parallel data into a serial data channel. The device used is the 6402 Universal Asynchronous Receiver Transmitter

(UART), which uses CMOS technology for low power, and is able to operate at clock speeds of up to 1 MHz. The UART's own control logic is used to generate many of the control codes required within the KTI, and thus forms an important part of the control logic discussed below.

As used here, the UART receives the 8 parallel data lines from the ADC and transmits them as a serial stream, lowest byte first. The formatting comprises adding a start bit (low) at the beginning of the sequence, and then finishing it with a parity bit and one stop bit (high). The parity bit is low if the data byte contains an even number of highs, and high if there is an odd number. The device used to receive the serial data can then check the parity bit to ensure that there has been no data corruption during transmission. In the case of the synchronisation code embedded in the serial data, a unique code is achieved by adding two stop bits instead of only one. Figure 41 shows typical data and sychronsation (sync) codes, and figure 42 the whole cycle. Two cases are shown since there is a slight difference between the two clock speeds due to relative timings within the start-up procedure. Since a data word is 11 bits, and a sync word 12 bits long, the whole cycle of 8 data words and 1 sync is 100 bits long, the same as the Met Processor cycle length. Figure 42 also includes the Met data in a typical synchronisation.

This completes the flow of data through the KTI. The data output is buffered for transmission to wherever it is to be received for storage and analysis.

4.4.6 Control logic

An important part of the KTI is concerned with controlling the various components so that they work reliably together and transmit data of the required format. The logic can be analysed into two functions. Firstly, there are the circuits to maintain the continuous running of the KTI, and secondly there are those which control the start up of the system so that its running state is predictable.

Underlying all this control logic is the system clock. The KTI contains a crystal controlled oscillator at 10 MHz, divided down to give the clock frequency of 1 kHz or 500 Hz required for the system operation. A switch on the front panel allows either of these rates to be chosen. (The UART actually uses this frequency multiplied by 16, dividing it down internally). There is provision for this KTI clock to be reset regularly by a signal derived from data transmitted over the radio (kite) link, and thus the KTI clock may be kept synchronised with what has now become the system master clock aboard the kite. If the radio link is not used in this way, the KTI takes over the role of system master. The synchronisation of the clocks depends on being able to match the two oscillators to within 1 part in 10^4. With crystal oscillators this is easily achieved.

Counter output decimal	binary	ADC channel	Remarks	Word being transmitted
0	0000	0	set two stop bits	sync
1	0001	1		data 1
2	0010	1		data 2
3	0011	1		data 3
4	0100	1		data 4
5	0101	1		data 5
6	0110	1		data 6
7	0111	1		data 7
8	1000	1	load null word into UART	data 8

Table 4.3: Control logic counter states for the Kite Tether Instrumentation unit.

UART continuous running

The UART control signals help maintain the continuous running of the KTI. At the end of the transmission of a data or sync word one of the UART status flags pulses high. This is used to increment a scale of 9 counter. Table 4.3 lists the counter states, and the special operations associated with each state.

Note that analogue input 1 corresponds to ADC channel 0 and the transmitted data word 0. This is because electronic counters start at 0, whereas human beings like to start counting at 1.

The counter's three lowest bits address the multiplexor, while the fourth bit switches the UART inputs to the null array. It does this by opening 8 analogue switches in the ADC output lines, allowing the UART inputs to fall to 0 V. When the counter output is zero a signal is sent to the UART to generate two stop bits. The lag between loading the null word and setting two stop bits is because the UART uses a buffer register so that the data being transmitted was received from the ADC on the previous cycle.

A series of monostables triggered by UART status flags initiate the ADC conversion and UART loading. The UART buffer register is maintained with valid data which ke ;ps the UART transmitting continuously. Since the system timing is controlled by a combination of counters and monostables, it is not as flexible as one based purely on counters. This is because monostables generate fixed delays, while a counter's delay depends on the clock frequency. However, the current design is simpler that one based purely on discrete counters would be, and still meets all the requirements.

UART start-up

Starting transmission in a reliable way and leaving it in a reproducable free-running state needs its own control logic. Two controls concerned with this are situated on the KTI front panel. The switch has two positions : "stop", in which all transmission

is stopped, and "ready" when the system is primed, ready to start transmission as soon as a suitable start pulse is received. The push-button below (labelled "start") generates such a pulse. Alternatively, the reset pulse derived from the radio data may also start transmission. This ensures that the relative phasing of the radio and tether data is fixed.

Other control functions

An important part of the KTI's function is to control the operation of the other parts of the experiment system. This is achieved by transmitting the KTI clock and a cycle sync signal derived from the control counter (see table 4.3) : this cycle sync is generate while the counter is in state 0, which is also the period when the tether sync word is being transmitted. The KTI clock (500 or 1000 Hz as selected) and the cycle sync are available, buffered, on the KTI rear panel.

The Met Processor has inputs for an external clock ("EXT CLOCK") and a signal to start transmission ("MIN"). The KTI clock is fed to the external clock input and the cycle sync to MIN. With this arrangement the Met Processor output is synchronised with the tether data, and the phasing between the two serial data outputs is reliably defined as in figure 42 for example.

4.4.7 Radio

A radio receiver is incorporated into the KTI. This is a standard model radio control receiver (for amplitude modulated signals). The output of the receiver is available, buffered, at a socket on the KTI rear panel.

This is a facility intended for applications outside the current work, although the KTI control and synchronisation is designed to work with this extension.

4.5 Data Collection and Storage Equipment

The output of the experiment equipment is transmitted through 3 serial data lines, with one line each for tether and met data, and a third for the system clock required to read the data. If the system is being used to measure wind profiles with a kite, then the met data is no longer needed, and only two output lines are used.

Figure 43 shows the equipment used for data collection and storage. The FM tape recorder is optional, most experiments used the computer to store the data in real time. Although the tape recorder is able to store 1 or 2 hours' data without a break, it was not used in practice since experiments typically lasted only 15 minutes, which is within the capacity of the computer. Also, using the computer to store data

directly generated far fewer errors than if the data had been stored on tape and then read into the computer.

Each data cycle produces 8 bytes of tether data (1 for each channel) and 6 bytes of met data (1 for each DVA). At the usual sampling frequencies (n_s) of 5 or 10 Hz, this corresponds to 70 or 140 bytes per second to be stored. Since the data cycle length for both the tether and the met data is 100 bits, the baud rate at which data is transmitted is 500 or 1000 Hz.

An Apple II microcomputer with 64 k of RAM (the direct access semiconductor memory of the computer) is used to collect and store the data (1 k is a unit of memory size equal to 1024 bytes). Running typical data collection programs leaves about 30 k available for data storage in RAM, and the floppy discs used for permanent storage hold 137k on each side. Thus one experiment (filling one side of a disc) may last for about 15 or 30 minutes (n_s = 10 or 5 Hz respectively). Experiments last for 15 minutes usually, so 1 or 2 fit neatly onto each side of a disc. Because of the limited RAM available, data is collected in units of about 4 or 7 1/2 minutes (n_s = 10 or 5 Hz respectively), and written to disc in these units. About 6 s of data is lost between units while the data is being written to disc.

The Games Paddle connector of the Apple II is used for data input since it is designed for single bit inputs such as serial data lines. The system clock uses input PBO, tether data FBI and met data PB2 (these are three lines available on the Games Paddle connector). A simple interface (one comparator for each data line) was built to ensure the signals at the computer were well-defined and to protect the computer from overloads through the data lines. Specially written data handling programs were written to read the incoming data and store it for later analysis.

4.6 Site Details and Experiment Procedure

4.6.1 Site details

Figures 44 and 45 show the flying sites used for all experiments. Figure 44 gives a plan of the surrounding area, while figure 45 shows the layout of the flying site itself. The experiments are performed in the southern corner of Cranfield airfield, using winds from either due north or within the range south through west to north-west. The flying site was covered by rough grass of typical height 0.2 m in the winter, growing to 0.5 m in the summer. To the north is the airfield, which during the winter is covered either with short grass or tilled soil (and the occasional runway). In the summer barley is grown on the area closest the flying site. To the west the land is arable, and beyond the edge of the airfield (300 to 400 m away) slopes away gently. For both these directions there are no significant obstructions within 2 or 3 kilometres, apart from occa sional trees and one or two isolated buildings, and none of these within 500 metres.

Figure 45 shows the location of the tower supporting the anemometers and the different tether positions used. The aim is to position the tether about 30 to 35 m upwind of the anemometers so that the anemometers measure the wind as close as possible to the kite.

Figure 46 shows diagramatically the items of equipment used and their interconnections. The main building is about 100 m from the Wind Hut, and the tether about 50 m beyond that. Coaxial cable is used to transmit the data.

4.6.2 Experiment procedure

Given suitable weather conditions for an experiment, the procedure is as follows :

a) obtain permission from Air Traffic Control (this is necessary since the site is within 5 km of an airfield),

b) set up the tether about 30..35 m upwind from the anemometer tower,

c) aim the anemometers into the mean wind, removing protective covers and checking alignment,

d) make all electrical connections checking for continuity,

e) check data reception at the computer (inside the main building) and that the computer is ready to collect data,

f) launch the kite to be flown, tethered to a parking tether near the instrumented tether,

g) perform the experiment(s), which comprises:

i) start the computer program,

ii) run an initial period of calibration with the tether line hooked to the reference tension and direction,

iii) the period flying the kite, typically 10 to 12 min,

iv) a final period of calibration back on the reference,

v) when the program has finished, protect the collected data and prepare the computer for the next experiment if more experiments are to be performed (repeat steps i..v),

h) pack equipment away after all experiments completed / kites all damaged / daylight has faded.

A record is kept of site and weather details for use in the data analysis. These are entered in a log which is also used to make notes during the kite flights, so that any special features of the flight or weather which may be important for the analysis later are recorded. The site and weather measurements which need to be made are:

1. tether reference inclination and direction (azimuth),
2. anemometer reference direction,
3. tether base distance from anemometers and bearing of anemometers from tether base,
4. mean air temperature and pressure

With this information the kite's position relative to the anemometers, and the kite azimuth relative to the wind direction can both be calculated. The air temperature and pressure give its density to the accuracy required.

Chapter 5

EXPERIMENT SOFTWARE

Section 5 describes the programs written to collect, analyse and display the data. The programs are only described in detail if they are important for either the data collection system, or for the analysis of the data. Since so much data has been collected, in terms of bytes of information, the only feasible way to analyse it is by computer : these programs therefore play an important part in the analysis of the data as well as its storage and collection, and considerable effort has gone into writing and checking them.

The programs fall into three groups. First there are those concerned with the data collection. This covers the whole process from reading the serial data lines and to leaving the data in a suitable form for analysis. The second group of programs operates directly on this prepared raw data, and performs the bulk of the analysis of the experiment results. Some of these programs condense data into record files, and it is on these condensed data files that the third group of programs operates.

All these programs have been written on, and for use on, the Apple II microcomputer. The language used is Pascal, which is flexible enough to handle a wide range of tasks well, and clear enough to enable complex programs to be written comparatively easily. Most of the graphical output has been produced on a plotter (the Hewlett-Packard HP 7470A) coupled to the Apple II computer.

5.1 Data Collection and Validation

These programs have all been written especially for collecting the tether and met data. Four programs are used , which together take the data from its initial serial format as received by the computer to a final data file stored on disc along with a data summary file containing all the experiment parameters and the information required for its analysis.

5.1.1 Program STORE/TM

This program reads the serial data lines and stores the data on disc. The procedure (DATAREAD2A) which reads data in is written in Assembler and operates within the Pascal environment : it is the core of STORE/TM. Around this is the Pascal shell program (STORE2A) which opens and closes the files as appropriate, passes parameters relating to the data phasing to DATAREAD2A and keeps a check on the amount of data stored to stop collection when the experiment is complete. Procedure DATAREAD2A linked with STORE2A gives program STORE/TM.

The limitations of memory size in the Apple II mean that the largest practical array of data which may be stored is 63 blocks (1 block = 512 bytes). Each sampling period produces 14 bytes, so this corresponds to 2304 sampling periods, ie. 230.4 or 460.8 s (10 or 5 Hz sampling frequency respectively). Up to 4 of these 63 block units may be stored from one experiment.

Program shell STORE2A

The functions performed by this program are :

a) open a file, checking it is large enough to receive to all the data,

b) print the program heading giving details of its operation and the inputs required,

c) accept input specifying the relative phasing of tether and met data and the number of 63 block units to be recorded (up to a maximum of 4),

d) run procedure DATAREAD2A the correct number of times, writing the data to disc each time,

e) close the data file, making it permanent.

A convention for naming experiment data files has been adopted. A prefix “T” or “TM” is used depending on whether just tether or tether and met data is being collected. Following this is the date, and then finally the experiment number on that day (if more than one experiment is stored per file then the first experiment number is used). Eg. “TM10JUN3” means the data file contains tether and met data collected during experiment number 3 on 10-Jun.

Procedure DATAREAD2A

DATAREAD2A is a machine code program written to read the serial data lines and store the data in an array in memory. Figure 47 gives as outline of DATAREAD2A’s functions. A more complete flow diagram is shown in figure 48, where each box represents a function which can be executed by a few lines of machine code.

baud rate =	1 kHz	500 Hz
SYNC	0	0
SPEED	17	18
C3	1	2
C4	2	2

Table 5.1: Typical DATAREAD2A counter values.

Figure 42 shows the data lines available and their relative synchronisation. Four counters are used to indicate position within the data cycles, two each for the tether (Cl and C2) and met (C3 and C4). Figure 42 shows portions of the two serial data lines with their appropriate counter values.

Any relative phasing of the two serial lines may be handled by adjusting the variables SPEED and SYNC which are passed to DATAREAD2A. On the start bit of tether data word number SYNC (of 0..7) the met counters take the values C3 = SPEED mod 8 and C4 = SPEED div 8. The values for normal operation (as in figure 42) are given in table 5.1.

A moderate drift in the relative phasing of the two data lines may be corrected for by adjusting the value of SPEED within DATAREAD2A. The code to do this uses the fact that the first 6 met data channels contain a high followed by 7 lows, and monitors the position of one of these highs. A drift of up to one clock pulse every data cycle may be handled without losing any data. The variable SPEED is returned to STORE2A : if any clock pulses are missed or gained, SPEED will have changed from its initial value.

Error Checks

In addition to the met synchronisation check via the variable SPEED the tether data is checked to see that each word is received uncorrupted. The start, parity, and stop bits are checked by DATAREAD2A, and any error found is flagged. The error "flag" used here is to replace any byte generating an error with the value 255. Thus a search through the raw data for a 255 will reveal all the errors found (as well as any valid items that also happen to be 255).

Raw Data Format

The 14 bytes of data received per data cycle are stored sequentially, the first 8 bytes being tether data (channels 1..8 respectively) and the last 6 the met data (channels 7..12). This mini-array consisting of the 14 bytes of data for one sampling period is often referred to here as a record. Figure 49 shows an example of a raw data file (including an error which has been patched). Channel 8 is connected to the counter and channels 3,4 and 7 are blank in this case. Each 63 block unit written

to disc contains 2304 of these records. The Pascal operating system uses the same physical arrangement of data for a type specified by Packed Array [0..2303, 1..14] of 0..255. An array of this type is a very convenient way of recalling the data, and in fact may be generalised to any Packed Array [a..b,1..14] of 0..255 where the total number of records (b+1-a) is some multiple of 256 (so the array occupies a whole number of blocks). The record index in the range 1..14 specifies the data channel: 1..8 are the tether channels and 9..14 the met channels. In general the most efficient way of reading the raw data back from disc is to create a packed array of this type and blockread it back from the disc file ("packed", "blockread" and "type" are all standard Pascal terms and are used as such here).

5.1.2 Program FLAGFIND

This program is used after STORE/TM. Its two main tasks are to search for any error flags set and to pick out signal pulses embedded in the data. In addition to this it displays portions of the data file for inspection and allows individual file elements to be modified.

Error Detection and Correction

One option within FLAGFIND sifts through the raw data looking for elements indicating potential errors. For the tether data this is done by checking channels 1..7 for any bytes equal to 255. Channel 8 is not included since it is normally connected to a counter which generates the code 255 regularly. Errors in met data are indicated by values which are unusually low or high, ie. less than 128 or greater than 200 or 250 (depending on the sampling frequency). Since a non-orthogonal triad is used for the DVAs, no DVA reading should be negative, ie. less than 128, and the counts of 200 or 250 correspond to windspeeds of about 20 or 15 m s^{-1} at sampling frequencies of 10 and 5 Hz respectively. Any met values outside this range are considered to be suspect.

If an error is detected, the program displays the suspect data and the records around it. Usually it is obvious from a visual inspection whether the data is valid or not. If it is, then the program is set searching for the next error, if a genuine error is found then there is the option of patching over it using a linear interpolation between valid points either side in that same channel. Figure 49 shows a printout of an error before and after this patching procedure. A record is kept of all alterations made, and there is always a copy of the original data to refer to in case of any doubt about the "correction" made. The main justification for this procedure is that if too many spikes of 255 are left in the data then they give a misleading value for the variance and related measures. If too many errors are found, the data is not used further. Typically, reading data into the computer in real time, no more than one or two errors are found, and often none at all. However, using the FM tape recorder gave anything from several dozen to a few hundred, with the worst cases being completely

spoilt. This was the main reason for storing by computer in real time.

Signal Pulse Detection

This procedure searches the data channel containing signal pulses for the appropriate pattern. In general terms a signal pulse is identified by a length of data at 0 followed by a jump to one of the 5 specified levels, and then a return to 0. The record number and level of any pulses found are printed out. The procedure is not infallible -an occasional pulse is missed -but does find about 90 %. The remainder are then easily found using what pulses have been found, the experiment written log, and the procedure within FLAGFIND which displays any selected portion of the data file.

5.1.3 Program DATALOG/TM

This program produces a compact visual record of the whole experiment. Five channels of information are plotted : line inclination, azimuth and tension, and wind speed and direction (derived from the Porton anemometer). Since the Porton wind direction channel is normally used for the signal pulses, these too are displayed. This visual log is used to complement the written one produced during the experiment, and is very useful in identifying particular features of the kite flight. However, some detail is lost since 30 consecutive records are averaged for each point plotted. An example of a typical log is shown in figure 50. The inclination shows an interesting dip between 8 and 9 minutes -this is the sort of feature which would be examined more closely to check the data is still representative -in this case it appears to be due to the kite coming down in low wind, perhaps with the line going completely slack at times. Signal pulses have caused the discontinuities in the wind direction trace around 2 and 14 minutes.

5.1.4 Program DATASUM/TM

Programs STORE/TM, FLAGFIND and DATALOG/TM take the data from its initial serial input to the form of a checked and documented raw data file on disc. The final stage of data preparation is to produce a data summary file containing all the experiment parameters required to interpret the data.

Data summary file format

All the data summary information is stored in an array, specified in Pascal terminology as Array [1..8, 1..16] of real. Figure 51 shows the complete array and the items stored in each location.

Procedure PREPROCESS

PREPROCESS calculates means and standard deviations from the raw data for all 14 channels over a specified range of records. For channels 1..8, the slopes and intercepts needed to convert the raw data to absolute values (angles in radians etc.) are entered and stored. The kite azimuth is defined so that it is 0 for a kite flying exactly along the mean wind. The wind data of channels 9..14 is used to calculate two matrices, one each for 10 and 22 m. These rotation matrices (LAB_{ij}) operate on the three triad DVA components (V_j / m s^{-1}) to give the component W_{0i} in standard orthogonal axes Oxyz.

$$W_{0i} \;=\; LAB_{ij}V_j$$

The standard axes Oxyz are defined so that the mean wind lies along Ox. Oz is the vertical axis (upwards) and Oy completes a right handed triad. However, it is important to note that a positive value of W_{0i}. means that the wind has a positive component coming in along that axis; thus $W_{03} > 0$ corresponds to a wind with a downward component.

In addition to these results, the data summary is also loaded with parameters which will allow the calculations to be repeated exactly in case the program is changed and its results need checking.

Trend Removal

If there is significant change in the reference data values over the period of the experiment, then a linear trend may be subtracted from the data. The trend T at record R with endpoints (T_1, R_1), (T_2, R_2) is defined by

$$T \;=\; \frac{T_1(R_2 - R) + T_2(R\_R_1)}{R_2 - R_1} - \frac{(T_1 + T_2)(R_2 - R_1)}{2}$$

Using this definition, the mean over the whole flight period is unchanged and thus the original slope and intercept are still valid. This trend removal is valuable since the linear trend introduces an error into the mean and increases the variance (by $d^2/12$ where d is the span of the trend).

The only channel occasionally needing trend removal is the tension, particularly on the more sensitive range. Trends of up to a few Newtons (equivalent) may be measured, and in such cases, especially if the signal tension is low, trend removal has a significant effect on the results. A record is kept of all trends removed to enable the original data to be recreated.

Procedure SITEDATA

This procedure stores details of the kite, site, and line in the data summary file, and also performs calculations relating the tether and anemometer positions with the mean wind. Figure 52a is a site plan diagram showing the angles, and figure 52b introduces the distances so that the position of the kite relative to the anemometers may be calculated.

Site Geometry

The angles ψ are bearings from magnetic north, and angles ϕ are tether azimuth measurements. The site measurements include the bearing of the anemometers from the tether, the tether reference direction and the anemometer reference direction. $\phi = 0$ is chosen to be the mean downwind direction and increases in an anti-clockwise direction whereas the bearings increase clockwise. The mean horizontal wind components are U and V, then

$$\begin{aligned} \psi_w &= \psi_{a,\mathrm{ref}} - \pi - \tan^{-1}(V/U) \\ \phi_{t,\mathrm{ref}} &= \psi_w - \psi_{t,\mathrm{ref}} \\ \psi_k &= \psi_w - \phi \end{aligned}$$

Figure 52b gives angles relative to the mean wind direction to calculate the kite position relative to the anemometers with line length (l) and the line horizontal projection (rk) as :

$$\begin{aligned} X &= ra\cos(\psi_a - \psi_w) - rk\cos\phi \\ Y &= ra\sin(\psi_a - \psi_w) + rk\sin\phi \\ Z &= l\sin\theta \end{aligned}$$

The distances are approximate since any line curvature or stretch has been ignored.

SITEDATA performs all these calculations and stores the results (X, Y, Z, ra, ψ_r, ψ_a, $\psi_{a,\mathrm{ref}}$) in the data summary file. A logarithmic fit for the wind profile, using the mean wind values at 10 and 22 m is used to extrapolate the windspeed to the kite height. The roughness length and friction velocity are both stored in the summary array, and the estimated mean windspeed at kite height (W_z) is used to calculate a mean time lag for wind eddies to travel from the kite to the anemometers (lag = X/W_z). This time lag is also stored.

Kite parameters

SITEDATA stores important kite and line parameters relating to the experiment for use by later analysis programs. Figure 53 shows the definitions used for the bridle angles of the kites flown in these experiments.

5.2 Raw Data Analysis

Five programs are included in this group. Two provide displays of the data, which may be used either to check details in the data files, or to provide a more qualitative impression of the data. The remaining three programs calculate various statistical measures of the data for a more quantitative analysis.

5.2.1 Program ANGLEPLOT

ANGLEPLOT produces kite locus plots, with inclination plotted against azimuth for a specified period during the experiment. If the range is chosen with a small time step, then detailed manoeuvres can be studied. If instead a much longer period of the kite's flight is sampled, then the resulting cloud of points shows the positions explored, and the cloud's density gives the amount of time spent in each region. To provide clearer plots, several consecutive data points may be averaged for each point plotted. An example of the output is shown in figure 54. The upper example is a scatter plot, and the other two are kite loci, where the kite's path in the inclination -azimuth plane is shown.

5.2.2 Program DATAPLOTv2

DATAPLOTv2 provides a fully detailed plot of the most important experiment measurements. It displays information from a 300 record segment of the raw data file, plotting the kiteline inclination, azimuth and tension along with the windspeed and its vertical and cross-wind components (as measured at 22 m). The data summary file is used so the output is correctly calibrated.

An example plot is shown in figure 55. The information displayed allows a qualitative examination of the data. This is a very useful check on some of the more complex analysis programs, in that any results derived must at the very least be consistent with the basic information displayed by DATAPLOTv2.

5.2.3 Program STATS1v5

This is probably the most important data analysis program here. It calculates means and standard deviations for each of the data channels, as well as for several derived quantities such as angular velocity and log(reaction). These are all interpreted as dimensional values or derived coefficients before finally being stored in the results data file. Table 9 lists the quantities stored which have been calculated from the raw data by STATS1v5. This program has developed with the analysis so some of the results stored are now redundant.

The program runs in two stages. It first passes through a specified range of the raw data calculating a set of sums. In the second stage these sums are interpreted as quantities relevant to kite performance, eg. mean tension, lift coefficients, etc. These results are all stored for further analysis.

Raw data sums calculated

Several parameters need to be chosen to control the data analysed. Apart from specifying the raw data to be used, the main parameter is an averaging period (AVG). This is used to define rates of change for several quantities. The value of the time lag for the wind between the kite and the anemometers is also used. The wind data is delayed by this lag in an attempt to use the wind data relevant to the tether measurements being processed.

Channels 1..8: the linear and squared sum is calculated for each of these channels (the raw data values are summed, undimensionalised).

Channels 9..11, 12..14: using the dimensionalised vane readings V_j (j = 1..3) the following sums are evaluated for each triad: V_j and V_jV_k , j,k = 1..3

All the following sums are evaluated within a separate summing procedure, which is used every AVG records (where AVG is the averaging period specified for STATS1v5). There are two reasons for using this separate summing procedure. Firstly, some quantities involve rates of change, and these are only defined over a suitable averaging period. Secondly, some of these quantities use more involved mathematical calculations which tend to be comparatively slow to execute. It thus speeds up the program significantly with little loss of information if they are only evaluated every AVG records rather than for every single record.

Kite tangential velocity: inclination and azimuth are averaged over AVG records along with their average rates of change over that period. The kite velocity (V_k) at line length (l) over that period is:

$$V_k^2 = l\left(\dot{\theta}^2 + (\dot{\phi}\cos\theta)^2\right)$$

Kite flight angle: this is the angle subtended by the kiteline and the downwind direction, and is equal to $cos^{-1}(\cos\theta\cos\phi)$. Every AVG records the mean inclination and azimuth over that period are calculated and used to evaluate the kite flight angle. Both the linear and squared sums are evaluated.

log(windspeed): the average windspeed aver a period of length AVG is calculated, and its logarithm to base 10 summed. Logarithms are used to make any power-law relationship between variables more apparent. To simplify the computation, the log of the windspeed squared is calculated rather than have to take a square root each time. This just means that the result is doubled. Since the wind speed doesn't have significant amounts of energy at high frequencies, no valuable information is lost by only evaluating this sum every AVG records rather than every single one.

log(apparent windspeed): since in general a kite moves about, its apparent windspeed, which determines the forces on it, is different from the windspeed measured by a stationary anemometer. In an attempt to allow for this an estimate of the apparent windspeed is calculated.

$$\begin{aligned} \mathbf{V}_a &= \mathbf{V}_w - \mathbf{V}_k \\ \text{thus } V_a^2 &= V_w^2 - 2\mathbf{V}_w \cdot \mathbf{V}_k + V_k^2 \end{aligned}$$

The subscripts are for the apparent (a), kite (k) and wind (w) velocities.

The cross term is ignored in these calculations, its contribution is assumed to be negligible. This introduces only a very small error of typically 0.2 %. Section 6.3.6 gives details. The remaining expression is then simply the sum of the squared kite and wind velocities, both of which are evaluated as described above. The log of this sum of squares is the quantity summed.

log(reaction): for analysis of kite performance the reaction force is more fundamental than the line tension. It is calculated using the following equation,

$$\begin{aligned} \mathbf{R} + \mathbf{T} + \mathbf{w} &= 0 \\ R^2 &= T^2 + 2\mathbf{T} \cdot \mathbf{w} + w^2 \text{ kite values} \\ &= T^2 + 2TW\sin\theta + w^2 \text{ tether values} \end{aligned} \tag{5.1}$$

$\mathbf{R}$ = reaction, $\mathbf{T}$ = tension, $\mathbf{w}$ = kite weight. Again it is the logarithm of this quantity which is summed for later analysis.

Interpretation of raw data sums

Means and variances are calculated from these sums, and interpreted as to obtain the quantities listed in table 9. The data file in which the results are stored is handle

by program KITEDATA (described later). The method used to obtain each of the stored quantities is now described.

$< i >$ means quantity number i evaluated here. This shorthand is used for those quantities which are derived from earlier ones.

1..6: inclination and azimuth data are read directly from raw data channels 1 and 2. The data summary file indicates which channel has been used for tension, and also supplies the slopes and intercepts to transform raw data values into their dimensional counterparts. The mean and standard deviation are calculated from the sums evaluated. Angles are stored as degrees and tensions in Newtons.

7..14: to obtain these results, the 9 sums obtained for each triad are used with the wind rotation matrix (LAB).

$$
\begin{aligned}
W_{0i} &= LAB_{ij}V_j \\
s(W_{0i}) &= \left[\frac{\Sigma W_{0i}^2 - \Sigma^2 W_{0i}/N}{(N-1)^{1/2}}\right]^{1/2} \\
\text{where} &\quad \text{(summing over repeated suffices)} \\
\Sigma W_{0i} &= LAB_{ij}\Sigma V_j \\
\Sigma W_{0i}^2 &= LAB_{ij}LAB_{ik}\Sigma V_j V_k
\end{aligned}
$$

The quantities for the total vector are given by,

$$
\begin{aligned}
W &= \left[W_{01}^2 + W_{02}^2 + W_{03}^2\right]^{1/2} \\
W &= \left[s^2(W_{01}) + s^2(W_{02}) + s^2(W_{03})\right]^{1/2}
\end{aligned}
$$

Those values considered to be most relevant to the later analysis are stored in the results file.

15,16: as for channels 1..8 the linear and squared sums are used to give the mean and standard deviation, noting however that since the angle is only evaluated every AVG records, the effective number of data points is N' = N div AVG and not N. The two quantities are stored in units of degrees.

17: the line specification (stored in the data summary file) and windspeed at 10 m are used to estimate the line curvature. This correction applied to the mean line inclination at the tether gives the estimated line inclination at the kite. This is expected to be a more reliable measure of kite performance than the tether inclination. The difference between the two inclinations should be no more than a few degrees : anything greater indicates that the results should be treated with caution, since the tension vector changes significantly along the kiteline.

The line curvature theory of section 3 is used to extrapolate the tether tension and angles to the kite. This correction is first order only, ignoring any wind profile and treating the line as a single rigid link. However, for small curvatures this correction should be all that is required. This mean inclination at the kite is stored in units of degrees.

18,19: these values are left blank by STATS1v5, to be used by KITEDATA, the program which analyses the results data files.

20: the bridle angle used to characterise the bridle setting used.

21: as described above, the kite velocity is calculated from the rates of change of line inclination and azimuth (defined over AVG) and the line length. Since the mean velocity will be very small for any kite returning close to its original position, the root mean square velocity is a more useful measure

$V_{k,\mathrm{rms}} = [\Sigma V_k^2/N']^{1/2}$

22: the summing procedure calculates the sum of $\log(W_{22}^2 + V_k^2)$ Dividing by N' gives the mean values stored.

23: The tension vector extrapolated to the kite and the kite weight together give the aerodynamic reaction at the kite as:

$$R^2 = (mg)^2 + 2mgT_k \sin\theta_k + T_k^2$$

R is stored in the data file in Newtons.

24: this is simply $< 6 > / < 23 >$ and gives a non-dimensional measure of the tension variation.

25: the summing procedure calculates the sum of $\log(R^2)$. Dividing by N' gives the mean value stored.

26..29, 33..36, 46..49: these force coefficients are obtained by dividing the relevant force by the dynamic pressure multiplied by the kite area. The dynamic pressure is based on the kite's apparent wind velocity,

$$q = \frac{1}{2}\rho(W^2 + s^2(u) + s^2(v) + s^2(w) + V_k^2)$$

The lift and drag are defined with respect to the mean wind direction over the sampling period.

$$\mathbf{ew} = (u, v, -w)/W$$

ie. the unit wind vector in the tether axes. Then with the tension at the kite (T_k), and kite weight (mg), the reaction, then the lift and drag are obtained as

$$\begin{aligned} \mathbf{R} &= -\mathbf{T}_k - m\mathbf{g} \\ D &= \mathbf{ew}.\mathbf{R} \\ L &= (R^2 - D^2)^{1/2} \end{aligned}$$

The coefficients are then calculated using the dynamic pressure (q) and the kite area (S, from table 2),

$$\begin{aligned} C_R &= R/qS \\ C_D &= D/qS \\ C_L &= L/qS \end{aligned}$$

The coefficients are stored in the order C_R, C_L, C_L2, C_D (for locations 26..29 respectively).

These coefficients, when corrected for the estimated windspeed at the kite height using a logarithmic profile, are stored at locations 33..36.

A further correction is applied by using the flight angle to define the relevant lift and drag components rather than the mean kite azimuth and inclination. A kite which moves in an arc about the downwind direction may have a high lift to drag ratio but show up poorly if only the mean azimuth and inclination are used as for the previous sets of coefficients. These coefficients are stored at 46..49.

30,31: these two angles are calculated from the mean wind components at 22 m over the sampling period:

$$\begin{aligned} \text{azimuth} &= \tan^{-1}(v/u) \\ \text{inclination} &= \tan^{-1}(w/(u^2+v^2))^{1/2} \end{aligned} \tag{5.2}$$

The azimuth and inclination are stored as items 30 and 31 respectively (in units of degrees).

32, 50: the summing procedure gives the sum of $\log(W^2)$.

37..40, 52..57: these are the parameters used in calculating the sums from from the raw data files, and are respectively,

37: the averaging period (AVG, in records) used to define the kite velocity, kite flight angle and the log sums,

38: LAG (in records) allowed for between the anemometers and the tether data,

39: the first record analysed,

40: the number of records analysed (N).

52..54: kiteline mass, diameter and length respectively

55, 56: kite mass and lifting area

57: air density

These values allow any results to be traced back to the original data for checking.

41, 42: the logarithmic wind profile model is used to extrapolate the mean wind from 22 m (W_{22}) to that at the kite height (W_z). The standard deviation is given by its 22 m value multiplied by the ratio W_z/W_{22}.

43: $< 43 >=< 21 > / < 42 >$

44, 51: $< 32 >$ is scaled to kite height by adding twice the log of the ratio W_z/W_{22} to $< 32 >$. $< 51 >=< 44 > /2$.

An important precaution with a program such as this is to check all operations thoroughly, to ensure that the program is doing exactly what it is intended to do. This has been done for this program by comparing its results with values calculated independently by hand from real data values. The program appears to be operating correctly, no discrepancies have been found.

5.2.4 Program STATS2v4 and v5

This program performs a correlation between two of the raw data channels. The results are stored in a correlation data file, and displayed either as a straightforward tabulation of values or plotted to give a visual presentation of the results. The correlation between two channels x(t) and y(t) is calculated from,

$$r(t) = \frac{\sum x_n yn + t - \sum x_n \sum y_{n+t}/N}{\left[\left(\sum x_n^2 - \sum^2 x_n/N\right)\left(\sum y_{n+t}^2 - \sum^2 y_{n+t}/N\right)\right]^{1/2}}$$

The raw data may be used in several ways, with the user free to specify : a) the raw data file to be used, b) the first record sampled, c) the number of records averaged (AVG) for each data point (a simple form of numerical filtering), d) the steplength through the raw data, e) the total number of data points used (N), f) the maximum delay for which the correlation is evaluated, and g) the timestep in which the delay is incremented from 0 to its maximum value.

The two channels correlated may be any two of the following:

1..8: tether data channels,

9..11, 12..14 : wind components u,v,w in standard axes at 10 and 22 m respectively,

15,16: windspeed at 10 and 22 m respectively,

17..19: kite velocity components in tether axes (Oxyz),

20,21: rate of change of inclination and azimuth respectively, defined over AVG records,

22,23: wind azimuth at 10 and 22 m respectively, 24,25 : wind inclination at 10 and 22 m respectively,

26: scalar product of kite and (22 m) wind velocities,

27: power law estimate of windspeed (W) based on tension (T), the coefficient (m) and exponent (n) need specifying. $W = mT^n$

(Channels 17..21 and 26 use the averaging period (AVG) to define the period over which the rate of change is calculated.)

The program evaluates r(t) using the parameters above. In addition to r(t), the value of the denominator (suitably dimensionalised) is stored for the first and last correlations evaluated. These allow a dimensional value of the correlation to be obtained (useful when calculating power spectra from autocorrelations), and any non-stationarity in the data to be detected.

Figure 5.1 shows in a simple diagram the data used for the correlation. As the delay increases, the two data channels correspond to increasingly different periods. For the original definition of the correlation based on integrals over all time, this doesn't lead to any error, but for a finite digital implementation care must be taken to ensure that spurious results are not generated. Essentially this requires that the extra data used at the end of channel 2 is similar in its general features to the data now no longer used at the beginning. Spurious results may be guarded against by keeping the maximum delay always much shorter than the total length of data used. As a check, the values of the denominator for the first and last correlation should show no significant change (no more than a few percent).

If either of the two data sequences contains a linear trend, then this will add a constant to the correlation calculated. The extra variance due to a linear variation through an interval D is $D^2/12$. As long as this is significantly less than the remaining variance, then the linear trend may be ignored. This reveals itself as a constant bias to the results.

STATS2v5 is a revision of v4 to calculate autocorrelations only. It is much faster than v4 since it takes advantage of the data being common to both channels. Apart from that modification, the two programs are identical.

The program has been checked by comparing its results with values calculated independently by hand from real data, and by running it on test data of known functions which can be evaluated analytically. By both of these checks, the program has been found to be operating correctly.

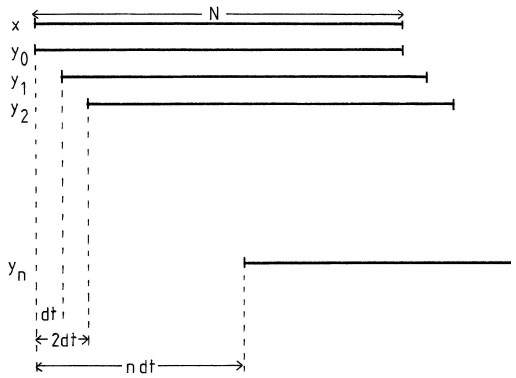

Figure 5.1: Representation of the data correlation method used.

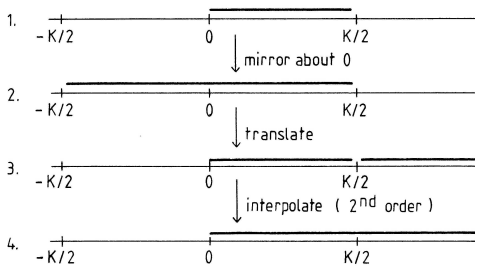

Figure 5.2: Processing correlation output to obtain the power spectrum.

5.2.5 Program STATS3v3

STATS3v3 analyses the raw data into its frequency components. A Fast Fourier Transform algorithm is used, coded to take advantage of the fact that the input data is wholly real. The input takes the form of 2^N real numbers ($N \leq 10$), read from the raw data file, and dimensionalised using the data summary file. This means that the output may be used to calculate the variance of the original data in its correct dimensional units. STATSSvS is also able to access the correlation results files of STATS2v4 to calculate power spectra from autocorrelations. Several forms of display are possible, either a tabulation of the results or one of a range of plot formats.

The expression used to evaluate a frequency component of the original data x(k) (k = 0..K-1) is

$$X(m) \quad = \quad x(k)e^{j2\pi mk/K} \text{ for m = 0..K-1}$$

As with STATS2v4, the input can be derived form the raw data in a variety of ways, specified by the following parameters : a) original raw data file, b) first raw data record number, c) averaging period (AVG) -several data points may be averaged for each point for the FFT, d) steplength (STEP) through the raw data between input values (STEP = AVG normally), e) the number of points to be input (K, must be a power of 2).

The data channel for analysis may be any of the 27 available for the correlation programs STATS2v4 and v5.

Using autocorrelation results

The Fourier transform of an autocorrelation gives the power spectrum of the original data directly. STATS3v3 has been written to use the autocorrelation results produced by STATS2v4 or v5. The following parameters should be specified : a) correlation results file title, b) correlation record number (0..63 are stored in each file), c) the averaging period (AVG correlation points) for each FFT input value, d) steplength through the correlation results between input points, e) the number of points to be analysed (a power of 2, up to a maximum of 2^9).

To use autocorrelation results, the program assumes symmetry about zero, so that the K/2 points read from the correlation results file are mirrored about zero to give the K points input to the FFT. Figure 5.2 shows this procedure in more detail. Three steps are used. In the first, the K/2 points are mirrored about zero to produce K-l points. The next step is to translate the points -(K/2-1)..-1 up by K into K/2+1..K-1; and then finally a second order fit is used for the point x(K/2) giving the K points required for the FFT. The second order fit used is given by :

$$x(K/2) = [4x(K/2 - l) - x(K/2 - 2)]/3$$

Since the correlation results are normalised, the values of the denominator stored along with the correlation results are used to dimensionalise the Fourier transform output.

Interpretation and display of results

The output of the FFT algorithm is a set of K complex numbers, X(m) for m = 0..K-1. These are most usefully presented as intensities $XX^*(m)/K$. Parseval's theorem allows these intensities to be identified with the variance at frequency m, since the total variance is given by the sum of intensities over all non-zero frequencies. Most of the displays here use relative variances, with the variance at frequency m divided by the total variance. These values along with the total variance give all the useful information.

Although the intensities are defined for m = 0..K-1, there is redundancy and all the information is contained by frequencies m = 0..K/2. The original data should have been filtered to remove frequency components above m = K/2 (the Nyquist frequency) so that there is no physical variance at these frequencies : the apparent variance is a feature of the mathematical technique (based on the indistinguishability of positive and negative frequencies for real variables) and the apparent variance may be taken to correspond to m = -(K/2-1)..-1.

Four different displays are used, one tabulation and three plots. The formats use the relative and total variances, and the frequency index m interpreted as a frequency in Hz. Since FFT results tend to be "spiky" the three plots have the option of smoothing the data before plotting. A simple travelling average is used such that the value plotted for component m is 50% true component m and 25% each of the components either side.

$$\begin{aligned} E0 &= \text{the total variance} = \sum_{m\neq 0} X^*X(m)/K^2 \\ e(m) &= E(m)/E0 = \frac{X^*X(m)}{E0K^2} \text{ (the relativ variance)} \\ n(\text{Hz}) &= m.ns/(STEP.K) \end{aligned}$$

n gives frequency as a function of sampling frequency (ns) and steplength through the original data (STEP/records).

a) tabulation : lists the relative variances for m = 1..K/2 and X(0)/K,

b) standard format : relative variance (linear scale) is plotted against frequency (log scale),

c) meteorological format : nE(n)/E0 (linear scale) is plotted against frequency (log scale). Using this format, equal areas under the curve represent equal variances,

d) logarithmic format : log(E(n)/E0) is plotted as a function of frequency (log scale). This reveals any power law relationship between E(n) and n as a straight line.

Correlation file results

The K/2 points read from the correlation file are used to give the K points required for the FFT input as described above. For an autocorrelation, the results of the FFT are already proportional to the variance of the original raw data, and so need to be handled slightly differently than normal FFT results.

The total variance is now given by

$$E'0 = \sum_{m \neq 0} Re[X(m)]/K$$

and the relative variance by

$$e'0 = \frac{Re[X(m)]}{E'0K}$$

These values are then used in the various display procedures.

The correlation denominators stored with the correlation results enable these variances to be dimensioned, so that the dimensioned variance is given by

$$E(m) = E'(m).\text{correlation denominator}$$

The sum over all non-zero frequencies of E(m) gives the full variance. Thus the corresponding sum of E'(m) should be unity. In practice this second sum may be other than unity if insufficient frequency components have been calculated, ie. if the maximum correlation delay is too short or the timestep in the delay too long. Displays from correlation data then include both the correlation denominator giving the full "true" variance for that raw data, and the sum over all non-zero frequencies of E'(m) which by its closeness to unity is an indicator of how completely the autocorrelation has sampled the signal variance.

Transfer functions

The results of the FFT may be stored to calculate transfer functions. A subsidiary program (ARR8FILE) handles these FFT results and performs the calculations.

Program validation

With a program as involved as this, it is important to check its operation thoroughly. Four independent checks are used. Some simple cases have been evaluated by hand from real data. Then test functions have been used whose output may be checked analytically (eg. square wave). A separate program evaluates Fourier transforms using a "longhand" algorithm rather than the Fast Fourier Transform algorithm, and finally the program operation has been checked against versions written by other members of EPRG. On all these tests the program operation is satisfactory.

5.3 Data Record Analysis

This last group of programs used for data analysis use data which has already been partly processed. Only those programs which extend the analysis are described here, many of them simply display the results in one form or another.

5.3.1 Program ANEMOMETER

This program may be used to study the relationship between the wind velocity and line tension. It accesses the results of STATS1v5 (for the mean reaction at the kite (R) and the windspeed extrapolated to kite height (W_z). A power law relationship specified by its coefficient (m) and exponent (n) gives an estimate (W_r) of windspeed from the reaction, and then ANEMOMETER calculates the variance for this estimate relative to W_z. If the results warrant it, the error ($W_z - W_r$) may be fitted by a quadratic function of W_r to remove more of the variance.

5.3.2 Program ARR8FILE

ARR8FILE handles a general file of type array [0..7] of real (in Pascal jargon). This file type is used by many of the subsidiary programs as a general data file, and in particular by program STATS3v3 to store the results of the frequency analysis for transfer function calculations.

The transfer function is the ratio between a system's input and output in the frequency domain. For example, the wind azimuth may be taken as input and the kite azimuth as output : the ratio between corresponding values of their power spectra gives the value of the transfer function for that frequency.

Once the data file has been loaded with the two FFT results, ARR8FILE can be used to pass through the file calculating the ratio between input and output. Since Fourier transforms tend to be "spiky", a travelling average is used to smooth the results and prevent isolated extremes from dominating the results. A triangular weighting function is used, so that if x(n) is the original function and y(n) the smoothed one with window size m, then

$$\begin{aligned} y(n) &= mx(n) + (m-1)[x(n-l) + x(n+l)] \\ &\quad +(m-2)[x(n-2) + x(n+2)] \\ &\quad ... + [x(n-(m-1)) + x(n+(m-1))] \end{aligned}$$

This weighting function is applied before the ratios have been calculated. A similar function (with m = 2) is available to smooth the FFT results displayed by STATS5v5.

5.3.3 Program KITEDATA

This program accesses the result records produced by STATS1v5 and helps analyse them. It can be used to group results together so that experiments with similar bridle settings or windspeeds for example can be compared. Items 18 and 19 of table 9 are completed by KITEDATA. $< 18 >$ is the average line inclination for the group of experiments and $< 19 >$ the deviation from this mean for each experiment. Apart from this, the program is concerned with displaying results in one form or another.

As part of its more general analysis functions, KITEDATA calculates standard statistical sums for linear regressions between variables. These may be obtained for any of the results of STATS1v5, ie. any of the quantities of table 9.

5.3.4 Program KITEDBASE

A conveniant means of storing basic kite information is in a data file. KITEDBASE creates a suitable data file, and allows extra information to be added easily, updating existing records. Table 10 lists all the information contained in these kite database records. Items 0..5 are entered manually and then KITEDBASE calculates the remaining values as indicated in table 10.

Chapter 6

EXPERIMENTS PERFORMED and ANALYSIS PROCEDURE

This section presents the results obtained from the kite experiments and describes the procedure used to analyse them. The results obtained are presented (section 6.1) in the form of a list of all the experiments performed, together with brief meteorological and site details. Several empirical parameters need to be established before the full analysis can be performed, and these are described in section 6.2. This also includes such information as identifying experiments which need special care in their analysis due to very low tension or highly variable winds. The final part of the chapter (6.3) is a quantitative discussion of the errors relating to the experiments and the results obtained.

6.1 Kite Experiments Performed

This section presents a list of all the kite experiments performed, along with brief details of the weather, sites used and kites flown.

6.1.1 Experiments performed

For convenience, Table 11 contains details of all the individual experiments performed. The experiments are grouped together according to the date on which they were performed, and numbered for that day in chronological order. For each experiment, table 11 contains the following information :

Start : the start time of the experiment (hours.minutes) in GMT or BST as appropriate. Previous to the start time quoted, there will have been about a minute of instrument calibration.

T/s : the duration of the experiment in seconds. This figure has been rounded to

the nearest 10 seconds. In some cases, the experiment may consist of two shorter parts, interrupted by either a kite landing, or bad data reception, and the duration quoted is the sum of these two parts.

n/Hz : the sampling frequency used to record the data.

Kite type : indicates which kite was flown (abbreviations are explained at the foot of the table, after the listing for 22-Aug-85). These kites are all described more fully in Table 2 and section 6.1.2 below.

b : the bridle setting. For kites for which this is relevant, the bridle angle (as defined in figure 53) is given, rounded to the nearest degree. For kites with only one bridle setting b is left blank.

Line type : indicates the type of line used. The letter gives the material used (Nylon, Polyester or Kevlar) and the number is the line's rated breaking strength in kgf. Table 6 contains fuller details of line properties.

l / m : the line length used in metres (unstretched length).

Wind dir : the mean wind direction (at 22 m) during the experiment, in degrees (magnetic). This is calculated as described in section 5, and then expressed as the conventional wind direction rather than its heading, a difference of 180°.

vel : mean windspeed in m s^{-1} at 22 m over the period of the experiment.

turb : the mean turbulent intensity at 22 m. Defined over the experiment as the standard deviation of the windspeed divided by the mean windspeed.

Kite posn/m : the mean position of the kite during the experiment relative to the foot of the anemometer tower. All distances are in metres, X : distance of the kite upwind of the anemometers, Y : distance of the kite to the left of the anemometers (as viewed from the tether, across the mean wind), Z : the height of the kite above the ground. These values are calculated assuming the line has no stretch or curvature. Although neither of these assumptions is true in practice, the errors in useful experiments are small enough to be ignored to the accuracy to which these values are required.

For all experiments apart from one, the information recorded comprises the line inclination, azimuth, and tension (at the tether), the wind speed and direction (as measured by the Porton anemometer and wind vane), and the met data from the two mica DVA triads (one each at 10 and 22 m). The one exception is experiment 1 on 26-Nov-84. In this case, the DVA data is so badly corrupted that it is useless : only the tether and Porton data remain valid.

Table 12 lists the flying site used for each day's experiments (following the pattern of figure 45), and gives the local weather forecast for that day, to indicate the general weather conditions. The mean air temperature and pressure are also included, together with the calculated air density according to the ICAO standard atmosphere (see section 5.2 (STATS1v5)).

Figures 56a..k group the experiments according to kite type, showing the wind conditions flown in for each kite tested. Each point corresponds to approximately 5 minutes of kite flight, with different bridle settings differentiated where appropriate.

Some kites have been tested widely, others only in a restricted range of conditions. Figure 56k is included for completeness. These kites are not examined further here since they are either unsuitable as wind probes (Rotor) or are similar to other kites which are more thoroughly tested, and so provide no extra useful information (the Dunford Delta duplicates the (Skycraft) Delta, and the Winged Box the Cody).

As well as providing a catalogue of the experiments performed, Figures 56a..k give an approximate indication of the range of wind speeds over which the kite may be flown, since the usual practice was to attempt to fly any kite thought suitable for the prevailing conditions. For some experiments, the kite spent so little time flying stably, the line curvature was so great, or the load cell thermal drift so large, that the data recorded at the tether is an unreliable record of the kite performance. These experiments are not used for analysis sensitive to these errors.

6.1.2 Kites flown

Altogether, twelve different kites were flown in the experiments, chosen to represent the range of single line kite designs. All of them are included in Table 2, and are illustrated in Plates 1 to 11 (the two Tailed Sleds are identical except for size, the large one is twice the area of the small one). Each of these kites is now described briefly in turn.

Cody : This is a rigidly-braced winged box kite. The central box has two cells, each with a fore and aft compartment, and the wings are built around the diagonals of the box. This particular kite is an Extended Wing Cody, ie. the upper front wings have an extended span compared with a standard Cody. The other wings are basically devices to ensure the kite is kept rigidly braced. Small adjustments in the kite bracing result in comparatively large changes in the kite's natural attitude in the air, making it difficult to repeat experiments exactly.

Delta (Skycraft) : A standard delta design is used, with the two leading edge spars ending about 0.3 m from the nose, and able to move independently. A central spine and a spreader complete the structure, which is flexible enough to adapt to different wind conditions. The line is attached to a small triangular keel which gives the kite some directional stability. In strong winds the tips tend to be pulled in and aft as the covering billows out and the keel deepens.

Dunford Delta : Again a delta planform is used, but this time a one-piece fibreglass leading edge spar curves across the whole span. The keel is formed by two triangles coming down from the covering to a spreader bar, leaving an open channel in between. A tail (a small drogue) is supplied for use.

Flare : This kite was designed and built at Cranfield and intended as a platform for

carrying small payloads. A large area is supported by a fairly light structure, and uses a small box frame on the underside to provide some extra rigidity and vertical surfaces for directional stability. Compared with the Cody, which has about the same span and mass, the Flare is much more flexible and has about twice the lifting area.

Gibson Girl : This is a classic box kite design, produced in the Second World War. It is fairly large, with a light aluminium frame which braces the kite into shape, but is liable to distort in strong winds. The kite is flown edge-on to the wind, using either of two bridle points, one each for light and strong winds.

Malay (Skycraft) : This is a version of the standard Malay kite, but uses a metal former to hold the wings at a definite dihedral angle, rather than having one continuous spar bowed to create the dihedral. The kite may be flown with or without the tail supplied. It is very sensitive to bridling, and will not fly outside a fairly narrow range of settings.

Parafoil : This standard rectangular parafoil is made by Green's of Burnley. It uses small vents on the underside to inflate the wing section, and has one standard bridle setting, which because of the number of shroud lines cannot easily be altered. It is always flown with the drogue supplied.

Rotor : The rotor kite tested is little more than a toy, so its performance is unlikely to be optimal. It is not tested further since other kites are much better suited as anemometers.

Tailed sled : These were built at Cranfield to a pattern given for the TALA kites. The design is a standard plain sled, with no vents or taper. Without a tail the kites are almost unflyable : the tail is crucial to the kites' flight. Of those tested, only the tail supplied with the Malay is suitable. With this tail (5 m long), the kites fly very well in a wide range of wind conditions, although having small areas they generate only small forces. Only one bridle setting is available.

Vented sled : This was again built at Cranfield, this time using a pattern (the Grauel sled) from Pelham (1976). No tail is required, but this sled doesn't have quite the same wind range as the tailed sleds with the Malay tail.

Winged box : The diagonal of a standard single cell box kite is extended to support two triangular wings, with the box flown edge-on to the wind. The bridle allows some adjustment of incidence, but the kite does not have a wide range of wind conditions in which it may be flown. This is because it is fairly heavy, but not strong enough to fly well in strong winds.

6.2 Analysis Procedure

The data from the experiments listed in section 6.1 above is stored on floppy disc. The data preparation programs of section 5.1 need to be used before the main analysis programs described in sections 5.2 and 5.3 can be used.

6.2.1 Data preparation programs

Program FLAGFIND sifts through the data files searching for errors and signal pulses. Those errors found were almost all due to bad recording by the FM tape recorder. Most data files could be corrected, although parts of some files were so badly corrupted that the anemometer data is unusable. These portions are not used in the analysis. Later experiments did not use the FM tape recorder and are practically 100 % error free -those *errors* remaining are all due to sensors going off scale.

All the signal pulses embedded in the data were found, most by FLAGFIND directly, and the remainder by visual inspection of the data file displays. These signals mark the limits of calibration and experiment periods, and are also used to flag special features of the flight -mostly periods to be avoided in the later analysis.

DATASUM/TM prepares the data files for analysis. The calibration periods at the start and end of the experiment allow trends over the experiments to be detected. The inclination and azimuth show no significant change over the duration of any experiment. The tension measurement however is sensitive to air temperature, and many of the data files need to be corrected for drifts in tension offset over the experiment. The criterion used to decide whether a trend needed removal was simply whether or not the change in reference level was greater or less than 1 least significant bit (lsb). If the change is less than 1 lsb, then trend removal can contribute nothing to the data integrity.

Lastly, the mean wind velocities calculated at the start and end of each experiment may be compared to see how much the wind has changed over the experiment. To quantify the variability of the wind, the difference between these two velocities and their mean is divided by that mean, and expressed as a percentage,

$$r\% \quad = \quad \frac{|\underline{W1} - \underline{W2}|}{|\underline{W1} + \underline{W2}|} \cdot 100 \tag{6.1}$$

Figure 57 shows this ratio graphically for each of the kite experiments performed. In neutral conditions, with experiments lasting about 10 minutes and 1 minute calibration periods at either end, r is usually in the range 2..8 %. A level of 10.. 15 % or greater is chosen to identify those experiments for which the non -stationarity of the wind is significant. This level is somewhat subjective, but seems to be a

suitable value for the experiments performed. Most of the winter experiments fall below this threshold, but those recorded during June and August, especially, tend to be significantly non-stationary by this criterion. This information is used to indicate those experiments needing extra care in their analysis (especially correlations and frequency analysis), rather than to exclude the data as unusable. In fact, those experiments with significant variation in the wind are useful in testing the response of kites to changing wind conditions.

As each experiment was being recorded, a record was kept of any significant features of the flight. These features have all been recorded on each experiment's visual log (produced by DATALOG/TM), together with signal pulse positions and important errors detected, so that the log represents a complete, compact record for each experiment.

6.2.2 Data analysis parameters

The data recorded during each experiment comprises a simultaneous record of the wind velocity at the anemometers and the line tension vector at the tether. Because of the short line lengths and relatively high wave speeds along the kiteline, the tension at the tether may be taken to represent the tension at the kite quite closely (see section 3). The kite always flies some distance away from the anemometers and is often moving relative to the tether, so that the wind information does not directly represent the wind experienced by the kite. An allowance is made for this in four ways.

a) due to the distance of the kite upwind of the anemometers there is a lag between the wind experienced by the kite and that measured at the anemometers.

b) an estimate of kite velocity is required to be able to analyse the measurements in terms of the apparent wind at the kite rather than just the mean wind velocity. The apparent wind is the difference between the kite and wind velocities, and is the wind experienced by the kite.

c) since the wind structure changes, in time, as it is transported downwind at the mean wind velocity, and in space, from the kite to the anemometers, a suitable averaging period needs to be defined so that the fluctuations in the wind at one position relative to the other become negligible. This averaging period must take account of the separation between kite and anemometers, the scale of typical variations in the wind, and the behaviour of the kite, so that the results obtained are representative of the general kite performance rather than just particular features of individual kite manoeuvres.

d) the kite does not generally fly at exactly the same height as one of the anemometer triads, and so a correction for the variation of windspeed with height is required.

a) Lag for separation of kite and anemometers

Table 11 includes information on the mean kite position relative to the anemometers (see section 6.1.1). Program DATASUM/TM, which calculates these values, extrapolates the mean winds over the experiment (at 10m and 22 m) logarithmically to obtain a value at the kite height. The downwind separation (X) divided by this windspeed then gives the time lag between the mean kite position and the anemometers, and is stored in the data summary file for each experiment. When STATS1v5 is used, the wind information delayed by this lag relative to the tether data is used, since this is the wind expected to be relevant to the kite at that time.

b) Averaging period to define angular velocity

The kite velocity is obtained from the known line length and the angular velocity. The angular velocity must be defined over a suitable averaging period : if it is chosen too short, the resolution in velocity becomes very poor, and the mean square kite velocity is overestimated. If it is chosen too long, the higher frequency velocity components are filtered out, and the mean square velocity is underestimated.

A suitable compromise is obtained by examining the dependence of calculated velocities on averaging period, and may be checked by comparing calculated velocities with values estimated from a trace of kite angular position against time (as produced by DATAPLOTv2). This analysis has been performed and suggests that the best averaging period is 0.5..0.8 s. This corresponds to between 5 and 10 angle increments per averaging period in the cases examined. The averaging period is dependent on the mean angular velocity, since at higher velocities a sufficient number of increments is obtained in a shorter time.

The averaging period used in practice is in the range 0.5..0.8 s, taking the longer period when the kite is moving more slowly.

c) Averaging period for general kite performance

Most of the interest of this work is in general kite properties, which should be relatively insensitive to details of the wind structure and kite motion. Since the apparent wind exactly at the kite position is not known, these properties cannot be measured instantaneously, but must be obtained from suitable averages. To ensure that the mean wind is representative of the mean wind experienced by the kite, the averaging period used must be long enough to remove fluctuations due to structure in the wind, kite dynamics, and the displacement of anemometers relative to the kite. However, the period should not be so long that the wind has changed significantly during that period, otherwise the kite performance measured is representative only of a broad range of windspeeds. Several different techniques have been used to estimate suitable sample sizes and each is now described.

Program DATASUM/TM uses details of the site geometry and wind velocity to calculate the mean displacement of the kite from the anemometers, and the mean wind velocity. The largest eddies which will effect the anemometers and kite differently are those about as large as this displacement, and will pass by in a time equal to the displacement divided by the mean wind speed. Any one averaging period should be

long enough for several of these eddies to pass by. In practice, *several* is taken to be about 20, since this should allow for the spatial variation in the wind, as well as the fact that although a kite's mean position may be quite close to the anemometers, it may have excursions taking it some distance away from them.

Autocorrelations have been calculated for most experiments, using both the wind and the kite data channels. Some care is needed in interpreting autocorrelations, since, due to the normalisation used, the ratio between variances is investigated rather than the absolute variance. Thus an independent check on the absolute variance is also used.

The decorrelation time has been obtained by visual inspection from each of the autocorrelations calculated, and is used to assess suitable averaging periods for each experiment. These decorrelation times are listed in Table 13, along with the displacement-sized eddy periods discussed above. It can be seen that the largest wind decorrelation times correspond to unstable (convective) weather conditions in the summer months and that the wind decorrelation times are almost always longer than the kite decorrelation times. This is due to a significant amount of medium frequency variance in the kite signals, which generally swamps the lower frequency components. Typical decorrelation times at the kite height are 20..50 s.

Taking the frequency analysis a stage further, the autocorrelations may be used to derive power spectra for the data, and then to produce a transfer function for some aspect of the kite system. The simplest example relates the kite azimuth (as output) and the wind azimuth (as input). At very low frequencies, the kite azimuth follows the wind azimuth exactly. At higher frequencies however, the kite's own motions begin to exaggerate certain frequency components in the wind and the kite azimuth no longer follows the wind azimuth closely. The averaging period should be long enough to contain all the frequencies corresponding to significant kite motions. From considering transfer functions calculated from actual data, the averaging period should be at least 50.. 100 s typically.

Lastly, the data for a few experiments has been analysed using a variety of averaging periods, and the results then combined to provide an average result for each parameter. For example, a 6000 record length may be treated as one length of 6000 records, or two of 3000, three of 2000, etc. In each case the one, two, three,... estimates of the parameter are combined, and the standard deviation calculated for the combined estimate. It has been found that up to a period of about 300 s, the standard deviation decreases steadily for increasing length of averaging period. This suggests that the data should be treated in sections as long as practical, up to 300 s at least.

Taking all these points together indicates that the averaging period should be fairly long, up to about 250..300 s. In practice, this is restricted by the lengths of valid data available, and by underlying non-stationarity in the wind. However, averaging periods of around 300 s prove to be a practical compromise.

d) Wind **Profile Correction**

During experiments, the kite is usually flying close to the 22 m height of the upper anemometer triad, which is the one used for the wind relevant to the kite.

If there is any variation in wind velocity with height then there is a small error if the kite is not exactly at 22 m. This may be corrected to first order by extrapolating the wind velocity from the 10 and 22 m triads to the kite height.

Examination of typical kite heights (Table 11) and the mean windspeeds at 10 and 22 m, shows a mean shear of about 1 % m^{-1} at these heights, and thus a typical correction of a few percent. Cases in which the correction may be much larger are those with the kite flown on 60 m lines. These experiments are used to study the effect of line length rather than to calibrate a kite anemometer, and so second order errors in the windspeed are not crucial.

6.2.3 Remaining analysis details

A final point relevant to the operation of the analysis program STATS1v5 concerns a first order correction to the tether tension made by extrapolating the tether tension up to the kite. This is done by allowing for the kiteline weight and curvature, using the equations derived in section 3. The 10 m windspeed is used in calculating the line windage, and the elasticity of the line is ignored.

6.3 Error Analysis

The previous two sections have described the experiments performed and the analysis procedure. This section reviews the various sources of error affecting the results, and estimates the confidence limits on those results. The list below shows the stages at which errors may be introduced, and briefly describes the types of errors involved.

1. Tether measurements -Line angle and tension, with sources of error including tether arm weight, bearing friction and temperature drift; all of which must be considered relative to the digital resolution used.

2. Tension extrapolation along the kiteline -Both the tension magnitude and line angle change along the line, and some correction must be made for this.

3. Wind measurements -How accurate are the anemometers? How well is the air density known ?

4. Wind velocity extrapolation to the kite position -Since the kite is not at the same place as the anemometers, errors are involved in relating the wind at the anemometers to that expected at the kite.

5. Relating tether and anemometer measurements -This includes consideration of the site geometry and the correction made for the velocity of the kite relative to the tether.

6. Analysis techniques -Simplifying assumptions are made in several of the programs used to analyse the data.

7. Systematic errors -Faults in experiment procedure, equipment, or analysis techniques may bias the results systematically.

Table 13 summarises the main errors and related parameters for the primary measurements of line tension vector and wind velocity. As in Table 11, the experiments are numbered chronologically for each date. The kite type indicates the kite flown in each experiment, using the same abbreviations as Table 11.

The other quantities recorded in table 13 are described here. Three types of error affect line inclination : these are tether arm weight (wt), bearing friction (f) and line curvature (cat). All three errors are given in degrees. The main error affecting the azimuth measurement is bearing friction (f) : the estimated error is again given in degrees. For tension, the largest uncertainty in the measurements is due to changes in offset with temperature. This is indicated by change in a reference reading between calibration periods before and after each kite flight. This reference drift is expressed in Newtons and also as a percentage of the mean line tension during the flight. A positive value indicates that the reference reading increased. For all three of these tension vector components, the significance of the uncertainty depends on its magnitude relative to the digital resolution of the system for that quantity.

The resolutions used are :

inclination :	0.405 °
azimuth :	0.764 °
tension:	0.150 or 0.580 N (depending on range used)

The three parameters listed for the wind are :

dWz/W22 : the correction factor used to extrapolate the 22 m wind velocity to the kite height (using a logarithmic profile)

decorr : the integral time scale, or decorrelation time, obtained from autocorrelations calculated for various wind velocity components

Rka/W : the mean distance between kite and anemometers divided by the 22 m wind velocity. This gives an estimate of the time for eddies the size of this separation to pass.

Not all the columns are filled, since in many cases (eg. inclination wt and f, azimuth f, and tension ref drift) the errors are much smaller than the digital resolution, and contribute negligibly to the total error. Those values included are the larger ones

only. The wind decorrelation times are incomplete since correlations have not been calculated for all experiments : where several values are given in one location several different wind components have been investigated.

The information of table 11 is also relevant to some aspects of the error analysis and is usefully read in parallel with table 13. The following sections discuss the various sources of error in turn, using the scheme itemised above.

6.3.1 Tether measurements

Section 4.1 (Kite Tether) describes the sensors used to measure line angle and tension at the tether, and considers possible sources of error. For the servo potentiometers measuring angle, the main sources of error are friction about the relevant axis (f), the weight of the angle sensing arm (wt), and the linearity of the potentiometer calibration.

The resolution in inclination is 0.405°, so that even in the worst cases the friction error is negligible. The tether arm weight becomes important at low tensions and low inclinations, so that it is the smaller kites in light winds which are effected. The values in table 13 are only average values, there will be instantaneous values greater than these, especially if the line temporarily went slack. This sort of behaviour is noted during the experiment, and the results analysed carefully, avoiding unreliable sections of the data.

The major limitation on the azimuth measurements is the friction about the tether's vertical axis. This is especially serious at low tensions and high inclinations, and as shown in table 13, can easily lead to errors of several degrees. The angle tabulated (f) is that at which the couple due to the line tension misalignment at the end of the tether arm is just sufficient to overcome the bearing friction. Details of angular position less than this value are not reliably measured. Again, the value given is calculated from average values, so at times the error will have been less, at other times much more.

The digital resolution in azimuth is 0.764° : only those errors larger than this are important. It is generally the smaller kites flying at large inclinations or in low winds which are most prone to these errors. Since both angles are measured with servo potentiometers, the underlying linearity of the potentiometers conditions the accuracy to which angle may be measured. Figure 31 shows a typical potentiometer calibration, and indicates that over an interval of 90° (eg. inclination), the linearity is good to about 0.4°, and over the azimuth range of 180° is accurate to about 0.6°. Thus in both cases the linearity corresponds to about one unit of digital resolution over the whole interval.

Tension is the third quantity measured at the tether, and the main problem is the load cell's sensitivity to temperature. From calibration experiments the Kulite load cell is known to have an effective temperature coefficient of about 3.5 NK. Thus the

tension drifts recorded correspond to temperature changes of parts of a Kelvin, over periods of up to 12 minutes. Only those drifts greater than the digital resolution (0.150 N or 0.580 N, depending on range) have been included in table 13. An important feature of the error is its variation over the day. Usually there is an increase initially, followed by a period of fluctuation, and finally a gradual decrease. This corresponds to the daily variation of temperature, so that it is reasonable to assume that the offset variation is roughly linear over an experiment except during those periods when temperatures are likely to fluctuate significantly on timescales of less than about 15 minutes. Thus the offset drift is assumed to be linear except for experiments showing significant drift in the early afternoon or on days when bright sunshine was occasionally blocked by cloud. The corresponding temperature drift errors of the detrended data are thus normally an order of magnitude less than the reference drift.

Examining table 13 shows that for small kites in low winds, especially during summer, the reference drift may be as large as the mean line tension, and so introduces significant uncertainty. The larger kites, with higher tensions, can generally be expected to have tension accurate to about 1 % of mean tension.

All the sensor errors discussed above are static errors. The sensors' dynamic responses are such that the static errors dominate, and so the dynamic responses need no further consideration in the error analysis.

The one remaining aspect of the error analysis for the tether instrumentation is the digital resolution of the system. For the angle measurements, this is straightforward since the ranges of inclination and azimuth are the same for all kites. For tension there is the difficulty of the wide dynamic range which must be accommodated, not only during one kite flight but also from kite to kite. It is not easy to ensure that each kite is well matched to the load cell full scale, and especially with the small kites (low tensions), the mean tension may only correspond to 10..30 digital units. This means that details in the tension

fluctuations at low tension cannot be resolved accurately. However, the statistical measures such as mean and variance are not severely affected until their typical values correspond to only a few (less than 5 say) digital counts.

6.3.2 Tension extrapolation to the kite

The tension vector is measured to the tether, but for the analysis should be known at the kite. The understanding of the kiteline developed in section 3 allows tension to be extrapolated along the line, given a knowledge of the line and the wind. Since most experiments were flown with short lines (30m), the extrapolation is a small correction and can be made in one step.

As an indication of the size of the corrections made, the change in inclination is given in table 13, listed under Inclination (cat). These values are accurate to about 0.3°,

ie. approximately the digital resolution available. With the kites used, the typical line curvature is rarely less than 1°, and may be as much as 5° over 30m. These are mean curvatures, and provide first order corrections to the mean inclination. Some kites allow the line to go slack briefly, and the tether arm may fall quickly even though the kite is still flying well. This behaviour needs to be noted during the flight and the exaggerated kite speed and angle variance estimates should be ignored.

Since most of the experiments flew the kite close to downwind, the azimuth is generally quite small, and not affected significantly by the tension extrapolation from the tether to the kite.

The line tension changes due to the height of the kite above the tether and the line's weight per unit length. Typical line masses are 0.15 to 1.3 g m^{-1} , so that even a change in height by 10 m only changes tension by 0.015 to 0.13 N. Thus the tension extrapolation is easily accurate enough, since the minimum tension resolution is 0.15 N, and kite height can be estimated to within +/- 3 m.

6.3.3 Wind measurements

Section 4.2 describes the equipment used to measure the wind, and includes details of the static and dynamic response of the anemometers. The triads have an effective distance constant of 0.35..0.40 m, and the individual anemometers give a resolution in windspeed of 0.12Z or 0.243 ms (operating at 5 or 10 Hz respectively), although due to the relationship between consecutive readings, the error in the mean over any period should still only be +/- 1 count, ie. 24.3 mm, over that whole period. The digitisation introduces extra variance into the measurements, but this is not significant as long as more than about 5 pulses are received in each sampling period. (5 pulses corresponds to a windspeed of about 0.6 ms if sampling at 5 Hz.).

Thus for the experiments here, the anemometry introduces no significant errors, and responds to all structures in the wind greater than 0.3 5..0.40 m in size.

The air density is calculated from measurements of its mean temperature and pressure during the experiment. During the afternoon, when the experiments were usually performed, both temperature and pressure were normally fairly steady; temperature varying by perhaps +/- 2 K, and pressure by up to 2 mb. These correspond to an uncertainty in air density of up to 0.7 %. Only the calculation of kite force coefficients uses air density.

6.3.4 Wind velocity extrapolation to the kite position

The analysis of kite performance assumes that the wind at the kite's position is known, whereas in the experiments the kite and anemometers may be separated by 5..40 m. It is very important therefore that the procedure for extrapolating wind

measurements at the anemometers to the kite position is well understood.

The displacement between kite and anemometers is analysed into three components : longitudinal (parallel to the mean wind, assumed horizontal), lateral (horizontal, and perpendicular to the mean wind), and vertical. For a uniform site, it may be assumed that horizontal displacements do not affect the long-term statistical properties of the wind, such as mean velocity, variance and power spectrum, and that instantaneous winds differ mostly due to eddies of scales less than the separation.

A simple understanding of how well a measurement of the wind at one point represents that at another is developed in Monin and Yaglom (1971). There it is shown that the integral time scale (or more exactly, twice the integral time scale) obtained from an autocorrelation of wind velocity, gives the size of an independent *sample* of the wind. An experiment lasting for N such periods then effectively takes N samples of the wind velocity. The measured mean velocity is then an estimate of the distribution mean with a confidence level of the distribution standard deviation divided by $N^{0.5}$. Table 13 includes values of the integral time scale (decorr) where these have been evaluated. Since the experiments are usually analysed in lengths of about 300 s, and a typical integral time scale is 5..20 s, the confidence level on the anemometer mean as a representation of the distribution mean is 13..26 % of the distribution standard deviation. Typical standard deviations are 10..25 % of the mean wind, so that the confidence level on mean wind velocities measured over 300 s is usually in the range 1.3..6 % of the mean.

In practice, this is a conservative estimate of the coherence between the two wind velocities (at kite and anemometer), since there is a significant correlation between them. The final column of table 13 gives the timescale for eddies whose size is the separation between kite and anemometer. This shows that a 300 s sample of the wind includes typically 40..100 such eddies. For averaging periods much longer than the separation eddy timescales, the two mean wind velocities may be expected to agree very closely, and the confidence level on the mean wind at the anemometers representing that at the kite will be lower than the 1.3..6 % quoted above, probably closer to 0.5..2 %.

Even at a perfectly uniform site there will be a vertical wind profile : for vertical displacements this must be considered. A two parameter logarithmic fit is used here to model the wind profile, based on the mean winds measured at 10 m and 22 m. Table 13 lists the estimated percentage increase of the wind at kite height relative to the 22 m wind. The accuracy of these values may be estimated by comparing them with values produced by other models of the wind profile. Over all the experiments performed, the mean ratio of windspeed at 22 m and 10 m was 1.201 (+/-0.071). Using this ratio in three profile models gave the results of table 6.1, ie. the mean windspeed at 27 m is 4..7 % higher than that at 22 m.

The logarithmic fit best represents the physics of the wind profile, and so is probably the most reliable one to use. Its close agreement with the exponential model suggests a tolerance of about 0.5 % on the values shown, or equivalently about 0.1 % m. The linear fit overestimates the mean wind gradient by approximately 0.5 % m at about

Profile	$(W_{27} - W_{22})/W_{22}$ / %	Remarks
logarithmic	4.3	z(rough) = 0.198 m
exponential	4.9	exponent = 0.232
linear	7.0	slope = 1.68 % m^{-1}

Table 6.1: Comparison of wind profile models using parameters appropriate to the experiment site.

25 m : its only virtue is its mathematical robustness and simplicity.

6.3.5 Relating tether and anemometer measurements

This section considers the relationship between the tether and anemometer measurements in two ways. Firstly, the site geometry measurements are used to relate the kite position and direction to the anemometer position and wind direction, and secondly, the change in kite position is used to estimate a kite velocity relative to the ground, which is combined with the local wind velocity to give the apparent wind velocity experienced by the kite.

The site layout bearings are accurate to about +/-2° (tether reference direction, anemometer bearing from tether, and anemometer reference direction), so that the mean wind direction, which is nominally at tether azimuth = 0, may in fact be in error by +/- 6°. Thus a kite flying exactly along the mean wind may have its azimuth recorded anywhere in the range +/- 6°.

The site layout distances are accurate to 0.3 m, as is the unstretched line length (usually nominally 30 m). In flight, the line stretches by up to 10 % (eg. nylon line at 50 % bs, figure 23a), giving an uncertainty of an extra 1..3 m on the 30 m line length assumed. The line curvature is typically $1..5^0$ (table 13) and the site is effectively level. Combining all these values gives an underestimate of kite height of up to 3 m, and in position relative to the anemometers of +/- 3 m.

The procedure used to estimate kite velocity relative to the ground simply assumes a fixed line length, and uses changes in the kite's angular position over a suitable averaging period (section 6.2.2b). This technique is accurate to within about 15 %, which, since the root mean square kite velocity is roughly equal to the wind standard deviation, corresponds to an error in kite speed estimate of 1.5..4 % of the wind velocity.

There are several simplifications assumed; firstly, the kite's radial velocity has been ignored. Observations so far do not suggest it is an important factor, which is a little surprising since tension fluctuations can be quite rapid, and may correspond to movements by the kite of several metres. Possible reasons for the lack of effect include that the magnitude of these fast changes is fairly small, that the kite responds dynamically during these rapid changes in tension, and the quasi-static response assumed otherwise is not relevant, or that an easily stretched line (eg. nylon relative

to Kevlar) tends to act only as a filter on the tension fluctuations and doesn't modify kite behaviour significantly. Experiments have been performed with lines of different material, so that any significant effect due to the kite's radial velocity should be apparent.

A second simplification is to ignore changes in line curvature. Generally, the changes are very small, and so correspond to low velocities. However, if the line goes slack, suddenly giving a large curvature, this may appear as an unrealistically high value for the kite velocity. This is guarded against by noting *line flopping* in the experiment log during the kite flight, and then avoiding such sections of the data in later analysis.

6.3.6 Analysis techniques

Section 5 describes the programs used to analyse the information collected, and the various types of results obtained. Several of the programs use simplifying assumptions to make the analysis quicker and more straightforward. In most circumstances, the effect of these assumptions on the accuracy of the results is negligible, but it is important to be aware of the assumptions and their implications, so that those cases for which they do not work well may be identified.

One of the more important assumptions made is that the wind may be treated as a stationary variable, ie. that its statistical properties do not change significantly. This is hardly ever exactly correct -figure 57 shows how variable the wind can be. In practice, a check is kept on the non-stationarity of the wind using such tools as noting drifts in the mean wind velocity and autocorrelation results. If significant non-stationarity is found then related results are treated with caution. The effect of non-stationarity is to smear wind ranges, ie. a kite studied in a wind changing from 6 to 8 ms should show characteristics of the whole range. Frequency analysis techniques are also affected, since the stationary data for which the techniques are normally intended in now contaminated by an underlying trend. Both these effects are usually small, but occasionally they may become important.

A second simplifying assumption concerns the calculation of the apparent wind velocity ($\underline{V_a}$) from the measured velocity ($\underline{W}$) and the kite's velocity ($\underline{V_k}$),

$$\underline{V_a} = \underline{W} - \underline{V_k} \tag{6.2}$$

$$V_a^2 = W^2 - 2\underline{W} \cdot \underline{V_k} + V_k^2 \tag{6.3}$$

The square of the apparent wind involves the scalar product of kite and wind velocity, which is complicated and time-consuming to calculate. It is assumed that the mean value of the scalar product is negligible, much simplifying the calculation. This assumption is justified since calculations of a few specific examples show that the scalar product is typically no more than about 0.2 % of the squared apparent velocity, and so may be safely ignored. The reason for this low value is that it is the kite

position rather than the kite velocity which is well correlated with the wind velocity components.

These are two examples of simplifying assumptions made in the analysis techniques. There are others, but the intention is to keep the errors due to such assumptions less than about 0.5 %, so that they do not contribute significantly to the total uncertainty in the results.

6.3.7 Systematic errors

This section is more of a disclaimer than a quantitative analysis of system errors. The whole experiment system includes many different stages, from the basic experiment procedure, such as assembling equipment, making notes, through all the electronic circuits designed and built, to the programs used to analyse the information and obtain results, and it would be rash to assume that everything has been done perfectly. However, as much as is possible, the system has been thoroughly checked, and any unusual behaviour followed up until either a fault has been found or something interesting discovered. Experience has shown that this is the only realistic way to work.

Chapter 7

KITE PERFORMANCE

This section and the next present results obtained from the experiments listed in section 6. Even from the small range of experiments performed so far, a large amount of information is available which is only reviewed in this section. The aim here is to provide a general summary of kite performance over the range of kites flown and wind conditions tested. The next section takes the analysis further, in its application to kite anemometers, as an example of the use which can be made of the results.

The first section (7.1) briefly summarises the information already presented which is relevant to kite performance analysis. Section 7.1 presents results obtained by other workers (7.1.1), and compares these with the present research as a final calibration of the experiment system (7.1.2). Section 7.2 discusses the most significant features of kite performance, comparing all the kites tested, parameter by parameter. Lastly, section 7.3 draws together the performance characteristics by kite type, and attempts to relate these to features of the design.

7.1 Kite Performance Information

7.1.1 Previous kite performance results

Although kites have been around from before the turn of the century, relatively little "serious" aerodynamic research has been done with them. What useful information there is comes mainly from two periods. Firstly, during the Second World War kites were considered for aerial barrages (to supplement the barrage balloons in strong winds, when the balloons were less effective), and as part of this research effort, several different kites -mostly similar to the Extended Wing Cody flown here -were tested in wind tunnels. Secondly, in the 1960's and 70's aerofoils similar to the Rogallo Wing and Parafoil were tested, either as potential spacecraft reentry vehicles (once the spacecraft had slowed and entered the lower atmosphere), or as

lightweight aerofoils suitable for "aerial jeeps". Section 1 contains more details.

Two sets of kite aerofoil data measured in wind tunnels are both complete enough, and represent aerofoils sufficiently similar to some of the kites tested, to allow a useful comparison to be made between these wind tunnel results and the experiments performed here. The comparisons made use data from Naylor (1940) for the Cody, and Nicolaides and Tragarz (1971) for the Parafoil. The basic data is given in tables 14 and 15. The Cody data for 40 fts is used since this corresponds most closely to the windspeed at which most Cody experiments were performed (in terms of the kite's unit windspeed -table 2).

Jan Nowell's MSc thesis (Nowell, 1984) provides another useful source of kite performance data. Her work was done at Cranfield in July and October 1984, and evaluated various kites for bird-scaring. Three of the kites she used have also been flown in these experiments, and provide a useful comparison : the three kites are the Delta, Malay and the Vented Sled (referred to as the Red Delta, Malay and Double Vented Sled respectively by Nowell). Many other kites were also tested, and the results are a valuable reference for typical line inclinations and windspeed ranges in which those kites will fly.

7.1.2 Comparison between current and previous results

The wind tunnel data obtained from the work by Naylor (1940) and Nicolaides and Tragarz (1971) is suitable for use by the longitudinal kite model programs described in section 2.5 and Appendix B. This basic aerodynamic data allows the static longitudinal behaviour of the two types of kite, the Cody and Parafoil, to be modelled, and then these model results may be compared with those obtained experimentally from the work at Cranfield.

Figures 58a and b show the lift -drag polars obtained for the two kites. The agreement is very encouraging, especially for the Cody.

The Cody used in the Cranfield experiments has a larger wingspan than the one reported by Naylor. Although its higher aspect ratio may be expected to be reflected in lower drag, this is not apparent from the results shown. The points from the experiments in the natural wind appear to reach a lower maximum than those from the wind tunnel. Part of this is due to the averaging over a range of

windspeeds and angles involved in these open air measurements, and part is probably due to the wind turbulence occaisionally stalling the kite. Each point plotted actually represents an average over a range of incidences, and so the points towards the top of the lift -drag polar may include short periods of flight when the kite was stalled, which will lower the average significantly. Note that for both plots, the values obtained from the wind tunnel work provide a rough calibration of incidence against position along the lift -drag curve.

The results for the Parafoil do not show such a close agreement as for the Cody, but

Kite type	Airborne windspeed / m s^{-1}		
	min	max	range
Delta	1.7 (2..3)	10 (9..10,12)	8.3 (8..10)
Malay	2.2 (3)	10.3 (10)	8.1 (7)
Vented sled	1.7 (2..3)	13.3 (10..12)	11.6 (8..10)

Table 7.1: Kite airborne windspeed ranges from (Nowell, 1984) (values in brackets are estimated from current work).

the two experiment situations differ more significantly. For the Cody curves, both kites were fairly closely matched in size and windspeed, whereas for the Parafoil, not only is the wind tunnel model of twice the aspect ratio, but its airspeed is also much higher. Both of these trends favour the wind tunnel results in terms of lower drag, as is borne out by the figure. The general form of the curve is represented well, and interestingly indicates that the Parafoil kite can be flown at or beyond the stall -and must be reasonably stable there. The value of drag for zero lift for the Parafoil is obtained by extrapolating the drag vs lift curve back to the drag axis (zero lift).

Figures 59a,b and c show the comparison results for the Cody in more detail. Again, the agreement between the two sets of data is very pleasing, although the experiment results do not test the model very extensively. The general trends are however very encouraging.

Nowell (1984) contains results of experiments performed with the Delta, Malay and Vented Sled. Table 7.1 presents some of the results for these three kites.

The two sets of estimates agree quite well : the windspeeds quoted by Nowell are minimum and maximum instantaneous values, whereas those quoted for the current research are 5 minute means and tend to be more conservative. The two values given for the Delta maximum correspond to the limit of its steady flight, and the limit for being able to launch safely (even though the flight may not be very steady).

The second comparison relates to the line inclination angles measured. Figure 60 shows results measured by Nowell for the “Red Yellow Delta” alongside values measured here for the Delta (”Red Delta”). The performances are very similar, and show that the characteristics of the Delta are not too sensitive to details of its design. The agreement also lends confidence to the two experiment techniques.

The agreement between previous research and current results is generally good, and gives a measure of the reliability of the other results obtained from experiments. A note of caution however must be sounded, since both “force” comparisons, ie. the Cody and Parafoil, are made with large kites : for the smaller kites which have lower tension, the proportionate error in the force measurements and coefficients is much larger.

7.2 Kite Performance

In this section the main characteristics of kite flight are analysed. The discussion is based on the experiment results obtained. Figures 61, 62 and 64 to 74 each relate to one of the characteristics discussed, and within each figure the letters a..k refer to one of the kite types. All these figures are based on the analysis results of programs STATS1v5 and KITEDATA.

Certain aspects of notation are common to nearly all the plots, but are only mentioned at their first occurrence. Points which are unreliable are indicated by a prime (') if they are shown, and are often omitted from regressions if these are calculated. The two bridle settings of the Gibson are differentiated by using + for the 7/20 mph case (b = 56°) and * for 15/40 mph (b = 90°). The three kites which have not been widely tested are grouped together in plot k, and are the Dunford Delta (d), Rotor (r) and Winged Box (w). If a regression has been calculated, its slope is usually shown alongside the line.

7.2.1 Mean tension

Figures 61..64 show various aspects of the relationship between mean tension and windspeed. Figure 61 gives the basic data which has been analysed to give the results shown in figures 62 and 64.

The mean tension at the tether is given in figure 61 as a function of mean windspeed. Each point represents a linear average over typically 5 minutes' kite flight. For a), d) and e) the points plotted represent several different bridle settings, as indicated by the banding of the points.

The most significant features are,

1 : the typical magnitude of the tension for these kites in the winds tested is in the range 2..100 N;

2 : tension increases steeply with windspeed, and depends strongly on kite size.

There is some scatter about the trend for most of the kites. However, the tension errors due to a 0.5 K change in air temperature (+- 1.8 N) and the digital resolution of the measurements (0.15 or 0.60 N), are responsible for most of the scatter. Other sources of scatter are slight changes in the kite's rigging from flight to flight and the difficulty of averaging out the kite's dynamics. The load cell sensitivity to air temperature and the consequent difficulty in measuring low tensions (< 20 N) accurately is one of the main experiment limitations. Despite this, most of the tension measurements appear accurate to within +- 1 N at worst. The exceptions to this were mostly measured on 21-Aug-85, when the weather was bright and sunny, with plenty of convection (ie. large temperature differentials in the atmosphere).

The three plots for kites with variable bridles show a trend to increased tension

with decreasing bridle angle. Kite incidence tends to increase as the bridle angle decreases, so that, again as expected, tension tends to increase with incidence.

The next three figures (62..64) examine aspects of the relationship between mean tension and windspeed in more detail.

Figure 61 shows that tension increases with windspeed, but does not reveal any particular analytical features of the relationship. To test for some form of power law fit, a log -log plot of aerodynamic reaction against windspeed is used as shown in figure 62. The logarithms are true mean logs, and not logged means. Reaction is used rather than tension since the reaction is independent of kite weight. The windspeed has been corrected for kite height using the mean wind profile during the experiment. The slope of the linear fit gives an estimate of the index of the power law best approximating the relationship:

$$\begin{aligned} \text{If } R &= aW^n \\ \text{then } \log(R) &= \log(a) + n\log(W) \text{ i.e. slope} = \text{n} \end{aligned}$$

For each plot, the slope (n) is given, followed by the estimated percentage standard deviation. The primed points have been omitted from the fit since they are unreliable, usually due to thermal drift.

The most significant point is that none of the slopes are particularly close to the square law (n = 2) which might naively be expected : nearly all the slopes lie in the range 1.0..1.6. A reason for this is shown by the work on the static longitudinal kite model (section 2.5), where the kite weight was shown to cause significant changes in kite incidence with windspeed (figure 18). As a direct comparison with figure 62, figure 63 is a log plot of reaction against windspeed for the longitudinal kite models representing a flat plate and the Cody. The dimensionless windspeed varies from 1.5 to 10 (for the kites tested it is within the range 2..10), and gives slopes of 1.80 and 1.73, with standard deviations of 1.3 and 1.9 % respectively. This suggests that the longitudinal model explains only part of the difference in slope from 2.0, and that there may be effects other than those explained by the model. Such effects may include the three dimensional character of the airflow and the changing shape of a flexible aerofoil (ie. the kite) at different incidences and windspeeds. (The flat plate data is appropriate to an infinite aspect ratio and the Cody data was all recorded at the same airspeed.)

The longitudinal model also demonstrates that the variation of reaction with windspeed does not follow a power law exactly. This gives rise to some of the uncertainty in the slope, probably 1..2 % over the range of windspeeds tested.

Of the kites tested, the Delta shows the most pronounced non-linearity while still having a well-defined trend. This is due to its shape changing under increased wind pressure, as described in section 6.1.

At very high windspeeds it is believed that, provided the kite does not deform (which

in practice is unlikely), the reaction will tend towards a square law dependence on the windspeed. No tests here (or elsewhere, to the author's knowledge) have exceeded about 10 times a kite's unit windspeed to be able to test this idea.

The third set of plots (figure 64) shows the variation of reaction coefficient (C_R) with mean windspeed. For all kites there is a definite trend for C_R to reduce as windspeed increases -this reduction corresponds to the discrepancy between the actual power law index (the slopes of figure 62) and the square law assumed in the definition of C_R. To aid comparison with figure 18, the line parallel to the x-axis corresponds to a windspeed of 5 times that kite's unit windspeed.

The reaction coefficient summarises the attitude and shape of the kite, and depends on both these properties. As explained with the longitudinal models, the balance of moments causes the incidence to change with windspeed; this gives the main variation of C_R with windspeed. Those kites with variable incidence show this variation of C_R. with incidence directly (plots a), d) and e)). As a secondary effect, the changing shape of the kite is also reflected in the reaction coefficient. Thus for the Delta at high windspeeds, C_R starts to fall more steeply.

The magnitude of the reaction coefficient describes how "efficiently" the kite area is used to generate an aerodynamic reaction. Typical values are around 0.6, but at low windspeeds (high incidence), C_R may rise above 1. The Parafoil and the sleds generate comparatively large reactions, while the Gibson (a standard "box-kite") only gives small forces. For a full analysis, these plots should be read in parallel with the lift -drag polars (figure 73) to estimate how well-bridled the kite is to achieve a high C_R. All of the kites here are able to reach values of C_R above 0.5.

Figure 64k is interesting for the large coefficient of the Rotor kite. If pure force is required, the Rotor is very good : however, most of the reaction is drag and not lift. Of the other two kites, the Winged Box has a comparatively large C_R and the Dunford Delta a comparatively low value. K.

7.2.2 Mean angles

Line azimuth and inclination are both measured directly at the tether, and the results are shown in figures 65 and 66. The angles are plotted against the most important factor influencing them, ie. wind azimuth for kite azimuth and windspeed for kite inclination. Since kites in strong winds seem to move along an arc, the kite flight angle, defined as the angle between the line and the mean downwind direction (azimuth = 0), is calculated to test this. Figure 67 shows the variation of kite flight angle with windspeed. For plots 66 and 67 the angle standard deviation is also shown on the same axes, but is discussed later (section 7.2.4).

In figure 65, kite azimuth is plotted against wind azimuth. The most striking feature of these results is the wide variation in kite azimuth, as much as over 40° away from the mean wind direction (azimuth = 0). Most points represent half an experiment

period, with the mean wind defined over the whole experiment; thus a kite which followed the mean wind exactly would have points all lying on a line of unit slope through the origin, with each pair of experiment points symmetrically placed about the origin. Pairs of points from one experiment are shown joined by a dashed line.

Very few real kites approach this ideal performance in azimuth. However, the paired points' slopes are generally close to unity, within the measurement errors, so the main scatter is due to azimuth offset variation from flight to flight. The offset, which may be as large as 20..30°, is due to some asymmetry, usually in the kite construction. Those kites which can be inverted (ie. the sleds) demonstrate this neatly by having two clusters of points either side of the origin (65j shows this most clearly, including a pair of points from one experiment in which the kite crashed and then relaunched itself inside-out; the tailed sleds were almost always flown with the longerons on the inside of the sled).

The asymmetry of the more complex designs is due in part to asymmetry of the rigging, which is easily changed (inadvertently) from flight to flight. The simpler designs are more robust in this respect. Another reason for the scatter in azimuth is simply that some designs are less sensitive to mean wind azimuth than others. The Delta (c)) is comparatively insensitive, while other kites with more vertical surface area seem slightly better. However, those kites always flown with a tail or drogue (g), h) and i)) seem to follow the wind azimuth most closely. This suggests that the design of the kite is no more important than the tail or drogue used with the kite in determining the kite's response to changing wind direction. A tail tends to smooth the kite's response to changes in wind azimuth, so that the kite responds only to larger eddies (from the size of the tail length upwards), and thus should be more stable in response to the small eddies which might otherwise disturb it.

Figure 66 shows the variation of line inclination at the kite with windspeed. Line inclination also depends on wind inclination, but the range of mean wind inclinations explored is small, especially when compared with the changes in mean line inclination due to windspeed, and these therefore dominate the results.

The results for each kite are characterised by the maximum inclination achieved and by the change in inclination with windspeed. Most kite inclinations show an initial rise with windspeed, reaching a peak, and then decreasing.

The initial rise is due to the decreasing importance of kite weight as windspeed increases. This is described by the longitudinal model, and kite inclination is simply the inverse tangent of the ratio of (lift -weight) to drag. Thus a higher inclination corresponds to more lift (L) per unit drag (D). Several kites achieve 60° (L/D = 1.7), and some as high as 65° (L/D = 2.1), but none have been regularly measured much higher than this. Ranking the kites according to highest typical inclinations measured (not necessarily the highest ever recorded), gives :

65°	Cody; Delta
60..65°	Flare; Parafoil
60°	Malay; Tailed Sled (l); Vented Sled; Winged Box
45..55°	Gibson; Tailed Sled (s)

The decrease from the maximum value is generally due to the kite's flight becoming more erratic at higher windspeeds, bringing down the average inclination. To allow for this, the kite flight angle is calculated, and shown in figure 67. Figures 66 and 67 should be read together since the difference between them is due to kite azimuth, which may be important. Most kites show the plateau of figure 66 extended in figure 67, indicating that the kite is in fact moving more in azimuth, and not necessarily changing much in terms of L/D. The decrease in kite flight angle is a truer measure of L/D, and of those kites tested, only the Malay shows a marked reduction in L/D at high windspeeds.

7.2.3 Tension variation

Figure 68 shows plots of variation in tension against variation in windspeed for each kite tested. The tension and windspeed variations are represented by their standard deviations divided by their means for each experiment.

If a standard power law relationship is assumed between reaction (R) and windspeed (W), then

$$\begin{aligned} R &= aW^n \\ \frac{dR}{r} &= n\frac{dW}{W} \end{aligned}$$

Thus the ratio of the proportions of small changes gives another estimate of the power law index. As a first approximation the slopes through the origin for figure 68 are expected to be close to the corresponding slopes shown in figure 62. Table 7.2 lists the two slopes for each kite.

Thus typically, the slope estimated from the tension variation plots (figure 68) is lower than that from the mean reaction plots (figure 62) by 20 %. Of the two sets of plots, those of figure 68 show a much greater scatter of points, so that these slopes are less certainly defined. Some kites show much less scatter than others, eg. the estimated standard deviation on the slope is 2.9 % for the Malay, but 11.5 % for the Gibson (7/20 mph).

A posible reason for the difference in the two power law slope estimates involves the kite's frequency response. Figure 62 measures this variation at low frequencies and figure 68 at higher frequencies. The situation is complicated, but investigations of kite dynamics suggest that a kite's behaviour does change in character with timescale.

kite	power law exponent	
	$\log(R)$ vs $\log(W)$	$s(T)/R$ vs $s(W)/W$
Cody, 74°	1.51	1.40
Delta	1.17	0.91
Flare, 87+°	1.54	1.09
Gibson, 56,90°	1.33, 1.30	1.11, 1.00
Malay	1.01	0.85
Parafoil	1.31	1.34
Tailed sled, large	1.26	0.92
Tailed sled, small	1.65	0.87
Vented sled	1.53	1.07

Table 7.2: Tension vs windspeed: power law estimates using two different methods.

7.2.4 Angle variation

Figures 69..72 show various aspects of the variation of kite angle. There are two main influences : the kite's own unsteadiness, which is a function of its design and the wind conditions, and secondly, the response of the kite to changing wind direction.

The kite's unsteadiness varies most strongly with windspeed. Figures 66 and 67 include plots of inclination and flight angle standard deviations against windspeed. Generally, both are insensitive to windspeed, until at high windspeeds the kite becomes very unsteady and the inclination variance begins to increase, eg. the Delta at W $>$ 9 m s^{-1}. Even in these conditions the flight angle variance is generally constant, implying that the kite tends to restrict itself to an arc about the mean downwind direction. Movements along this arc correspond directly to changes in azimuth but only generate small changes in inclination. This is as observed, if windspeed is taken as an indicator of the kite's unsteadiness and thus motion along the arc, since azimuth variance increases with windspeed whereas that for inclination or flight angle usually does not over the windspeeds tested.

Figure 69 shows the relationship between windspeed and azimuth standard deviation. There is a tendency for the two to be correlated, with some kites showing this much more clearly than others (eg. Parafoil compared to the Gibson). Also, different kites have a different "gain", in that at a given windspeed some show much less variance than others : the steadier the kite, the lower its variance. The two tailed sleds are the steadiest kites measured, especially considering that their experiments include mean windspeeds above 12 m s^{-1} (it was their steadiness which allowed these experiments -other kites wouldn't fly).

The Delta is interesting in that its transition to unsteady flight has been measured. Below 8..9 m s^{-1} its flight is generally very good and reasonably steady, but above this it starts to become very unsteady, until by about 12 m s^{-1} it is unflyable. Other kites show similar behaviour, but are not gradual enough to allow the change to be measured.

Figure 70 shows the kite velocity (rms) as a function of windspeed. This is another measure of kite steadiness -although a kite moving quickly is not necessarily on the verge of being unflyable. Linear least squares fits have been calculated and are shown along with the data. There generally seems to be an intercept in the range 0..3 m s^{-1} , and then a slope of 20..50 %. The intercept is not very well defined, but does hint at a minimum windspeed for flight.

A low value for the slope tends to indicate the steadier kites, but this does not always apply (eg. the Malay scores well on the kite velocity slope but is not a particularly steady kite). The magnitude of the slope indicates that the kite velocities are about the same as the wind standard deviation for the steadiest kites. The less steady kites tend to exaggerate the variation in the wind velocity.

Figures 71 and 72 show the kite's response to changing wind direction (azimuth and inclination respectively). The wind variation is characterised by the crosswind and vertical components of turbulence (normalised by the mean wind velocity) respectively. For both figures, a least squares fit through the origin has been calculated and is shown along with a reference slope corresponding to 1 radian per unit wind variation. Data from a kite able to follow the wind exactly would lie close to this reference slope, so that comparing the actual mean slope with the reference gives an indication of the fidelity of the kite's response to the wind. All three sleds, the Delta at low windspeeds, and the Gibson (15/40 mph) appear to follow the wind fairly closely, while the others exaggerate the wind variation by their own unsteadiness. The Parafoil is particularly poor.

These experiments used comparatively short lines. On longer lines, the limitation of a finite kite velocity will becomes important and prevents the kite from registering small-scale changes in wind azimuth. This is one aspect of the low-pass filter effect of line length discussed in section 2.4.3.

Figure 72 examines kite inclination relative to the vertical component of turbulence. Again, a least squares fit through the origin is shown, along with the unit reference slope. An "ideal" response is not as straightforward as for

azimuth, since the kite's weight is also involved, however, at windspeeds safely above the kite's unit windspeed, the kite should follow changes in wind inclination with unit gain. Changes in inclination are subject to the same filtering due to line length and finite kite velocity as azimuth.

Kites flying steadily tend to have slightly less than unit gain. This may be due to the effect of the kite weight, but probably a more important reason is the inability of the kite to register small / fast changes in inclination down at the tether. Thus, the tailed sleds only register 60..70 % of the vertical component of turbulence by changes in inclination at the tether.

As usual, some kites tend to respond more predictably than others. The Delta (at low windspeeds), Malay and Tailed sleds are good, while the Flare, Gibson and Parafoil are poor.

7.2.5 Force coefficients

The measurements of wind velocity and line tension, together with details of the kites, allow lift and drag coefficients to be calculated. These are shown in figures 73 and 74.

Figure 73 gives the lift-drag polars as measured for each kite. Most of these are similar to the curves for standard aerofoils at incidences below the stall. Few of the kites flown have measured points above the stall -the Parafoil being the main exception. Plots e), h), i) and j), for the Gibson and the sleds, are less conventional, presumably due to their very low aspect ratios. It would be useful to have some wind tunnel results to compare with these plots, but kites such as these do not seem to have been tested. For the smaller kites flying at lower tension, the uncertainty in the points plotted is comparatively large, especially those points measured at low windspeeds (corresponding to large values of the coefficients).

Figures 59a and b provide a valuable comparison between these experiment results and previous values obtained from wind tunnel experiments for the Cody and Parafoil. In both cases, the two sets of points show encouraging agreement.

A useful extra piece of information from these comparisons is an estimate of the actual range of incidences explored by the kites in the natural wind, even with a fixed bridle setting. Thus the Cody probably explores the incidence range 7..20°, and the Parafoil 5..20°.

Lifting line aerofoil theory predicts a variation of drag with lift, with the drag due to lift proportional to the lift squared. This is examined in figure 74 where drag coefficient is plotted as a function of lift coefficient squared. The slope of a line through these points gives an estimate of aspect ratio, and the intercept is the drag at zero lift, ie. the minimum drag coefficient.

$$\begin{aligned} \text{slope} \;=\; m \;&=\; (l+d)/(\pi AR) \\ AR/(1+d) \;&=\; 1/(\pi m) \text{ is the estimate of aspect ratio} \end{aligned}$$

The term d is a small correction for non-elliptical lift distributions, and may be as much as 0.15. Lifting-line theory is implicitly high aspect ratio -the chord-wise extent of the aerofoil is ignored -so it is not strictly applicable to most kites, whose aspect ratios vary from 0.5..4. However, the results often do follow a generally linear trend, and allow useful estimates of effective aspect ratio to be made.

Of the plots shown, those for the smaller kites are hampered by significant uncertainty at low tensions (generally the largest coefficients). The Parafoil provides the best example for estimating the aspect ratio, where a geometric aspect ratio of 1.0 corresponds to an estimated value of 0.85. Since the Parafoil has a rectangular planform, the small correction (d) is about 0.07 (Glauert, 1926), giving a revised estimate of aspect ratio as 0.91.

Typical values of the drag coefficient at zero lift are 0.05..0.20. It is difficult to obtain precise values due to the scatter of the points, and a trend which in some cases (eg. the Cody and Delta) has a significant non-linear component.

The coefficients plotted in figures 73 and 74 are defined using the kite area as given in table 2. A kite with low values of the coefficients indicates one in which the lifting area is not being used to generate large mean pressure differences, as if some parts of the lifting area may be redundant or under-used. Of the kites tested, the Parafoil and the sleds operate at the highest values of the coefficients. (The Rotor is even higher, but at a very low L/D ratio. It has different basic characteristics, so that a direct comparison is not appropriate). If the lifting area has been wrongly estimated, the error in the area will be reflected in the magnitude of the coefficients (overestimating the area reduces the coefficients) and the slope of the drag due to lift plot (over-estimating the area steepens the relationship, ie. underestimates the aspect ratio).

7.3 Kite Types

The previous section analyses kite performance by property, such as mean tension : this section brings together aspects of kite performance by kite type, and provides a summary of the main features of each of the kites tested.

Cody

The Cody is fairly large and complex. It is a strong design, but too heavy to fly in light winds. The Cody version tested (an Extended Wing Cody) would fly in winds of 4..12 m s^{-1} , and is happiest at 6..9 m s^{-1}. It is sensitive to its rigging adjustment, so that some of the scatter in the results is due to slight changes in the rigging, especially its symmetry, between flights. This Cody's unit windspeed is 2.61 m s^{-1} , so that it was never flown in winds strong enough for incidence to be independent of windspeed.

Its mean line inclination (at the kite) and flight angle are close to 70° at best, giving a very good L/D of almost 3. It does not follow the wind azimuth as well as some other kites, but is typical in its response to changes in wind speed and inclination.

Angles of incidence up to the stall can be achieved by changing the bridle, but no points beyond the stall have been measured. This may be due to a comparatively sharp stall. Maximum measured lift coefficient is about 0.6. The aspect ratio estimated from the drag variation with lift is low at only 0.48. This suggests that the kite should be treated as one single aerofoil with chord equal to the kite length. The curvature apparent in the induced drag plot indicates that non-linear terms are important, which again is an indication of the low aspect ratio.

Delta

The Delta tested is typical of the design. It is a light kite, and able to fly in winds as low as 2..3 m s^{-1}. The upper windspeed limit is around 9 m s^{-1} for steady flight. At high speeds the kite deforms significantly, tending to reduce its loading. The measurements show a clear relationship between kite reaction and mean windspeed, but due to the changing shape and incidence of the kite, the relationship is not a simple power law.

Up to 9 m s^{-1} , the Delta follows the wind to a similar degree as other kites, but above this speed its own instability becomes more dominant, and by 12 m s^{-1} makes the kite virtually unflyable, as it veers wildly about the sky. The maximum line inclination achieved is about 70° (L/D = 2.7), comparable with Cody.

Due to the kite's changing shape, its lift-drag polar is not as simple as a rigid aerofoil's. More precise measurements will help in defining the behaviour, but at low windspeeds, extra incidence may cause increased camber, while at high windspeeds the extra loading tends to sweep back the wing tips and deepen the keel, tending to reduce the lifting area.

Flare

The Flare tested here was designed to carry small payloads (up to 1 kg) at windspeeds of 4 m s^{-1} upwards. The framework is quite light and flexible, much more so than the Cody. It has been flown in windspeeds of 3..9 m s^{-1} , and over the range 4..7 ms is extremely steady. The bridle may be adjusted, but all bridle angles greater than about 88° have the same effect since the rear bridle leg is then completely slack. The reaction coefficient is comparatively low, with a maximum measured of 0.75, and typical values around 0.4.

Maximum line inclination is just over 60°, giving a best L/D ratio of about 2. The Flare has complex rigging like the Cody, and it too is sensitive to small changes in symmetry -but not as much as the Cody. It follows the wind azimuth slightly better than the Cody, but is not as good for inclination.

The lift-drag polar is similar to the Cody's, but not as sharply defined, possibly due to the more flexible structure. The geometric aspect ratio is 1.8 compared with 0.94 estimated from the relationship between lift and drag coefficients. The effective lifting area may have been over-estimated by including the horizontal surfaces of the box structure below the main lifting surface -ie. these "stabilising" surfaces provide no extra lift. This over-estimation would account for part of the underestimate of the aspect ratio.

Gibson

This is a classic box kite design. It has two bridle settings; one with a bridle angle of 56° for windspeeds of 7..20 mph, and the other of 90° for 15..40 mph. These two bridle settings are clearly distinguished in the plots of tension or reaction against windspeed, and both show a similar variation with windspeed. Reaction coefficients

are quite low; only 0.5 or 0.25 for the 7..20 and 15..40 mph bridles respectively.

The Gibson does not fly at high angles of inclination -typically only 50..55°, corresponding to a L/D ratio of about 1.3. The mean inclination decreases with increasing windspeed as the kite moves more in azimuth -the flight angle stays more or less constant. The angles are quite variable, so that despite its simple design, the Gibson is not a good indicator of wind direction.

The lift-drag polar shows a comparatively large increase of drag with lift, ie. a low effective aspect ratio, suggesting that the aspect ratio relevant to the kite is closer to the "aspect ratio" of the whole frame than that of the individual panels around the box.

The standard box-kite thus combines a strong structure with flight at a low reaction coefficient, ie. a low loading. Both these help its survivability in strong winds, in keeping with its reputation.

Malay

The Malay (or Eddy) is the standard "kite-shaped" kite with some dihedral added for stability. The model tested has been flown in winds of 4.. 10 m s^{-1} , and has a useable range of 3..10 m s^{-1}

At low windspeeds it has a good performance, but as the windspeed increases above 6 m s^{-1} the shape changes so that its L/D is degraded and also its reaction coefficient decreased. The change in C_R combines with the usual change in incidence with windspeed to give an aerodynamic reaction which is almost directly proportional to windspeed. This direct proportionality is probably related to the good correlation between windspeed fluctuations and tension fluctuations.

The Malay tested is not a very steady flier, so that it is generally a poor indicator of the wind direction -in azimuth, inclination, and its variation.

Despite the apparent change in shape with windspeed, the lift -drag polar still has the usual form. Since the Malay wings taper linearly to a point at the wing-tips, the aspect ratio correction factor (d) is 0.13, giving the corrected aspect ratio estimate of 1.9. This agrees comparatively well with the geometric value of 2.0. Further experiments would confirm this agreement, but the Malay does seem to have quite straightforward lift -drag characteristics : its comparatively high (for a kite) aspect ratio of 2, and simple design probably contribute towards this.

Parafoil

Tension measurements show the Parafoil to be a fairly powerful kite in that it operates at quite high reaction coefficients (0.6.. 1.1). Tension variation with mean windspeed follows a clear trend ($W^{1.3}$), but the relationship between standard deviations of windspeed and tension is not so well defined.

Probably due to its use of a drogue, the Parafoil follows the wind azimuth well, without any strong bias to one side or the other. Its inclination peaks at just over

60° (L/D = 1.75), but falls away at higher windspeeds as its motion in azimuth becomes more pronounced. The flight angle stays constant at around 60° once the windspeed has reached 6..7 m s^{-1} (below this the kite weight reduces the line angle).

High windspeeds make the kite unsteady, so that kite velocity and azimuth variation both show strong dependence on windspeed, but kite inclination and azimuth standard deviations are poorly correlated with the corresponding wind turbulent intensity components.

The lift -drag polar corresponds well with values measured for a parafoil in a wind tunnel (section 7.1.2), allowing for the different aspect ratios, and shows that the Parafoil can be flown stably beyond the maximum lift coefficient in a stalled condition. The estimated aspect ratio (0.91 when corrected for wing planform) agrees well with the geometric value of 1.0.

Tailed sleds

Two tailed sleds were tested, one nominally twice the area of the other, and both were built to the design used for the TALA sleds. The tail is very important, so that with no tail or an unsuitable one, the kites are very erratic fliers, whereas a good tail transforms them into the steadiest kites tested. The tail normally used was 5 m long, and did not twist up. Since both the tailed sleds have a small area and generated small forces, the proportional uncertainty in the measured forces is quite large, and has made interpreting the kite behaviour difficult. This is reflected in the uncertainty of the measured relationships between reaction (coefficient) and windspeed.

Both kites fly happily in windspeeds of from 3..12 m s^{-1} , and appear steady enough to be able to survive in even stronger winds without any difficulty.

The sleds tend to fly at high values of C_R (implying that the true lifting area may be under-estimated, and that their design, with large end-plates to the aerofoil, is able to generate large pressure differentials), with typical values ranging from 0.6 at high windspeeds to over 1.2 at the lowest windspeeds. The variation of tension is not very well measured, and to clarify this aspect of the performance more precise measurements are needed.

Both sleds achieve a steady value of inclination and flight angle, of almost 60° for the large sled and just over 45° for the small one. Probably due to their long tails, both sleds show little bias in azimuth, but the standard deviation of azimuth depends more on windspeed than on the crosswind component of turbulence. Both kites show a good correlation of line inclination standard deviation with the vertical component of turbulence. There is a clear variation of kite velocity with windspeed, but not so steep as to indicate that the kite is becoming unstable.

The calculation of the lift and drag coefficients is subject to the errors involved in measuring the forces, however, the lift -drag polar is much more like that of the Gibson than the other kites. The low aspect ratio of the sleds is partly responsible for this, and also the drag of the tail. The main reason for the difference between

the two sleds is the proportionately more important drag of the tail for the smaller kite. The tail drag coefficient is probably not constant since it is likely to feather in strong winds; this provides a further complication for the relationship between lift and drag coefficients.

Vented sled

The Vented sled behaves similarly to the large tailed sled (they have about the same lifting area). The performance results are again degraded by the inaccuracy of the tension measurements. The kite tested has been flown in winds of 3..9 m s^{-1} : its absolute limits are probably 2..3 and 10..12 m s^{-1}

As with the other sleds the vented sled has a high typical reaction coefficient of 0.7 or greater, and shows the usual variation of reaction coefficient with windspeed.

The kite inclination reaches 60° by 6 m s^{-1}, and then falls away to about 55° at 9 m s^{-1}. Kite flight angle stays constant at about 60° once above 6 m s^{-1}. The kite tested flies about 20° from the mean wind direction -due to some asymmetry in its construction (flying the kite inside-out reverses this bias). A tail was not normally used, and there is more variation in azimuth than for the tailed sleds.

Tension standard deviation is closely correlated with windspeed standard deviation, and (again as for the other sleds) kite velocity shows a close, but not steep, relationship with windspeed. Inclination and azimuth standard deviations are not closely correlated with the relevant turbulent intensity components, suggesting that the vented sled has its own dynamics somewhat independent of wind structure, which are responsible for much of the observed angle variation.

The lift -drag polars are again uncertain due to the inaccurate measurement of low tensions. However, the form is similar to the tailed sleds, ie. typical of a very low aspect ratio.

Miscellaneous

The three kites included in this category are the Dunford Delta, the Rotor and the Winged Box, all of which were only very briefly tested. In general form, the Dunford Delta most resembles the (Skycraft) Delta already tested more fully. The Winged Box is similar to the Cody in that it combines a central box with some extra lifting surface. The Rotor is unlike all the other kites tested, and its performance is also quite different.

The Dunford Delta has a performance similar to the Skycraft Delta (which has been tested more thoroughly), but is not generally quite so good, ie. it does not seem to fly as steadily or with such a high L/D ratio.

The Winged Box is similar to the Cody in most respects, although its maximum inclination and flight angle are not quite as high. It has a large bias in azimuth (over 40° away from the mean wind direction).

The Rotor's main feature is its high reaction coefficient ($C_R > 2$ at 8 m s^{-1}).

The L/D ratio is quite low however (about 0.7), which limits the usefulness of the Rotor for the usual kite applications, such as hoisting payloads, traction, and any tasks requiring the kite to achieve a good altitude. There may however be other applications for which the high reaction coefficient can be used.

Chapter 8

KITE ANEMOMETERS

Kite anemometery is one of several techniques for measuring wind velocities at heights of up to several hundred metres, and has several features making it particularly attractive. The main alternatives are:

a) Tower mounted anemometers -These give the most accurate and reliable readings, but for all but a few special experiment sites, they are prohibitively complicated and expensive. At certain sites they may also be a serious obstruction.

b) Doppler systems -Either light (lidar), radio (radar) or sound (sodar) may be used. Sensitive detectors are needed for the returned signal, along with sophisticated signal processing. These systems also tend to be complicated and expensive although they are more mobile than towers.

c) Tethered balloons -The balloon is used as an aerial platform, either to carry the anemometers itself or by suspending them along the tethering cable. The problem with balloons is that they tend to get blown down in strong winds. They are also fairly bulky and expensive to operate.

d) Free balloons -These have to be tracked, with the wind velocity deduced from their movement (allowing for the balloon's normal rate of ascent). Radiosondes are often carried to transmit information on air temperature and pressure. Because of their horizontal movement, a large number of tracked balloons are needed to study airflow around individual features such as ridges, mountains or coasts, and is often impractical.

e) Aircraft -Either manned or remotely-piloted aircraft may be instrumented as probes to study the lower atmosphere.

These are suited only to very short-term surveys, and are expensive to operate, especially manned aircraft. Large areas can be covered quickly though.

f) Smoke trails -The distortion of a rocket's exhaust trail

indicates local wind velocity. For detailed measurements the trail must be observed carefully, and in strong winds the rockets tend to be unstable.

A good kite anemometer is well suited to measuring wind velocity at heights up to several hundred metres, with an accuracy much better than 1 m s^{-1} (for averages over several minutes). It can also give an indication of the level of turbulence. The system is fairly simple (especially the most vulnerable part, the kite) allowing a low-cost, robust piece of field equipment. The kite's position is controlled by the line length and tether position, *so* that wind velocity can be measured at particular locations. Kites can be flown from most sites, although some, such as the lee of a large obstruction, are not suitable. All kites need a certain minimum windspeed to be able to fly, usually around 2–3 m s^{-1} , so that kites alone cannot measure windspeeds below this. The upper windspeed limit depends on the kite's strength and steadiness and may be up to 30–40 m s^{-1} for a good design.

8.1 Ideal Kite Anemometer

The longitudinal model of section 2.5 indicates that for steady winds, kites can measure windspeed and inclination exactly, using the line inclination and tension at the kite. Kite azimuth gives wind azimuth, and thus the complete wind velocity is known. Practical kite anemometers face several limitations though. The most important one is the unsteadiness of the wind. This transforms the system into one which is dynamic, and so must be analysed more carefully. Suitable averaging periods must be used to obtain useful measurements, and the steadiness of different kites becomes an important factor. Other limitations include the accuracy to which the tension and angles may be measured, although in principle this is not a serious difficulty apart from the usual problems of field measurements. The weight of the kite sets a minimum windspeed for launch, and its strength and steadiness give an upper windspeed limit. The line weight and diameter cause a change in tension and angle along the line and also limit the maximum altitude attainable. The line length and kite size both tend to limit the maximum frequencies measurable.

Ideally, a kite anemometer should have the following properties:

a) able to fly steadily in a wide range of windspeeds,

b) be reliable and accurate in its measurement of windspeed and direction,

c) easily rigged and launched,

d) robust, and able to withstand occasional crashes,

e) have sufficient lift to reach altitudes of several hundred metres,

f) and perhaps enough lift to carry small payloads (up to about 500 g),

g) the instrumentation should be robust and portable, and provide outputs in convenient formats and units.

The kites tested (section 7) are evaluated here for kite anemometry with these ideal characteristics in mind. The next section (8.2) reviews an existing kite anemometer system (TALA). Section 8.3 evaluates the kites for measuring mean wind velocity, and section 8.4 considers their dynamics and how well turbulence is measured. Section 8.5 then draws these together by kite type, identifying the best kites for anemometry.

8.2 Review of existing kite anemometers

The recent use of kites to measure wind velocity comes from work by Dr. C.F. Woodhouse and Ray Holland (Whitney, 1978) who designed and constructed the TALA system. Since 1976 this has been used several times, either to evaluate it against existing systems, or as an active research tool, measuring wind profiles in various locations. No other kite anemometry has been reported.

The available TALA literature falls into three categories. First is that produced by the manufacturer, Approach Fish Inc., consisting of various instruction manuals. Second is a series of evaluations of the system, usually comparing TALA with existing anemometers to check its reliability and accuracy. Third is a smaller group of reports in which it has been used as a research tool.

"Instructions for a Hand-Held Wind Measuring Device (TALA)" (Approach Fish) quotes the results of two wind tunnel calibrations over windspeeds of 2–22 m s^{-1}. Form these, the dependence of windspeed (V, m s^{-1}) on line tension (N, Newtons; assumed at the kite) is given for the standard TALA as,

$$V = 0.5144(N/0.01779)^{0.51} = 4.015N^{0.51}$$

Inverting this relationship gives

$$N = 0.06550V^{1.96}$$

which is very close to a square law -much closer than for any of the kites measured here. This is partly due to the higher windspeeds used in the wind tunnel, since at these speeds, the variation of incidence with windspeed becomes much less important.

The calibrations are quoted for standard temperature and pressure. Corrections for other air densities are presented, and may be as much as 10 %.

The recommended sampling technique is to read windspeed (from a calibrated spring scale) every 2 or 3 seconds for a period of 2 minutes at each altitude. The mean and

variance of these measurements gives estimates of mean windspeed and its standard deviation. The kite height is estimated from the angle of inclination of the kite from the tether and the line length, with a small correction for line curvature.

Baker, Whitney and Hewson (1979) describe several comparisons between conventional tower mounted anemometers and TALA. Heights range from 17–200 m with windspeeds of 7–16 m s^{-1}. Mean winds over periods of 3, 5 or 10 minutes are given, and show agreements of 1–3 % between the tower and TALA. Two versions of the TALA system are used : the spring scale already mentioned, and an electronic version with analogue voltage outputs. The spring scale was read every 15 s for 5 minutes and the analogue voltages were sampled every 4 s for either 3 or (ideally) 10 minutes. The wind decorrelation time is not given, so the number of independent wind measurements made is not known.

Ray Whitney's MSc thesis (1978) contains a full description of the TALA sled, but the experiment results are unreliable.

Kunkel (1981) is an evaluation of the TALA with analogue electronic outputs, based on two years' experience and development. Both TALA kites are used : the standard (0.15 m), and the large one (0.30 m) for use in low winds or to high altitude (500 m instead of 300 m). The digital system developed takes samples every second, and calculates means and standard deviations from these over user -specified sampling periods. The calibrations relating force (F, newtons), windspeed (V, m s^{-1}) and air density (p; .£,,= air density at 55°F and 1013.25 mb) for the two kites are

$$\begin{aligned} V &= 4.0 \left(\frac{\rho}{\rho_0}\right)^{1/2} F^{0.49} \\ V &= 3.86 \frac{\rho}{\rho_0} (-0.639 + F^{1/2} - 0.0238F) \end{aligned}$$

The calibration for the standard TALA can be rewritten for the ICAO standard daytime temperature and pressure (15°C, 1013.25 mb), giving

$$V = 4.016 \left(\frac{\rho}{\rho_0}\right)^{1/2} F^{0.49}$$

This differs slightly from that given in the TALA hand-held model's manual. The ratio difference reaches 9 % by windspeeds of 40 m s^{-1}: no explanation is given for this change in calibration.

As a comparison, the coefficients derived from these calibrations are shown in figure 75 alongside experiment measurements made here. Kunkel's report finishes with examples of some wind profiles measured up to 300 m.

Kaimal, Baynton and Gaynor (1980) report on an experiment organised to compare techniques for measuring winds up to several hundred metres. Each method was

Variable	Kite	No. points	Mean wind	rms difference from tower	
			m s^{-1}	m s^{-1}	
Wind from W	standard	25	4.31	0.96	22
	large	12	8.64	1.72	20
Wind from S	standard	25	4.31	0.82	19
	large	12	8.64	1.15	13

Table 8.1: TALA comparison with standard tower anemometers (taken from Kaimal, Baynton and Gaynor, 1980).

compared with a standard instrumented tower. The calibration quoted is similar to that for the hand-held device but not identical (an exponent of 0.508 rather than 0.510). The report is quite brief, but does mention a simple investigation of kite inclination (ie. altitude) versus windspeed, which supports the results here.

One TALA claim conflicts with this study : they claim that "the maximum effect of catenary drag on the measured tension at the ground is five orders of magnitude smaller than the tension produced by the airfoil itself". The kiteline theory developed in section 3 applied to the TALA system indicates that tension changes of 1 % or more are possible. The discrepancy is probably because TALA have taken the tension change per unit length to be the tension change along the whole line. On lines of several hundred metres, the total change is easily 1 %, and may be as much as 20 % on long lines in light winds.

Apart from this, the comparison is useful. The results are analysed into two orthogonal components, and the TALA measurements compared with those of the standard tower anemometers. Table 8.1 summarises the results.

Each point is assumed to represent an average over several minutes according to the usual TALA practice. These results suggest that TALA is reliable to within about 1 m s^{-1} , which is not as good as the values quoted previously, eg. Baker, Whitney and Hewson (1979). No reasons for this increased error are given.

The University of Hawii has used TALA kites to study wind profiles around the Kahuku headland, Oahu. The work also involved developing an improved tether head with digital data outputs for automatic operation. Eight of these automatic units were used, along with a few of the usual manual units for checking and adding extra detail. Daniels and Oshiro (1982a,b) describe studies made from the beach and the foothills at Kahuku, and Daniels (1982) uses the results to make a study of the turbulence.

The development and experiment work appears to have been thoroughly done. Several problems were encountered and it took a considerable effort to sift through the data to remove unreliable portions. The majority of the data consists of recordings of instantaneous line tension and angles sampled every 2 minutes over periods of several days. In addition, data was recorded every second for periods of about an hour

to allow wind turbulence studies to be made. In parallel with these measurements, the outputs of standard cup anemometers and windvanes were also recorded.

Several aspects of the Kahuku study are particularly relevant to this thesis. Daniels and Oshiro (1982b) describe a comparison in which all eight kites were flown close together (at about 10m lateral spacing). Mean velocities over 4–5 hours agree within about 0.4 m s^{-1} at the lower level (about 25 m) and 0.15 m s^{-1} at the upper level (72–96 m). Especially at the lower level, the variation is partly due to non-uniformity of the site. Correlations between the (2 minute) readings are generally low, indicating significant variance due to the smaller eddies, even at these close spacings. In his turbulence analysis, Daniels (1982) notes that the kite-measured wind spectra show peaks at frequencies in the range 0.1–1.0 Hz, instead of a steady decay. He suggests that this may be due to the kite's motion, as it chops through eddy structures elongated along the mean wind. Stationary anemometers do not sample the wind in the same way, and Daniels suggests that for wind turbine applications the kite may give a more useful measure of the turbulence, since it sees similar structures to a moving turbine blade.

These Kahuku Kite-Wind studies provide useful information about the use of kite anemometers, but no evaluation of different kite designs, or calibration of the kite for turbulence studies has been attempted. In this thesis it is suggested that the peak in the kite measured spectra is more a feature of the kite as a mechanical system than of the way in which the kite measures the wind. The failure to consider kite system dynamics puts Daniels' turbulence analysis in question.

To summarise these reports, it seems that TALA is accurate to better than 1 m s^{-1} for mean windspeeds measured over periods of several minutes. The sled design used is good since it is able to fly in very strong winds, although the kites used are too small to carry any significant payloads. The turbulence estimates have not been reported in detail, although work at Cranfield suggests that the system dynamics are important. This is a factor which has not been explored in any of these TALA reports.

8.3 Mean Velocity Analysis

This mean velocity analysis is based on the 5 minute average results reported in section 7. The correlation and frequency analysis work suggests that there should be no significant change in results for small changes in this averaging period.

8.3.1 Mean windspeed

To calibrate a kite for windspeed, a relationship giving windspeed as a function of line tension and perhaps angle is required. The longitudinal model of section 2.5 shows that tension is almost independent of wind inclination, and thus to a good

approximation the tension alone gives the windspeed. At this stage, to take out any variation due to the kite's weight, the aerodynamic reaction rather than the line tension is used. By analogy with the square law "expected", a power law fit is used as a first approximation to the relationship between windspeed and reaction.

The exponent (n) of the power law is given by the slopes from figure 62. A least squares fit of reaction to the power n against windspeed (corrected for kite height) gives the coefficient (m) for the power law relationship. Figure 76 shows calibrations based on these relationships for most kites tested. The scatter is typically 0.5 m s^{-1} , although some kites are better than others. The small kites are handicapped by larger relative errors in the tension measurements, but even so the scatter is not significantly worse than for the large kites. However, removing unreliable data points has left some of the kites with only a small number of valid ones, eg. the large Tailed Sled.

The calibration correction of figure 76 shows a clear trend for some of the kites. This can be partly removed by adding a quadratic correction to the power law fit, and has been done for the Delta and large Tailed Sled, as shown in figure 77. With this extra iteration, the calibration is good to within about O.2 m s^{-1} over a windspeed range of almost 10 m s^{-1}. The Delta and the Tailed Sled are the best kites for measuring windspeed in conditions similar to those of the calibration experiments.

In section 8.4.1 below, there is a discussion of kite dynamics based on these experiment results. There it is suggested that the line length and kite drag combine to give a pendulum motion, as described in section 2.4.4, which is important for the system's dynamics and which affects large kites on short lines most strongly. Thus much of the scatter in the calibration of the Cody and Parafoil may be due to this pendulum motion, and may be significantly reduced on longer lines. Unfortunately, no calibrations have been possible using lines longer than 30m since the anemometer tower height is only 25 m. If longer lines do increase the damping for these large kites, then they may be best suited to higher altitudes. They also have the advantage of being able to carry small payloads.

These calibrations are based on 5 minute averages of windspeed and reaction. Correlations have been calculated between the measured windspeed and that estimated from the tension for various averaging periods to see how sensitive the calibrations are to the averaging period used. Figure 78 shows the results of these correlations. The absolute value of the correlation depends on the closeness of the fit as well as the averaging time, so to study the averaging time only, the shape of the curves is most important, and especially where they start to fall steeply. Above about 30 s most of the correlations have levelled off, thus small changes in averaging periods longer than this are not important. The larger kites tend to have less uniform curves, indicating features of the motion which favour particular timescales. The smaller kites have smoother curves, probably due to more effective damping of their motion, and their falls start around 10–20 s. The Tailed Sled and the Gibson have the smoothest curves, followed by the Delta and the Malay. This corresponds to the Delta and Malay being slightly less steady than the Sleds or Gibson, especially in

strong winds.

8.3.2 Mean wind direction

Of the two angles measured, the range of mean inclinations explored is too small to be able to report any firm conclusions from the experiments. However, the longitudinal model indicates that to a good approximation, the change in mean line inclination is equal to the change in mean wind inclination. These changes in wind inclination can be measured, given a reference inclination (horizontal wind), and using a suitable averaging period so that kite dynamics do not interfere.

A simple model for a kite's response to changes in inclination described in section 2.4.3, suggests a low pass filter effect of line length on angle measurements.The time constant (t) is a function of line length (1) and kite velocity per unit error angle (V), and is given by

$$t = 2\pi l/V$$

Values of 30 m (l) and 10 m s^{-1} (V) give a time constant of about 20 s. It can be seen that on long lines, kites will not be able to measure changes in angle accurately unless over periods of several minutes or more. An added complication is that the kite changes its position as it adjusts to the new line inclination, and moves through any features much smaller than the line length.

Figure 65 has already presented plots of mean kite azimuth against wind azimuth. The most reliable kites are those with tails, which appear to damp down unsteadiness in azimuth. For these kites, eg. Tailed Sleds, mean azimuth measurements are accurate to within about 5°.

A simple stability model (section 2.4.4) similar to that for the inclination, but taking its basic ingredients as the kite's mass, drag and line length, indicates a pendulum motion. The period (t) of the natural frequency is a function of windspeed (W), line length (l), kite solidity (μ), size (L) and drag coefficient (C_R) given by :

$$t = \frac{2\pi}{W}\left(\frac{2lL\mu}{C_D}\right)^{1/2}$$

Inserting typical values ($W = 7$ m s^{-1} ,$l = 30$ m, $\mu = 0.2$, $C_R = 0.3$) gives a period of 6 s. This corresponds fairly well with measured kite motions, although in practice the period is usually 10 s or more. The difference may be due to the chaotic input from wind turbulence and damping of the system.

This analysis shows that for reliable azimuth measurements, an averaging period of a few minutes will usually be suitable, although on longer lines the low-pass filter effect becomes the most important (the pendulum motion appears to be damped by long lines).

8.4 Kite Dynamics and Turbulence

A kite flying in the wind is a dynamic system. Since the wind and tether measurements were recorded at fairly high sampling rates (5 or 10 Hz), they may be used to study aspects of kite dynamics. The results help describe the kite's response to turbulence and thus the use that can be made of kites to measure wind turbulence.

8.4.1 Kite dynamics

The main techniques used to reveal patterns in the kite dynamics are correlations and Fourier analysis. The Fourier transform results may be used to derive transfer functions relating kite system inputs (the wind) and outputs (kite motion and line tension). These techniques for analysing experiment data allow comparisons to be made between real kite behaviour and various theoretical models, for example those presented in section 2.4.

Correlations have been calculated for all kites and wind conditions, and are useful for estimating the timescale of significant changes in a quantity. A few examples of autocorrelations are shown in figure 79. Two representative experiments are shown, the first is 14-Dec-84/2 and the second is ll-Jun-85/7, being respectively a large kite (Cody) in winter and a small kite (large Tailed Sled) in summer. Both these experiments are in quite strong winds. The Cody one has been analysed in most detail. The relationships between wind correlations are similar for all experiments so only the one experiment is shown in detail. The main points to note are :

a) of the wind components, the longitudinal one has the longest timescale and the vertical one (at heights of about 25 m) the shortest,

b) the longitudinal wind component (b) and windspeed (a), and the lateral component (c) and wind azimuth (e), have almost identical autocorrelations,

c) the wind component autocorrelations (a–e, i–j) contain a wide spectrum of frequencies, while the kite autocorrelations (f–h, k–l) are generally smoother, ie. relatively fewer high frequency components,

d) autocorrelations j and k, and, especially i and 1, are quite similar, indicating the Tailed Sled follows the wind well, while e and f, a and h, are much less closely related, suggesting the Cody's response is less characteristic of the wind and more a property of the kite system,

e) the summer autocorrelations do not tend to zero, indicating an underlying trend throughout the experiment, ie. a very large eddy : winter correlations do not usually have this feature since large convection cells are much rarer.

Many of these points can be explored more fully using Fourier analysis as shown in figure 80. Fourier transforms have been used on the autocorrelations of figure 79 to produce the power spectra of figure 80. The plot format is such that equal

areas represent equal variance within each plot (although not necessarily between plots). The wind spectra (80a–e, i–j) show the wide range of frequencies present, with a general decrease in amplitude above a frequency somewhere between 0.01 and 0.1 Hz. The longitudinal wind component (80a–b, i) contains the lowest significant frequencies. The Cody kite spectra (80f–h) all have a sharp peak around 0.1 Hz. The Tailed Sled spectra also have a peak at about the same frequency, but not quite so pronounced.

The next stage in the analysis is to calculate transfer functions, ie. the ratio between input and output for the kite system. The kite response is thus normalised by dividing by the wind input. Figure 81 shows four transfer functions : two calculated for each experiment. The first is kite azimuth relative to wind azimuth, and the second is windspeed estimated from tension relative to measured windspeed. All four response functions have a significant peak at around 0.1 Hz. Below this frequency, the functions are generally close to a "unit gain" as indicated by the dashed line. Above the peak frequency, the azimuth transfer functions fall to zero, while the windspeed (essentially tension) falls down towards unity, for the frequencies measured. The Cody peaks tend to be sharper than those of the Tailed Sled.

Rather than show correlations, power spectra and transfer functions for all the kites flown, figures 82 and 83 show just the transfer functions since these conveniently summarise the response of the kite to the wind. Figure 82 shows kite azimuth relative to wind azimuth, and figure 83 shows windspeed estimated from tension relative to true measured windspeed.

The transfer functions shown are fairly representative for each kite over the windspeeds measured. The dashed line represents unit gain (an output following the input exactly would lie along this line). At very low frequencies all transfer functions are expected to tend towards this unit gain; the fact that some of these examples do not is a measure of the accuracy of the technique. (Since this technique is based on ratios, cases where the actual variance is small anyway are very sensitive to even small errors.)

Azimuth transfer functions all have a peak around 0.1 Hz and then fall to zero at frequencies above this. The position of the peak corresponds roughly to the "pendulum" motion described in section 2.4.4. However, a brief comparison of the frequencies of the peaks of figure 82 with the frequencies predicted by the pendulum model does not show a good correlation. At the moment it is not known whether this is due to the chaotic input of the wind or whether the frequency measured is in fact largely due to some other effect. Further experiments to investigate this point would be useful.

The peak is most pronounced for large or comparatively unsteady kites, eg. Cody, Delta (in strong winds), Malay and Parafoil (If the mean windspeed varies significantly the peak will be smeared over a range of frequencies). The mean windspeed affects kite steadiness, so that the Tailed Sleds, the small one especially, show great steadiness considering the high windspeeds in which they have been tested and the small peaks at those windspeeds. As a comparison, the Delta at 10.9 m s^{-1} is very

much less stable. The function decay at frequencies above the peak is compounded by the low pass filter effect of a finite kite velocity and the line length. On very long lines it may dominate and suppress the pendulum mode. For reliable azimuth measurements, the averaging period should be longer than that of both the pendulum motion, which is a function of windspeed, line length and kite solidity, and the low pass filter.

Windspeed transfer functions again show the peak, possibly linked with the pendulum mode. The peak is shifted towards higher frequencies : a factor of 2 is expected from the simple pendulum model. However, compared to the azimuth responses, those for windspeed show much more frequency content at even higher frequencies. This is mainly due to the lack of damping for the longitudinal waves at these frequencies compared to the lateral waves communicating azimuth. For some kites and windspeeds (eg. 83d,e,g and h) the kite's flight pattern is rather jerky, with sudden pulls on the line. This shows up as an exaggerated response at high frequencies. Others are not quite so erratic, and the high frequencies here are not as dominant. The sleds especially (83k–o) show little extra high frequency activity apart from the pendulum mode. A second mode of the kite system shown in some windspeed transfer functions is the first of the line's own normal modes, as considered in section 3.3.2. The frequencies are usually too high to be measured (tension measurements are filtered to remove frequencies above 3 Hz), but for comparatively low tensions or heavy lines, and without significant damping, the fundamental is measured (eg. 83a–c).

8.4.2 The influence of line properties

Several experiments were performed to study the effect of the kiteline on the measurements made. Windspeed transfer functions are a convenient way of presenting the results, and are shown in figure 84 for comparisons dealing with line length (30 or 60 m, 84a–d) and line material (nylon or Kevlar, 84e–g). The left-hand plots are the standard reference cases, ie. 30m nylon lines, and variations from these are on the right.

The Tailed Sleds were used to study line length since they are steady fliers and also quite small, so that changes are expected to show more clearly. Two features reveal themselves on the longer lines. Firstly, the higher frequencies (above about 0.3 Hz) are suppressed, and secondly, the peak corresponding to the pendulum mode is accentuated. The first indicates increased damping on the longer lines, presumably due to the extra line length's movement through the air. The second point indicates that the kite system's motion is more organised on the longer lines. The pendulum model may provide a qualitative explanation if it can be shown to become less vulnerable to small perturbations as its length increases.

Larger kites will not be so strongly affected by a 30 m increase in line length since a kiteline's unit length is proportional to the square root of its breaking strength (section 3.2.2 and figure 22d).

Figures 84e–g provide a comparison between nylon and Kevlar lines. Two cases with nylon are shown as a check on transfer function repeatability. The two modes -the pendulum motion around 0.1 Hz and the kiteline fundamental just above 1 Hz -can be seen in all three plots. The stronger peak for the pendulum mode with Kevlar is not significant : it is possible that the difference could be due mainly to a steadier mean wind for the Kevlar experiment. The responses at the kiteline fundamental show important differences however. The main feature is the much increased response for the Kevlar line. This is due mainly to its higher elasticity (much lower stretch at a given tension), so that a kite on a Kevlar line is much less compliant to the wind. It therefore shows more high frequency response due to sudden jerks in response to gusts. A secondary factor may be the reduced damping for a Kevlar line, since it has less windage than a nylon line of comparable strength and its wave velocities are much higher.

These results suggest that the line material is important only at frequencies comparable to the kiteline fundamental and above. Below this, the kite system does not appear to be affected significantly. Since most kite anemometer applications are unlikely to use tension information at or above the kiteline fundamental, line material is not a significant factor for system dynamics. A more stretchy line has the advantage of reducing shock loadings on the system, and thus tends to increase its useful life and reduce the safety factors needed. It should be remembered however, that the lower weight and windage of Kevlar lines compared with nylon are a great advantage for kites at high altitude or in very strong winds, even if the extra high frequency response is not.

8.4.3 Measurement of wind turbulence

Having measured the mean wind velocity, the next most useful measurement is the wind turbulence. The TALA system uses the variance of repeated windspeed measurements to estimate the turbulence, but there appears to have been no consideration of kite system dynamics. The results here show that for frequencies above about 0.1 Hz (on 30 m lines) these dynamics are very important, and so need careful consideration.

The windspeed power spectrum measured by kite is a product of the real windspeed spectrum (eg. figure 80a,i) and the kite transfer function. The resulting spectrum is thus biassed towards the natural frequencies of the kite system. Comparing windspeed power spectra with the kite transfer functions shows that typically 50–75 % of the windspeed variance is at frequencies below 0.1 Hz, outside the range where kite dynamics are important. The resulting measurements should give a reliable estimate for 50–75 % of the variance. Suitable assumptions about the windspeed spectrum would then allow this to be scaled up to an estimate of the full variance.

Wind direction measurements also need to be considered carefully relative to the kite system transfer function. For angle measurements, there is also the low pass filter effect of line length (described in section 2.4.3) which operates over longer

timescales than the pendulum mode, especially on long lines. These factors make it difficult to make useful estimates of variance in the wind direction from tether measurements.

An alternative approach to the measurement of wind turbulence has already been suggested by the results presented in section 7. Figure 68 shows tension variance plotted against windspeed variance, and figures 71 and 72 show variation in line angle against wind direction for azimuth and inclination respectively. These empirical calibrations should be treated with caution since the system dynamics, which have been shown to be so important, are completely ignored. The calibrations shown are almost certainly relevant only to the line lengths and windspeeds used to derive them. However, with this qualification, some kites appear to have a good correlation between wind variance and tether measurements, and may thus be used as a fairly direct measure of wind turbulence. For windspeed variance, the Cody, Delta, Malay and Vented Sled all have useful correlations. For azimuth and inclination, most kites flying reasonably steadily give some indication of wind direction variance, but rarely to better than 0.03 in the relevant turbulence intensity component. The Delta (at low windspeeds), Flare and Malay give the best results for azimuth, and the two Tailed Sleds for inclination.

8.5 Summary by Kite Type

This section draws together the results of the kite anemometer and dynamics analysis to provide a summary by kite type.

Table 16 shows the anemometer calibrations calculated from the experiments (as described in section 8.3), with an estimate of the accuracy of those calibrations. Figures 76 and 77 show the calibrations graphically; figure 76 uses the simple power law and figure 77 includes a quadratic correction for the Delta and large Tailed Sled, since these two kites show reasonably clear trends in the power law calibrations. Using these calibrations (based on 5 minute averages), kites may be used to measure mean windspeed to within about 0.2 m s^{-1} over a windspeed range of 3–13 m s^{-1} (large Tailed Sled). At low mean windspeeds (below 4–5 m s^{-1}) the Delta may perform better than the Sled since it has a larger area and so generates larger, more easily measured forces, and it also has slightly better light wind performance. Above this, the Tailed Sled is preferable because of its steadiness.

The following comments describe the main features of each kite as an anemometer in turn :

Cody : This is a comparatively heavy kite, and shows strong peaks in its transfer functions corresponding to the pendulum mode on the short lines tested. Because of this it does not measure the wind very well, although on long lines the pendulum motion may be sufficiently damped to give a useful anemometer which also has enough lift to carry small payloads. The empirical calibrations

suggest that the Cody may give useful estimates of wind variance.

Delta : At windspeeds up to about 10 m s^{-1} the Delta flies well. It can be flown in mean winds as low as 3 m s^{-1}. Within this range it measures windspeed well (to within about O.2 m s^{-1}), but becomes too unsteady to be usable in stronger winds than 10 m s^{-1}.

Flare : Two types of behaviour were observed corresponding to whether or not the rear leg of the bridle was allowed to go slack. If it is kept taut (bridle angles up to 86°), the kite is a useful indicator of windspeed and flies fairly steadily, although not in such a wide range of windspeeds as the Tailed Sleds, and its calibration range is comparatively limited. If the bridle is allowed to go slack (bridle angles above 87°), the sudden jerks as it occasionally pulls taut make estimates of windspeed less reliable. Up to moderate windspeeds, it flies very steadily (better than the Cody or Parafoil) and measures wind azimuth satisfactorily.

Gibson : Both bridle settings perform similarly, but require different calibrations. Being a heavy kite, it does not fly in light winds, and its upper limit is about 12 m s^{-1} (on 30 m lines as tested). It is fairly steady in flight, but tends to jerk the line, so that its windspeed calibration is not as accurate as some other kites.

Malay : As tested, this is not a very steady kite in azimuth, and so shows up the pendulum motion quite strongly. It is not well suited as a kite anemometer, except that the empirical calibrations suggest it may be useful for measuring wind variance, in certain wind conditions.

Parafoil : This is quite large and not very steady in azimuth, so shows the pendulum motion. However, this does not interfere as strongly with the windspeed measurements as for other large kites, and so may be a useful anemometer on longer lines.

Tailed Sleds : Both these kites are steady and well damped, so that the pendulum motion does not interfere stongly with angle and tension measurements. The small kite appears to be better damped, but not to the extent that kite system dynamics can be ignored. Both kites fly in a very wide range of windspeeds (with a suitable tail), from 3 m s^{-1} to at least 15 m s^{-1} , and probably higher still. The mean windspeed calibration based on tension is accurate to about 0.2 m s^{-1} for the large Tailed Sled, over 4– 15 m s^{-1}. Probably due to the tail used, these sleds follow mean azimuth closely, and also appear to provide an accurate measure of wind inclination variance. Their main drawback is their small size, which means that the forces to be measured are small and that no significant payloads can be carried.

Vented Sled : As with the Tailed Sleds, the Vented Sled is well behaved in azimuth, although not over such a wide range of windspeeds, being limited to about 10 m s^{-1}. Its dynamics are reasonably well damped, but not as well as

the other sleds tested. Empirical calibrations indicate the Vented Sled may provide good estimates of windspeed variance.

The best kites for anemometry are the Delta and large Tailed Sled. Because of its steadiness in a wids rage of wind conditions, the Tailed Sled is the more useful anemometer, provided that the tension can be measured sufficiently accurately. On lines long enough to damp out kite system dynamics, the larger kites (Cody, Flare and Parafoil) may be as accurate, and are also able to carry small payloads. So far however, no calibrations have been performed to check

this suggestion. Mean winds over periods of several minutes are measurable to within about 0.2 m s^{-1}. The full turbulence spectrum cannot be measured accurately due to the interference of kite system dynamics. However, fluctuations in tension or the variance of short period mean windspeeds may both provide useful estimates of the turbulence intensity.

Chapter 9

SUMMARY AND CONCLUSIONS

This last section. summarises the work of this thesis. It is presented in the form of an itemised list, under two headings. The first group relates to the equipment and techniques developed, and the second to the results derived from the data collected.

Finally, there is a brief discussion of the contribution of this work to other areas, and recommendations for further work.

9.1 Equipment and techniques developed

- An instrumented kite tether has been designed and built for testing single line kites. It is designed for a maximum tension of 100 kgf, and is a practical piece of field equipment which one person can operate.

- The Kite Tether Instrumentation (KTI) records line tension, inclination and azimuth, and may sample at either 5 or 10 Hz. It also has facilities for accepting up to 4 other analogue voltage inputs which are recorded in parallel with the tether data. It converts the data into a digital code which is then transmitted serially for storage as a single channel. The KTI also controls the collection of detailed anemometer data, and ensures that the whole experiment synchronisation is maintained. A standard 12V car battery is a suitable power supply.

- Accurate digital anemometers were mounted on a 25 m tower so that kites could be flown nearby for calibration experiments. The wind velocities measured should relate as closely as possible to the wind at the kite. The anemometers may be used in windspeeds up to about 20 m s^{-1}

- Several kites were constructed, including one designed here (large Flare). The sleds were built to standard designs.

- A data collection system was used, based on an Apple II microcomputer. Using the available memory, continuous data records can be made for 230 s (10 Hz) or 460 s (5 Hz), and up to 4 such units may be recorded with only a 6 s break between them.

- Programs have been written for the Apple II to collect the data in real time, to check its validity and prepare it for analysis, and to perform the analysis itself. The analysis programs use several statistical techniques, including simple means and variances (interpreted to give information such as lift coefficients, etc.), correlations, and Fourier analysis (using a Fast Fourier Transform algorithm). Also, several programs have been written to handle intermediate results calculated direct from the raw data, and to present the results in a useful format.

  is suitable for any single line kite in windspeeds up to 20 m s^{-1}, as long as the

- The experiment procedure developed may be run by only one operator, and suitable for any single line tension does not exceed 30 kgf.

- Information relevant to kite studies has been collated (for the first time) from a wide range of subject areas. This background of material properties, aerofoil and wind structure understanding is needed for progress with kites.

- Several simple mathematical models have been developed to study particular aspects of kite flight and the whole system of a kite, its line, and the wind, and to provide comparisons with the experiment results obtained. The energy stored as the kiteline's potential energy is shown to be the largest component for most situations, especially with long lines under high tension. The energy incident in the wind is comparatively large so that response times for the system should be quite short.

- A study has been made of the kiteline, and its influence on kite flight. Static line profiles may be calculated for arbitrary windspeed profiles and line properties, and from any initial conditions.

9.2 Results obtained; kite performance and anemometry

- A representative selection of single line kites has been flown in a range of wind conditions. Each experiment lasts for typically 12 minutes' flying time, and the data is stored on floppy disc ready for analysis.

- The kites tested were : Cody (extended wing), Delta (Skycraft), Flare (own design), Gibson Girl (box kite), Malay (Skycraft), Parafoil (Greens), Tailed Sleds (TALA design, built at Cranfield and using the Skycraft Malay tail) and Vented Sled (design from Pelham, 1976). In addition, the following kites were tested briefly, but not taken any further since they were either not considered

suitable as kite anemometers of duplicated other kites : Delta (Dunford), Rotor (a Magnus effect kite) and Winged Box.

- All the kites tested showed a clear trend for the reaction coefficient to decay with windspeed, usually towards a level around 0.3..0.6. This is as predicted by a static longitudinal model developed, and is due to the diminishing effect of kite weight at higher windspeeds.

- Lift and drag coefficients have been calculated for the kites over the range of bridle settings used (if appropriate), and are based on the total projected surface area in the plane of the lateral and longitudinal kite axes. Typical lift coefficients are in the range 0.4..0.8 (the box kite tends to be lower, and the Parafoil and sleds higher). Typical drag coefficients are 0.15..0.4 (the Parafoil and sleds are again higher).

- Maximum mean line inclinations are in the range 45..65°, as follows : 65° -Cody, Delta; 60..65° -Flare, Parafoil; 60° -Malay, large Tailed Sled, Vented Sled, Winged Box; 45..55° -Gibson, small Tailed Sled.

- Kite steadiness tends to decrease in strong winds, and often limits the usefulness of the kite. Some designs are much better than others though, eg. the Tailed Sleds both fly well in winds as strong as have been measured. Tails seem to help steadiness, and are crucial to the flight of some kites (the Tailed Sleds are very poor fliers without a suitable tail).

- Comparisons between the kite results obtained here and other work performed (mostly in wind tunnels) tend to show significant agreement, and give confidence in the techniques developed.

- Transfer functions are used to characterise the response of kites to the wind. They have been calculated for kite azimuth relative to wind azimuth, and windspeed estimated from line tension relative to measured windspeed. They provide a good summary of kite system dynamics as well as clarifying the kite's response to turbulence, and thus the turbulence information available from kite measurements.

- The principal features of kite system dynamics which are suggested treat it as a mechanical system responding to a chaotic input and are : a low pass filter effect of line length on angle measurements, a pendulum motion due to the line length and kite drag, and the kiteline fundamental (transverse waves). The pendulum motion is most effectively damped on the lightest kites, and appears to be mainly a feature of heavy kites.

- The best kites for anemometry are the large Tailed Sled and the Delta, either of which may measure mean winds over several minutes to within about $0.2\ \mathrm{m\ s^{-1}}$. Because of its steadiness, the Tailed Sled is generally the better anemometer, although the Delta is better for light winds.

- Because of kite system dynamics, kites are not suitable for measuring wind turbulence at frequencies above about 0.1 Hz on 30m lines. This still leaves 50..75 % of the variance which is measurable by kites. On longer lines, the frequency cut-off is expected to fall to lower frequencies roughly as (line length) (using the pendulum model).

9.3 Conclusion

Having listed specific achievements of the work here it is useful to consider its contribution in a wider context. Although kites have been used in a variety of different applications there has so far been no attempt at a structured study of kites themselves. It is hoped that this work may inchoate such a study by providing a proved experimental technique and results measured in the natural wind, as well as a framework for the analysis and presentation of those results allowing useful comparisons to be made.

Several applications should be able to use the results obtained here. The existing kite anemometer work has been placed in a broader background: the technique is sound, although measurements of turbulence need careful consideration of the kite system dynamics. Other applications, such as kite sailing and aerial platforms, now have a range of experimental results measured in natural wind available, and a technique for measuring kite flight in field experiments allowing detailed analysis of the results. The range of kites tested, although small, is the beginnings of a library of kite performance data which should be of use to anyone needing to design kites for particular applications.

This is by no means an exhaustive study of kites and there are several areas of further study or development which would benefit from more work. Firstly, the range of kites tested is small compared to the vast range available, and there is much scope for more detailed work here, either by testing new designs, by studying the effect of modifications to a basic design, by flying kites in a wider range of wind of wind conditions (to extend the anemometer calibrations), or by broadening the study beyond single line kites on comparatively short lines. In particular it would be useful to test steerable kites (usually two or more lines) for kite traction. If these were to be done, perhaps the most significant improvement to the tether instrumentation would be to improve the reliability of the tension measurements. At present, the sensitivity of the load cell to temperature fluctuations is a serious problem, and has invalidated a significant proportion of the data collected. If the facilities are available, it would also be useful to have measurements of the lateral and longitudinal variation of the wind velocity, allowing a more accurate extrapolation to the kite's position.

A second method of extending the work would be to study one of several areas raised in the present research. The area of steerable kites has already been mentioned as a useful new set of experiments to be performed. A more complete study would also

develop the kite stability ideas presented here (Is the pendulum model correct, how could it be made more quantitative? How do kite tails work?), and may overlap with steerable kites or a consideration of the performance of kite trains, or the influence of the kiteline on system stability -all of which are useful areas of further study.

To conclude, it is hoped that this thesis will help lay a sound foundation for kite studies, especially kite anemometry, and that the broad physics approach which has been used contributes by presenting a whole picture rather than focussing on particular features.

References

Arbouw, J. (1982). Electricity generated by flying windmill. *Engineers Australia*, 17–18.

ASME. (1980). *Metals handbook.* American Society for Metals.

Baker, R., Whitney, R., & Hewson, E. (1979). A low level wind measurement technique for wind turbine generator siting. *Wind Engineering*, *3*(2), 107–114.

Bent, G. (1982). *The immediate extraction and display of insect flight trajectories from infra-red remote sensor signals.* PhD thesis, Ecological Physics Research Group, Cranfield Institute of Technology.

Berman, S., & Stearns, C. (1977). Near-earth turbulence and coherence measurements at Aberdeen Proving Ground, Md. *Boundary-Layer Meteorology*, *11*, 485–506.

Bradshaw, P. (1975). *An introduction to turbulence and its measurement.* Oxford University Press.

Bryant, L., Brown, W., & Sweeting, N. (1942). *Collected researches on the stability of kites and towed gliders* (Reports and Memoranda No. 2303). Aeronautical Research Council.

Cochrane, J. (n.d.). The Dunford aerial photographic system. *Aerial Archaeology*, *4*, 8–11.

Daniels, P. (1982). *Kahuku kite wind study: III Turbulence analysis* (Tech. Rep.). Department of Meteorology, University of Hawaii.

Daniels, P., & Oshiro, N. (1982b). *Kahuku kite wind study: I Kahuku beach boundary layer* (Tech. Rep.). Department of Meteorology, University of Hawaii.

Daniels, P., & Oshiro, N. (1982a). *Kahuku kite wind study: II Kahuku foothills* (Tech. Rep.). Department of Meteorology, University of Hawaii.

Day, I. (1982). Jacob's Ladder. *Yachts and Yachting*, 67–72.

De Laurier, J. (1972a). A stability analysis for tethered aerodynamically shaped balloons. *Journal of Aircraft*, *9*(9), 646–651.

De Laurier, J. (1972b). *A stability analysis of cable-body systems totally immersed in a fluid stream* (Contractor Report No. NASA CR-2021). NASA, Washington.

DuPont. (n.d.). *Kevlar 29, Kevlar 49, Summary of properties and of applications.*

Dusariez, M. (1985). *Kite aerial photography worldwide association newsletter.* (Bruxelles, Belgique. ISSN 0773 6207)

Ericsson, I., & Reding, J. (1971). Unsteady airfoil stall, review and extension. *Journal of Aircraft*, *8*(8), 609–616.

Farrow, R., & Dowse, J. (1984). Method of using kites to carry tow nets in the upper air for sampling migrating insects and its application to radar entomology. *Bulletin of Entomological Research*, *74*, 87–95.

Glauert, H. (1934). *Heavy flexible cable for towing a heavy body below an aeroplane* (Reports and Memoranda No. 1592). Aeronautical Research Committee.

Glauert, H. (1959). *The elements of aerofoil and airscrew theory* (2 ed.). Cambridge University Press.

Gougeon brothers. (1979). *The Gougeon brothers on boat construction; wood and WEST system materials.* Pendell Publishing Co.

Hardy, A., & Milne, P. (1938). Studies in the distribution of insects by aerial currents, experiments in aerial tow-netting from kites. *Journal of Animal Ecology*, *7*(2).

Hart, C. (1967). *Kites, an historical survey.* Faber and Faber, London.

Hobbs, S. (1994). Calibration and performance evaluation of a lightweight propellor anemometer for micrometeorological research. *Boundary-Layer Meteorology*, *68*, 259–273.

Hoerner, S. (1965). *Fluid dynamic drag.* S.F. Hoerner, N.J., USA.

Hoerner, S., & Borst, H. (1975). *Fluid dynamic lift.* L.A. Hoerner, N.J., USA.

Hollingdale, S., & Richards, G. (1939). *First report on the development of a kite barrage* (ref. D.I. 150 R / 39, item no 56 A/5/38, D.I. 101). RAE Farnborough.

Ibbetson, A. (1978). Topics in dynamic meteorology : 6. Some aspects of the description of atmospheric turbulence. *Weather*.

Irvine, H. (1981). *Cable structures.* MIT Press, Cambridge, Mass., USA.

Jackson, S. (1942). *Free flight tests on kites in the 24 ft wind tunnel* (ARC R&M No. 2599). RAE Farnborough.

Jenkins, G. (1981). Kites and meteorology. *Weather*, *36*, 294–300.

Kaimal, J., Baynton, H., & Gaynor, J. (Eds.). (1980). *The Boulder low-level intercomparison experiment* (Report preprint No. 2). WMO. (Published by NOAA/NCAR, Boulder atmospheric observatory)

Kaye, G., & Laby, T. (1978). *Tables of chemical and physical constants* (14 ed.). Longman.

Kristensen, L., Panofsky, H., & Smith, S. (1981). Lateral coherence of longitudinal wind components in strong winds. *Boundary-Layer Meteorology*, *21*, 199–205.

Kuchemann, D. (1978). *The aerodynamic design of aircraft.* Pergamon Press, Oxford.

Kunkel, K. (1981). *Evaluation of a tethered kite anemometer* (AD A No. 097 082). US Army Electronics Research and Development Command, Atmospheric Sciences Laboratory, White Sands Missile Range, New Mexico, USA.

La Burthe, C. (1979). *Experimental study of the flight envelope and research of safety requirements for hang-gliders* (CP No. 2085 part II). NASA. (Proceedings: Science and Technology of Low Speed and Motorless Flight, NASA Langley Research Centre, 29-30 March)

Lighthill, M. (1978). *Waves in fluids.* Cambridge University Press.

Lissaman, P. (1983). Low-Reynolds-number airfoils. *Annual Review of Fluid Mechanics*, *15*, 223–239.

Lloyd, A., & Thomas, N. (1978). *Kites and kite flying.* Hamlyn, London.

Marvin, C. (1896). Kite experiments at the Weather Bureau (4 parts). *Monthly Weather Review, Washington.*

Marvin, C. (1897). The mechanics and equilibrium of kites. *Monthly Weather Review, Washington*, 136–161.

Met. Office (1961). *Handbook of meteorological instruments, Part II, Instruments for upper air observations.* HMSO.

Monin, A., & Yaglom, A. (1971). *Statistical fluid mechanics: Mechanics of turbulence, volume 1.* MIT Press, Cambridge, Massachusetts.

Moulton, R. (1978). *Kites.* Pelham Books Ltd., London.

Naylor, C. (1940). *Roof balance tests on a b type Cody kite in the 24 ft wind tunnel* (BA Departmental Note, Large Wind Tunnel No. 37). RAE.

Neumark, S. (1963). *Equilibrium configurations of flying cables of captive balloons, and cable derivatives for stability calculations* (Reports and Memoranda No. 3333). Aeronautical Research Council.

New Scientist. (1978). Wonderful flying machines for farmers. *New Scientist*, 344.

Nicolaides, J., , Speelman, R., & Menard, G. (1970). A review of parafoil applications. *Journal of Aircraft*, *7*(5), 423–431.

Nicolaides, T., J.D. (1971). *Parafoil flight performance* (Technical report Nos. AFFDL-TR-71-38, AD 731 143). UA Air Force.

Nowell, J. (1984). *The performance of kites with reference to bird scaring.* MSc thesis, Ecological Physics Research Group, Cranfield Institute of Technology.

Ormiston, R. (1971). Theoretical and experimental investigations of the sailwing. *Journal of Aircraft*, *8*(2).

Pasquill, F. (1962). *Atmospheric diffusion.* D. Van Nostrand Co Ltd, London.

Pelham, D. (1976). *The Penguin book of kites.* Penguin Books.

Pinnock, R. (1983). *Statistics of wind turbulence above a wheat canopy.* MSc thesis, Ecological Physics Research Group, Cranfield Institute of Technology.

Pocock, G. (1851). *The aeropleustic art, or Navigation in the air by the use of kites, or bouyant sails* (2 ed.). (unknown publisher).

Powley, M., & Wild, N. (1940). *The influence of kite characteristics on the performance of a kite barrage unit* (RAE ref Nos. D.I. 150, D.I.109). RAE Research Department, Exeter, General kite problems.

Reid, W. (1967). Stability of a towed object. *SIAM J. Appl. Math.*, *15*(1).

Richards, G., & Smith, T. (1942). *Report on kite duration flight* (Exe No. 121). RAE Research Department Exeter.

Robinson, & Lauermann. (1956). *Wing theory.* Cambridge University Press.

Roff, W., & Scott, J. (1971). *Fibres, films, plastics and rubbers.* Butterworths.

Rogallo, F., et al.. (1960). *Preliminary investigation of a paraglider* (TN No. D443). NASA.

Scannell, B. (1983). *Quantification of the interactive motions of the atmospheric surface layer and a conifer canopy.* PhD thesis, Ecological Physics Research Group, Cranfield Institute of Technology.

Schaefer, G., & Allsopp, K. (1980). Kite sails for wind-assisted ship propulsion. In *Proceedings, symposium on wind propulsion of commercial ships* (pp. 11–14). London. (paper number 9)

Schmidt, T. (1981). Kite sailing - a survey. *Boat technology international*, 11–14.

Shaw, C. (1980). *The aerodynamics of kites* (Tech. Rep.). Cambridge University, Department of Engineering. (Third year Lent term project report, Peterhouse College)

Shaw, N. (1926). *Manual of meteorology, Vol I, Meteorology in history.* Cambridge University Press.

Sweeting, J. (1981). *An experimental investigation of hang glider stability.* MSc thesis, Cranfield Institute of Technology.

Varma, S., & Goela, J. (1982). Effect of wind loading on the design of a kite tether. *Journal of Energy*, *6*(5), 342–343.

Ward-Smith, A. (1984). *Biophysical aerodynamics and the natural environment.* John Wiley and Sons.

Wellicome, J., & Wilkinson, S. (1984). *Ship propulsive kites - an initial study* (Tech. Rep.). University of Southampton, Department of Ship Science, Faculty of Engineering and Applied Science.

Wiley, J. (1984). *The kite building and kite flying handbook.* TAB books Inc.

Winters, R. (Ed.). (1969). *Newer engineering materials.* MacMillan.

Appendix A

Mechanical properties of struts, coverings and lines

A.1 Struts

The mechanical properties of interest are,

1. mass per unit length (m),
2. maximum tension (Tx),
3. maximum couple (Gx),
4. stiffness (k).

These may be calculated from a knowledge of the strut's density (ρ), elasticity (E), tensile strength (tx) and cross-section area (Ax).

a) mass per unit length

$$m = \rho/Ax \tag{A.1}$$

b) maximum tension

$$Tx = tx.Ax \tag{A.2}$$

c) and d) use standard beam deflection theory.

The strain of an elemental plane thickness dy distance y from the neutral axis of an arched beam is

$$\begin{aligned} \text{strain} &= y/R \\ \text{Total couple} &= \int_{\text{X-section}} E.(y/R).ydS = EI/R \end{aligned}$$

where I = second moment of area and dS is an elemental area.

The maximum strain (ex) is on the outer surface at y = ymax. The maximum stress (tmax) is thus

$$tmax = E.ex = E.ymax/R$$

The minimum radius of curvature is given by this equation with tmax = tx, and the maximum sustainable couple is then

$$Gx = EI/Rmin = I.tx/ymax \tag{A.3}$$

The stiffness is defined as the couple per unit curvature, thus

$$\text{stiffness} = G/(1/R) = EI \tag{A.4}$$

A.2 Coverings

The useful properties are mass per unit area (m) and maximum strength (tmax). The covering is defined by its thickness (t), density (ρ), tensile strength (tx) and bulk factor (bf).

Then

$$m = bf.\rho.t \tag{A.5}$$
$$tmax = bf.tx.t \tag{A.6}$$

gives the covering strength per unit length.

A.3 Lines

The most important physical parameters of kitelines are the diameter (d), mass per unit length (m) and elasticity (k). For lines, the elasticity is defined as the increase in tension per unit strain - for small strains. Since for real kitelines the breaking strength (bs) is the primary characteristic, this is used as the independent variable for most of the kiteline discussion. The material from which the kiteline is made is described by its bulk factor (bf), density (ρ), tensile strength (tx) and Young's modulus (E). Ax is the line's cross-section area.

$$\begin{aligned} bs &= tx.bf.Ax \\ \text{Thus } Ax &= bs/(tx.bf) \end{aligned}$$

$$\begin{aligned} \text{so } m &= \rho.bs/tx \qquad \text{(A.7)} \\ k &= E.bs/tx \qquad \text{(A.8)} \end{aligned}$$

The diameter is calculated assuming a circular cross-section

$$\begin{aligned} Ax &= \pi.d^2/4 \\ d &= 2.bs^{1/2}/(\pi.bf.tx)^{1/2} \qquad \text{(A.9)} \end{aligned}$$

Appendix B

Longitudinal Kite Model, Solution Techniques

This appendix gives details of the solution techniques used for the Longitudinal Kite Model of chapter 2.5. The symbols are as shown in figure 14 or in the list of notation.

The fundamental equations are

$$
\begin{aligned}
mg + T\sin\theta &= L\cos\beta + D\sin\beta && \text{(B.1)}\\
T\cos\theta &= D\cos\beta - L\sin\beta && \text{(B.2)}\\
(ac-ak)[L\cos\alpha + D\sin\alpha] + bk[L\sin\alpha &- D\cos\alpha] = \\
mg[(ag &- ak)\cos\gamma - (bg-bk)\sin\gamma] && \text{(B.3)}
\end{aligned}
$$

Equations B.1 and B.2 are obtained from the balance of forces vertically and horizontally, and B.3 from requiring zero net moment about the towing point K.

These fundamental equations are supplemented by several definitions:

$$\text{dynamic pressure} \quad q = \frac{1}{2}\rho W^2 \tag{B.4}$$

$$\text{drag coefficient} \quad C_D = \frac{D}{qS} \tag{B.5}$$

$$\text{lift coefficient} \quad C_L = \frac{L}{qS} \tag{B.6}$$

$$\text{dimensionless kite weight} \quad wq = \frac{mg}{qS} \tag{B.7}$$

$$\text{dimensionless windspeed} \quad u = wq^{-1/2} \tag{B.8}$$

$$\text{dimensionless line tension} \quad t = \frac{T}{mg} \tag{B.9}$$

$$\text{chord inclination} \quad \gamma = \alpha - \beta \tag{B.10}$$

Equations B.1 to B.10 are used to derive equations B.11 to B.18 which are actually used in the model solution. Subsidiary variables X and Y are used, defined by

$$\begin{aligned} X &= C_D \cos\beta - C_L \sin\beta \\ Y &= C_D \sin\beta + C_L \cos\beta \end{aligned}$$

$$\tan\theta = (Y - wq)/X \tag{B.11}$$

$$T = (mg/wq)[(Y - wq)^2 + X^2]^{1/2} \tag{B.12}$$

$$wq = [\frac{C_L^2 + C_D^2}{1 + 2t\sin\theta + t^2}]^{1/2} \tag{B.13}$$

$$\sin\beta = \frac{wq}{C_L^2 + C_D^2}[C_D(1 + t\sin\theta) - C_L t\cos\theta] \tag{B.14}$$

$$W = \left(\frac{2mg}{\rho S wq}\right)^{1/2} \tag{B.15}$$

$$bk = (ac - a_\delta - ak)\tan(\theta + \gamma) \tag{B.16}$$

$$a_\delta = wq\frac{ag - ac - bg\tan\gamma}{X(\tan\theta + \tan\gamma)} \tag{B.17}$$

$$\tan\gamma = \frac{bkX - (ac - ak)Y + wq(ag - ak)}{bkY + (ac - ak)X + wq(bg - bk)} \tag{B.18}$$

These equations are used in several ways, calculating one set of parameters as a function of the others. The different sets of input are :

A : the kite, specified by the lift, drag, and centre of pressure coefficients, together with the centre of mass position and the kite mass and lifting area,

B : the bridle, given either as a bridle point position or as a bridle locus (defined by its slope and intercept on the chord),

C : the wind, given as its speed and inclination to the horizontal,

D : the line, tension and inclination.

The different patterns of solution are :

(1) Calculate the bridle locus to achieve a specified inclination for a given kite and wind

The bridle point may lie anywhere on a straight line defined with respect to the chord axes Oab. In these axes the slope and intercept on the chord are given by

$$\begin{aligned} \text{slope} &= -\tan(\theta + \gamma) \\ \text{intercept} &= ac - a_\delta \end{aligned} \tag{B.19}$$

The procedure uses equation B.11, solving iteratively for the kite incidence giving the desired inclination. This incidence, together with the kite and wind information, is then used with equations B.10, B.16 and B.17 to give the bridle locus.

(2) Calculate kiteline tension and inclination given kite, bridle and wind

This is the "calculation" nature performs whenever a kite is flown, in the sense that flying a given kite in particular wind conditions specifies the kite, bridle and wind, and then the line assumes a definite tension. The technique used is again an iterative solution for the correct value of kite incidence, using equations B.10 and B.18 to find the incidence such that these two values of chord inclination agree. With this incidence, B.11 and B.12 are then used to calculate the line tension and inclination.

(3) Calculate the wind at the kite given kite, bridle and line tension vector

Note that this is the inverse of 2, and is effectively the task required of an anemometer in that a knowledge of the kite, its bridle and the line tension vector is used to infer the wind at the kite.

The incidence is again the optimised variable, this time using equations B.13, B.14 and B.18 to calculate the chord inclination, iterating until a satisfactory solution is found. The current values of u and bt then give (by equation B.15) the wind speed and inclination.

Lastly, as a check on the physical feasibility of any solutions obtained, the partial derivative of moment with respect to incidence may be calculated. A negative value of the derivative indicates a solution stable to small disturbances.

A version of 2 dealing only with dimensionless quantities is used to calculate the contours of wind speed and inclination as a function of line tension and inclination.

This plot models the use of the kite as an anemometer. This version is also used to study the effect of increasing windspeed on the incidence adopted by the kite, and thus the variation of the reaction coefficient with windspeed.

Appendix C

Equations describing the static kiteline

Appendix C presents the equations describing the quasi-static kiteline. The complete three dimensional equation is presented first. Then the various simplifications providing simplified or analytical solutions are described. Lastly, the procedure for the numerical integration used is given.

Figure 21 shows the forces acting on the kiteline (as described in section 3.1) and the geometry used in defining them. The effects of tension, line weight and aerodynamic force on a line element ds are now described in turn.

a) Tension

$$\begin{aligned} \text{Net tension acting on element ds} &= \mathbf{T}(s+ds) - \mathbf{T}(s) \\ &= \frac{d\mathbf{T}}{ds} ds \end{aligned} \tag{C.1}$$

b) Weight

The line mass per unit length (m) and acceleration due to gravity (g) give the line weight per unit length, and then the weight of the line element,

$$\mathbf{W} = (0, 0, -mg)ds \tag{C.2}$$

c) Aerodynamic force

This is best calculated in two parts: the normal reaction force and the friction along the line element.

The vectors **V** (wind velocity) and **n** (unit vector along the line element) are used to define the directions of these two components.

The normal reaction acts in a direction perpendicular to the line element and in the plane spanned by the vectors $\mathbf{V}$ and $\mathbf{n}$. $\mathbf{e}_r$ is the unit vector for the normal reaction, ψ the angle between $\mathbf{V}$ and the line element,and $\mathbf{e}_v$ the unit vector parallel to $\mathbf{V}$.

$$\mathbf{e}_r = \mathbf{e}_v/\sin\psi - \mathbf{n}/\tan\psi \tag{C.3}$$

The magnitude of the normal reaction is given by the reaction coefficient, C_R (typically 1.1, based on line diameter and unit length) and the wind component normal to the element ($V\sin\psi$). Then writing $\mathbf{r}$ for this normal reaction per unit length,

$$\begin{aligned} \text{normal reaction on element} &= \mathbf{r}ds \\ &= \frac{1}{2}\rho(V\sin\psi)^2 C_R ddsds\mathbf{e}_r \\ &= qdC_R\sin^2\psi\mathbf{e}_r ds \end{aligned} \tag{C.4}$$

where $q = \frac{1}{2}\rho V^2$

The friction force on the line element acts along the line element, and is similar in form to the reaction force, except that the reaction coefficient is replaced by the friction coefficient (C_F, typically 0.02) and the relevant wind component is that parallel to the line. Writing $\mathbf{f}$ for the friction force per unit length,

$$\begin{aligned} \text{friction force on line element} &= \mathbf{f}ds \\ &= qdC_F\cos^2\psi\mathbf{n}ds \end{aligned} \tag{C.5}$$

Static equation

These four force components may now be combined to give the equation of motion for the line element (quasi-static)

$$\begin{aligned} m\ddot{\mathbf{r}} = &\frac{d\mathbf{T}}{ds} + \mathbf{w} + qdC_F\cos^2\psi\mathbf{n} \\ &+qdC_R\sin^2\psi\mathbf{e}_r \end{aligned} \tag{C.6}$$

For the static line profile, the element acceleration (and velocity) is zero, so equation C.6 may be written

$$\frac{d\mathbf{T}}{ds} = -\mathbf{w} - qdC_F\cos^2\psi\mathbf{n} - qdC_R\sin^2\psi\mathbf{e}_r \tag{C.7}$$

This is the equation which must be satisfied by any static line profile. With suitable boundary conditions it may be applied to cases with, for example, several kites flown on one line, or a line which branches at several points.

To solve equation C.7, a coordinate system must be chosen, for the vectors to be written explicitly in those coordinates. Using the axes as shown in figure 21, the vectors are,

$$\begin{aligned} \mathbf{T} &= T\mathbf{t} \\ \mathbf{n} &= (\cos\theta\cos\phi, \cos\theta\sin\phi, \sin\theta) \\ \mathbf{w} &= (0, 0, -mg) \\ \mathbf{V} &= (V, 0, 0) \end{aligned}$$

The wind direction is assumed to be constant, and to lie along the x axis. Its magnitude is not fixed, but may vary as a function of height (z). Note that in this case (wind along Ox), the angle ψ is given by

$$\cos\psi = \cos\theta\cos\phi$$

Using matrix notation, the vector derivative from equation C.7 may be written in terms of component derivatives, and a matrix A

$$\frac{d\mathbf{T}}{ds} = A(\frac{dT}{ds}, \frac{d\theta}{ds}, \frac{d\phi}{ds}) \tag{C.8}$$

The vectors on the right hand side of equation (7) may be combined to give the vector.b, so that equation (7) is equivalent to

$$\begin{aligned} A(\frac{dT}{ds}, \frac{d\theta}{ds}, \frac{d\phi}{ds}) &= \mathbf{b} \\ \text{and so } (\frac{dT}{ds}, \frac{d\theta}{ds}, \frac{d\phi}{ds}) &= A^{-1}\mathbf{b} \end{aligned} \tag{C.9}$$

The inverse matrix is given by

$$A^{-1} = \begin{pmatrix} \cos\theta\cos\phi & \cos\theta\sin\phi & \sin\theta \\ -\sin\theta\cos\phi/T & -\sin\theta\sin\phi/T & \cos\theta/T \\ -\sin\phi/(T\cos\theta) & \cos\phi/(T\cos\theta) & 0 \end{pmatrix}$$

Solution techniques

This gives explicit expressions for the variation of T, θ and ϕ along the kiteline. Several types of solution are possible:

a) ignoring the aerodynamic forces on the line,

b) including a simplified aerodynamic force,

c) a full numerical integration of equation C.9.

Solutions a) and b) are usually restricted to the downwind case ($\phi = 0$). The three solution techniques are now described briefly.

a) line weight and tension only

In this case $\mathbf{b} = -\mathbf{w} = (0, 0, mg)$ and $\phi = 0$, so that equation C.9 reduces to

$$\begin{aligned} \frac{dT}{ds} &= mg\sin\theta && \text{(C.10)} \\ \frac{d\theta}{ds} &= mg\cos\theta/T && \text{(C.11)} \\ \text{and } \frac{d\phi}{ds}d &= 0 \end{aligned}$$

Using the slope (dz/dx, $= u_0$) and tension (T_0) at the origin, these equations may be solved exactly. L is a length scale for the line ($= T_0/mg$).

$$\begin{aligned} x &= L\left(\sinh^{-1}\left[\frac{s}{L+u_0}\right] - \sinh^{-1}[u_0]\right) && \text{(C.12)} \\ z &= \frac{T-T_0}{mg} && \text{(C.13)} \\ &= \left[1+\left(\frac{s}{L+u_0}\right)^2\right]^{1/2} - [1+u_0^2]^{1/2} && \text{(C.14)} \\ \cos\theta &= \frac{1}{\left(1+\left(\frac{s}{L+u_0}\right)^2\right)^{1/2}} && \text{(C.15)} \end{aligned}$$

b) line weight and tension with uniform wind and normal reaction only

In this case

$$\begin{aligned}\mathbf{b} &= -\mathbf{w} - qdC_R \sin^2\theta \mathbf{e}_r \\ &= (0,0,mg) + r(\sin\theta\cos^2\theta - \sin\theta, 0, \sin^2\theta\cos\theta)\end{aligned}$$

r is the reaction per unit length (equation C.4) and $\phi = 0$, so $\psi = \theta$

$$dT/ds = mg\sin\theta \quad \text{(C.16)}$$
$$Td\theta/ds = r\sin\theta + mg\cos\theta \quad \text{(C.17)}$$

Using $\sin\theta = dz/ds$, C.16 gives

$$T_0 - T = -mgz \quad \text{(C.18)}$$

where T_0 = tension at the origin.

Equations C.17 and C.18 may be non-dimensionalised using $L = T_0/r$, then

$$\begin{aligned}t &= T/T_0 \\ s' &= s/L \\ z' &= -z/L \\ x' &= x/L \\ \mu &= mg/r = 2\tan\alpha\end{aligned}$$

(α is a subsidiary variable introduced for convenience) Then C.17 and C.18 become

$$t\frac{d\theta}{ds'} = \mu\cos\theta + \sin\theta \quad \text{(C.19)}$$
$$1 - t = z'\mu \quad \text{(C.20)}$$

These may be solved to obtain a relationship between z' and θ

$$\ln(1 - 2\tan z') = \sin\alpha \ln\left[\frac{\cos\alpha - \cos\theta(1-\sin\alpha)}{\cos\alpha + \cos\theta(1+\sin\alpha)}\right] \quad \text{(C.21)}$$

The remaining variables of interest are obtained from

$$x' = -\int_0^{z'} \tan\theta dz' \quad \text{for x' = x'(z')} \tag{C.22}$$

$$s' = -\int_0^{z'} \sin\theta dz' \quad \text{for s' = s'(z')} \tag{C.23}$$

Although C.21 may be evaluated exactly, the integrals C.22 and C.23 need to be evaluated numerically: hence the use of tables or graphical solutions in the examples of this technique in Glauert (1934) and Neumark (1961).

c) full numerical solution of the static equation

A set of starting conditions is specified by T, θ, ϕ, s, x, y and z. The matrix A and vector **b** may then be evaluated at that point. A suitable step length along the line is chosen, and equation C.9 used to calculate the corresponding increments in T, θ and ϕ.

The increments in x, y and z are obtained by

$$\begin{aligned} dx &= \cos\theta\cos\phi ds \\ dy &= \cos\theta\sin\phi ds \\ dz &= \sin\theta ds \end{aligned}$$

In each case the angles used for the increment are taken as the mean of the values at each end of the line element, ie. $\overline{\theta} = \theta + d\theta/2$, etc.

Plates

Plate 1. Extended Wing Cody Warkite.

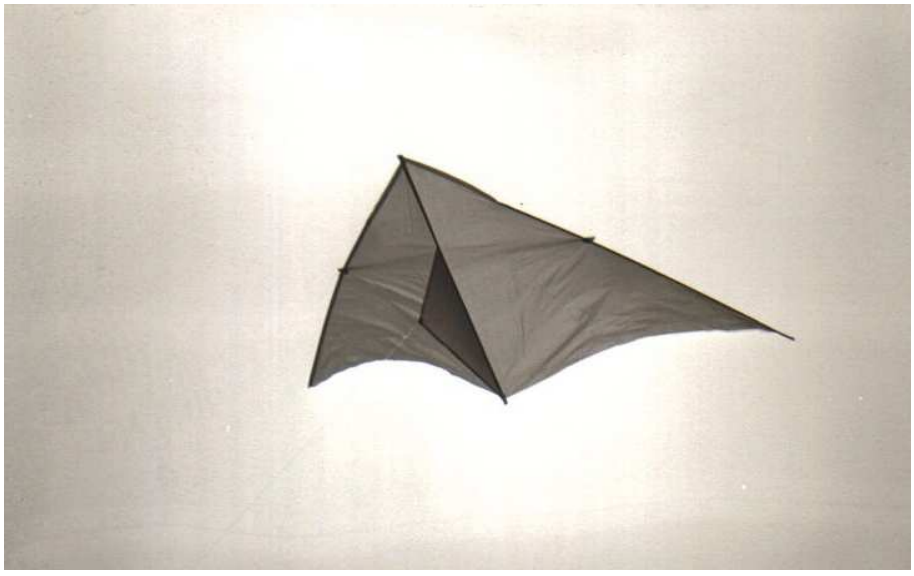

Plate 2. Delta (Skycraft).

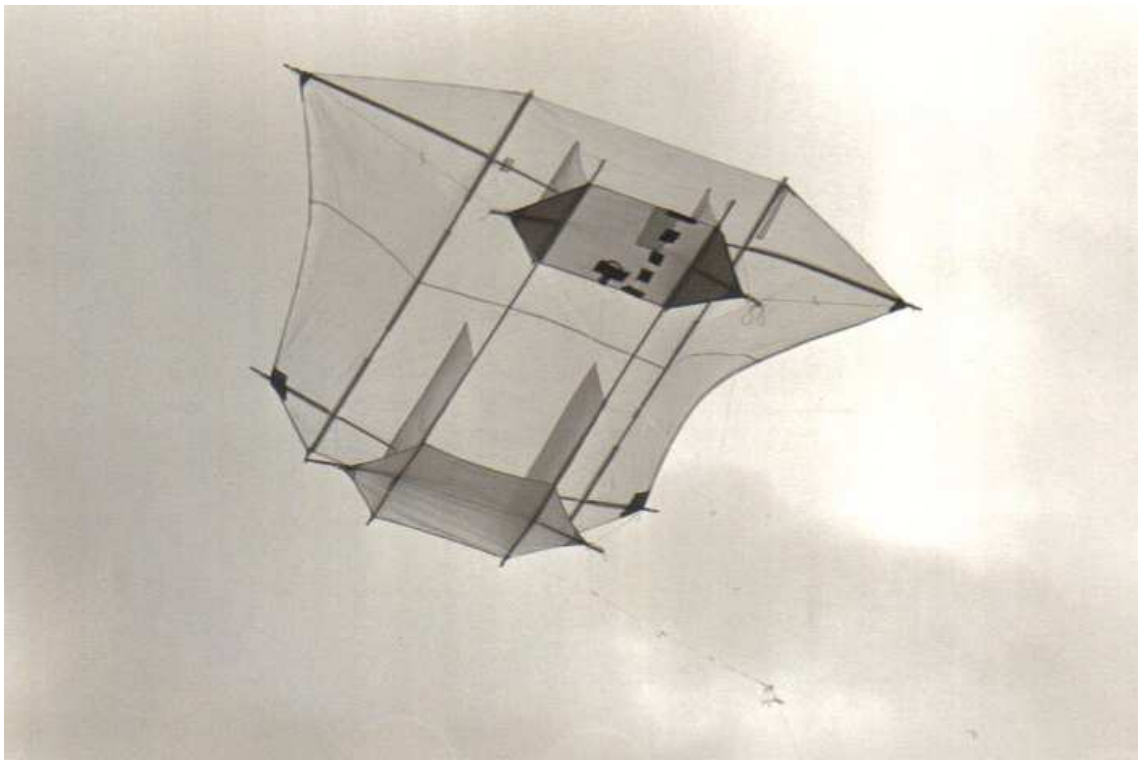

Plate 3. Large Flare (EPRG, Cranfield).

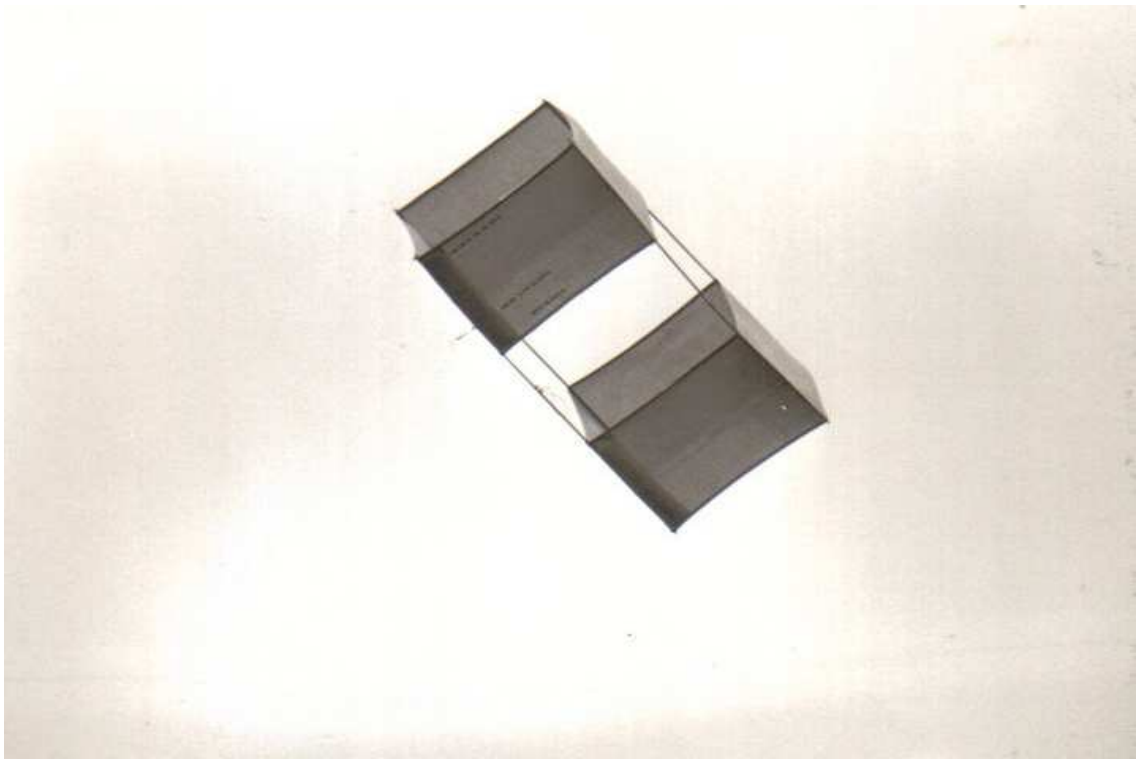

Plate 4. Gibson Girl (Second World War rescue kite - a box kite).

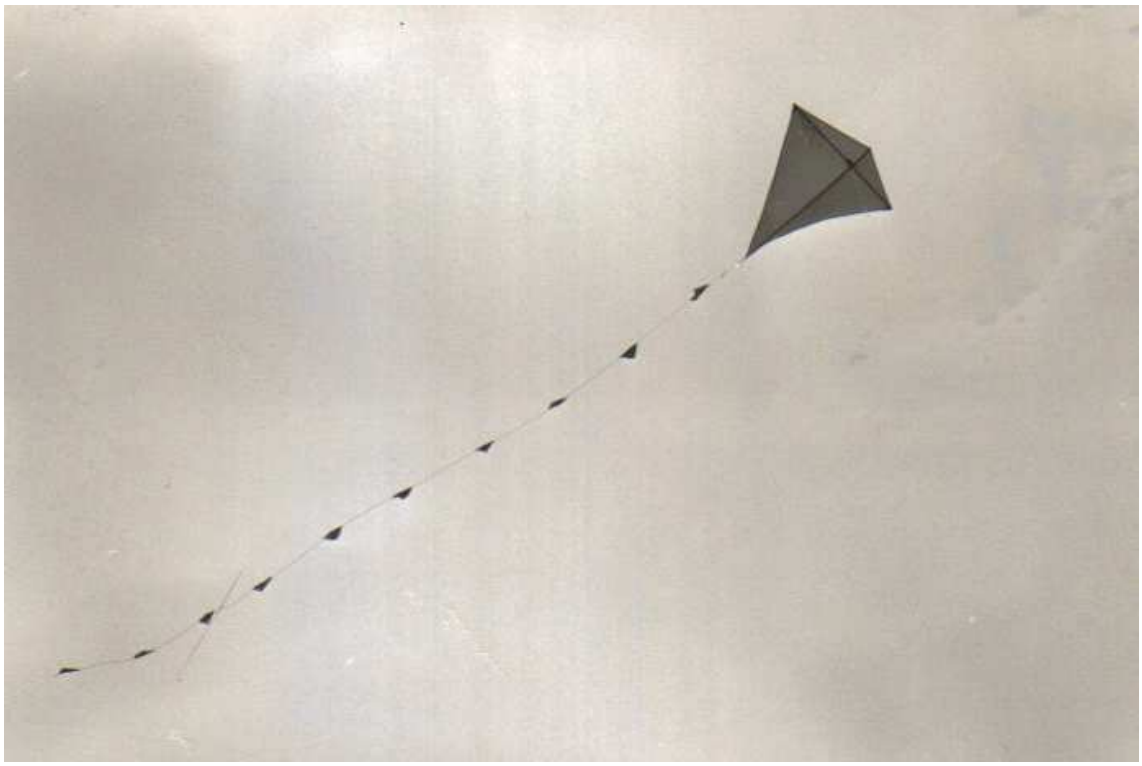

Plate 5. Malay (Skycraft).

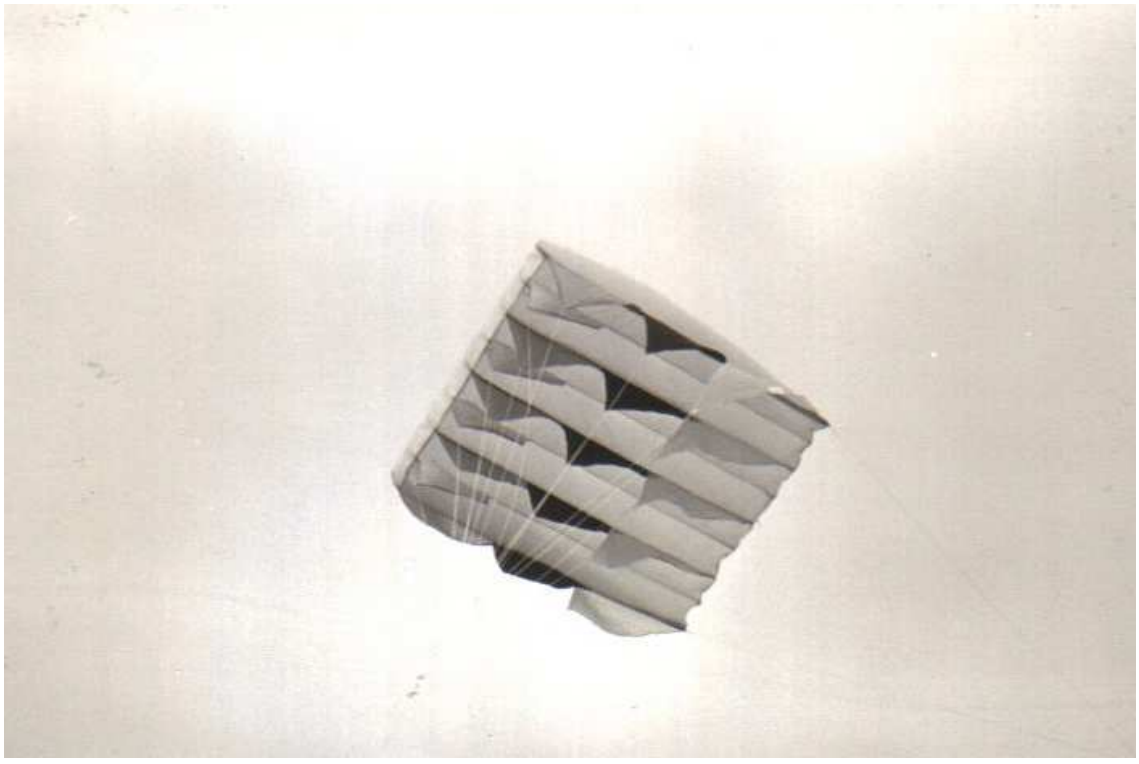

Plate 6. Parafoil (Greens of Burnley).

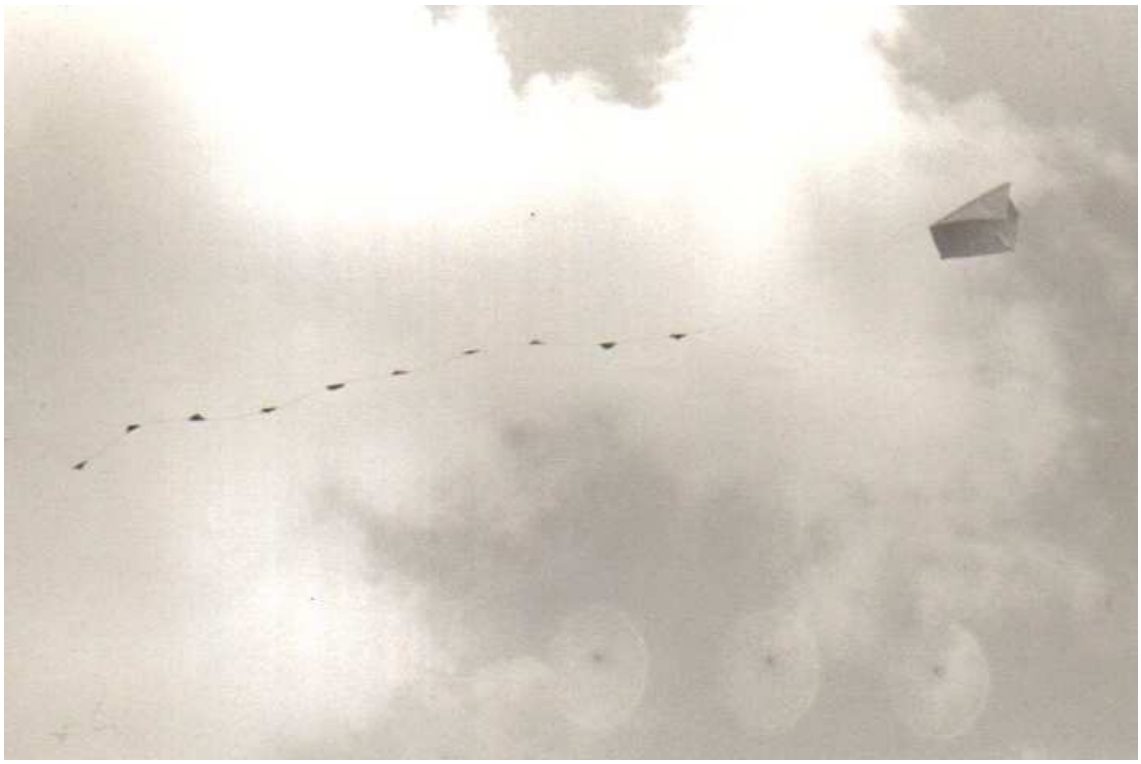

Plate 7. Large Tailed Sled (TALA design; EPRG, Cranfield, construction).

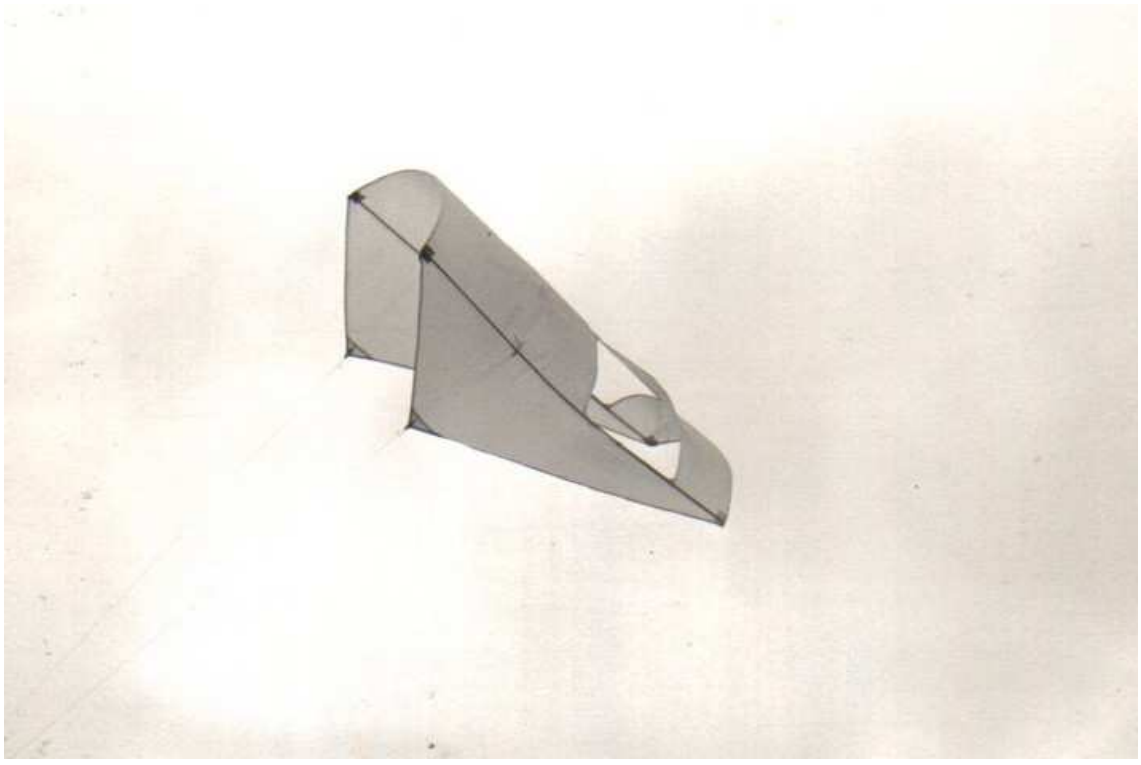

Plate 8. Vented Sled (Pelham design; EPRG, Cranfield, construction).

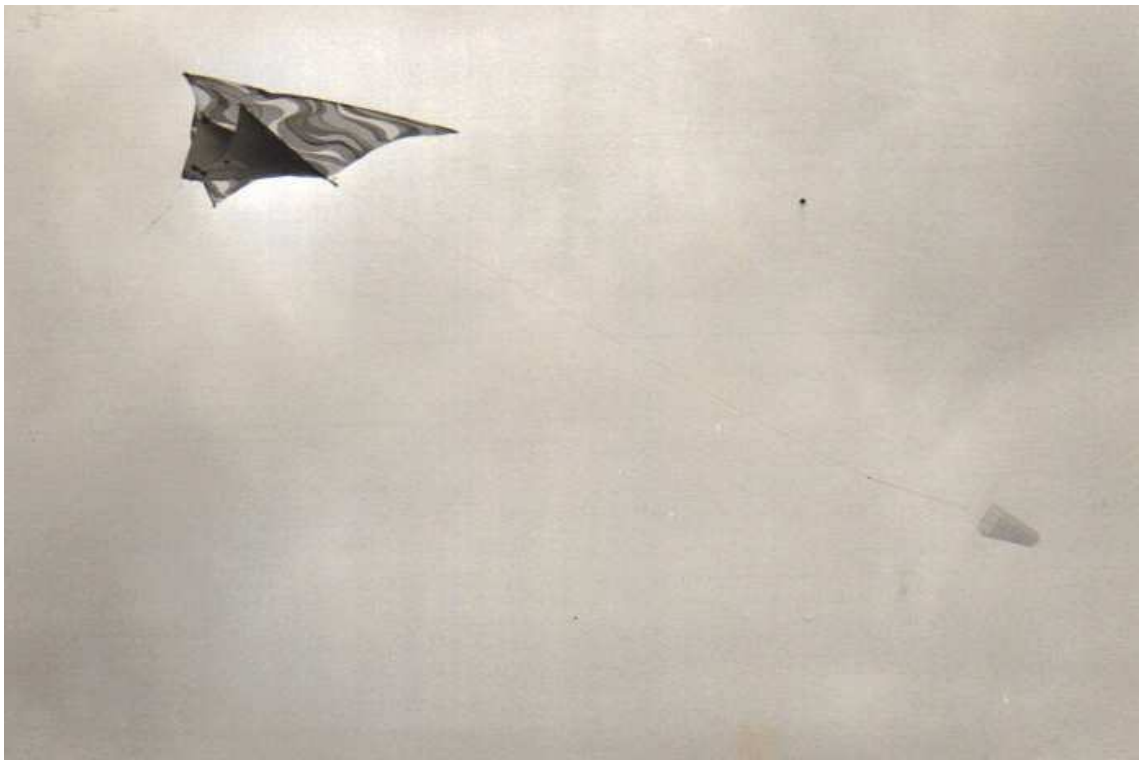

Plate 9. Dunford Delta (bird-scaring kite).

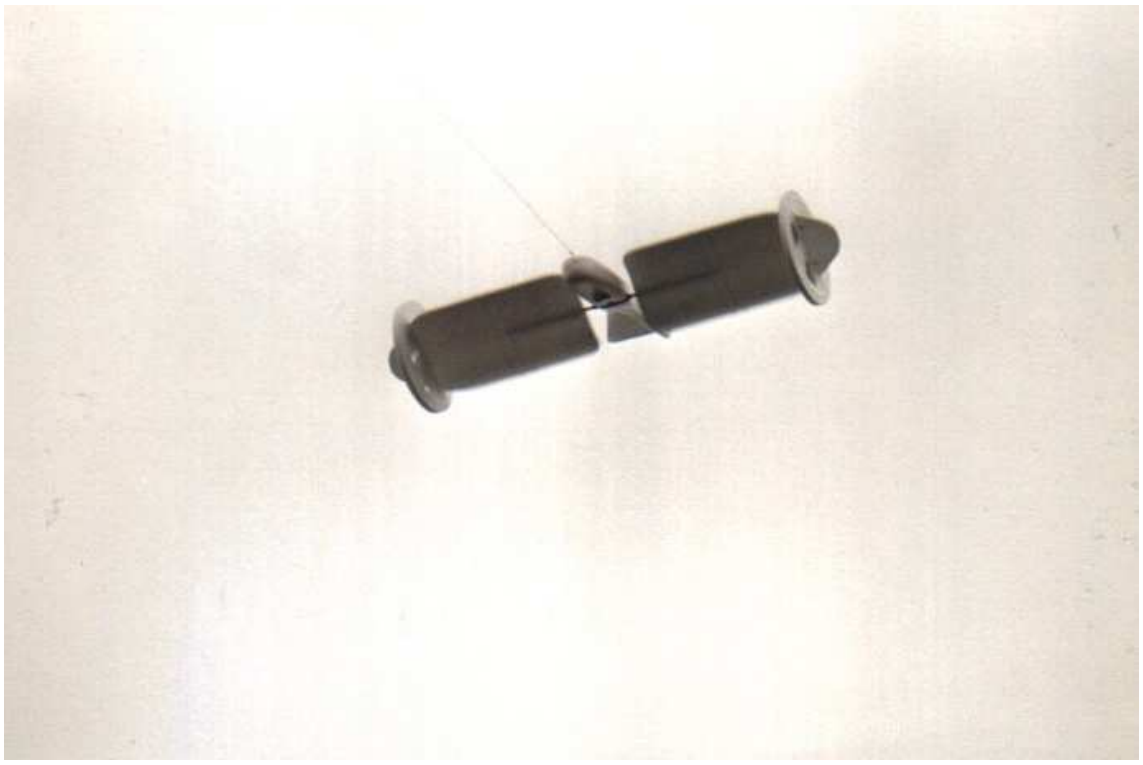

Plate 10. Rotor (Rotaplane).

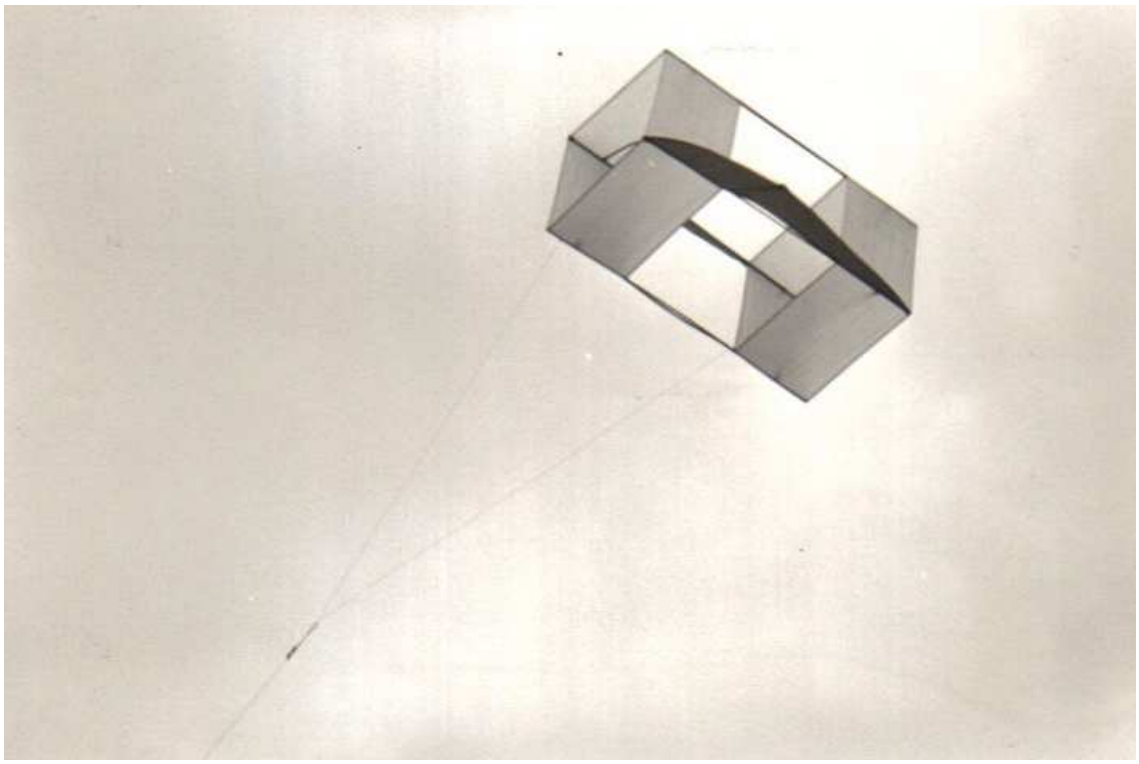

Plate 11. Winged Box.

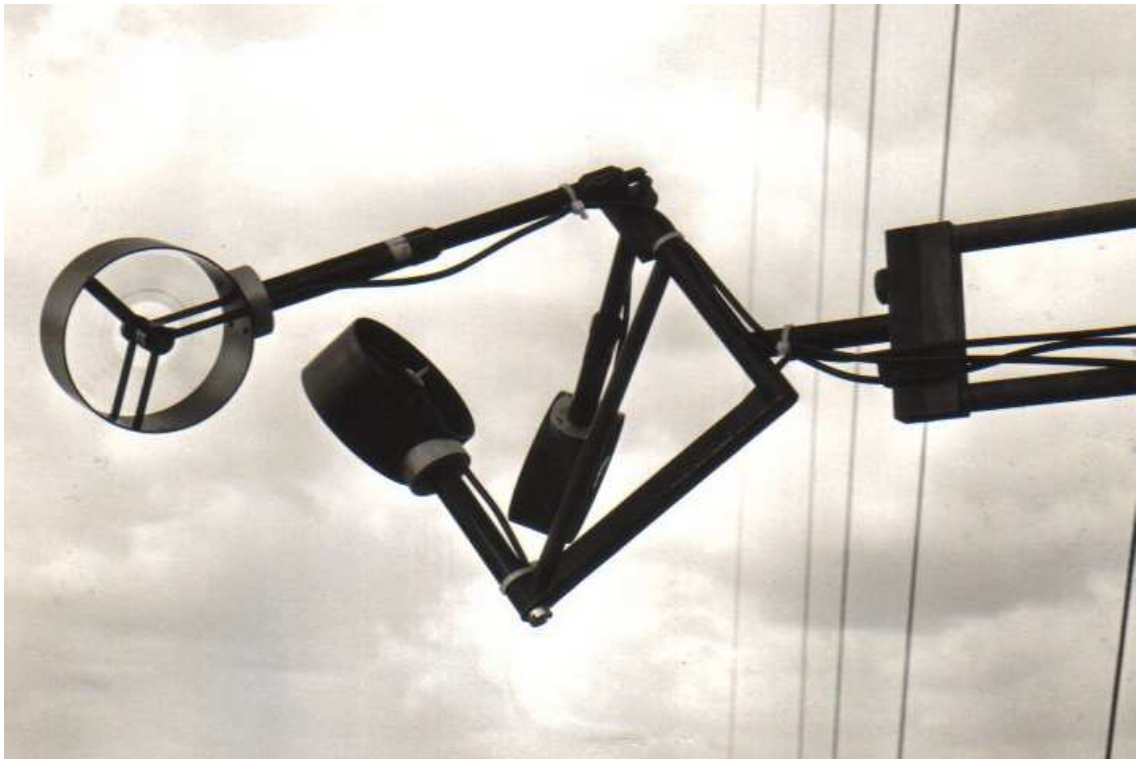

Plate 12. Non-orthogonal Digital Vane Anemometer triad.

Plate 13. Kite Tether Base and reference.

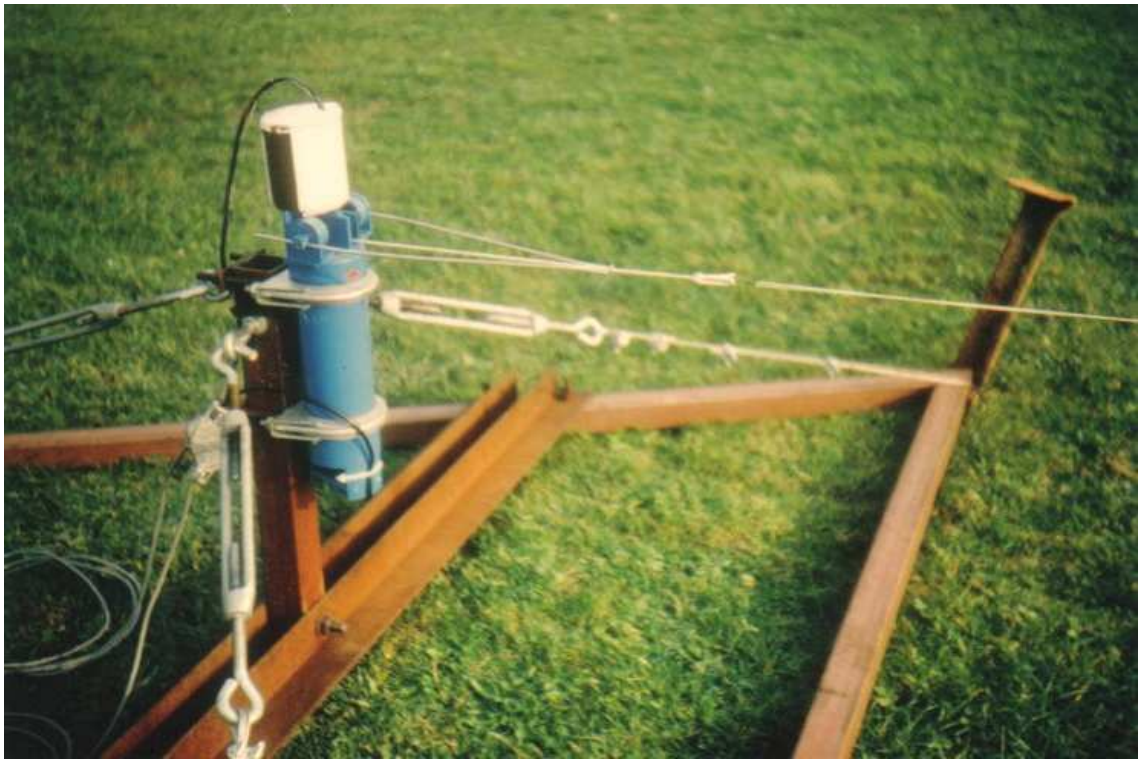

Plate 14. Kite Tether Head unit.

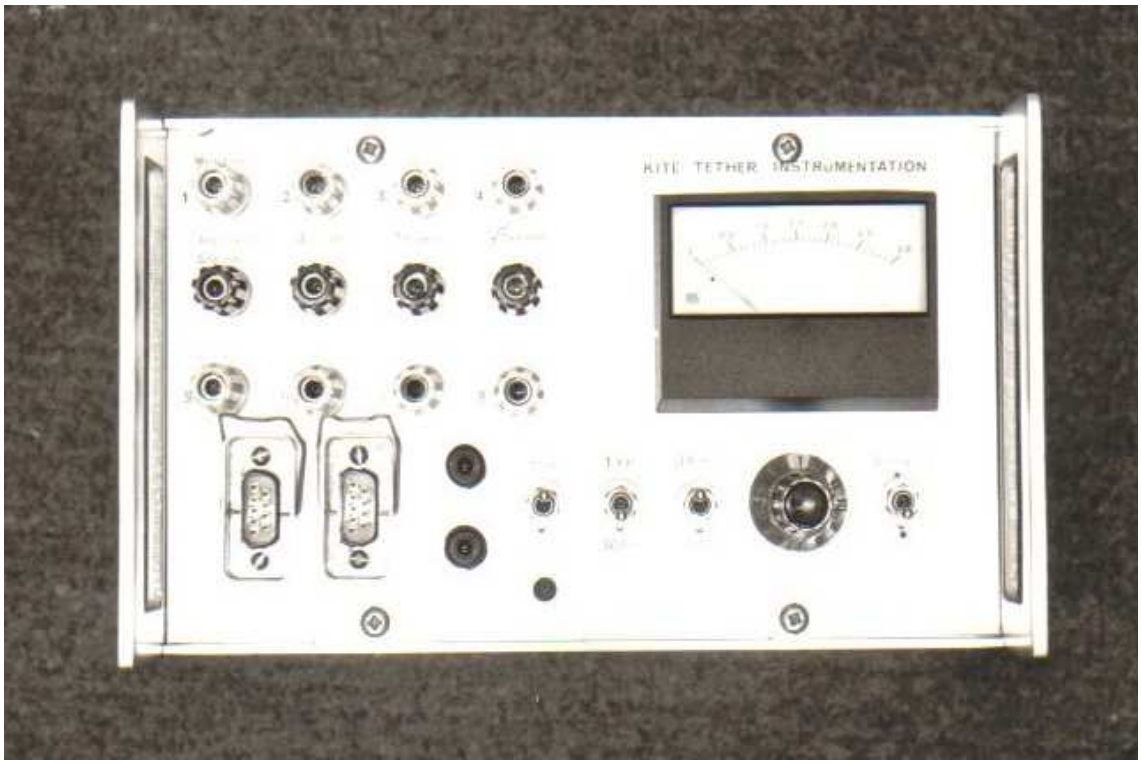

Plate 15. Kite Tether Instrumentation (front panel).

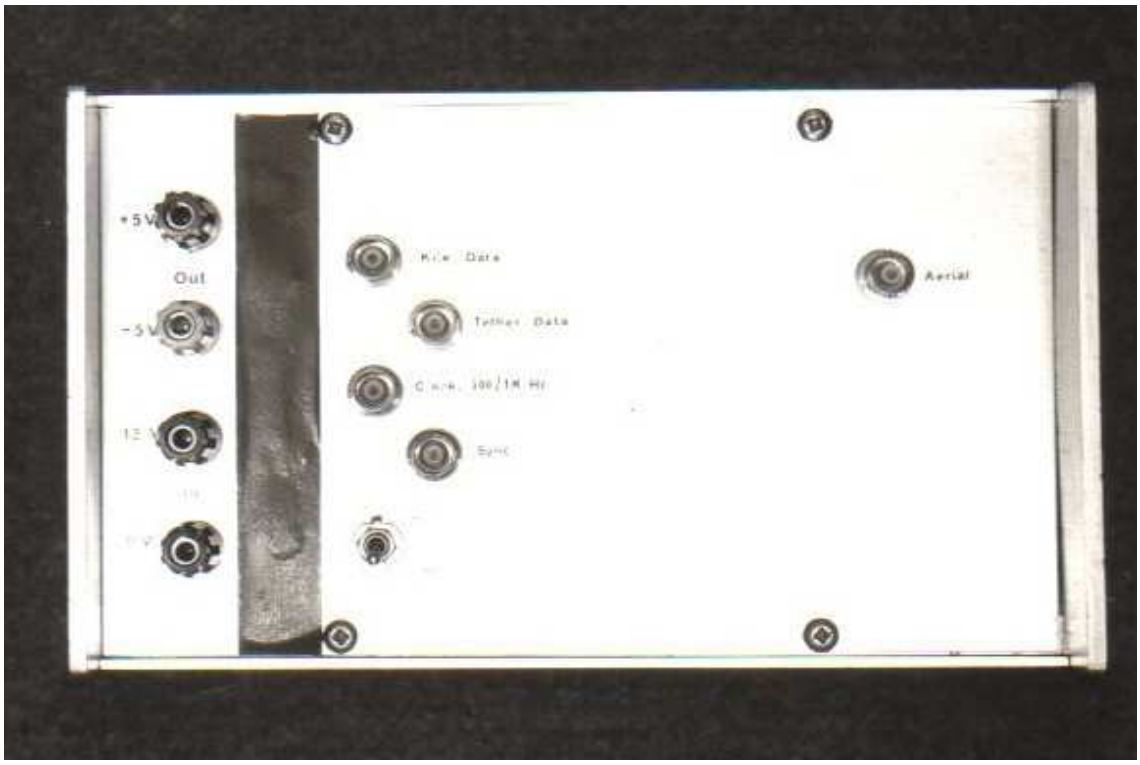

Plate 16. Kite Tether Instrumentation (rear panel).

Plate 17. Load Cell Interface and Pulse coder (front views).

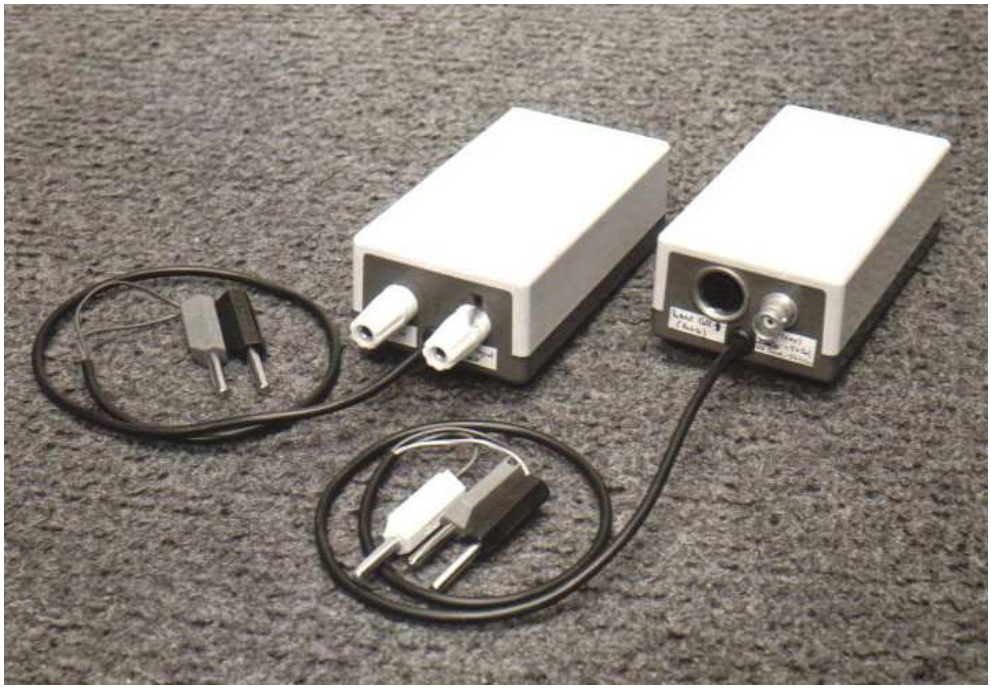

Plate 18. Load Cell Interface and Pulse coder (rear views).

Tables

1740's	Alexander Wilson, England, uses a train of paper kites. In 1749 he used them to lift thermometers for experiments.
1752	Benjamin Franklin, USA, uses a kite to show that lightning is electrical (taking sensible precautions).
1753	De Romas (France) performs electrical experiments with kites.
1762	Peter van Musschenbroek (Dutch physicist) publishes brief mathematical description of kite flight, having done several experiments.
1822	Sir William Parry and Rev. George Fisher use kites to lift thermometers for measuring the temperature profile in the Arctic -no temperature gradient was found.
1825-6	George Pocock uses steerable kites to tow carriages and for man-lifting. He publishes The Aeropleustic Art describing his work.
1835	Franklin Kite Club formed in Philadelphia, USA, to perform electrical experiments.
1841	J.P. Espy (Franklin Kite Club) publishes *The Philosophy of Storms*, with kites used as an important tool for studying columnar clouds.
1847	W.R. Birt uses hexagonal kites at Kew Observatory to carry meteorological instruments.
I860's - 1870's	Cleveland Abbe and Charles du Hauvel experimenting with instrument carrying kites.
1883	E.D. Archibald introduces the use of steel piano wire for the kiteline, and in 1887 he was flying kites in tandem up to 1500 ft to carry anemometers, cameras, etc.
1885	Alexander McAdie carries out kite experiments at Blue Hill, USA. Under Lawrence Rotch, the Blue Hill Observatory became an important centre of meterological research. Maillot man-lifting kite, France.
1888	Arthur Batut (France) starts using kites for aerial photography.
1891	William Eddy (USA) develops his bow kite, similar to the Malay.
1893c	Lawrence Hargrave (Australia) introduces the Box Kite.
1895-6	Blue Hill Observatory and US Weather Bureau start using Hargrave kites.
1898	S.F. Cody starts work on kites, eventually developing the Cody War kite, and a reliable man-lifting system.
1898-1908	Alexander Graham Bell uses kites as the basis of his work to build an aeroplane; introduces the Tetrahedral kite.
1906	S.F. Cody appointed to post of Chief Kite Instructor at Farnborough.
1938-42	Royal Aircraft Establishment and National Physical Laboratory performing experiments into kite performance and stability to develop a kite barrage.
1940's	Paul Garber's Target kite in use by the US navy.
1948	Francis Rogallo patents the Flexible kite, related to his parawing.
1950	William Allison patents the Sled, later improved by Frank Scott who added slots.
1964	Domina Jalbert introduces the parafoil design.
1976	Ray Merry and Andrew Jones first show the Flexifoil in public. C.F. Woodhouse and Ray Holland start using the TALA kite anemometer system.
1982	Jacob's Ladder captures the World Speed Sailing record in C class with 25.03 kt using kite traction.

Table 1. Research uses of kites from the 18th century onwards.

Kite		Class	Length (chord) m	Span m	Lift area m^2	Mass kg	Aspect ratio	Mass loading kg m^{-2}	Solidity	Unit w/s m s^{-1}
Kiskeedee, large		1	0.43	0.43	0.093	0.013	2.0	0.14	0.374	1.50
Cutter kite (Brookite)		2	0.98	0.75	0.365	0.096	0.8	0.26	0.355	2.05
Malay (Skycraft)	*	2	0.86	0.86	0.366	0.070	2.0	0.19	0.258	1.75
Delta (Skycraft)	*	2	0.83	1.71	0.706	0.121	4.1	0.17	0.167	1.66
Delta (Dunford)	*	2	0.81	1.63	0.660	0.180	4.0	0.27	0.274	2.09
Russell Hall		2	1.09	0.90	0.360	0.096	2.3	0.27	0.363	2.07
Flare (EPRG)	*	2	1.80	2.42	3.850	0.940	1.8	0.24	0.102	1.98
Flexavent (Possibility)		2	1.22	1.15	0.697	0.152	1.9	0.22	0.213	1.87
Powerkite (Stewkie)		2	2.65	2.93	3.000	1.550	2.9	0.52	0.244	2.88
Flying Machine (Dunford)		2	1.09	1.30	0.673	0.351	2.5	0.52	0.519	2.89
Daredevil (Dunford)		2	0.79	1.11	0.470	0.079	2.6	0.17	0.200	1.64
Stunter (Peter Powell)		2	1.23	1.15	0.730	0.275	1.8	0.38	0.360	2.46
Wembley kite (Mettoy)		2	0.75	1.03	0.530	0.079	2.0	0.15	0.167	1.55
Square Box		3	0.82	0.43	0.490	0.140		0.29	0.333	2.14
Gibson Girl	*	3	0.90	0.61	0.730	0.344		0.47	0.450	2.75
Hexagonal Box (Larus)		3	0.75	0.52	0.520	0.260		0.50	0.566	2.83
Box Kite (Blue Hill)		3	2.01	1.98	6.340	3.320		0.52	0.170	2.90
Cody, extended wing	*	4.1	1.09	2.36	1.910	0.840		0.44	0.260	2.65
French Rescue (Monday Lunch)		4.1	1.04	1.49	1.010	0.225		0.22	0.181	1.89
War Kite (Brookite)		4.1	0.86	0.81	0.478	0.192		0.40	0.474	2.54
Winged Box	*	4.1	0.81	1.15	0.765	0.195		0.25	0.238	2.02
Sled, vented (EPRG)	*	5	0.90	0.50	0.350	0.051	0.6	0.15	0.201	1.53
Tailed Sled, large (EPRG)	*	5	0.64	0.48	0.306	0.038	0.8	0.12	0.183	1.41
Tailed Sled, standard (EPRG)	*	5	0.45	0.34	0.153	0.023	0.8	0.15	0.314	1.55
Flexifoil		5	0.60	1.75	1.050	0.252	2.9	0.24	0.191	1.96
Parafoil (Green's)	*	6	1.30	1.33	1.730	0.520	1.0	0.30	0.187	2.19
Pocket Sled (Skycraft)		6	0.54	0.38	0.170	0.034	0.9	0.20	0.396	1.79
Glidakite (Stewkie)		7	1.17	1.17	0.680	0.140	2.0	0.21	0.204	1.82
Inflatakite (Stewkie)		7	2.65	2.73	3.600	1.030	2.1	0.29	0.123	2.14
Rotor (Rotaplane)	*	8	0.59	0.15	2.9	3.08	1.878	0.60	0.066	0.039

Table 2. Measured kite parameters.

Kite		Class	Mass loading kg m^{-2}	Solidity	Unit windspeed m s^{-1}	Remarks
Kiskeedee, large		1	0.14	0.374	1.50	Tail mass = 23 g
Cutter kite (Brookite)		2	0.26	0.355	2.05	
Malay (Skycraft)	*	2	0.19	0.258	1.75	Supplied with tail 5 m long
Delta (Skycraft)	*	2	0.17	0.167	1.66	
Delta (Dunford)	*	2	0.27	0.274	2.09	Used for bird-scaring, supplied with drogue
Russell Hall		2	0.27	0.363	2.07	
Flare (EPRG)	*	2	0.24	0.102	1.98	Equipped with small radio transmitter
Flexavent (Possibility)		2	0.22	0.213	1.87	
Powerkite (Stewkie)		2	0.52	0.244	2.88	Flies with deep keel - reduces lifting area and aspect ratio
Flying Machine (Dunford)		2	0.52	0.519	2.89	2-line kite
Daredevil (Dunford)		2	0.17	0.200	1.64	2-line kite
Stunter (Peter Powell)		2	0.38	0.360	2.46	2-line kite
Wembley kite (Mettoy)		2	0.15	0.167	1.55	2-line kite
Square Box		3	0.29	0.333	2.14	
Gibson Girl	*	3	0.47	0.450	2.75	Square box, used as rescue beacon
Hexagonal Box (Larus)		3	0.50	0.566	2.83	
Box Kite (Blue Hill)		3	0.52	0.170	2.90	Meteorological kite c. 1896
Cody, extended wing	*	4.1	0.44	0.260	2.65	Version of Cody's War Kite
French Rescue (Monday Lunch)		4.1	0.22	0.181	1.89	
War Kite (Brookite)		4.1	0.40	0.474	2.54	
Winged Box	*	4.1	0.25	0.238	2.02	Box dihedral = 45°
Sled, vented (EPRG)	*	5	0.15	0.201	1.53	
Tailed Sled, large (EPRG)	*	5	0.12	0.183	1.41	Used by TALA kite anemometer system for low windspeeds / high altitudes
Tailed Sled, standard (EPRG)	*	5	0.15	0.314	1.55	Standard TALA kite anemometer, must be flown with a suitable tail
Flexifoil		5	0.24	0.191	1.96	2-line kite
Parafoil (Green's)	*	6	0.30	0.187	2.19	Supplied with drogue
Pocket Sled (Skycraft)		6	0.20	0.396	1.79	
Glidakite (Stewkie)		7	0.21	0.204	1.82	Shrinks 10% (linear) on inflation
Inflatakite (Stewkie)		7	0.29	0.123	2.14	Shrinks 10% (linear) on inflation
Rotor (Rotaplane)	*	8	0.60	0.066	0.039	Fuselage length = 0.33 m, each wing panel span = 0.22 m

Table 2 (cont.). Measured kite parameters.

Material	Density kg m^{-3}	Elasticity GPa	Tensile strength MPa	Function (see *)		Reference
Balsa	170	6	20			a
Bamboo	400					a
Birch, yellow	620	14	114			a
Obeche	270					a
Ramin	590	15	127	s		a
Spruce, sitka	400	11	70			a
Cotton	1500	6–11	250–800	c	l	b
Hemp	1500	25–50	690		l	b
Silk	1400	7–10	340–600	c	l	b
Kevlar 29, fibres	1440	60	2650		l	c
Nylon, fibres	1140	2–5	400–900	c	l	b
polyester, fibres	1380	12–16	500–900	c	l	b
polyester, film	1380	3.5	160–180	c		b
polyethylene, film	950	0.2–1.7	5–35	c		b
polypropylene, fibres	905	3–7	300–600		l	b
polyurethane, film	1230	0.01	20–50	c		b
Tyvek, fibre	410		17	c		b
carbon fibre	1420	250	1450	s		d
fibreglass	1850	55	1380	s		d
aluminium, pure	2700	70	70	s		e
3L63	2700	70	450	s		e
magnesium	1740	45	60-190			e
steel, mild	7850	210	430–490			f
steel, piano wire	7850	210	1860–2330		l	f
titanium	4510	116	235–1100			e

Key to references:

a) Gougeon brothers (1979)
b) Roff and Scott (1971)
c) Du Pont (n.d.)
d) Winters (1969)
e) ASME (1980)
f) Kaye and Laby (1978)

* Function: s strut
c covering
l line

Table 3. Material physical properties

Material	Density	E	Tensile strength	X-section dia	X-section wall thickness	Mass	Max tension	Max couple	Stiffness
	kg m^{-3}	GPa	MPa			g m^{-1}	kN	Nm	N m^2
Ramin	590	15	127	1/8”		4.7	1.01	0.40	0.075
Ramin	590	15	127	1/4”		18.7	4.02	3.19	1.20
Ramin	590	15	127	3/8”		42.0	9.05	10.8	6.06
Ramin	590	15	127	1/2”		4.7	16.1	25.5	19.2
Ramin	590	15	127	5/8”		117	25.1	49.9	46.8
Aluminimum	2700	70	450	10 mm	20 swg	70.4	11.7	20.1	19.0
Aluminimum	2700	70	450	15 mm	20 swg	109	18.2	48.1	70.5
Aluminimum	2700	70	450	20 mm	20 swg	148	24.7	88.3	175
Aluminimum	2700	70	450	25 mm	20 swg	187	31.1	141	352
Aluminimum	2700	70	450	30 mm	20 swg	225	37.6	205	619
Aluminimum	2700	70	450	10 mm	22 swg	56.0	9.34	16.3	15.8
Aluminimum	2700	70	450	20 mm	22 swg	116	19.4	70.2	140
Aluminimum	2700	70	450	30 mm	22 swg	177	29.4	162	491
Aluminimum	2700	70	100	10 mm	20 swg	70.4	2.61	4.46	19.0
Aluminimum	2700	70	100	20 mm	20 swg	148	5.48	19.6	175
Aluminimum	2700	70	100	30 mm	20 swg	225	8.35	45.6	619
Fibreglass	1850	55	1380	3 mm		13.1	9.75	3.66	0.219
Fibreglass	1850	55	1380	4 mm		23.2	17.3	8.67	0.691
Fibreglass	1850	55	1380	5 mm		36.3	27.1	16.9	1.69
Fibreglass	1850	55	1380	7 mm		71.2	53.1	46.5	6.48
Fibreglass	1850	55	1380	10 mm		145	108	135	27.0

Table 4. Calculated strut properties

Material	Density	Elasticity	Tensile strength	bulk factor	thickness	mass	Strength meas.	Strength calc.
	kg m^{-3}	GPa	MPa		μm	g m^{-1}	kN m^{-1}	kN m^{-1}
Dacron	1380	14	800	0.7	150	145	20, 15	84
Mylar	”	3.4	170	1	13	18	1.6	2.2
Nylon, ripstop	1150	2.5	400	0.65	120	90	13,10	31
”	”	”	”	”	80	60	6.5, 9	21
”	”	”	”	”	60	45	7, 8	16
Polyethylene	950	1.0	25	1	38	36	0.8	1.0
Polyurethane	1230	0.01	30	1	40	49	0.6	1.2
Tissue paper	820		35		23	19	0.8,0.5	
Tyvek	410		17		104	43	1.8, 1.0	
silk						41		
nainsook						62		
cambric						91		
muslin						107		

Table 5. Measured kite coverings

Material	Strength	Mean dia.	Mass	Elasticity (10% bs)	Inferred bulk properties density	strength	elasticity
	N	mm	g m^{-1}	kN	kg m^{-3}	MPa	GPa
Kevlar,bare	900	0.85	0.76	25	1340	1600	44
”	1800	1.24	1.47		1220	1500	
”	3600	1.8	3.13		1230	1400	
Kevlar, sheath	1800	2.3	5.0	31	1200	430	7.5
”	3600	3.0	7.5	61	1030	500	8.6
nylon, twine	50	0.45	0.15	0.18	960	310	1.1
nylon, monofilament	160	0.66	0.41	0.72	1200	470	2.1
nylon, braid	220	0.8	0.65	0.86	1300	440	1.7
”	340	1.2	1.0	1.3	890	300	1.2
”	450	1.2	1.3	1.3	1200	400	1.2
”	670	1.6	1.7		810	320	
”	1800	3.0	6.4	7.7	910	250	1.1
”	3100	3.6	8.9		900	310	
”	5300	4.9	17		1000	320	
polyester, braid	200	0.7	0.49	2.4	1300	520	6.3

Table 6. Measured kiteline properties

kite:	Vented sled		Cody		Cody	
mass / kg	0.05		0.84		0.84	
area / m^2	0.35		1.9		1.9	
line:	nylon braid		nylon braid		Kevlar, bare	
strength / N	100		500		500	
diameter / mm	0.55		1.23		0.6	
mass / g m^{-1}	0.24		1.19		0.36	
windspeed / m s^{-1}	4	12	4	12	4	12
30 m line length						
KE kite / J	0.03	0.23	0.42	3.78	0.42	3.78
KE line / J	0.001	0.01	0.01	0.06	0.002	0.02
PE line / J	0.19	14.0	0.25	75.6	0.03	11.6
E total / J	0.22	14.2	0.68	79.4	0.45	15.4
I kite / J s^{-1}	14.2	384	77.2	2085	77.2	2085
I line / J s^{-1}	0.5	14	1.2	32	0.59	16
I total / J s^{-1}	14.8	399	78.4	2117	77.8	2101
t_r kite / ms	1.8	0.6	5.4	1.8	5.4	1.8
t_r system / ms	15	36	8.7	38	5.7	7.3
300 m line length						
KE kite / J	0.03	0.23	0.42	3.78	0.42	3.78
KE line / J	0.01	0.13	0.07	0.59	0.02	0.16
PE line / J	1.92	140	2.54	756	0.25	116
E total / J	2.0	140	3.03	760	0.69	120
I kite / J s^{-1}	14.2	384	77.2	2085	77.2	2085
I line / J s^{-1}	5.4	145	12.0	324	5.9	159
I total / J s^{-1}	19.6	529	89.2	2405	83.1	2244
t_r kite / ms	1.8	0.6	5.4	1.8	5.4	1.8
t_r system / ms	100	256	34	316	8.3	53

Table 7. Kite system energy analysis

No	Material	bs	T	profile	W10	length	upper end position			figures
							incl	x	z	
		N	% bs		m s^{-1}	m	deg	m	m	
1	Kevlar	900	10	const.	0	600	47.0	417	432	a
2	”	”	”	”	7	”	53.0	394	452	abce
3	”	”	”	”	15	”	84.5	269	523	a
4	Nylon	”	”	”	7	”	65.5	342	489	bd
5	”	50	”	”	”	320	88.8	132	283	d
6	Kevlar	900	5	”	”	600	61.9	358	479	c
7	steel	”	10	”	”	”	57.6	373	468	b
8	Kevlar	”	”	log	”	”	63.2	363	475	e
9	”	”	”	exp	”	”	40.2	373	468	e

Table 8. Kiteline cases used in Figure 22

548 records may be stored (numbered 0–547). Each record consists of a string giving the title of the raw data file used and then 57 real numbers as follows:

1	mean tether inclination / deg
2	" " azimuth / deg
3	" " tension / N
4	s dev of inclination / deg
5	" azimuth / deg
6	" tension / N
7	mean windspeed at 10 m / m s^{-1}
8	mean windspeed at 22 m / m s^{-1}
9	22 m wind component, u / m s^{-1}
10	22 m wind component, v / m s^{-1}
11	22 m wind component, w / m s^{-1}
12	s dev of 22 m windspeed / m s^{-1}
13	s dev of 22 m component v / m s^{-1}
14	s dev of 22 m component w / m s^{-1}
15	mean flight angle at tether / deg
16	s dev of flight angle / deg
17	mean inclination at kite / deg
18	mean inclination, several expts
19	$< 17 > - < 18 > = \Delta$ inclination
20	bridle angle / deg
21	rms kite speed / m s^{-1}
22	mean $\log(W^2 + V_k^2)$
23	mean reaction / N
24	s(T) / R
25	mean $\log R^2$
26	reaction coefficient (C_r)
27	lift coefficient (C_l)
28	C_l^2
29	drag coefficient (C_d)
30	wind azimuth / deg
31	wind inclination / deg
32	mean log (W_{22} squared)
33	C_r using logarithmic
34	C_l wind profile estimate
35	C_l^2 to define the
36	C_d kite coefficients
37	AVG
38	LAG
39	first record used
40	no. of records used
41	windspeed at kite height (W_z) / m s^{-1}
42	estimated s dev of W_z / m s^{-1}
43	kite speed / wind s dev at kite height
44	mean $\log W_z^2$
45	mean flight angle at kite / deg
46	C_r using logarithmic wind profile
47	C_l and flight angle at the kite
48	C_l^2 to define the
49	C_d coefficients
50	mean log(reaction / N)
51	est. mean log(W_z/ m s^{-1})
52	line mass per unit length / kg m^{-1}
53	line diameter / m
54	line length / m
55	kite mass / kg
56	kite lifting area / m^2
57	air density / kg m^{-3}

Table 9. KITEDATA results file format

64 records (numbered 0–63) are contained in each data file, with each record including the kite name, an array of 20 numbers giving the basic kite parameters, and finally a brief remark:

string		Name (with manufacturer's name in brackets) (32 characters max)
number	0	kite class (defined in section 2.1)
	1	length / m (the maximum chord over the whole kite)
	2	span / m (from tip to tip)
	3	lifting area / m^2
	4	mass / kg
	5	aspect ratio (if defined for this kite)
	6	length scale / m (square root of lifting area)
	7	mass loading / kg m^{-2} (mass divided by lifting area)
	8	solidity (kite mass / air density times length scale cubed)
	9	unit windspeed / m s^{-1} (windspeed at which dynamic pressure = kite weight per unit area)
	10–19	blank, available for expansion
string		Remark : a brief note of any special features of the kite or its use (72 characters max)

Table 10. Kite Database Record Format

Date: 30-Oct-84

No	Start	T	n	Kite: type	b	Line: type	l	Wind: dir	vel	turb	Kite position X	Y	Z
		s	Hz		deg		m	deg	m s^{-1}		m	m	m
1	12.21	520	10	Cody	74	N45	30	208	7.8	.27	16	12	27
2	37	440	”	”	65	”	”	214	7.3	.25	16	6	27
3	13.03	290	”	”	74	”	”	218	8.5	.21	17	5	27
4	12	280	”	”	77	”	”	210	8.1	.23	17	9	27
5	16.31	670	”	Flare	90	”	”	195	7.3	.19	10	16	26
6	46	380	”	Para		”	”	200	7.1	.14	12	15	26
7	17.05	450	”	Flare	86	”	”	209	6.1	.15	14	11	26
8	15	270	”	Delta		”	”	212	6.4	.17	16	10	27
9	22	240	”	”		”	”	207	6.6	.18	14	12	27

Date: 21-Nov-84

No	Start	T	n	Kite: type	b	Line: type	l	Wind: dir	vel	turb	Kite position X	Y	Z
		s	Hz		deg		m	deg	m s^{-1}		m	m	m
1	16.14	390	10	GG	56	N22	30	215	8.4	.17	12	22	24
2	23	420	”	Delta		N45	”	218	9.8	.15	13	22	24
3	35	460	”	GG	90	N22	”	211	8.7	.17	8	22	21
4	47	270	”	WBox	95	N45	”	208	8.8	.19	14	19	25
5	56	260	”	DD		”	”	207	10.6	.18	7	14	16
6	17.04	160	”	VS		N22	”	206	9.0	.15	7	36	24

Date: 26-Nov-84

No	Start	T	n	Kite: type	b	Line: type	l	Wind: dir	vel	turb	Kite position X	Y	Z
		s	Hz		deg		m	deg	m s^{-1}		m	m	m
1	14.23	330	10	GG	56	N22	30	18					22
2	33	370	”	Cody	74	N45	”	288	7.4	.20	23	-21	27
3	43	410	”	GG	90	N22	”	285	6.4	.20	14	-20	20
4	53	650	”	Flare	86	N45	”	280	6.7	.18	24	-15	27
5	15.09	300	”	Para		”	”	277	6.2	.19	20	-12	23
6	46	230	”	”		”	”	258	5.6	.12	19	0	21
7	55	330	”	Delta		”	”	260	5.7	.09	29	-9	27
8	16.03	400	”	Cody	74	”	”	268	5.6	.09	25	-8	26
9	13	400	”	VS		”	”	267	5.3	.11	21	-5	24
10	26	360	”	Flare	86	”	”	256	5.2	.10	26	1	26
11	36	360	”	Delta		N22	”	265	5.9	.11	28	-11	27

Table 11a. Kite experiments performed

Date: 27-Nov-84

No	Start	T	n	Kite: type	b	Line: type	l	Wind: dir	vel	turb	Kite position X	Y	Z
		s	Hz		deg		m	deg	m s^{-1}		m	m	m
1	11.51	330	10	GG	90	N22	30	200	13.9	.22	-1	18	11
2	12.00	420	”	”	”	”	”	204	13.8	.23	0	19	12

Date: 10-Dec-84

No	Start	T	n	Kite: type	b	Line: type	l	Wind: dir	vel	turb	Kite position X	Y	Z
		s	Hz		deg		m	deg	m s^{-1}		m	m	m
1	15.02	620	10	Flare	105	N22	30	238	5.3	.13	23	13	26
2	18	540	”	VS		”	”	246	4.9	.13	20	3	22
3	33	690	”	Delta		N34	”	244	5.2	.10	26	4	26
4	47	300	”	TS/l		N22	”	246	4.5	.10	19	16	20
5	16.11	700	”	Flare	95	”	”	247	4.8	.11	24	7	26
6	36	710	”	TS/s		”	”	241	5.8	.07	16	14	19

Date: 14-Dec-84

No	Start	T	n	Kite: type	b	Line: type	l	Wind: dir	vel	turb	Kite position X	Y	Z
		s	Hz		deg		m	deg	m s^{-1}		m	m	m
1	15.48	680	10	Para		N45	30	228	7.0	.17	20	20	26
2	16.36	720	”	Cody	74	”	”	213	8.6	.20	15	37	26
3	17.10	680	”	GG	90	N22	”	210	9.0	.20	6	19	18
4	31	680	”	”	56	”	”	209	7.9	.18	7	17	19

Date: 7-May-85

No	Start	T	n	Kite: type	b	Line: type	l	Wind: dir	vel	turb	Kite position X	Y	Z
		s	Hz		deg		m	deg	m s^{-1}		m	m	m
1	15.55	700	10	Delta		N22	30	21	10.9	.17	9	-5	21
2	16.33	740	”	GG	90	”	”	24	10.1	.20	5	-23	16
3	56	530	”	”	56	”	”	28	9.0	.20	5	-20	19
4	17.24	710	5	Cody	74	N45	”	30	8.6	.19	16	-7	26
5	49	740	”	”	65	”	”	29	9.3	.16	16	-4	25
6	18.14	760	”	”	77	”	”	28	8.5	.17	17	-6	26
7	40	220	10	Rotor		N5	25	16	7.9	.19	9	-7	12

Table 11b. Kite experiments performed

Date: 23-May-85

No	Start	T	n	Kite: type	b	Line: type	l	Wind: dir	vel	turb	Kite position X	Y	Z
		s	Hz		deg		m	deg	m s^{-1}		m	m	m
1	16.46	710	5	Delta		N22	30	193	3.5	.22	4	30	24
2	17.13	600	”	VS		”	”	216	3.4	.24	9	23	19
3	32	750	”	Delta		N5	”	218	4.5	.22	18	21	27
4	18.02	530	”	Flare	84	N22	”	226	5.1	.19	14	25	26
5	21	740	”	VS		N5	”	227	4.4	.16	9	34	24
6	40	260	”	Flare	96	N22	”	227	4.2	.20	11	24	24
7	19.03	750	”	TS/l		N5	”	228	4.0	.20	7	25	22

Date: 10-Jun-85

No	Start	T	n	Kite: type	b	Line: type	l	Wind: dir	vel	turb	Kite position X	Y	Z
		s	Hz		deg		m	deg	m s^{-1}		m	m	m
1	16.19	660	5	Para		N34	30	300	10.2	.16	17	-15	25
2	17.01	750	”	Malay	79	N5	”	316	6.3	.25	13	-12	25
3	30	740	”	Malay+	79	”	”	301	7.1	.18	18	-5	25
4	18.05	750	”	VS		”	”	303	6.4	.20	17	-18	26
5	25	440	”	GG	56	”	”	298	6.3	.24	12	-14	20
6	19.01	770	”	TS/s		”	”	269	6.3	.20	13	10	21
7	24	820	”	TS/l		”	”	275	4.8	.25	17	4	24

Date: ll-Jun-85

No	Start	T	n	Kite: type	b	Line: type	l	Wind: dir	vel	turb	Kite position X	Y	Z
		s	Hz		deg		m	deg	m s^{-1}		m	m	m
1	12.08	680	5	Cody	74	N45	30	225	8.3	.25	21	22	25
2	29	750	”	TS/l		N5	”	223	9.1	.22	19	14	25
3	49	730	”	Cody	77	N45	”	218	7.8	.23	19	26	26
4	13.15	740	”	TS/s		N5	”	216	8.6	.20	12	23	21
5	15.46	660	”	GG	90	N22	”	238	12.5	.23	18	-7	14
6	16.26	760	”	TS/s		”	”	243	11.9	.21	18	6	20
7	52	740	”	TS/l		”	”	240	11.2	.22	22	3	12
8	17.20	760	”	Malay+	79	”	”	233	9.9	.22	19	16	22
9	42	530	”	Malay	79	”	”	234	9.3	.22	20	14	23

Table 11c. Kite experiments performed

Date: 21-Aug-85

No	Start	T	n	Kite: type	b	Line: type	l	Wind: dir	vel	turb	Kite position X	Y	Z
		s	Hz		deg		m	deg	m s^{-1}		m	m	m
1	14.59	290	5	Delta		P20	30	233	9.3	.27	22	5	25
2	16.47	710	”	TS/s		N5	”	238	7.7	.27	19	8	22
3	17.08	730	”	”		”	60	241	8.9	.24	-4	4	41
4	44	710	”	TS/l		”	30	238	6.0	.29	23	4	25
5	18.05	740	”	”		”	60	224	7.2	.24	2	8	48
6	26	260	”	Cody	74	N34	30	240	4.0	.17	20	10	22
7	54	450	”	Flare	96	N22	”	203	4.2	.20	11	22	24
8	19.29	730	”	Malay	79	N5	”	194	5.5	.21	10	25	26
9	20.01	60	”	Flare	87	N22	”	186	4.5	.25	6	27	26

Date: 22-Aug-85

No	Start	T	n	Kite: type	b	Line: type	l	Wind: dir	vel	turb	Kite position X	Y	Z
		s	Hz		deg		m	deg	m s^{-1}		m	m	m
1	11.53	720	5	Cody	74	N34	30	262	7.7	.24	26	-6	27
2	12.14	720	”	”	77	”	”	267	6.5	.32	22	-7	25
3	15.12	730	”	”	65	”	”	249	9.6	.21	27	5	27
4	39	720	”	”	55	”	”	248	10.2	.25	24	9	25
5	16.08	710	”	”	74	”	”	256	9.0	.24	27	-2	27
6	32	730	”	”	77	”	”	251	8.8	.26	28	0	27
7	55	720	”	”	79	”	”	246	8.5	.30	28	3	27
8	17.20	730	”	”	82	”	”	249	8.4	.16	27	1	27
9	52	730	”	”	74	K90	”	248	7.6	.22	27	4	27
10	18.17	710	”	”	85	”	”	240	8.2	.20	25	9	26
11	50	670	”	Flare	88	”	”	280	6.1	.21	21	-24	26
12	19.13	730	”	”	80	”	”	271	5.9	.22	25	-21	26

Abbreviations used

Kites:		Lines:	
DD	Dunford Delta	N5	5 kgf nylon twine
GG	Gibson Girl	N22	22 kgf nylon braid
Malay+	Malay with tail	N34	34 kgf ”
Para	Parafoil	N45	45 kgf ”
TS/l	Tailed sled, large	P20	20 kgf polyester braid
TS/s	Tailed sled, small	K90	90 kgf Kevlar 29 braid
VS	Vented Sled		

Table 11d. Kite experiments performed

Date	Site	Local weather forecast
30 Oct 84	4	Dry, bright with sunny intervals in the morning, with cloud increasing from the West in the afternoon with rain/drizzle by evening. Temp: 16 deg C in afternoon. Winds: moderate south-westerly.
21 Nov	3	Mostly bright and dry, a few scattered heavy showers in the morning. In the late afternoon, cloud will thicken from the West, leading to rain in the evening. Temp : 12 deg C (pm). Very windy at times.
26	3	Dry and sunny today, temperature up to 10 deg C (pm). Wind: light westerly, backing to southerly overnight.
27	3	Cloudy, mostly dry at first, but some light rain. Mild - max. temperature 12 deg C. Wind : southerly light - moderate becoming strong in afternoon and overnight.
10 Dec	3	Dry and sunny with clear periods. Temp - 9 deg C max. Wind: light south-westerly.
14	3	Morning cloudy, becoming brighter in afternoon. Temp : 8 deg C. Wind : south-westerly, light becoming moderate to fresh.
7 May 85	1	Bright start, cloud increasing during morning, perhaps with becoming strong and gusty.
23	3	Afternoon dry with sunny spells and light SW breeze.
10 Jun	2	Mostly dry, fair amount of sunshine. Temp : about 17 deg C, Wind: NW, fresh at times.
11	3	Mostly cloudy and dry. Wind : fairly fresh from SW.
21 Aug	3	Generally sunny morning, one or two showers possible. Cloud thickening overnight.
22	3	Dry and bright, with sun soon breaking through. Wind: moderate westerly breeze.

Table 12a. Kite experiment site and weather details: local weather forecasts

Date	Mean conditions		
	pressure mbar	temp. deg C	air density kg m^{-3}
30 Oct 84	1006	15	1.216
21 Nov	987	12	1.206
26	1006	10	1.238
27	999	12	1.221
10 Dec	1012	9	1.250
14	993	8	1.230
7 May 85	998	15	1.206
23	992	15	1.199
10 Jun	997	16	1.201
11	1004	15	1.214
21 Aug	1000	20	1.188
22	1000	21	1.184

Table 12b. Kite experiment site and weather details: mean air density

Gaps in the table are because the errors are insignificant, except for the wind decorrelation time (decorr) which has not been calculated for all the experiments performed. Values of decorr do not change much over any one day.

Kite abbreviations				Errors	
DD	Dunford Delta	TS/l	Tailed sled, large	wt	weight
GG	Gibson Girl	TS/s	Tailed sled, small	f	friction
Malay+	Malay with tail	VS	Vented sled	cat	catenary
Para	Parafoil				

Date: 30-Oct-84

No	Kite	Inclination			Azimuth	Tension			Wind	
	type	wt	f	cat	f	ref	drift	dWz/W22	decorr	Rka / W
		deg	deg	deg	deg	N	% T	%	s	s
1	Cody			1.2		3.09	6.3	3.5	8,21	2.6
2	”	0.07		1.5	0.60			3.8		2.4
3	”			1.5		1.22	2.7	3.7		2.2
4	”			1.5				4.4		2.5
5	Flare	0.06		0.9		-1.53	-3.2	4.7	11,6,14	2.6
6	Para			0.9		-2.24	-4.6	5.6		2.8
7	Flare			0.9	0.38			4.4		3.0
8	Delta			4.8	2.57			5.3		3.0
9	”			4.2	2.33			5.7		2.9

Date: 21-Nov-84

No	Kite	Inclination			Azimuth	Tension			Wind	
	type	wt	f	cat	f	ref	drift	dWz/W22	decorr	Rka / W
		deg	deg	deg	deg	N	% T	%	s	s
1	GG	0.25		2.4	0.84			1.9		3.0
2	Delta			4.2	0.67	0.61	3.3	1.7	7	2.6
3	GG	0.57		4.5	1.25			-0.9	3	2.7
4	WBox		0.03	1.4	0.50			2.8		2.7
5	DD		0.05	4.1	0.49			-6.4		2.1
6	VS	0.28		3.0	1.69			2.0		4.1

Date: 26-Nov-84

No	Kite	Inclination			Azimuth	Tension			Wind	
	type	wt	f	cat	f	ref	drift	dWz/W22	decorr	Rka / W
		deg	deg	deg	deg	N	% T	%	s	s
1	GG	0.49	0.08		1.26	4.47	57.0	no valid met data		
2	Cody			1.5		-1.05	-2.3	2.7		4.3
3	GG	1.06	0.16	5.7	2.07			-1.3		3.8
4	Flare			0.9	0.48	-3.33	-7.0	2.3	18	4.3
5	Para			0.9	0.31	-1.92	-5.0	0.8		3.8
6	”		0.02	0.9	0.26	-1.93	-5.8	-1.1		3.4
7	Delta	0.38		3.0	3.04	-1.99	-29.0	5.2	4	5.4
8	Cody	0.12	0.03	1.5	0.87	-1.16	-5.1	4.5	9	4.8
9	VS	0.67		4.8	2.27	-1.74	-34.1	2.4		4.1
10	Flare			0.9	0.64	-1.16	-3.7	4.2		5.1
11	Delta	0.33		2.4	2.93	-1.16	-14.8	6.7		5.2

Table 13a. Experiment error summary

Date: 27-Nov-84

No	Kite type	Inclination wt deg	f deg	cat deg	Azimuth f deg	Tension ref N	drift % T	dWz/W22 %	Wind decorr s	Rka / W s
1	GG	0.39		2.4	0.39			-19.2		1.5
2	”	0.35		2.7	0.39			-13.7		1.6

Date: 10-Dec-84

No	Kite type	Inclination wt deg	f deg	cat deg	Azimuth f deg	Tension ref N	drift % T	dWz/W22 %	Wind decorr s	Rka / W s
1	Flare	0.14		0.9	0.88	-2.09	-10.0	3.1		5.0
2	VS	1.17	0.22	4.8	2.99	-3.20	-97.1	0		4.1
3	Delta	0.42		4.5	3.22	-3.39	-55.3	3.8	1	5.1
4	TS/l	0.59		2.1	1.21			-2.2		5.5
5	Flare			0.9	0.93	-1.74	-9.8	4.0	16	5.3
6	TS/s	1.59	0.24	6.2	2.74	-0.82	-29.7	-3.5		3.7

Date: 14-Dec-84

No	Kite type	Inclination wt deg	f deg	cat deg	Azimuth f deg	Tension ref N	drift % T	dWz/W22 %	Wind decorr s	Rka / W s
1	Para			0.9		-1.84	-3.6	3.9	6,6	4.1
2	Cody			0.9		-1.15	-2.0	4.8	4,2,7,10	4.7
3	GG	0.58		3.5	0.91	-1.01	-12.8	-4.6		2.3
4	”	0.35		1.8	0.59			-4.1		2.4

Date: 7-May-85

No	Kite type	Inclination wt deg	f deg	cat deg	Azimuth f deg	Tension ref N	drift % T	dWz/W22 %	Wind decorr s	Rka / W s
1	Delta	0.21		2.4	0.46	1.13	5.7	-0.6		0.9
2	GG	0.47		3.5	0.61	0.59	1.8	-3.3	20	2.4
3	”	0.25		2.4	0.50	-1.57	-9.5	-1.5		2.3
4	Cody			1.4		-1.14	-2.3	2.3		2.1
5	”	0.05		0.9		-1.45	-2.3	1.9	10	1.8
6	”			1.7		-1.79	-4.3	2.6	8,7	2.2
7	Rotor		0.15	1.6	1.36	-0.66	-15.0	-10.8		1.9

Date: 23-May-85

No	Kite type	Inclination wt deg	f deg	cat deg	Azimuth f deg	Tension ref N	drift % T	dWz/W22 %	Wind decorr s	Rka / W s
1	Delta	0.71	0.14	2.6	2.96	1.43	31.3	2.2	14,4	8.7
2	VS	1.24		3.3	2.08	0.33	9.2	-3.5		7.3
3	Delta	0.48		1.4	4.04	-0.83	-15.4	3.9		6.2
4	Flare	0.08		0.6	0.72			3.3	15	5.7
5	VS	0.93		1.5	3.12	0.16	4.2	2.3	12	8.0
6	Flare	0.21	0.04	0.9	0.86			1.9		6.3
7	TS/l	1.05	0.18	1.4	2.64			0	6	6.5

Table 13b. Experiment error summary

Date: 10-Jun-85

No	Kite type	Inclination wt deg	f deg	cat deg	Azimuth f deg	Tension ref N	drift % T	dWz/W22 %	Wind decorr s	Rka / W s
1	Para			1.1				2.5		2.2
2	Malay	0.54		1.8	2.31	-2.60	-42.9	2.6	10,15	2.8
3	Malay+	0.44		2.0	2.04	0.90	12.4	2.3		2.7
4	VS	0.44		2.0	2.52			2.8	10	3.9
5	GG	0.48		0.9	1.00	-1.58	-18.6	-1.8		2.9
6	TS/s	1.37		3.0	2.90	-3.84	-130.8	-1.3	7	2.6
7	TS/l	0.63		1.2	2.33	1.69	30.1	2.0		3.7

Date: 11-Jun-85

No	Kite type	Inclination wt deg	f deg	cat deg	Azimuth f deg	Tension ref N	drift % T	dWz/W22 %	Wind decorr s	Rka / W s
1	Cody			1.5				2.4		3.7
2	TS/l	0.29		2.0	1.37			2.7		2.6
3	Cody			1.4		-0.84	-2.1	3.6		4.2
4	TS/s	0.80		3.2	1.89	1.87	37.5	-1.1		3.0
5	GG	0.42		2.9	0.50	-3.95	-33.2	-10.8	9	1.7
6	TS/s	0.43		2.9	0.88	-2.22	-22.8	-1.8		1.6
7	TS/l	0.14		4.2	0.89	-2.51	-16.2	-11.9		2.2
8	Malay+	0.38		4.7	1.03	-2.73	-27.6	0		2.5
9	Malay	0.42		4.8	1.34	-1.00	-11.3	0.8		2.6

Date: 21-Aug-85

No	Kite type	Inclination wt deg	f deg	cat deg	Azimuth f deg	Tension ref N	drift % T	dWz/W22 %	Wind decorr s	Rka / W s
1	Delta			2.7	0.84	-1.99	-11.8	1.7		2.5
2	TS/s	0.57		2.3	1.49	5.02	74.9	0		2.7
3	”	0.73		6.0	1.55	2.52	44.9	9.6		1.9
4	TS/l	0.73	0.20	2.7	3.59			1.8		3.9
5	”	0.41		3.6	1.58	-6.64	-79.8	15.2		2.8
6	Cody	0.13		1.2	0.58	-1.69	-7.4	0		3.8
7	Flare	0.21		0.9	0.86	-1.74	-11.0	3.0	6	5.9
8	Malay	0.57	0.14	1.5	4.16	-1.74	-36.1	5.8		6.8
9	Flare			0.3				7.2		6.2

Date: 22-Aug-85

No	Kite type	Inclination wt deg	f deg	cat deg	Azimuth f deg	Tension ref N	drift % T	dWz/W22 %	Wind decorr s	Rka / W s
1	Cody	0.07		1.7		3.14	7.9	2.5		3.5
2	”	0.09		1.5	0.53	-5.81	-19.4	1.7		3.6
3	”	0.04		1.2	0.32			3.5		2.9
4	”	0.04	0.01	0.9	0.16	1.19	1.3	2.0		2.5
5	”			1.7		-2.93	-5.8	3.0		3.1
6	”			1.7		-2.93	-6.2	3.3		3.2
7	”	0.06		1.7	0.69			3.3		3.4
8	”	0.09		2.3	0.79	-1.82	-6.0	3.8		3.3
9	”			0.9		-2.90	-6.8	3.2		3.6
10	”	0.11		1.4	0.72	-1.23	-4.2	3.3	13	3.3
11	Flare			0.9	0.62	-1.35	-4.1	3.4	16	5.3
12	”	0.05		0.5	0.39	-2.08	-3.6	3.1		5.6

Table 13c. Experiment error summary

Airspeed ft s^{-1}	Airspeed m s^{-1}	Incidence deg	Cl	Cd	Cp
30	9.14	5.0	0.230	0.096	0.110
		7.8	0.381	0.128	0.117
		9.7	0.419	0.143	0.186
		14.4	0.556	0.212	0.250
		19.5	0.673	0.299	0.287
		24.6	0.711	0.382	0.332
		28.0	0.732	0.444	0.347
		31.1	0.728	0.480	0.336
40	12.19	5.0	0.236	0.123	0.075
		7.8	0.378	0.134	0.116
		9.6	0.423	0.148	0.175
		14.4	0.565	0.217	0.248
		17.1	0.646	0.271	0.275
		19.3	0.668	0.296	0.296
		24.2	0.726	0.382	0.324

Coefficients defined using area of 10.68 m^2 and kite length of 2.62 m.

mass	=	10.57 kg	chord	=	3 ft	=	0.91 m
area	=	10.68 m^2	length	=	8.6 ft	=	2.62 m

Table 14. B Type Cody kite wind tunnel data (Naylor, 1940)

Incidence deg	Cl	Cd	L/D
-6	0.070	0.135	0.508
-4	0.169	0.126	1.295
-2	0.272	0.128	2.062
0	0.372	0.131	2.734
2	0.468	0.137	3.281
4	0.570	0.146	3.827
6	0.674	0.153	4.297
8	0.773	0.165	4.566
10	0.823	0.183	4.422
12	0.816	0.218	3.693
14	0.765	0.256	2.974
16	0.719	0.285	2.542
18	0.695	0.311	2.216
20	0.690	0.343	2.010

area	=	360 ft^2	chord	=	4.09 m
aspect ratio	=	2.0	span	=	8.18 m
Re	=	3.8 x 10^6			

Table 15. Parafoil wind tunnel results (from Fig. 5 of Nicolaides and Tragarz, 1971).

A power law fit derived from 5 minute averages for reaction (R / N) and windspeed (W / m s^{-1}) is used for the basic calibration. The Delta and large Tailed Sled both also use a quadratic correction to improve the calibration, since their performance is good enough to warrant this.

Power law	$W = mR^n$
Quadratic correction	$W' = W + c_0 + c_1.W + c_2.W^2$

s(W) and s'(W) are the error standard deviations remaining after using the indicated kite anemometer calibrations.

Kite (bridle setting / deg)	Exponent (n)	Coefficient (m)	Range m s^{-1}	s(W) m s^{-1}	
Cody (74)	0.592	0.790	5.9–9.3	0.35	
” (77,79)	0.680	0.605	7.1–8.8	0.28	
Delta	0.789	1.023	3.4–9.8	0.49	*
Flare (84,86)	0.736	0.352	5.2–6.9	0.08	
” (87+)	0.627	0.618	4.3–7.9	0.22	
Gibson (56)	0.743	1.012	6.2–9.0	0.16	
” (90)	0.751	1.480	6.3–11.2	0.30	
Malay	0.945	1.066	6.2–10.1	0.31	
Parafoil	0.754	0.361	5.5–10.5	0.25	
Tailed sled (large)	0.789	1.314	4.0–13.1	0.45	*
” (small)	0.591	3.076	5.6–12.1	0.37	
Vented sled	0.648	1.768	4.2–9.1	0.19	

* these two calibrations are improved using the quadratic correction given by:

Kite	c_0	c_1	c_2	s'(W) m s^{-1}
Delta	-0.110	1.528	-4.677	0.22
Tailed sled (large)	-0.030	0.458	-1.315	0.14

Table 16. Kite Anemometer Calibrations.

Figures 79 and 80 use these data files and parameters.

Figure	Raw data file	Records first	Records last	Averaging period s
a–h	`SEH14B:TM14DEC2.DATA`	1350	7773	0.3
i–l	`SEH23B:TM11JUN7.DATA`	503	3689	0.4

Caption	Channel	Variance	Correlation file / record
a) Cody, windspeed	16	1.22 $m^2\ s^{-2}$	3/5
b) ” longitudinal wind component	12	1.23 $m^2\ s^{-2}$	4/1
c) ” lateral wind component	13	1.17 $m^2\ s^{-2}$	2/41
d) ” vertical wind component	14	0.59 $m^2\ s^{-2}$	4/2
e) ” wind azimuth	23	0.016 rad^2	2/40
f) ” kite azimuth	2	0.030 rad^2	3/6
g) ” tension	7	401 N^2	3/4
h) ” windspeed measured from tension	27	3.19 $m^2\ s^{-2}$	4/0
i) Tailed sled, large, windspeed	16	4.85 $m^2\ s^{-2}$	1/58
j) ” wind azimuth	23	0.018 rad^2	2/63
k) ” kite azimuth	2	0.052 rad^2	2/62
l) ” windspeed measured from tension	27	10.06 $m^2\ s^{-2}$	1/49

Table 17. Data used for autocorrelation and FFT examples.

Figures

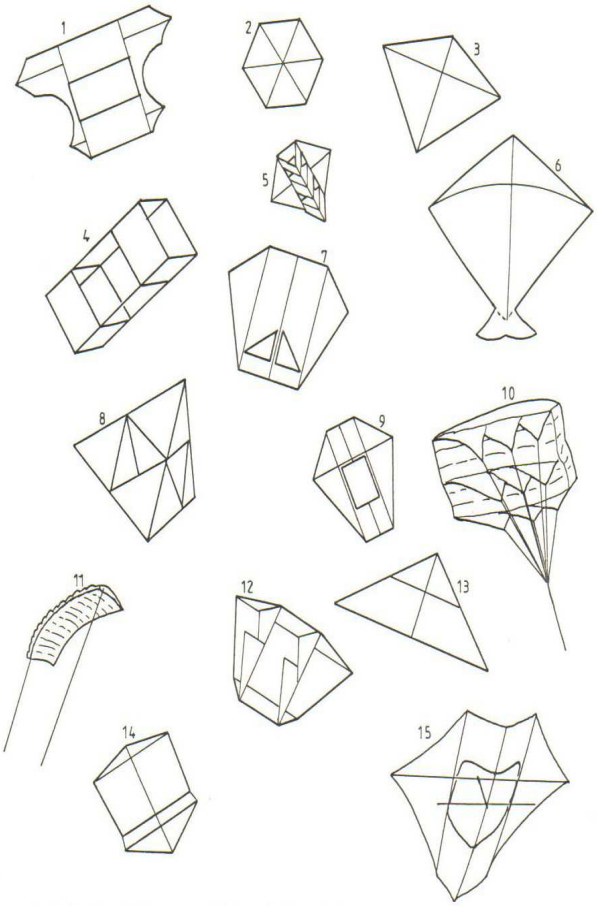

1 Cody War Kite
2 Hexagon
3 Malay
4 Square Box
5 French Rescue
6 Indian Fighter
7 Sled
8 Bell's Multi-celled Tetrahedral
9 Winged Box / Conyne
10 Parafoil
11 Flexifoil
12 Flare
13 Delta
14 Roller
15 Dunford Flying Machine

Figure 1. Examples of kite designs (not to scale).

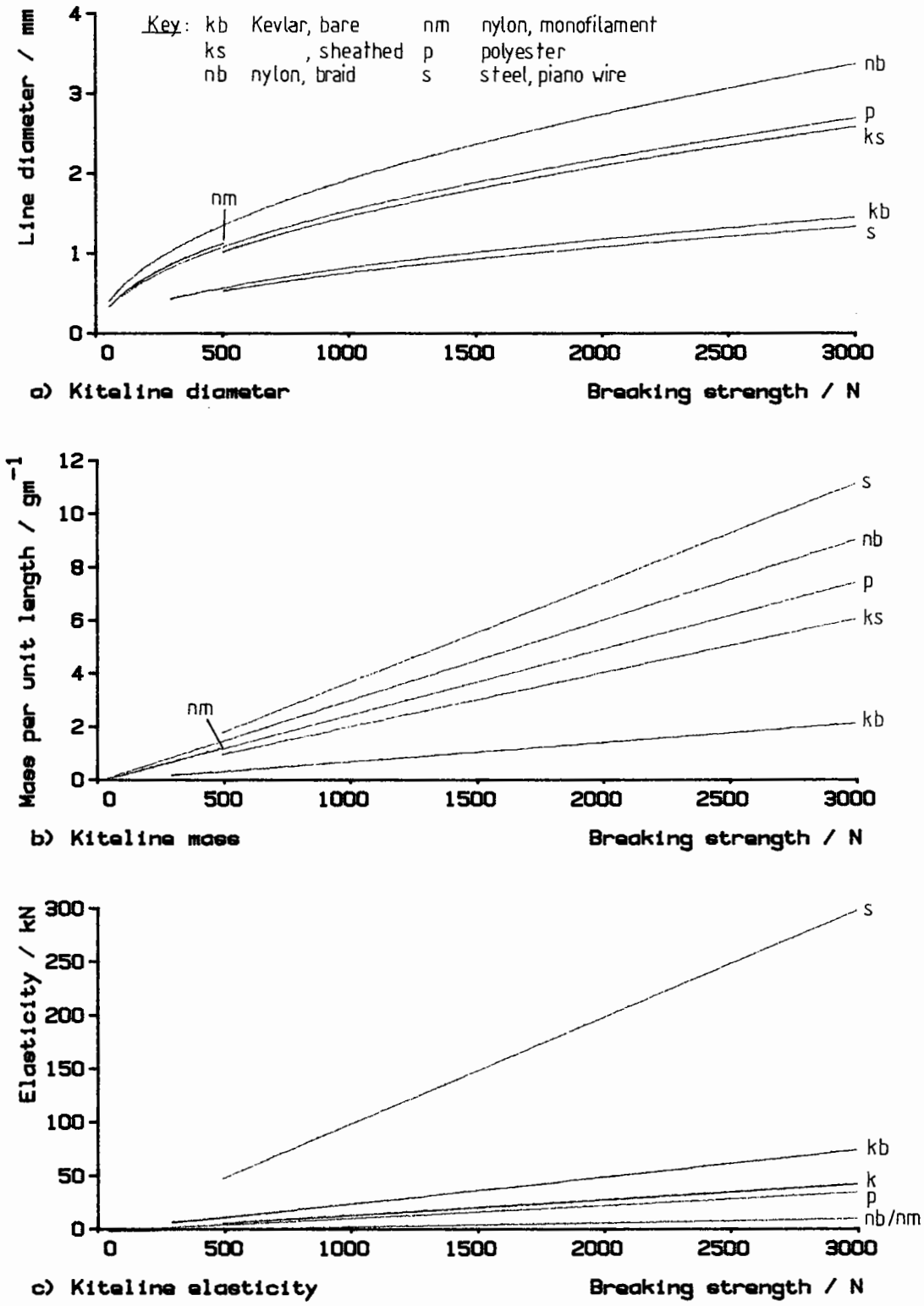

Typical kiteline properties

Figure 2

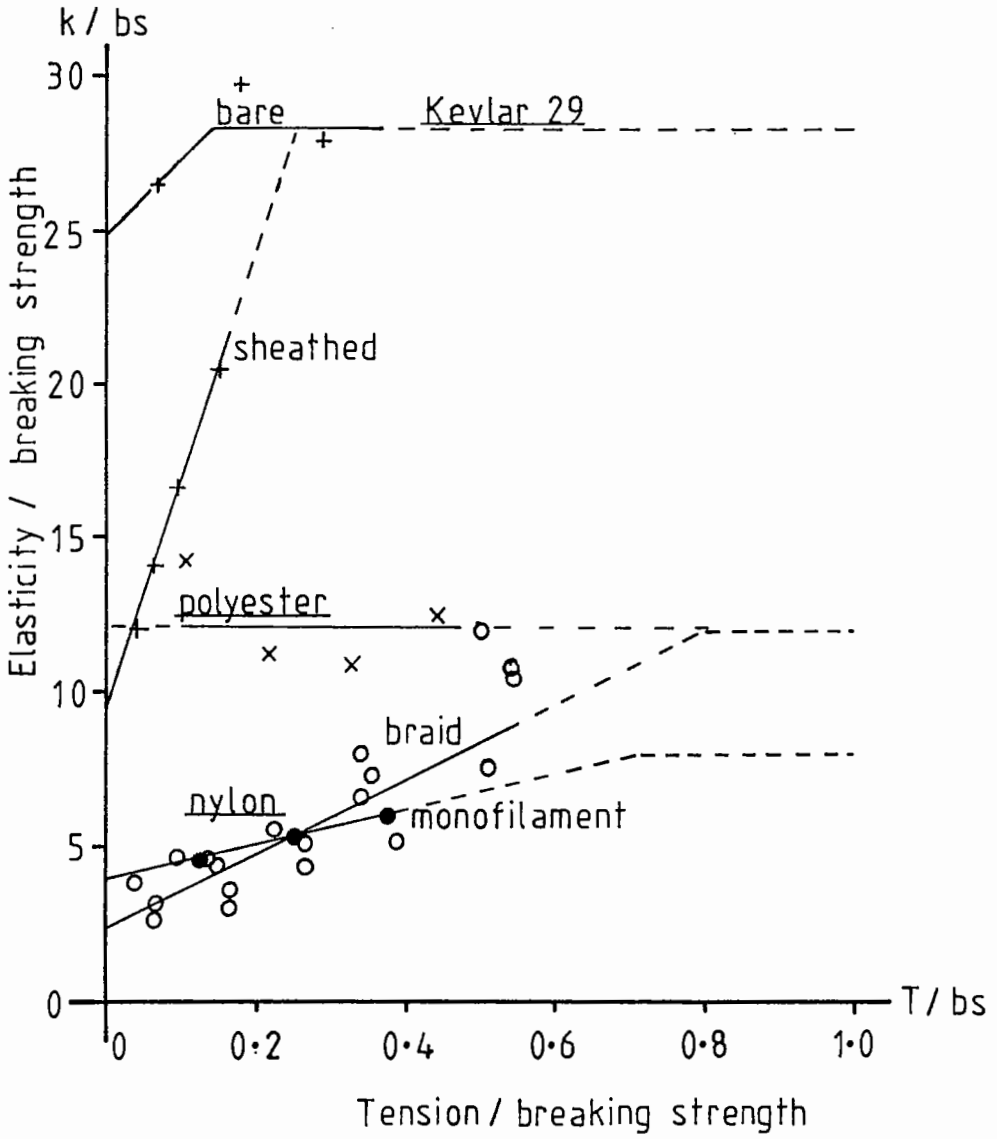

Normalised Elasticity vs Tension

Figure 3

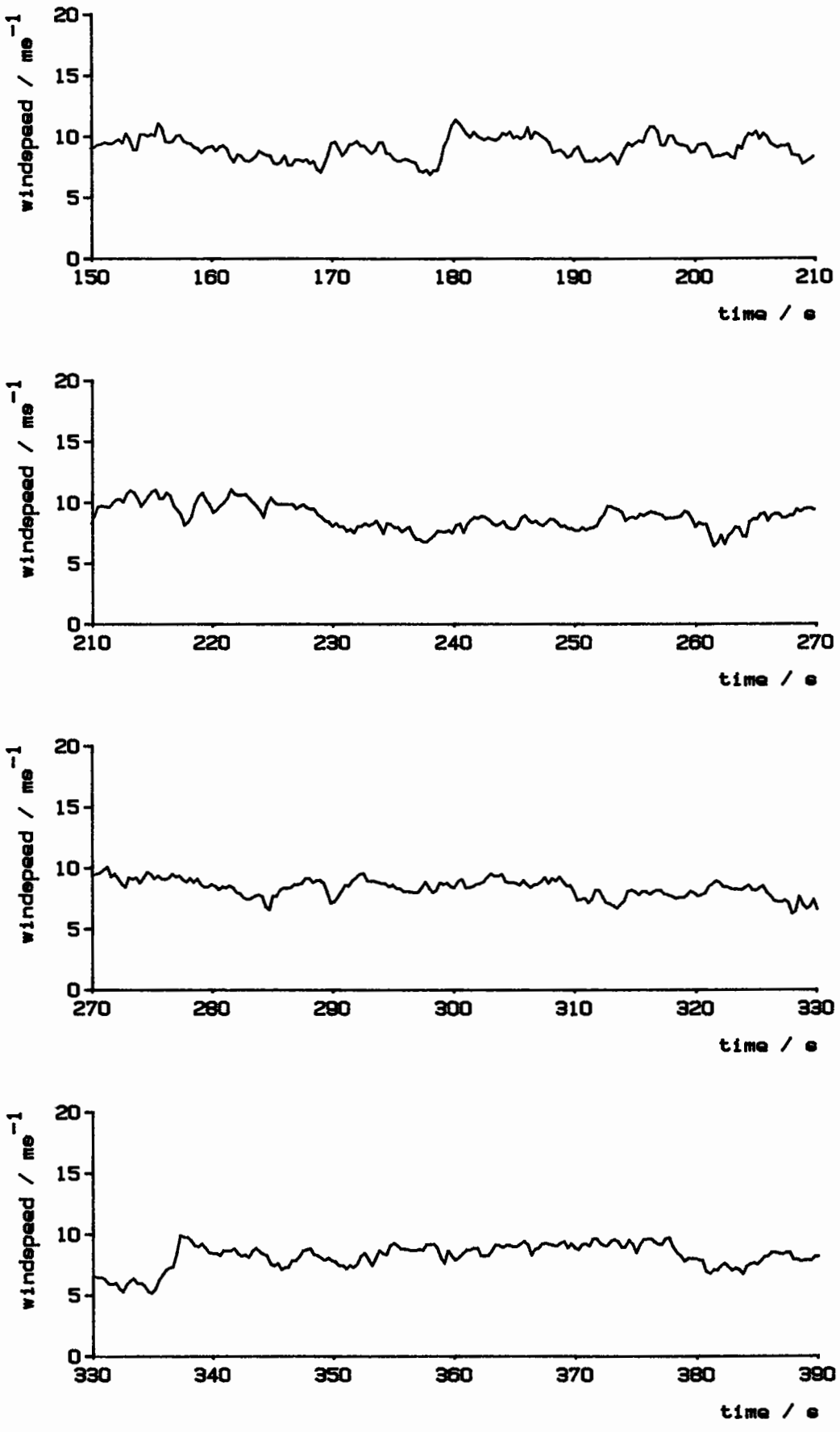

Windspeed trace example (22 m, 14 Dec 84, expt 2)

Figure 4

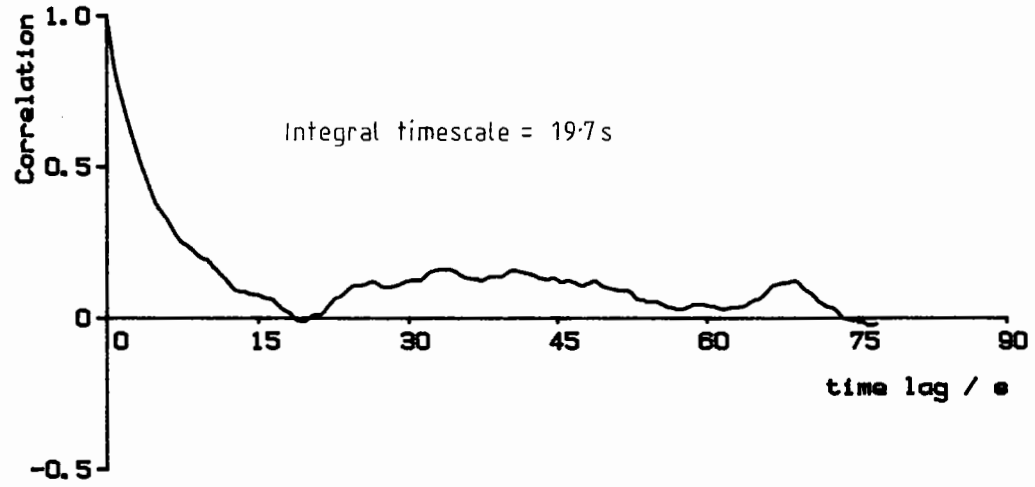

a) Autocorrelation of windspeed

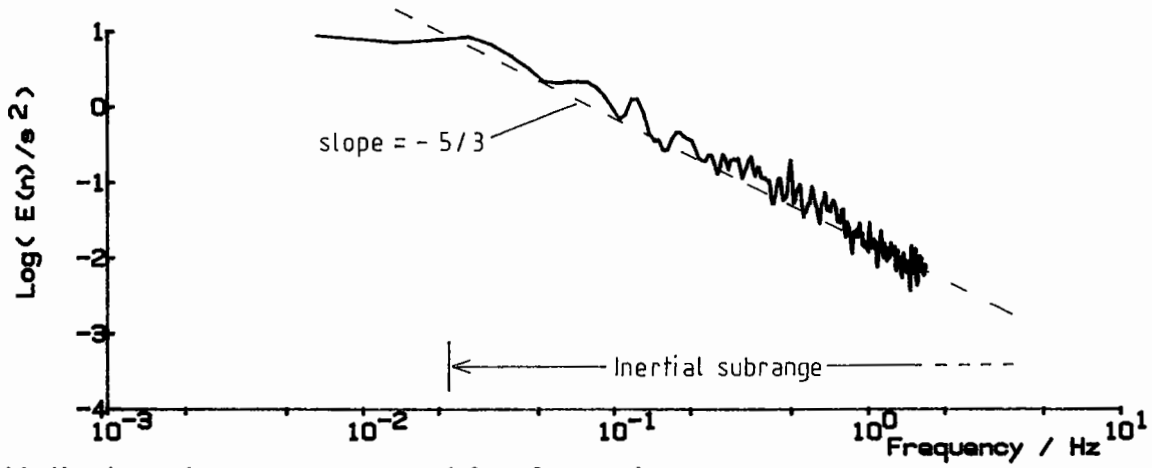

b) Windspeed power spectrum (log format)

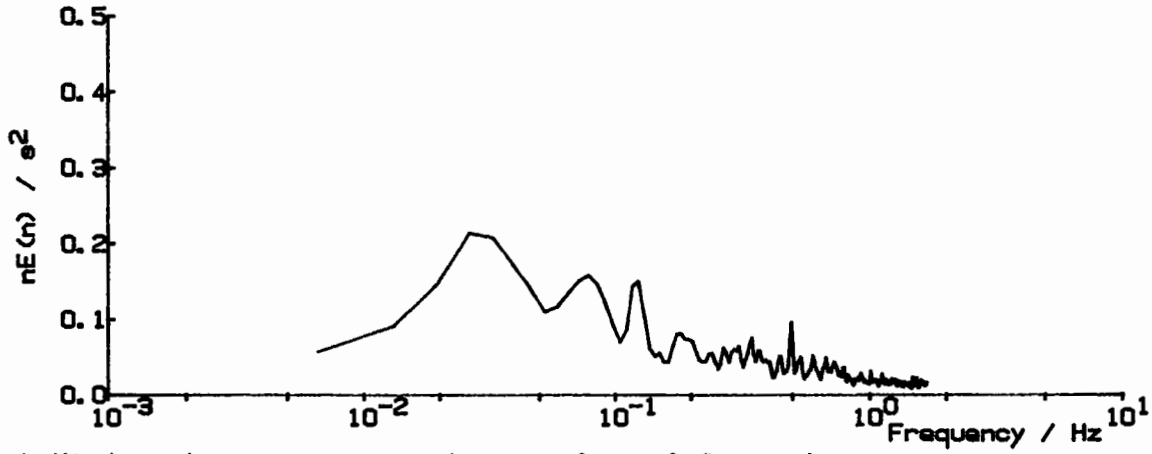

c) Windspeed power spectrum (meteorological format)

Windspeed frequency analysis examples (from Fig. 4) Figure 5

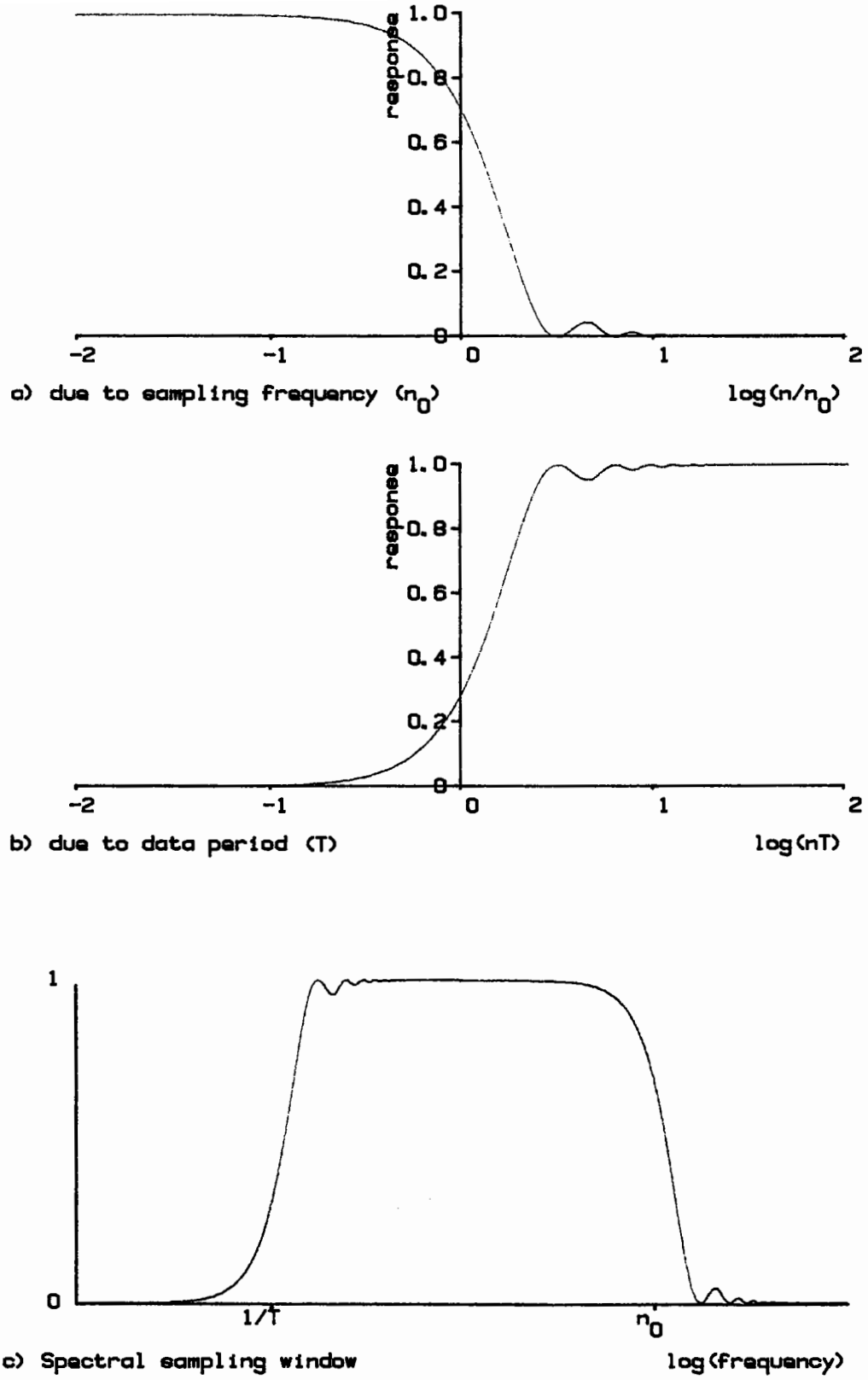

The effects of a finite sampling frequency and recording period

Figure 6

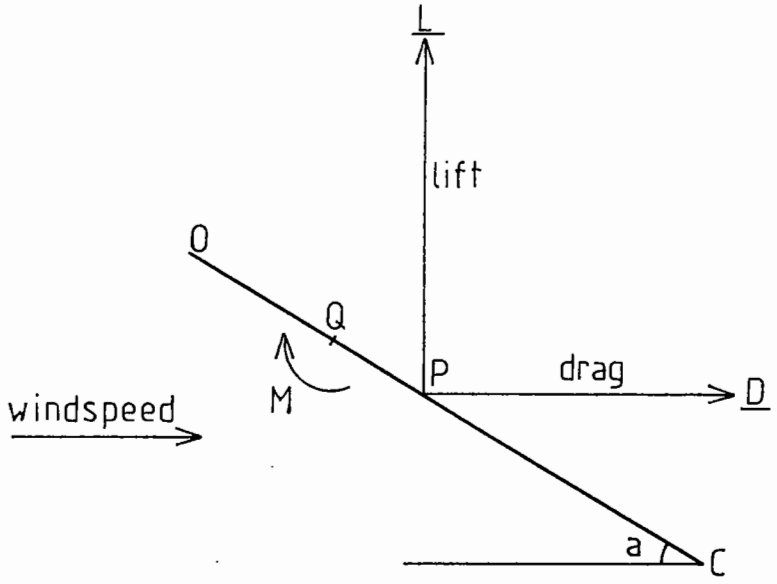

$$M = q\,S\,c\,C_m \quad \text{defines moment coefficient } C_m$$

$$C_p = \frac{OQ}{c} - \frac{C_m}{C_l \cos a + C_d \sin a}$$

Figure 7 Relationship between moment and centre of pressure coefficients

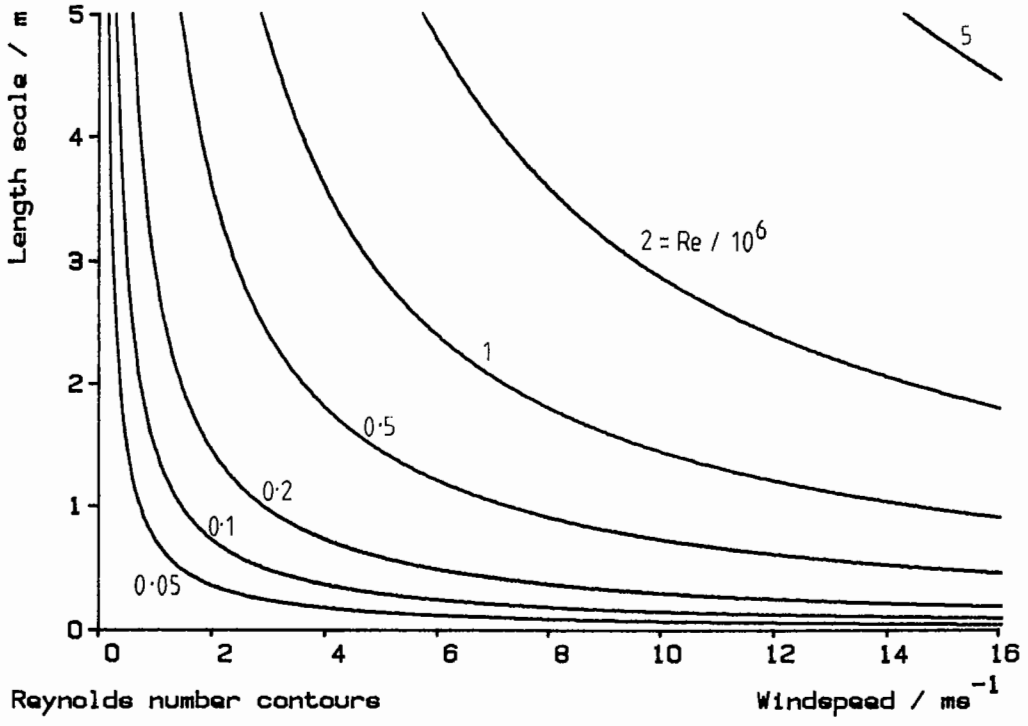

Figure 8

Figures 7 and 8

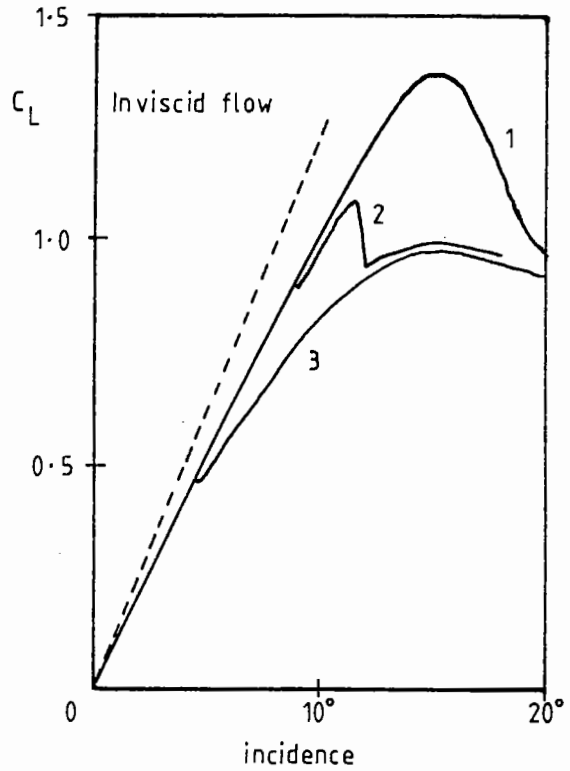

a) The behaviour of two dimensional aerofoils near maximum lift

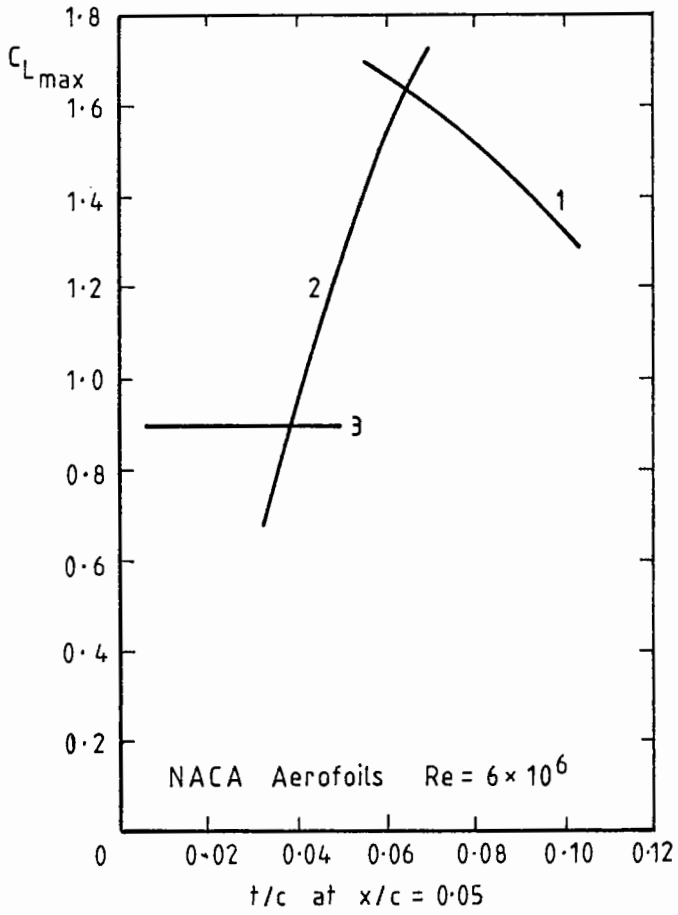

b) Maximum lift obtained on various two dimensional aerofoils

(Both figures taken from Küchemann, 1978) Figure 9

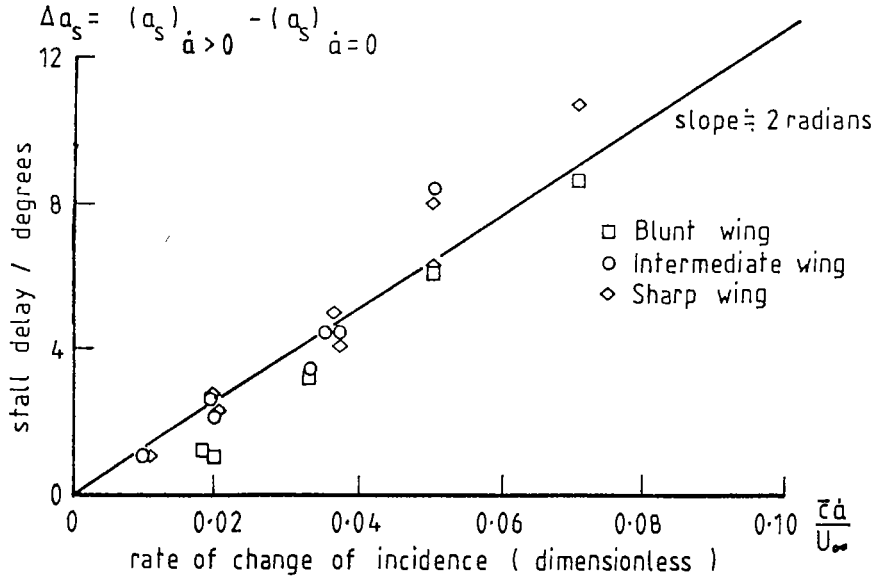

Oscillatory data for dynamic stall overshoot

(from Ericsson, 1971)

Figure 10

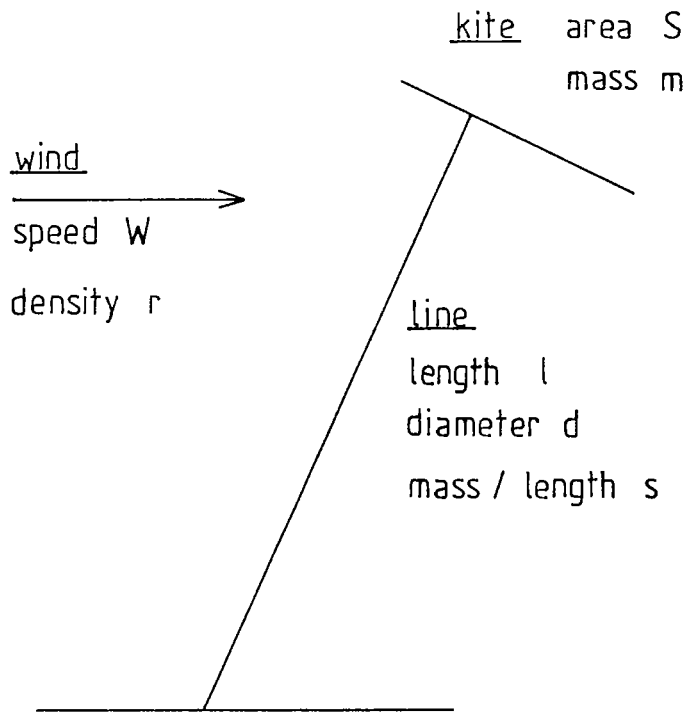

Elementary Kite System Model

Figure 11

Figures 10 and 11

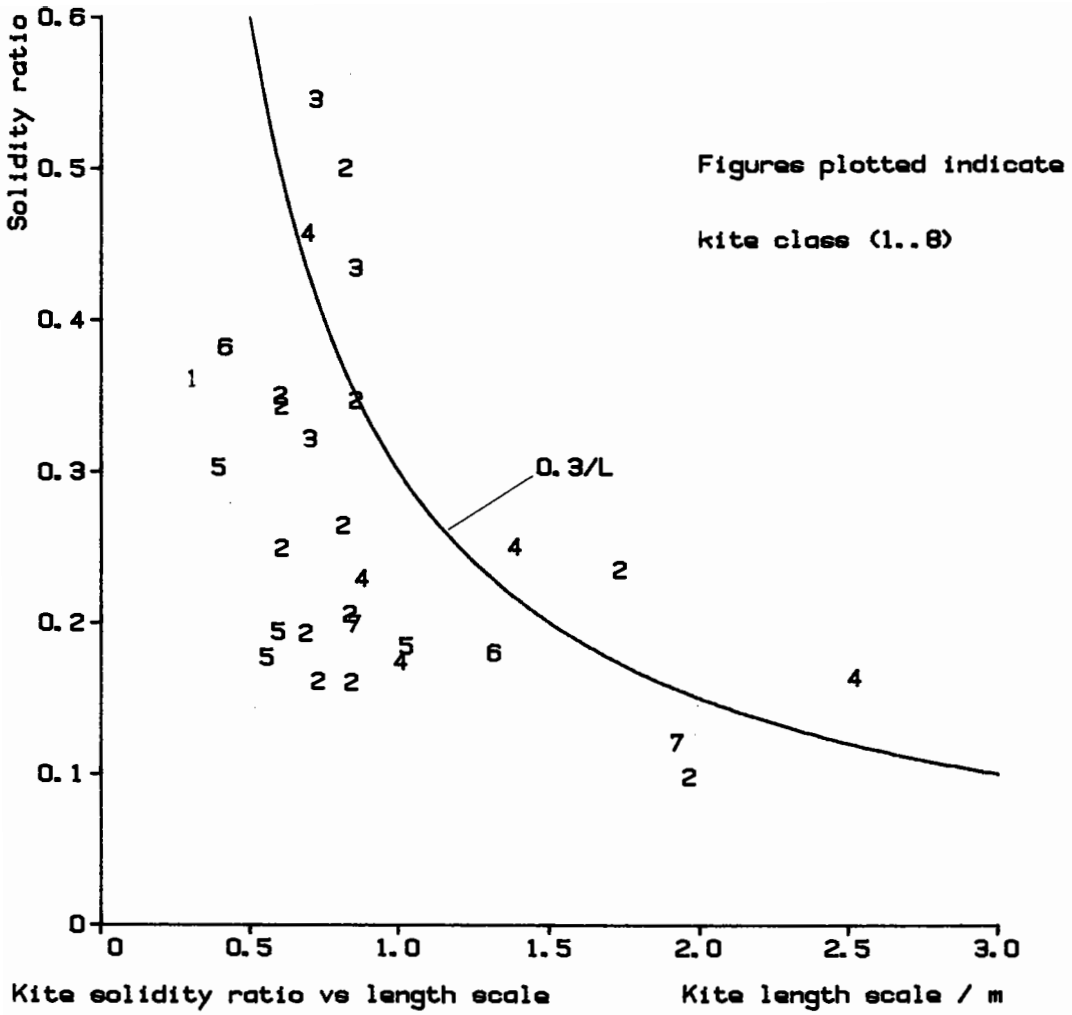
Solidity ratio
0.6
0.5
0.4
0.3
0.2
0.1
0
0
0.5
1.0
1.5
2.0
2.5
3.0
Figures plotted indicate
kite class (1..8)
0.3/L
Kite solidity ratio vs length scale
Kite length scale / m

Figure 12

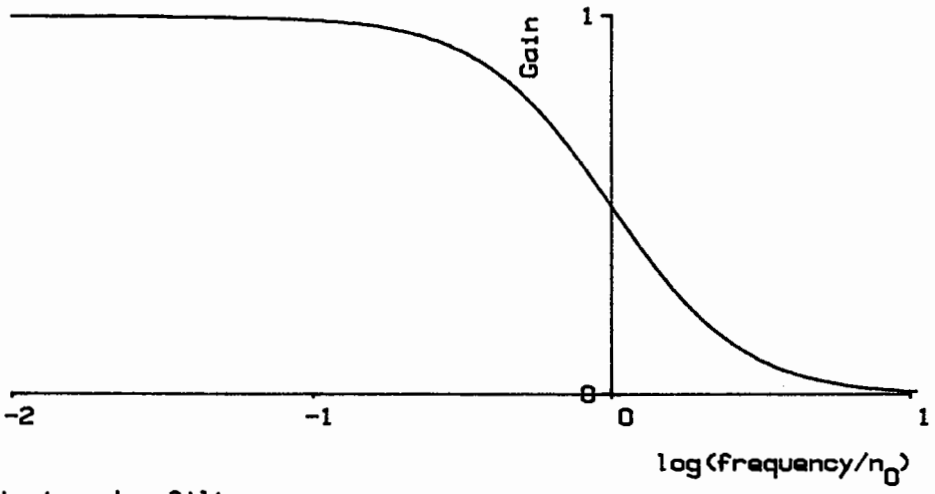

a) First order filter response

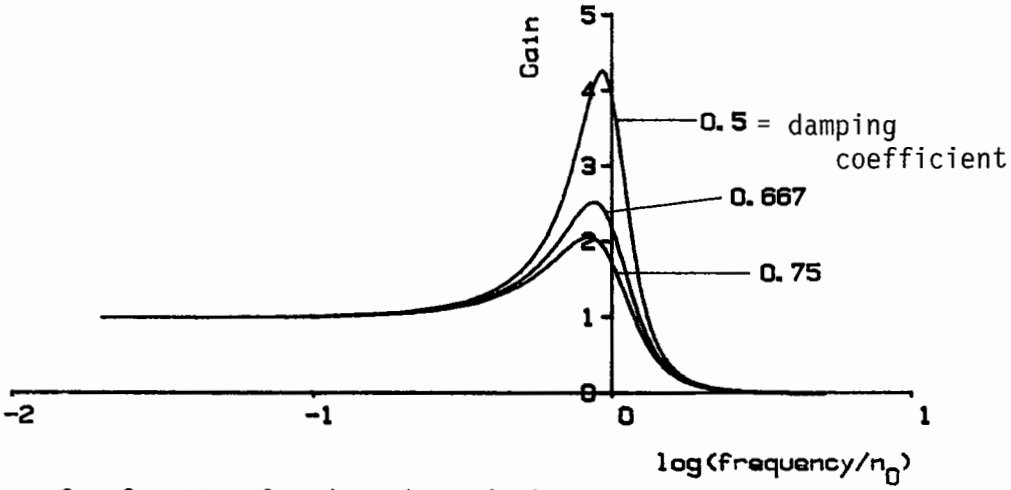

b) Transfer function for damped simple harmonic motion

Transfer functions for aspects of kite dynamics :

a) low-pass filter effect of line length

b) pendulum motion in azimuth

Figure 13

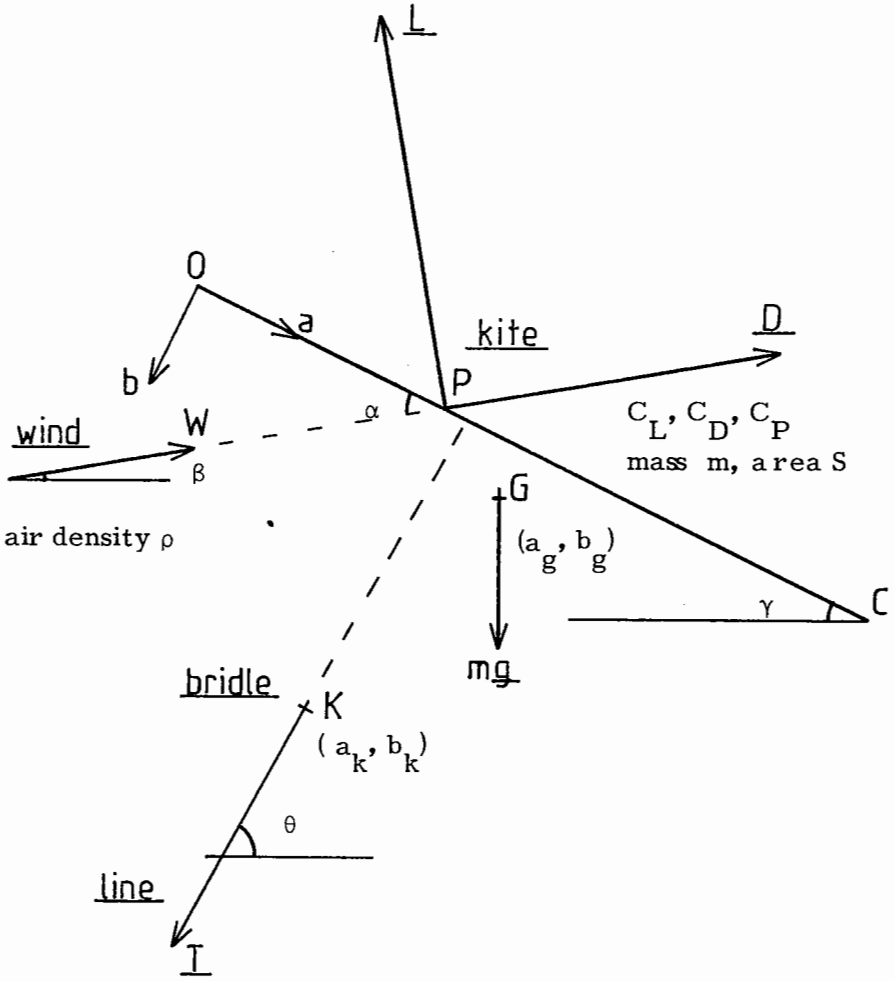

Longitudinal Kite Model

Figure 14

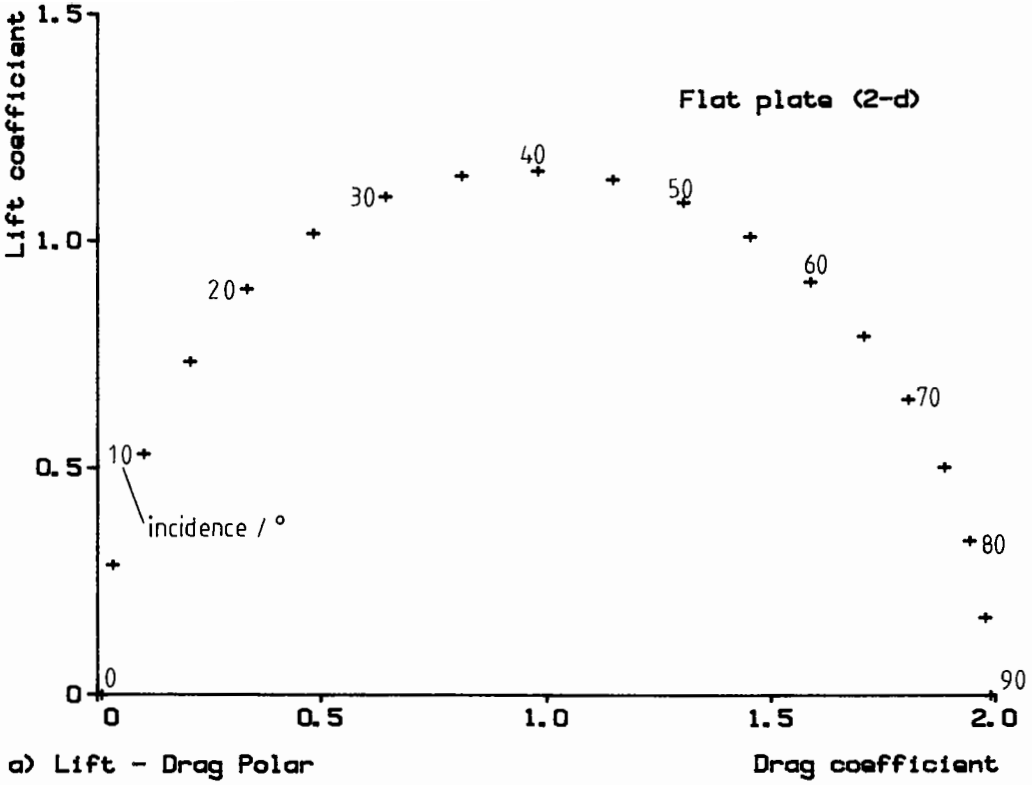

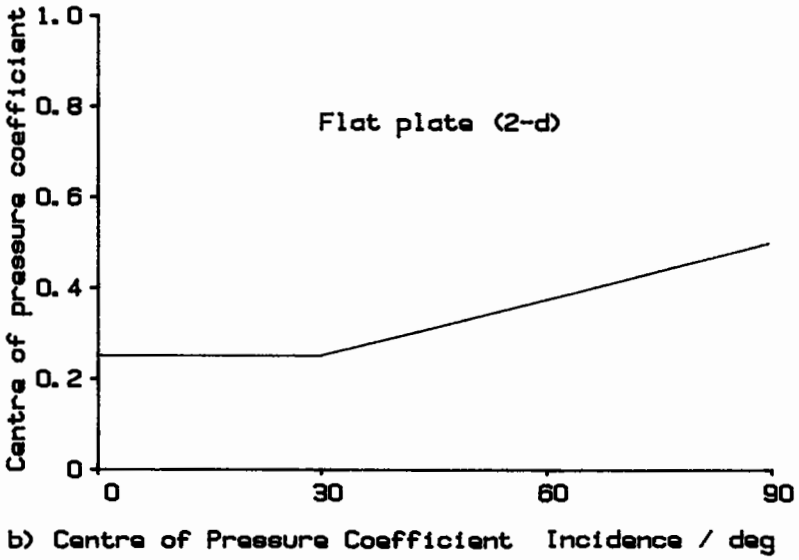

Aerodynamic characteristics of a 2-dimensional flat plate
(Hoerner 1965,1975)

Figure 15

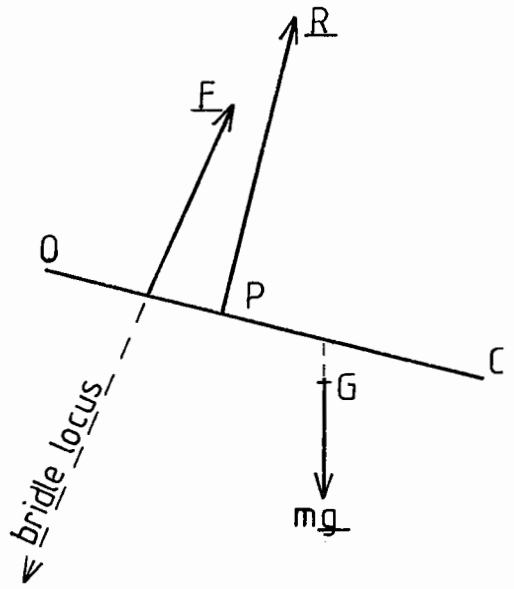

a) kite at low incidence

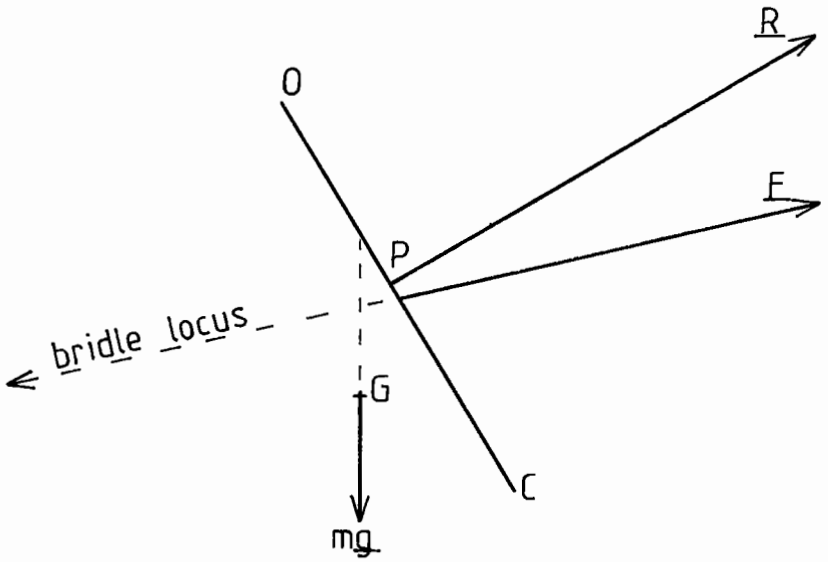

b) kite at high incidence

Longitudinal force balance for a kite in equilibrium

Figure 16

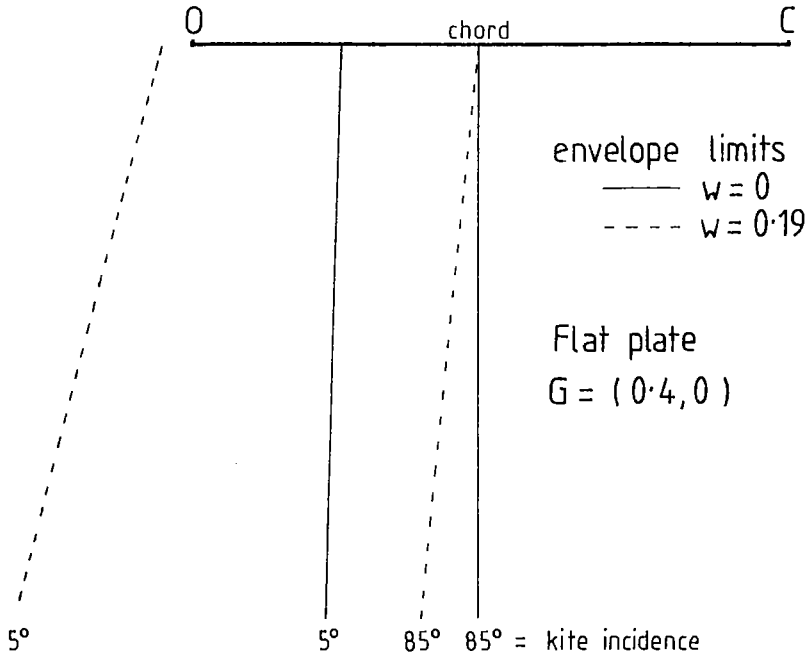

a) Bridle Envelopes for Two Kite Weights (non-dimensionalised)

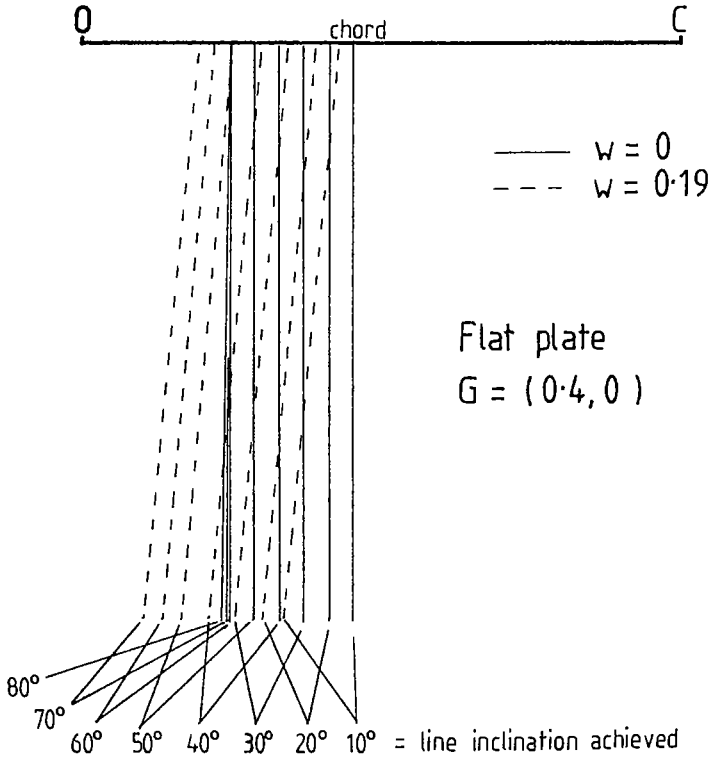

b) Bridle Loci at Two Kite Weights (non-dimensionalised)

Figure 17

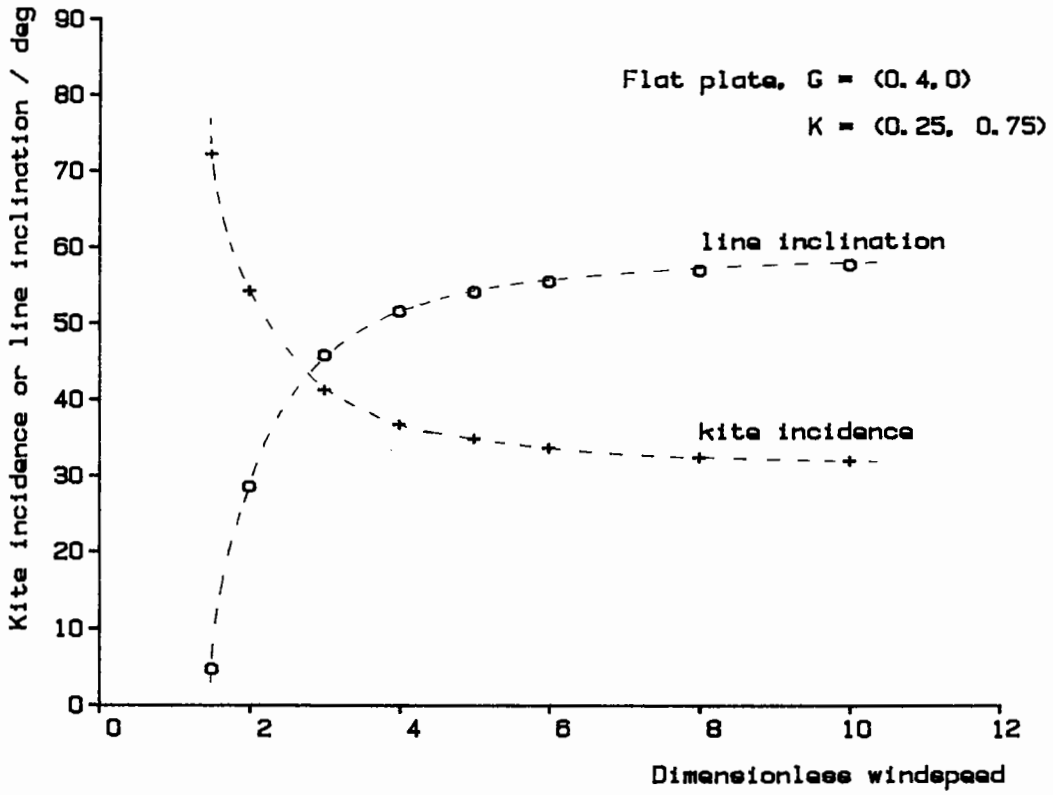

a) Inclination and Incidence vs Dimensionless Windspeed

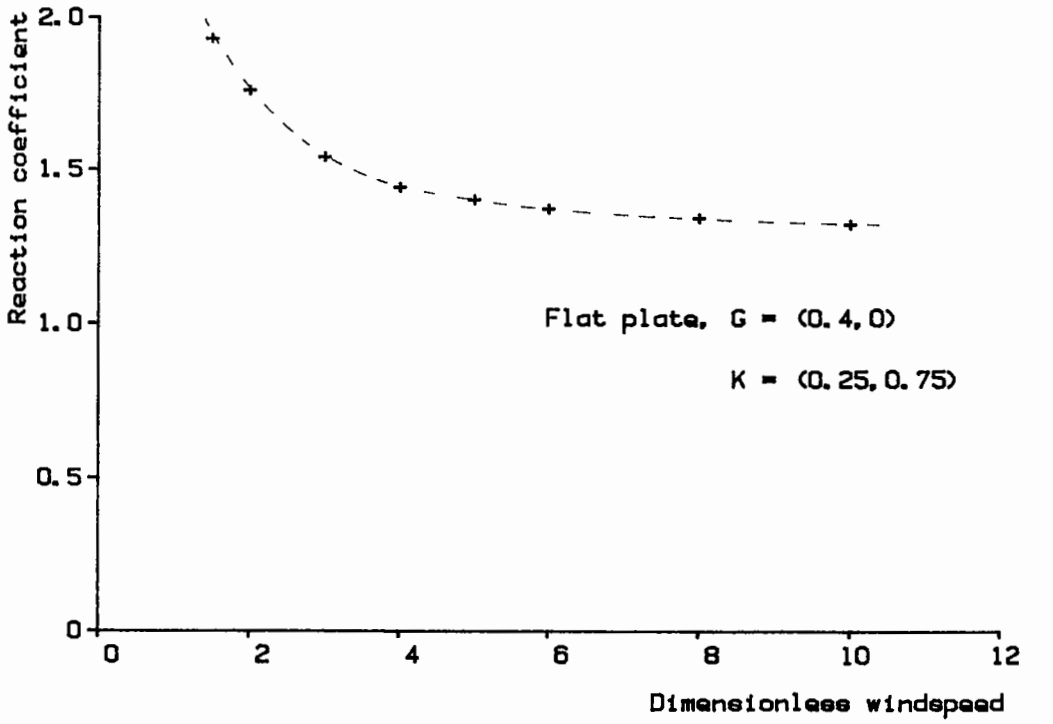

b) Reaction coefficient vs Windspeed (Flat plate)

Figure 18

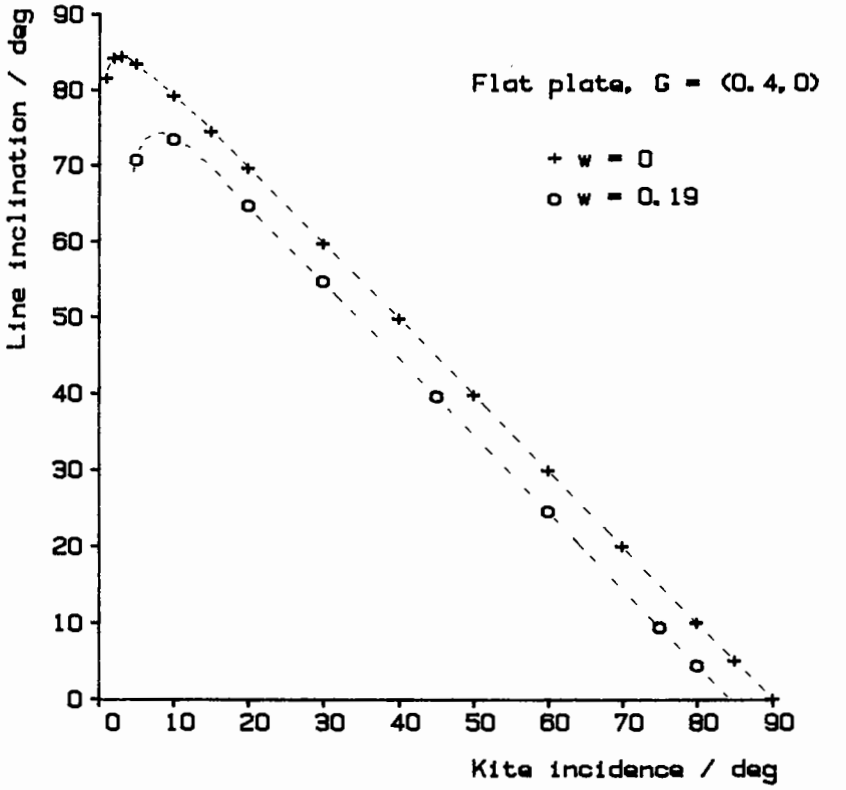

Line inclination vs kite incidence at two kite weights

Figure 19

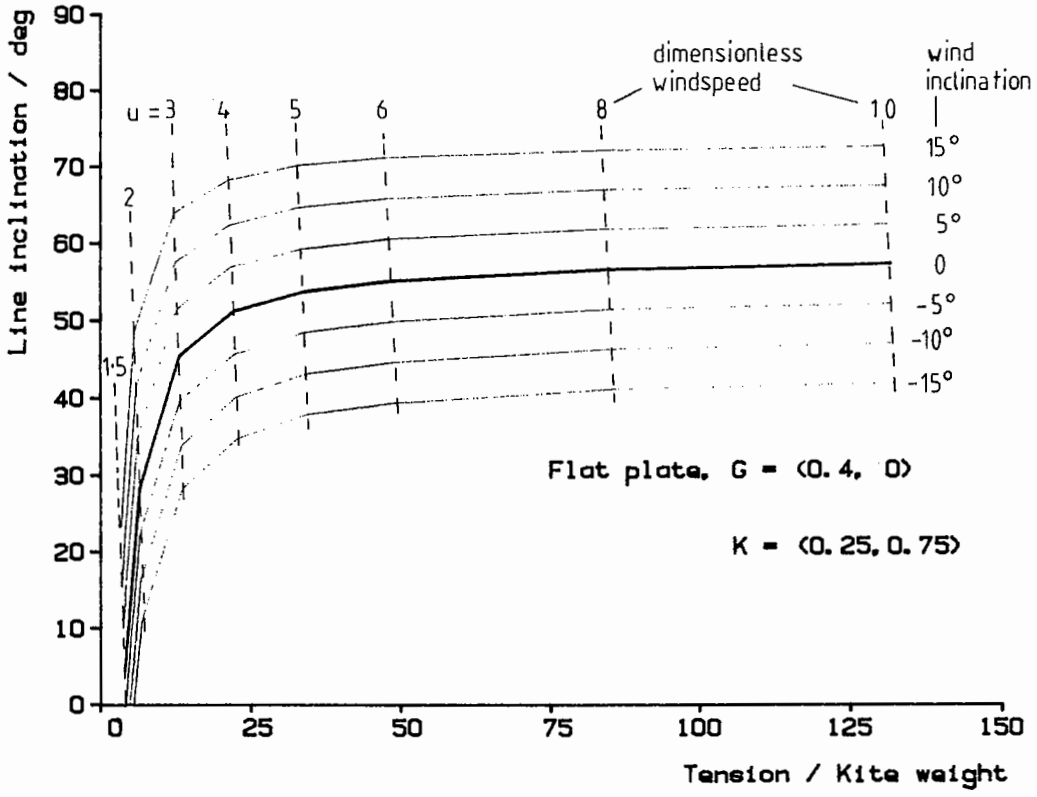

Wind velocity vs Line tension and inclination (Flat plate)

Figure 20

Figures 19 and 20

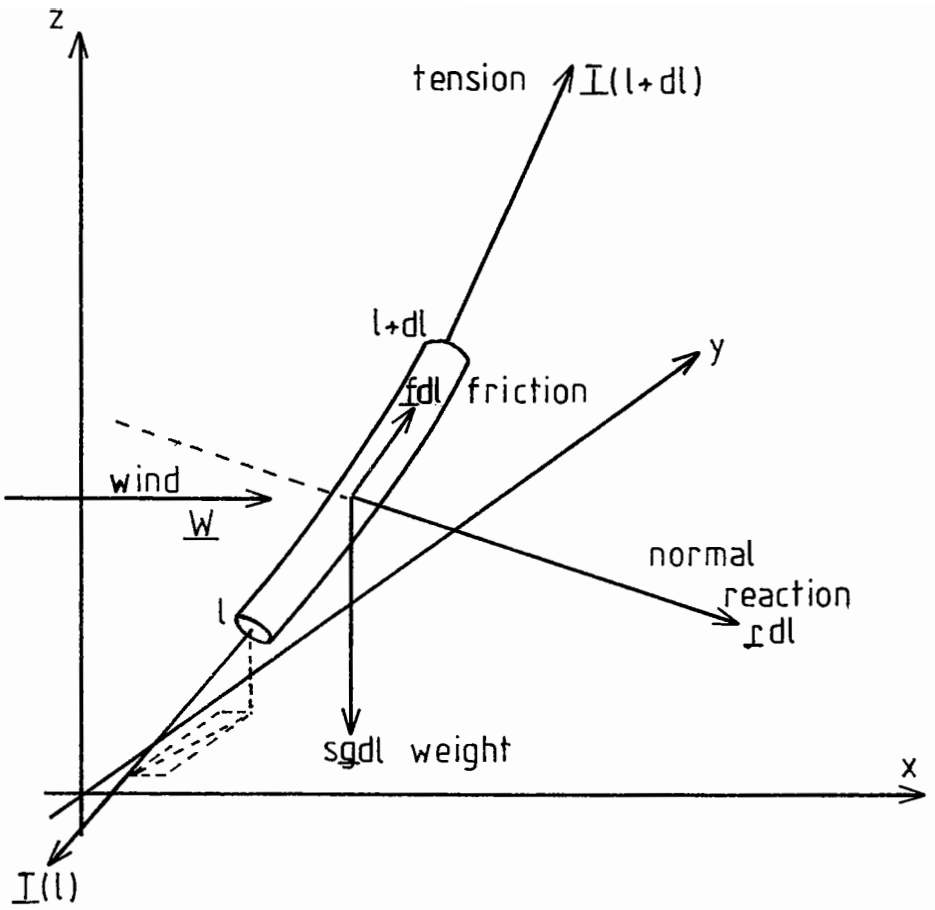

The Forces Acting on an Element of the Kiteline

Figure 21

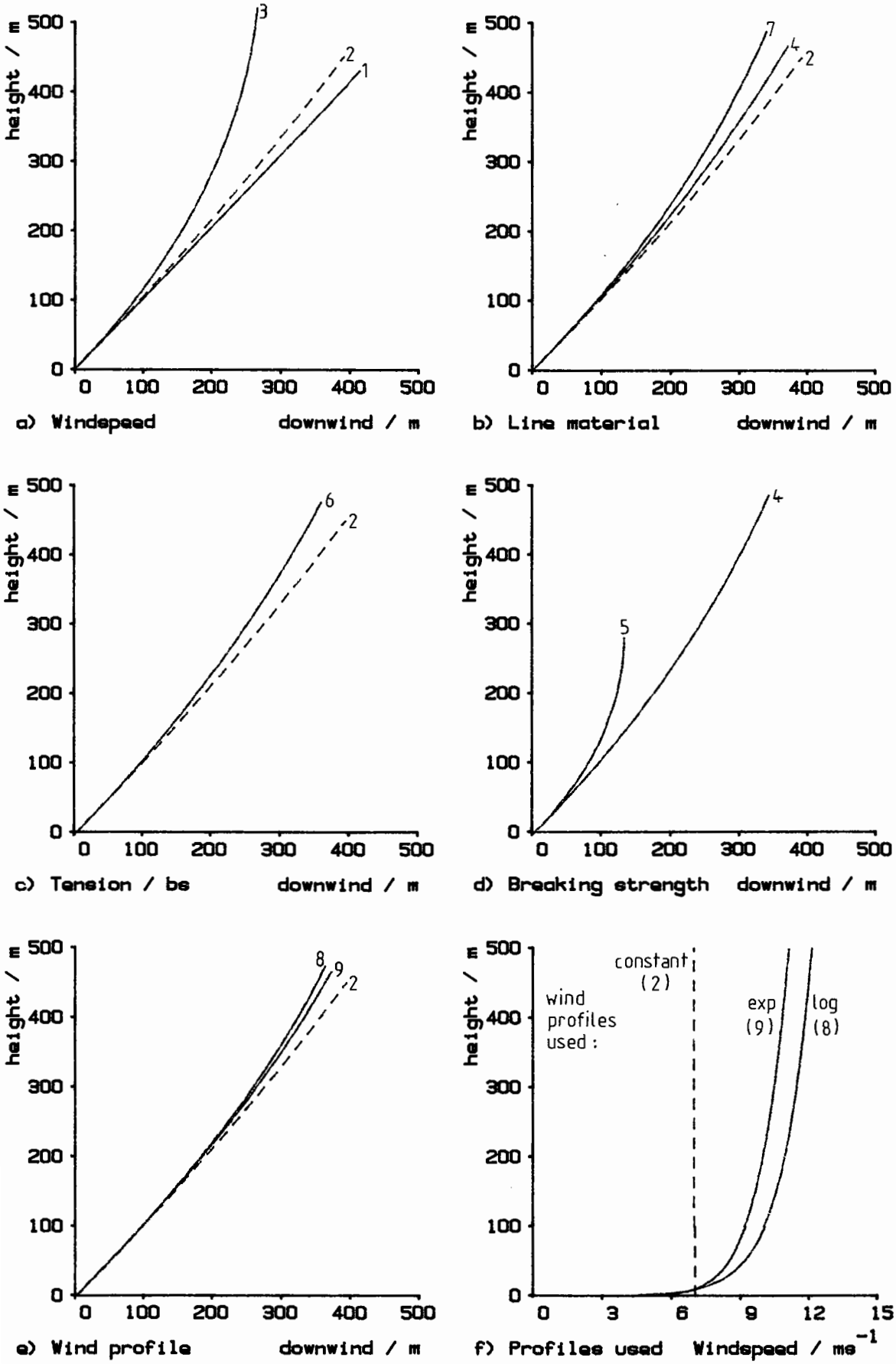

See table 8 for details of line profiles labelled 1 to 9

Kiteline profiles under various conditions

Figure 22

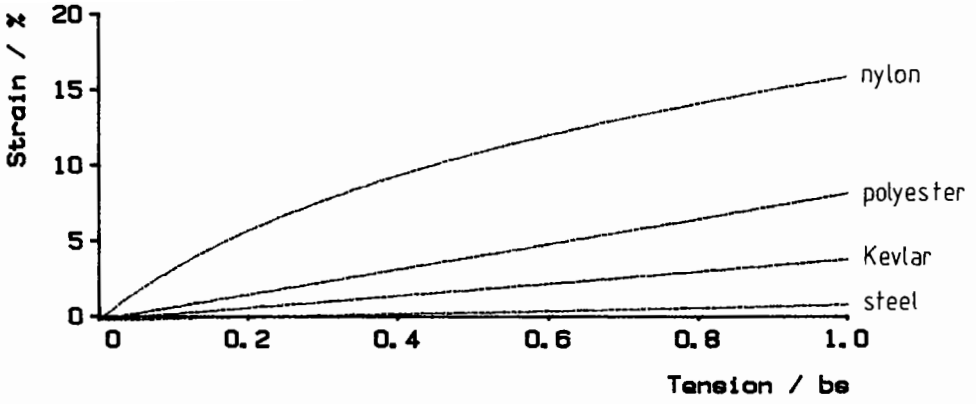

a) Kiteline strain as a function of tension

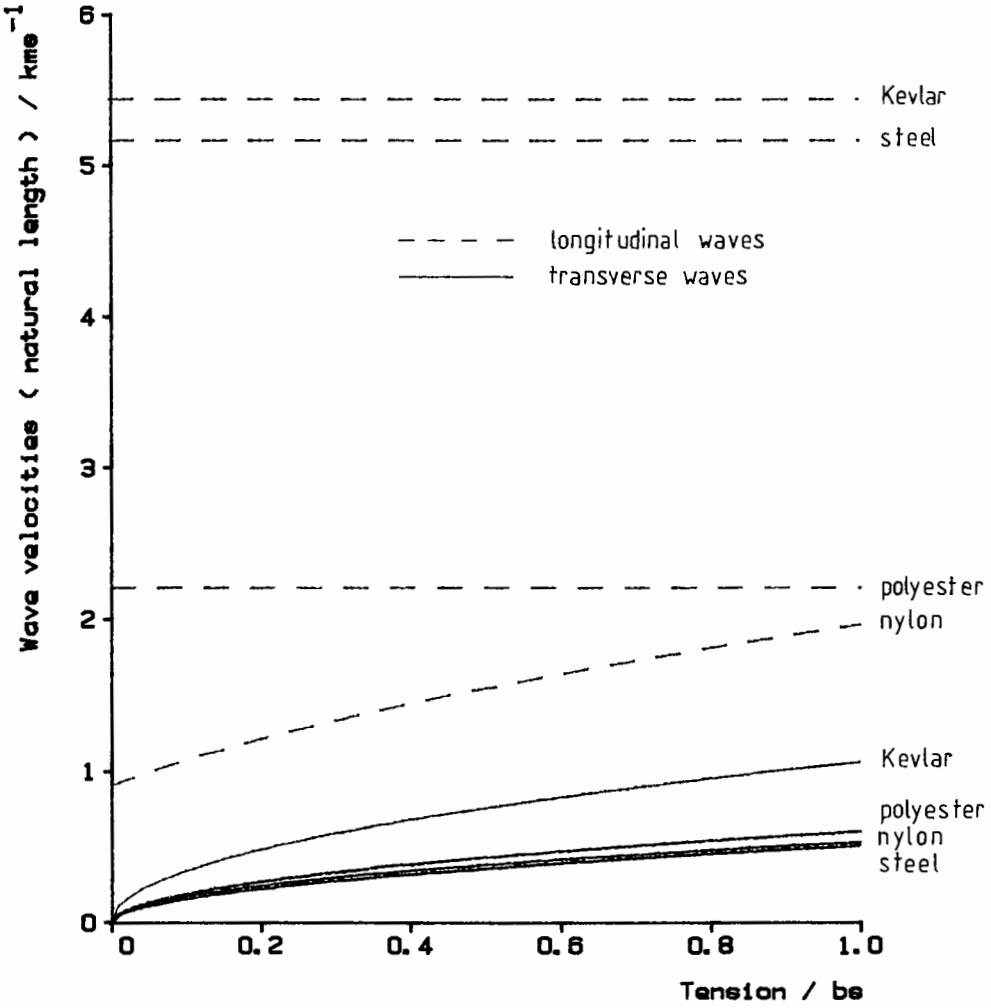

b) Wave velocities for various line materials

Figure 23

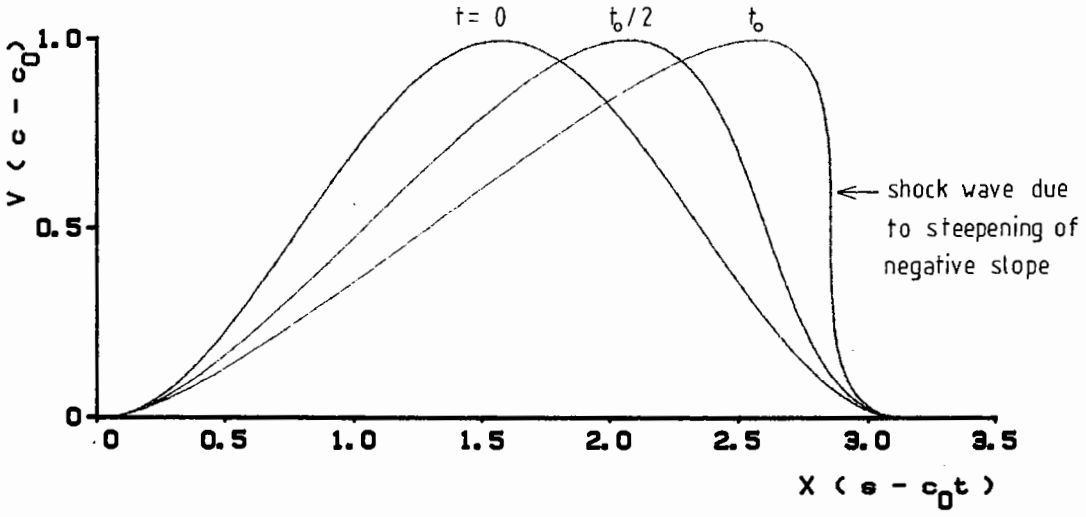

Example demonstrating shock wave formation

Figure 24

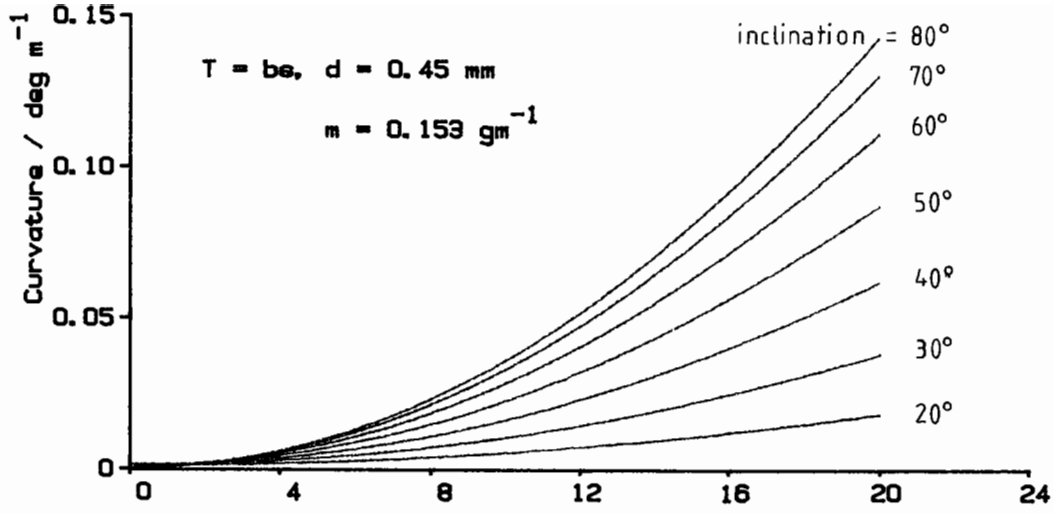

a) Line curvature, 5 kgf nylon twine

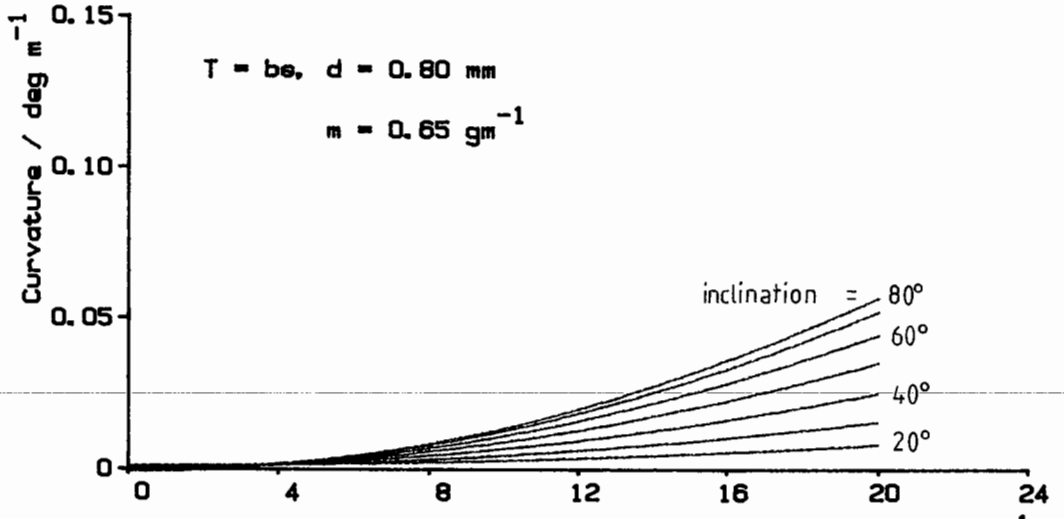

b) Line curvature, 22 kgf nylon braid

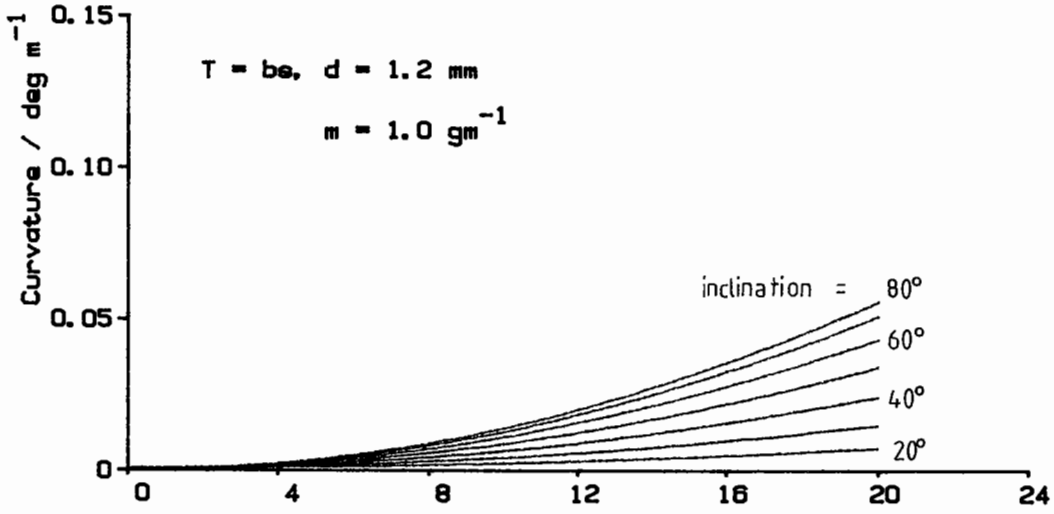

c) Line curvature, 34 kgf nylon braid

Figure 25

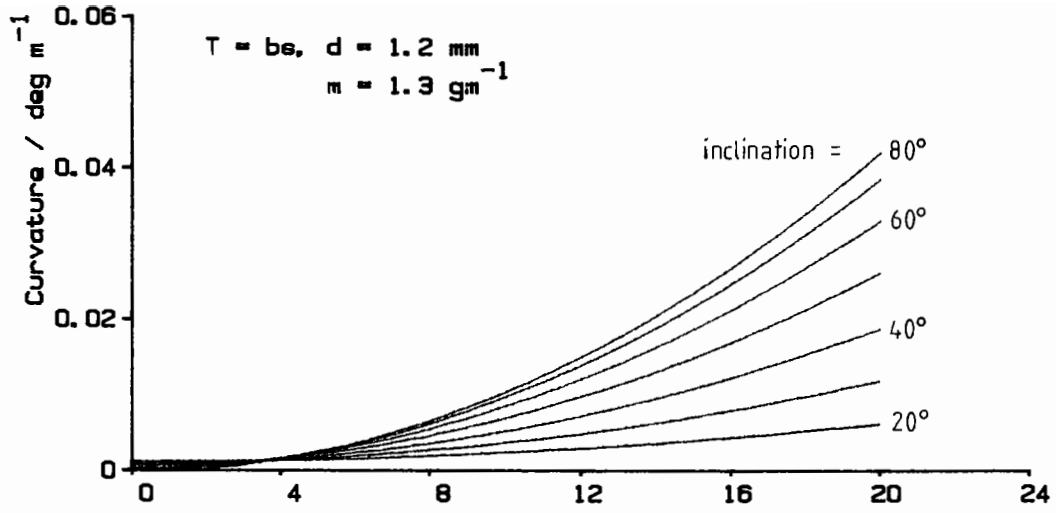

d) Line curvature, 45 kgf nylon braid

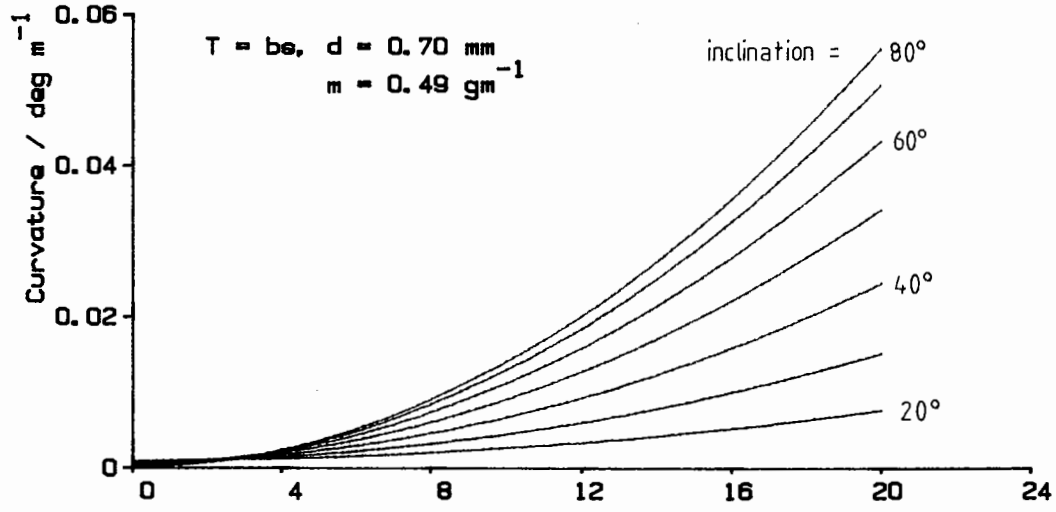

e) Line curvature, 20 kgf polyester braid

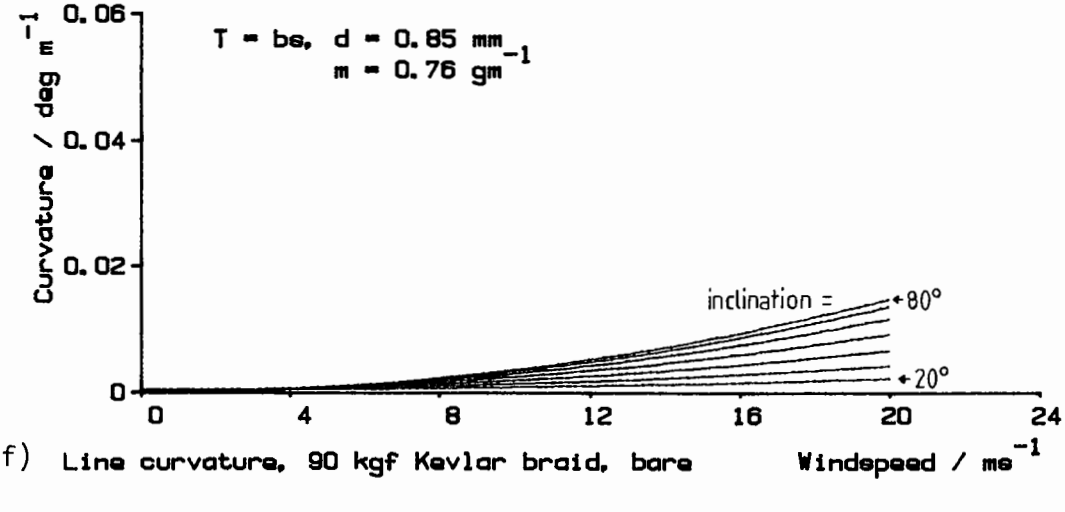

f) Line curvature, 90 kgf Kevlar braid, bare

Figure 25 cont.

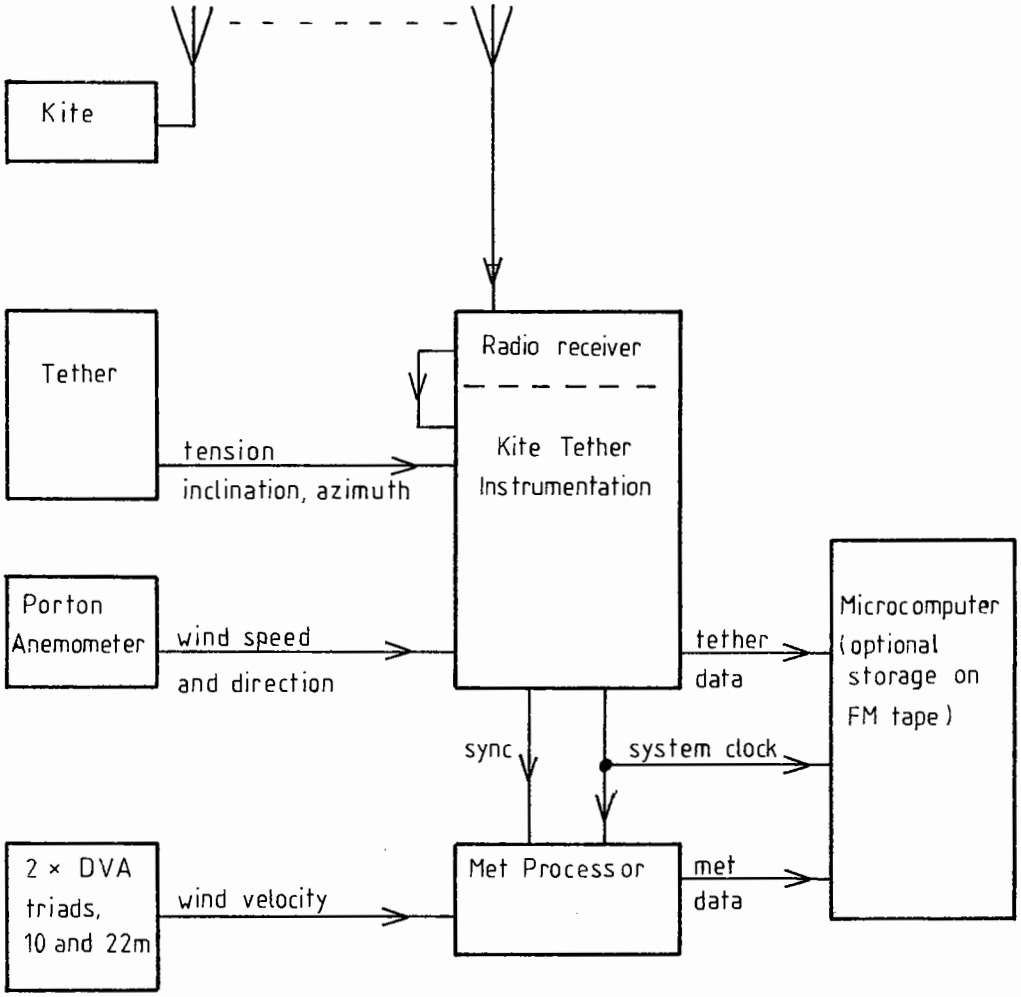

Experiment Data Collection System

Figure 26

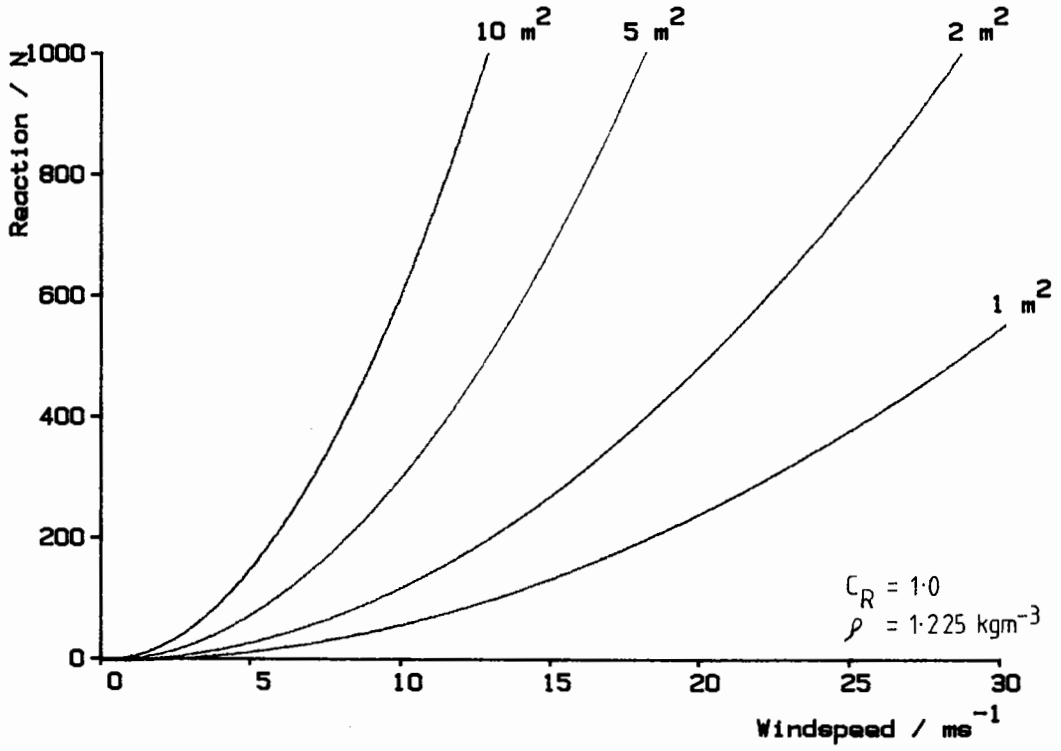

a) **Estimated Reaction Force variation with Windspeed**

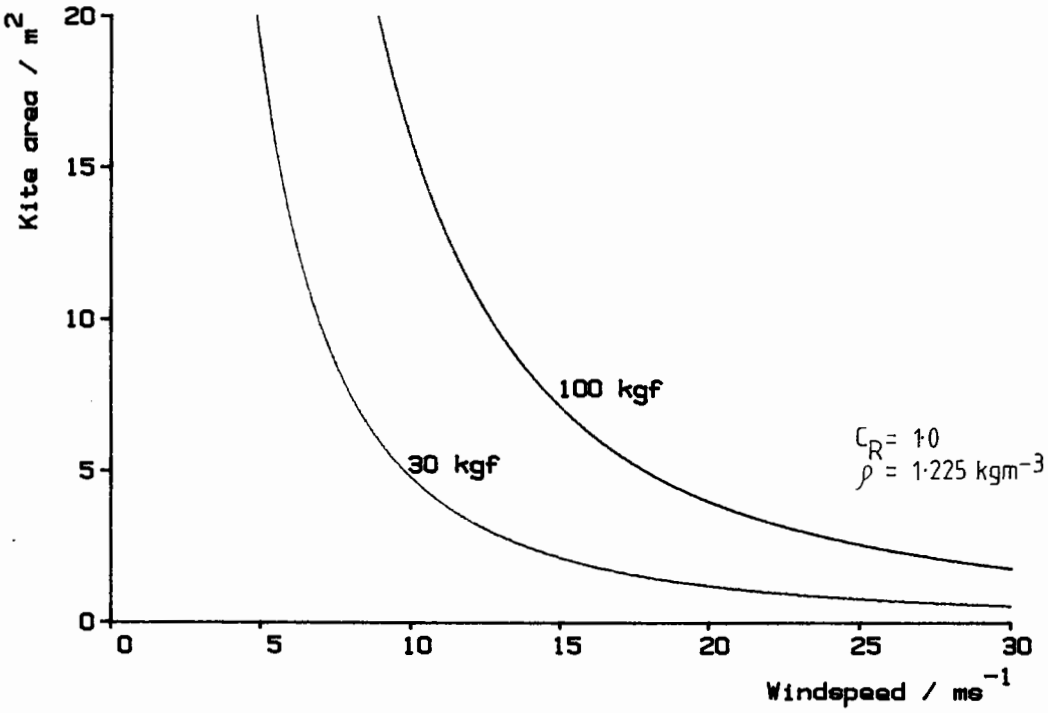

b) **Estimated Kite Area to generate specified Reaction Force**

Kite reaction vs windspeed and lifting area Figure 27

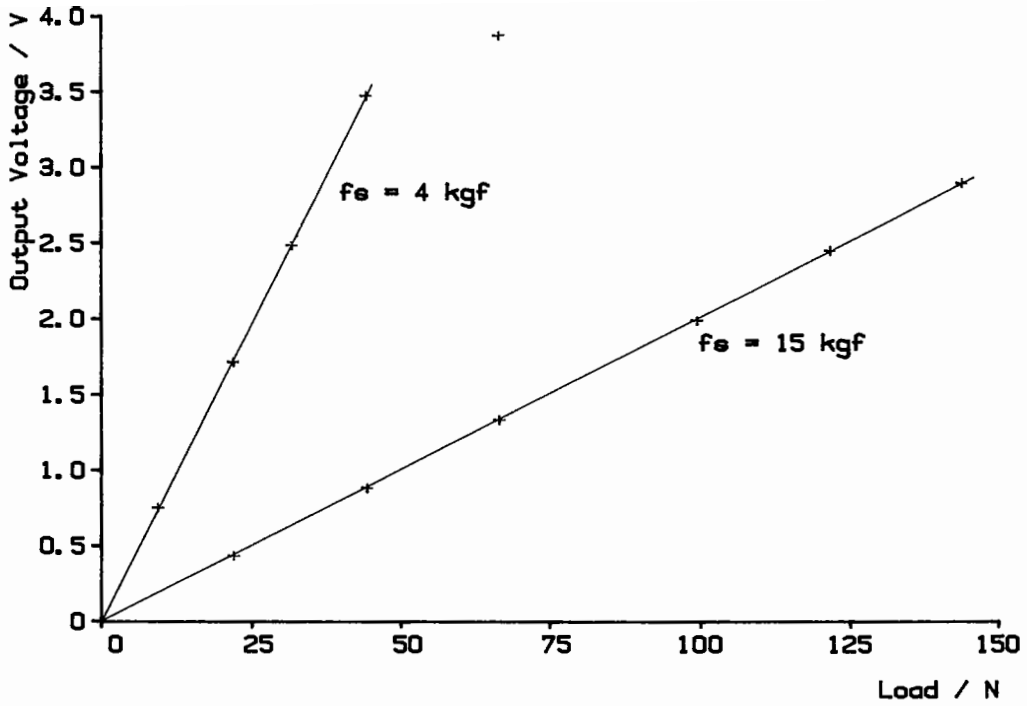

a) Kulite load cell (amplified) output voltage calibration

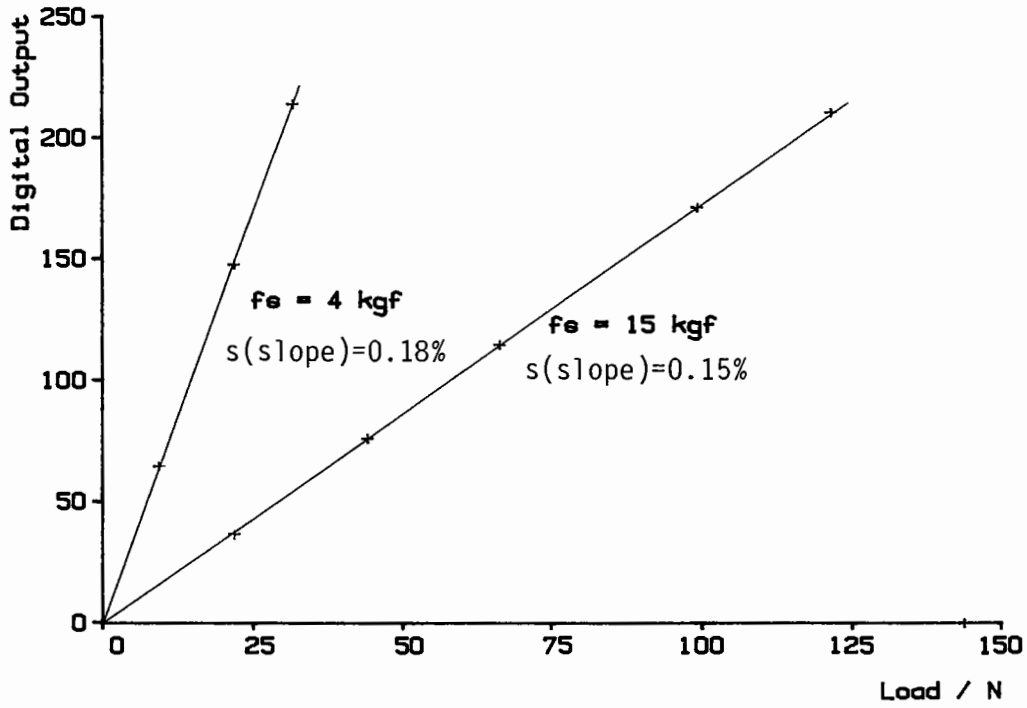

b) Kulite load cell / KTI digital output calibration

Kulite load cell calibrations Figure 28

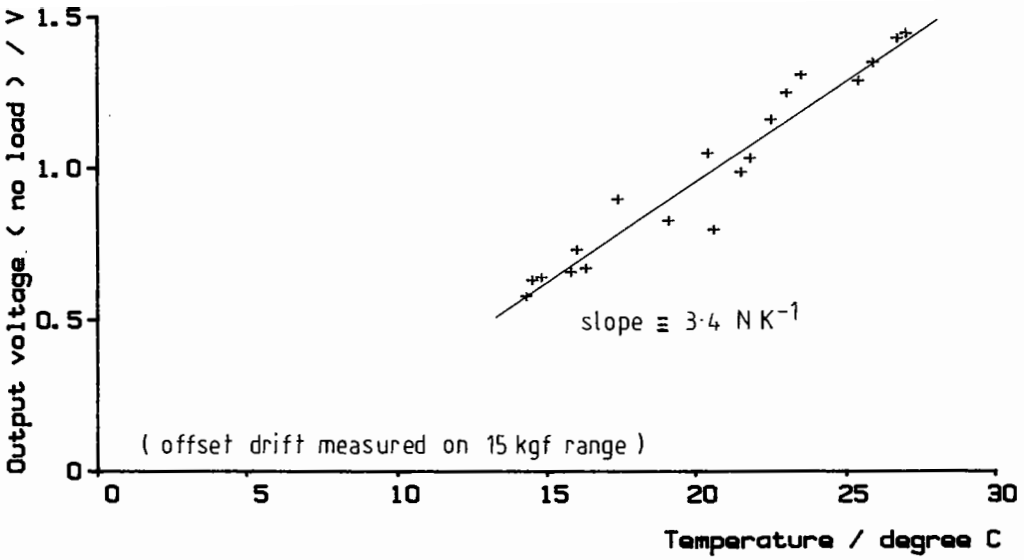

a) Kulite load cell offset temperature drift

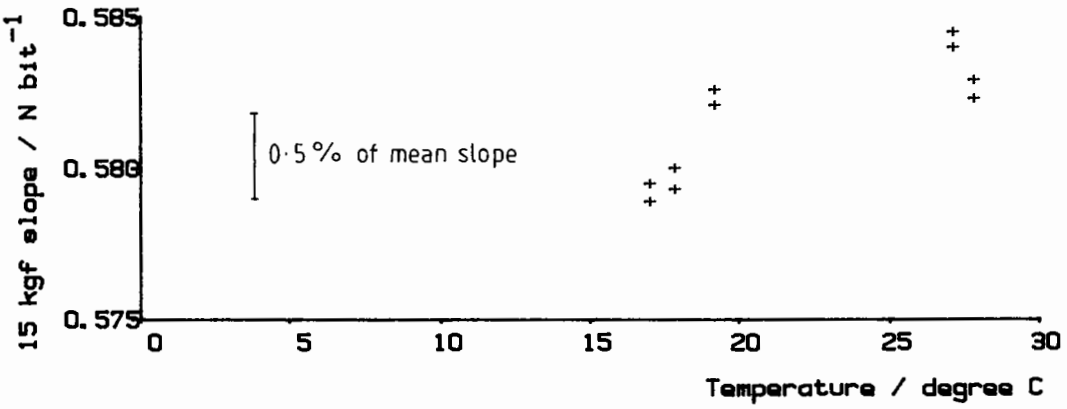

b) Kulite load cell calibration slope vs temperature

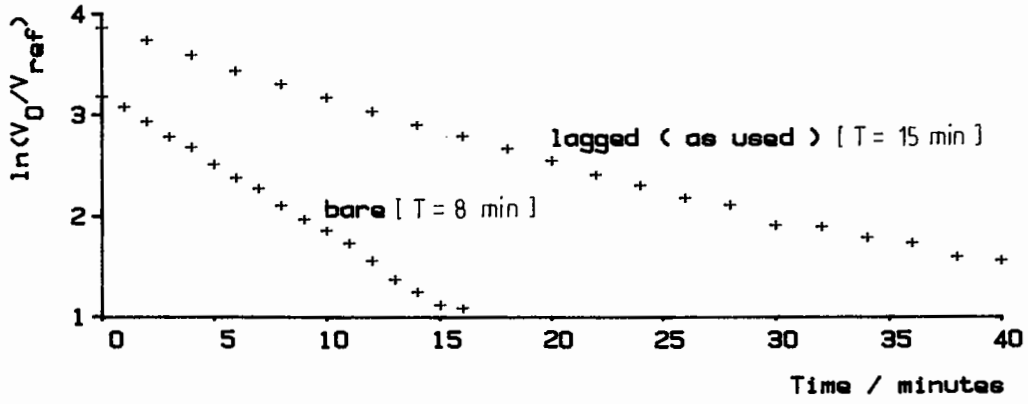

c) Kulite load cell thermal time constant in still air

Kulite load cell thermal properties

Figure 29

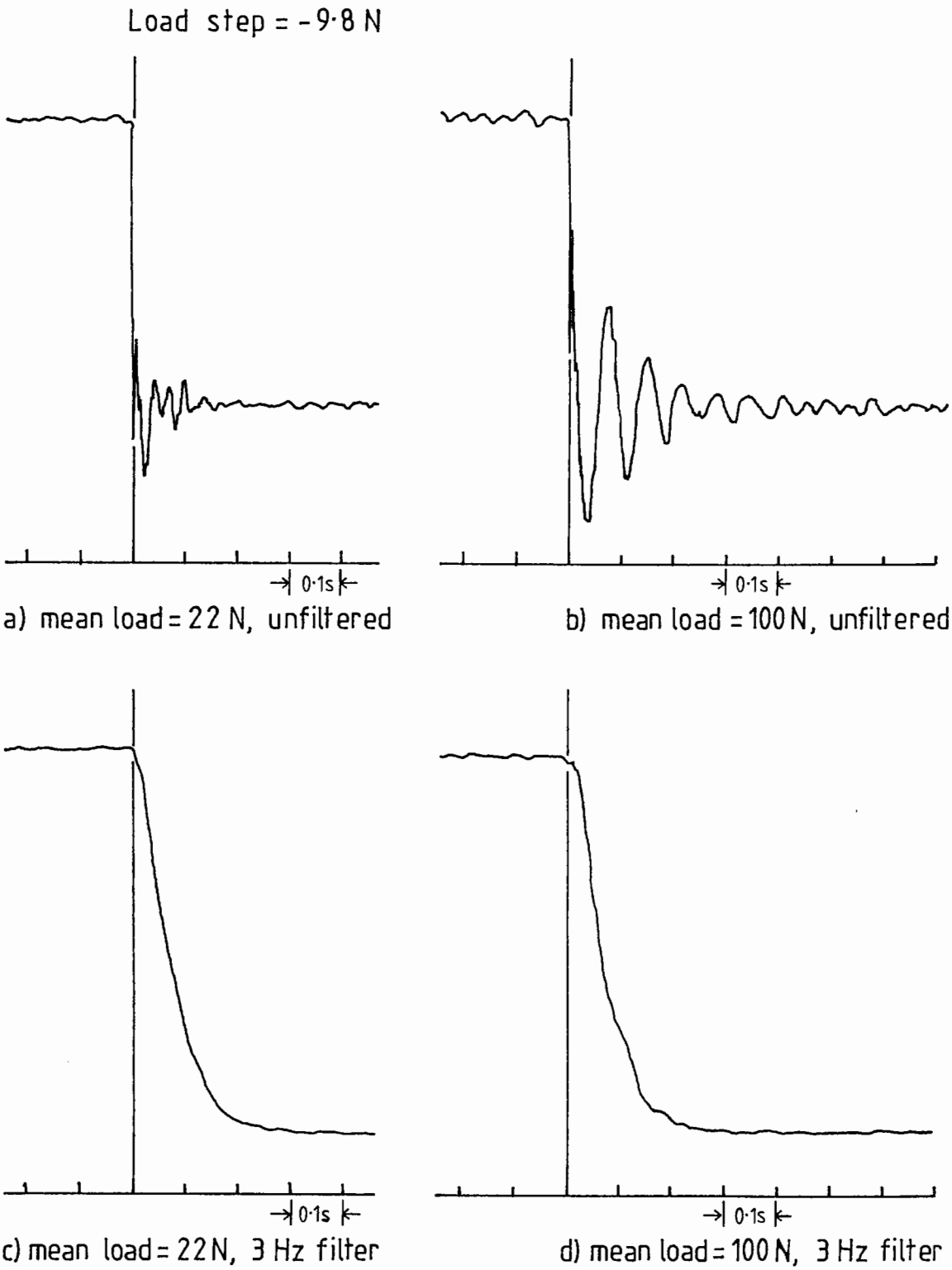

a) mean load = 22 N, unfiltered

b) mean load = 100 N, unfiltered

c) mean load = 22 N, 3 Hz filter

d) mean load = 100 N, 3 Hz filter

Kulite Load Cell Step Response

Figure 30

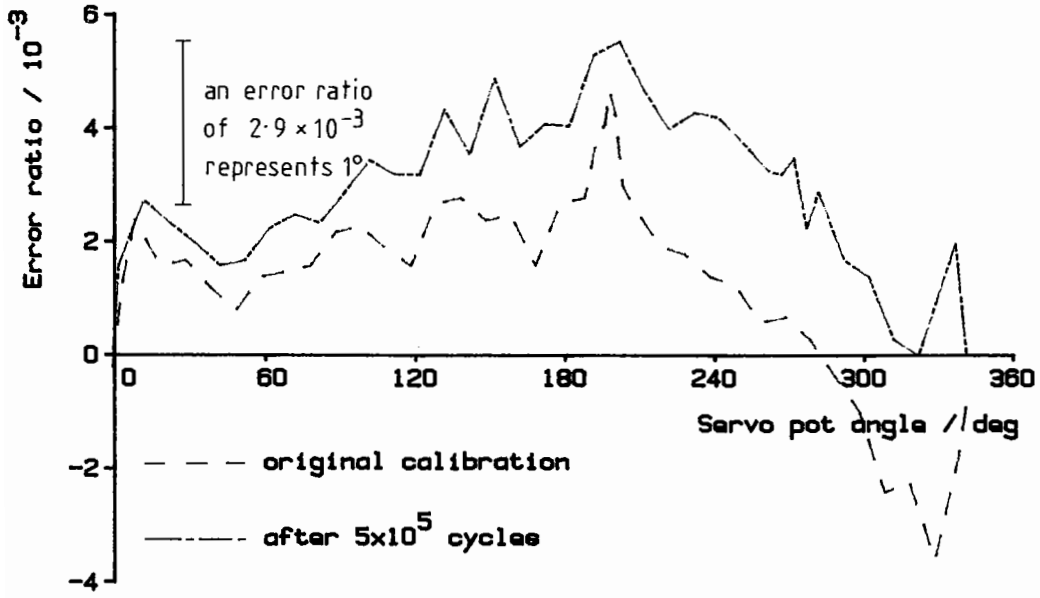

Servo potentiometer angle calibration results

Figure 31

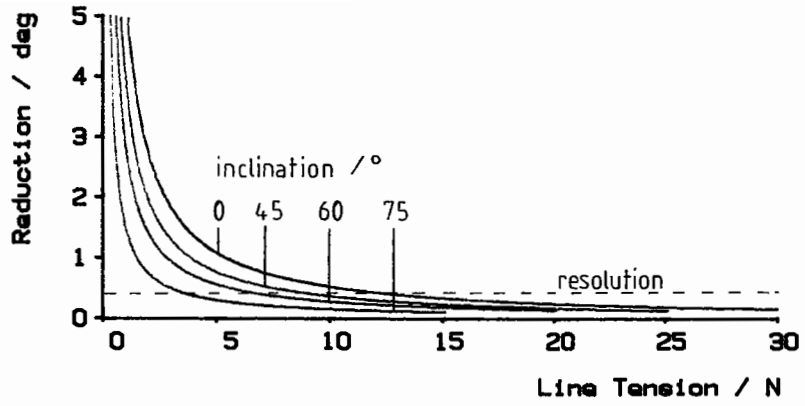

a) Inclination reduction due to tether arm weight

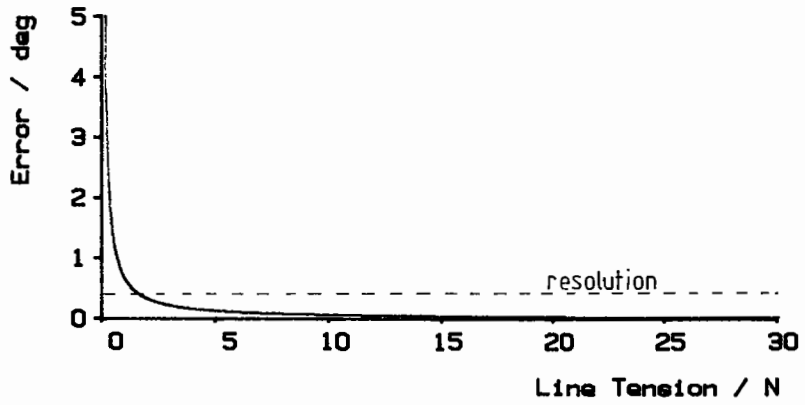

b) Inclination error due to friction

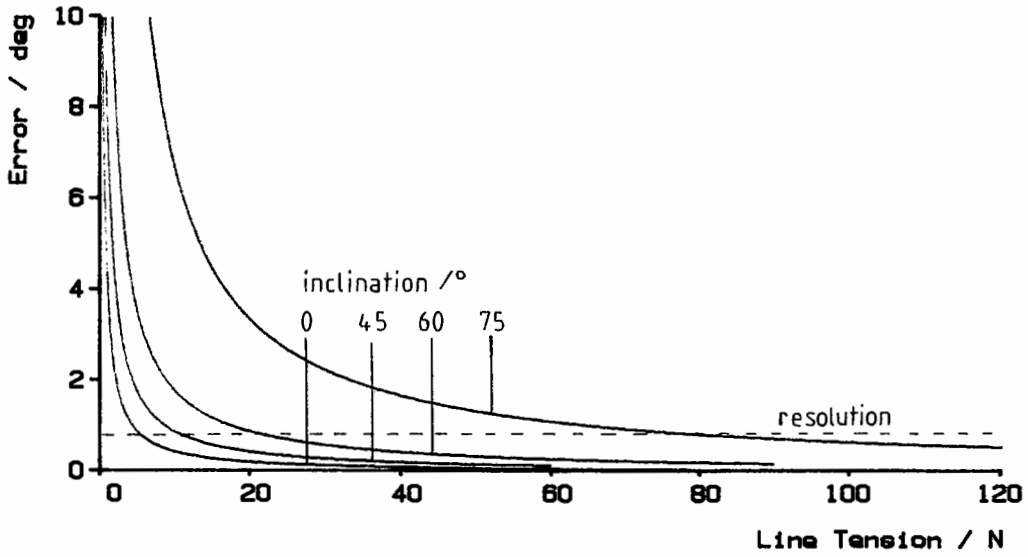

c) Azimuth error due to friction

Errors in tether angle measurements Figure 32

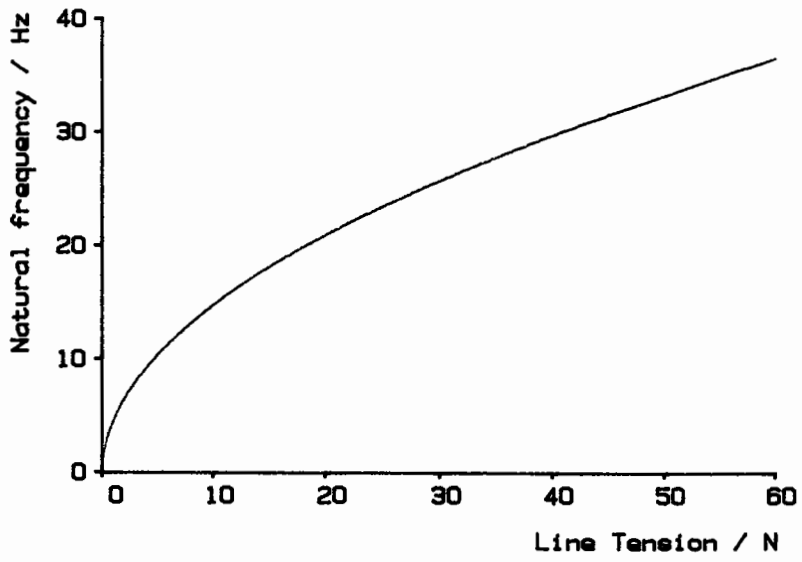

a) Inclination measurements

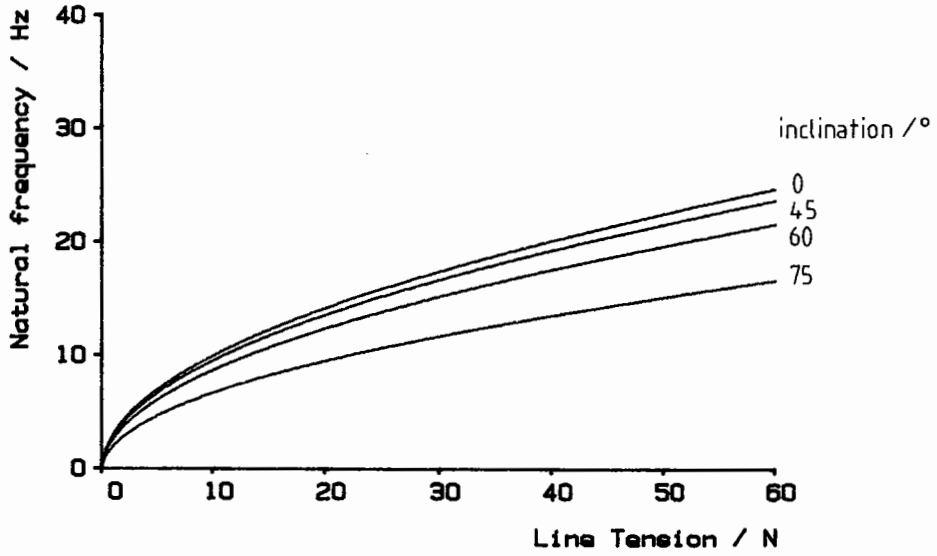

b) Azimuth measurements

Frequencies at which tether inertial response becomes significant

Figure 33

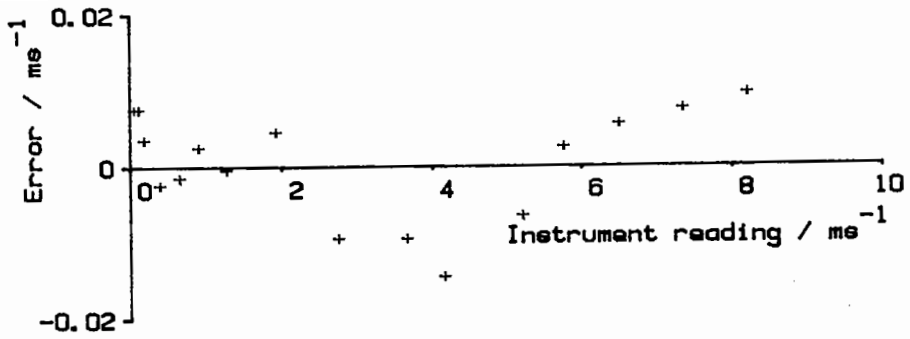

Mica-vaned DVA calibration results

Figure 34

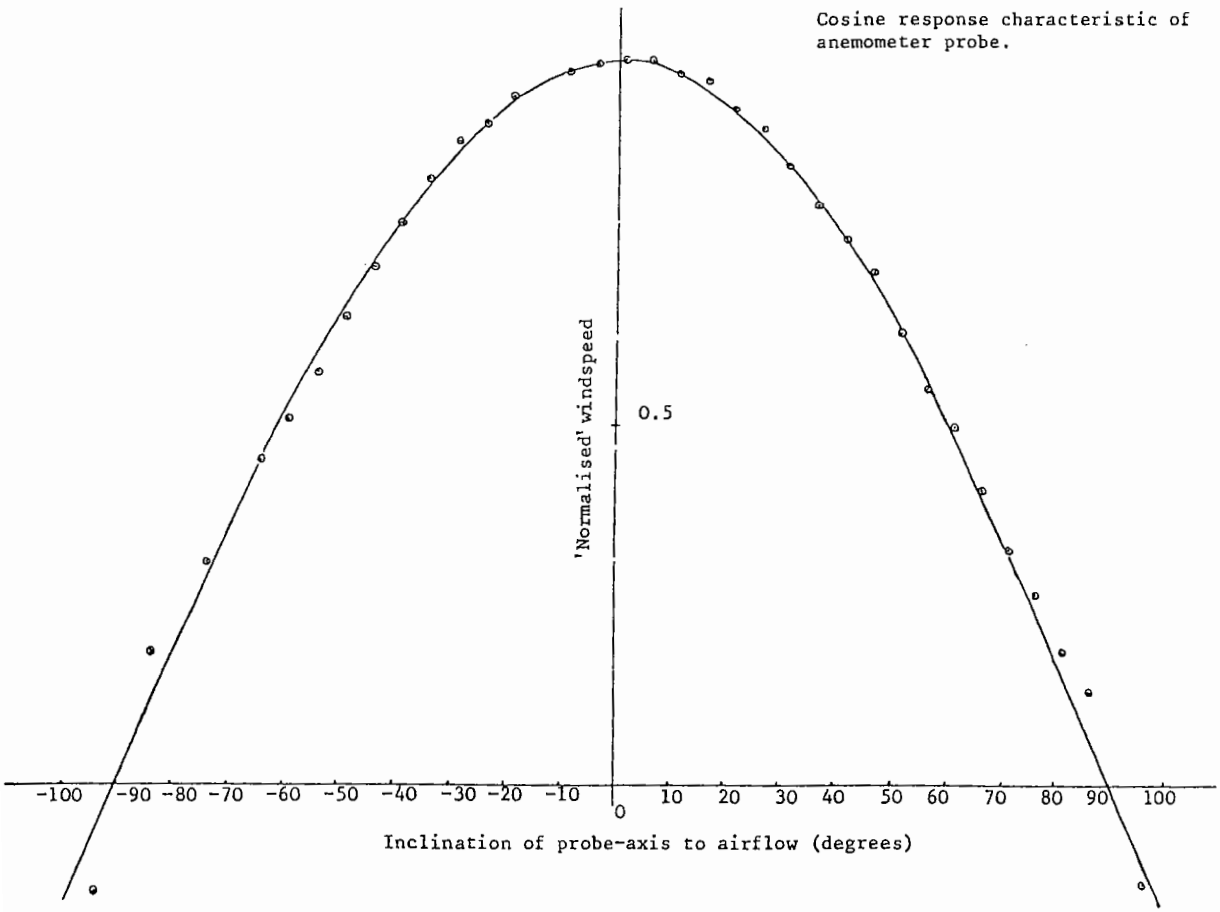

Figure 35 (from Pinnock, 1983)

Figures 34 and 35

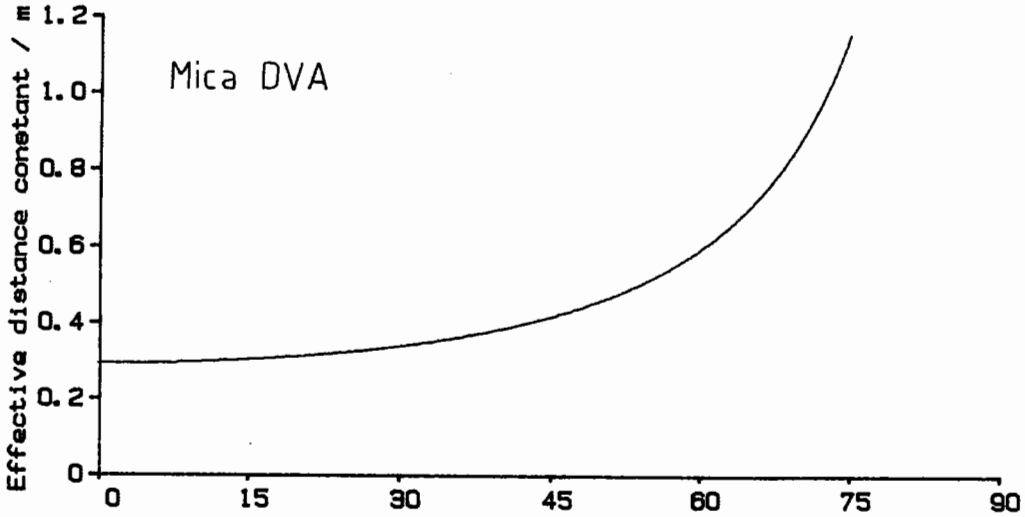

DVA distance constant vs inclination to wind velocity

Figure 36

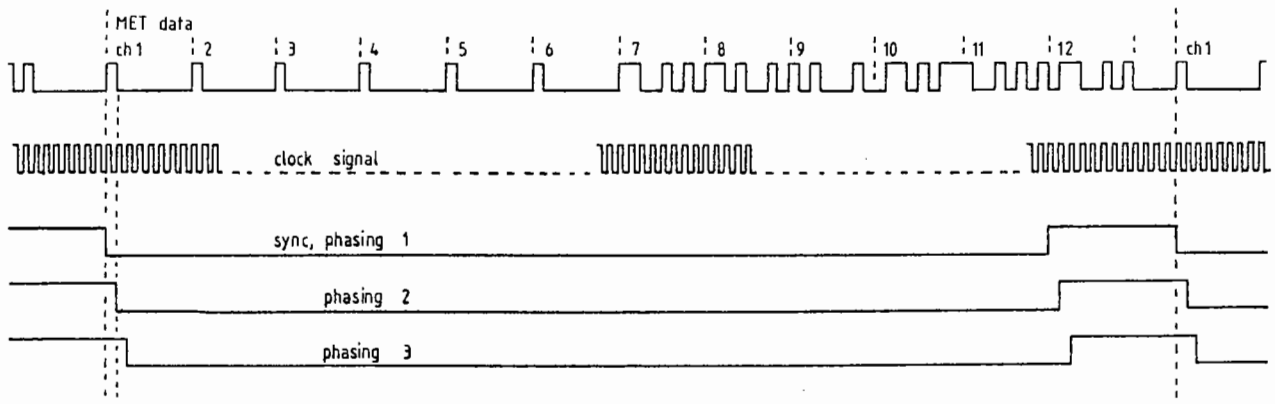

Typical Met Processor Output

Figure 37

Figures 36 and 37

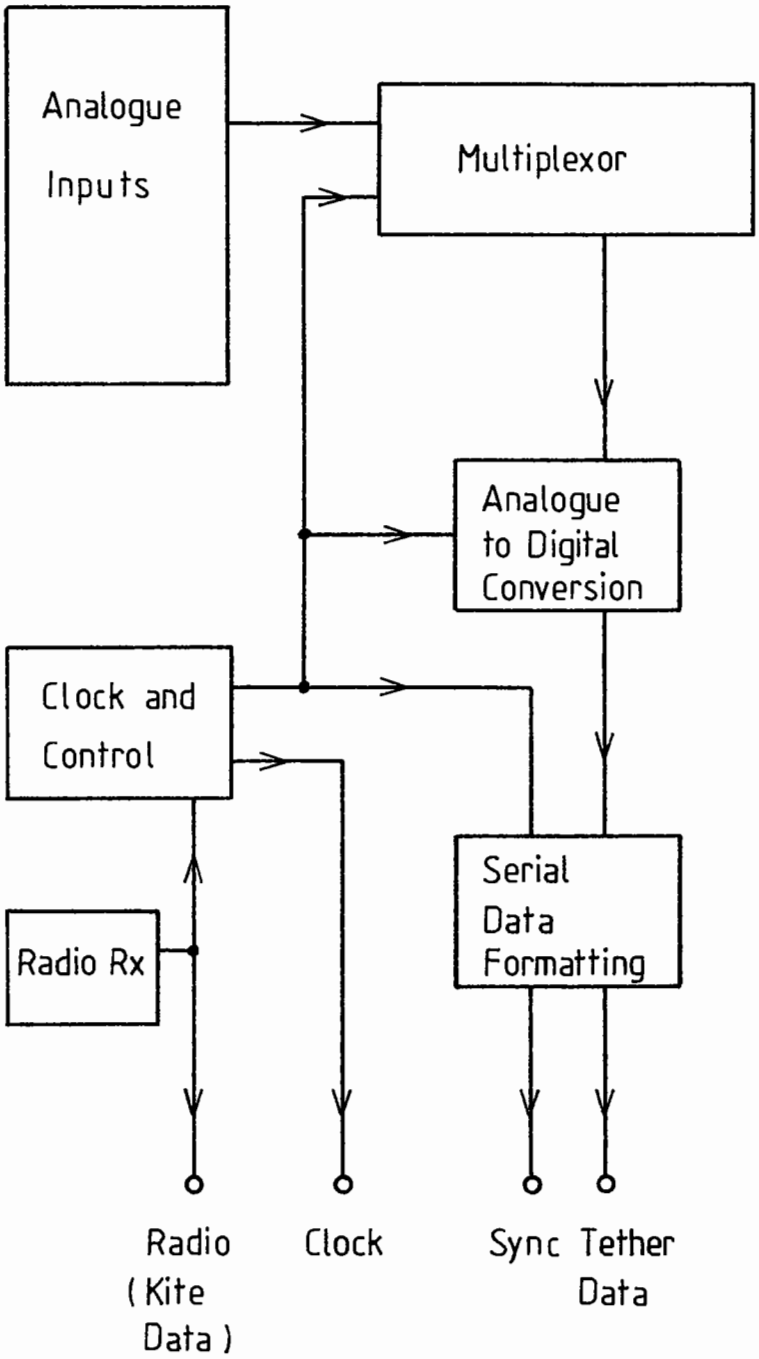

Kite Tether Instrumentation Block Diagram

Figure 38

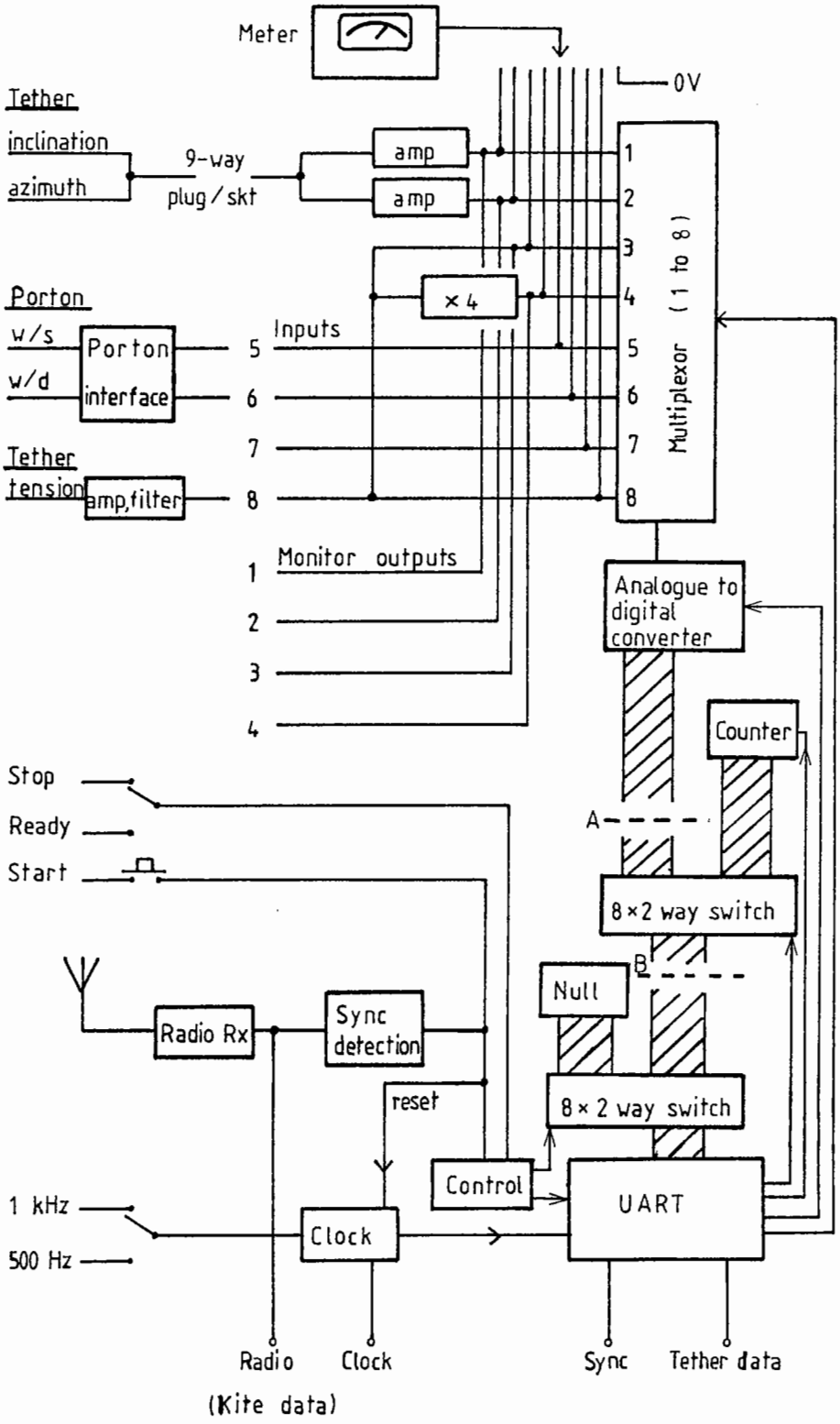

Functional Diagram of Kite Tether Instrumentation

Figure 39

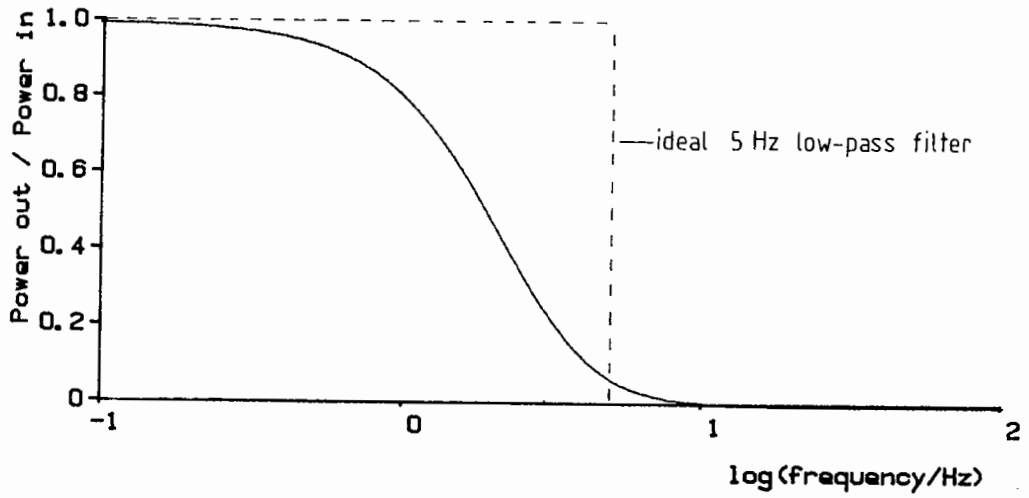

Load Cell Filter Transfer Function

Figure 40

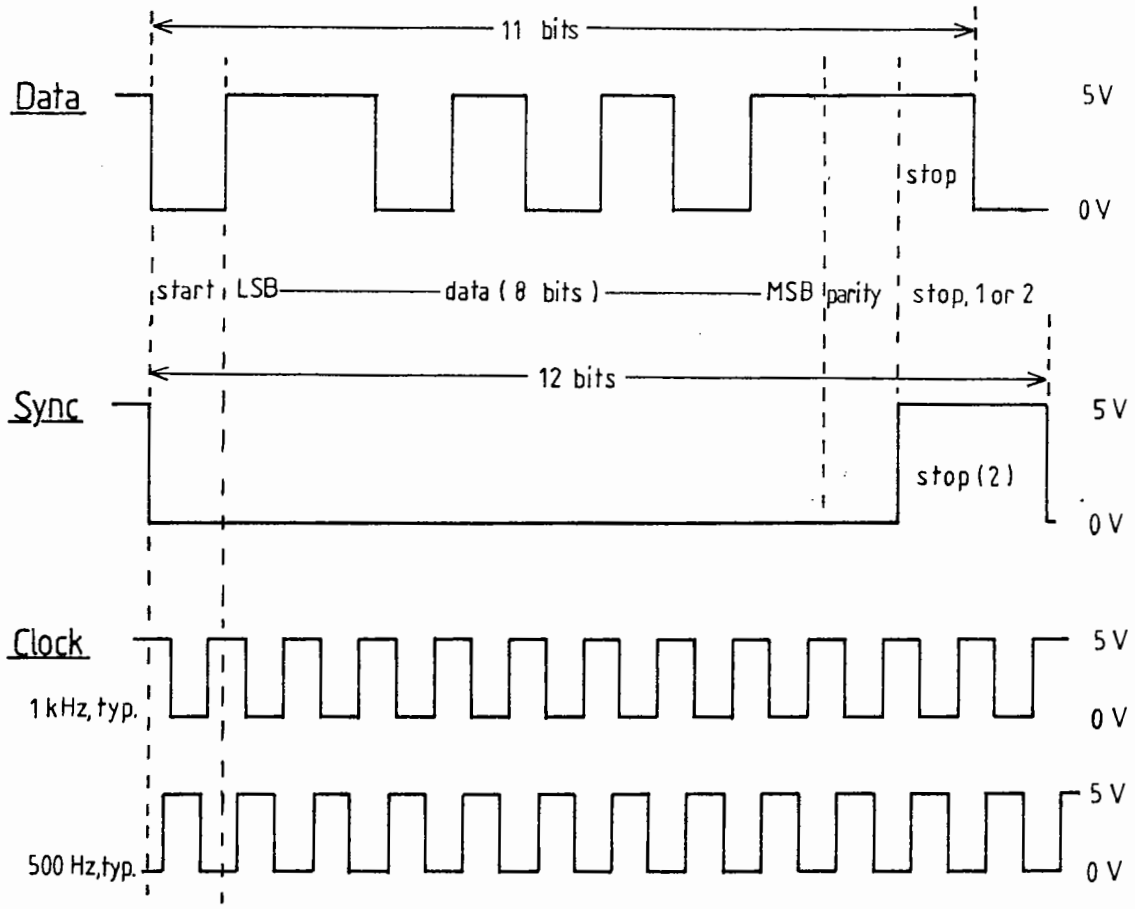

Typical Tether Data and Sync Words

Figure 41

Figures 40 and 41

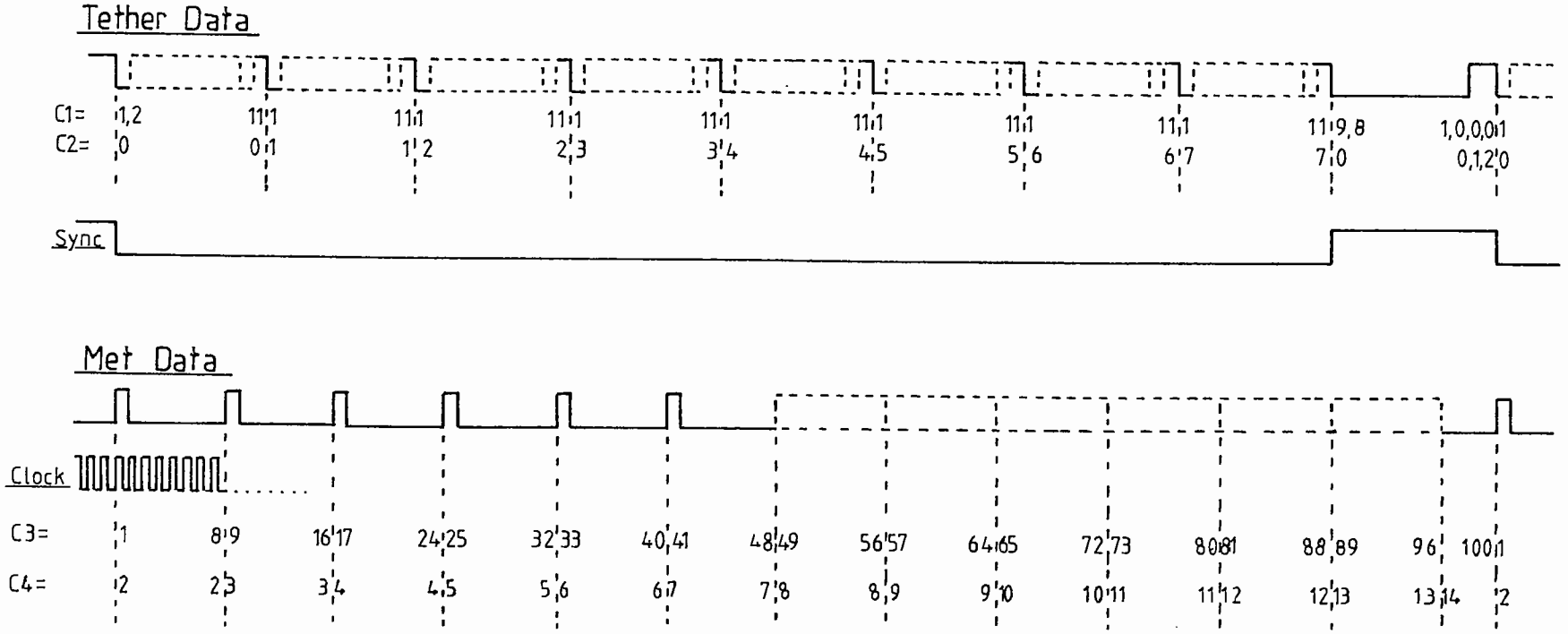

Serial Data Line Format and Synchronisation

Figure 42

Notes a) The counter values C1..C4 are as used by program STORE/TM. C3 is only used mod 8, so is arbitrary to any multiple of 8.

b) The phasing shown between tether and met data is appropriate to normal 1 kHz operation. Figure 37 shows the other phasings encountered.

c) For data collection, only the Tether Data, Met Data and Clock are required. The data cycle sync is coded into the Tether Data.

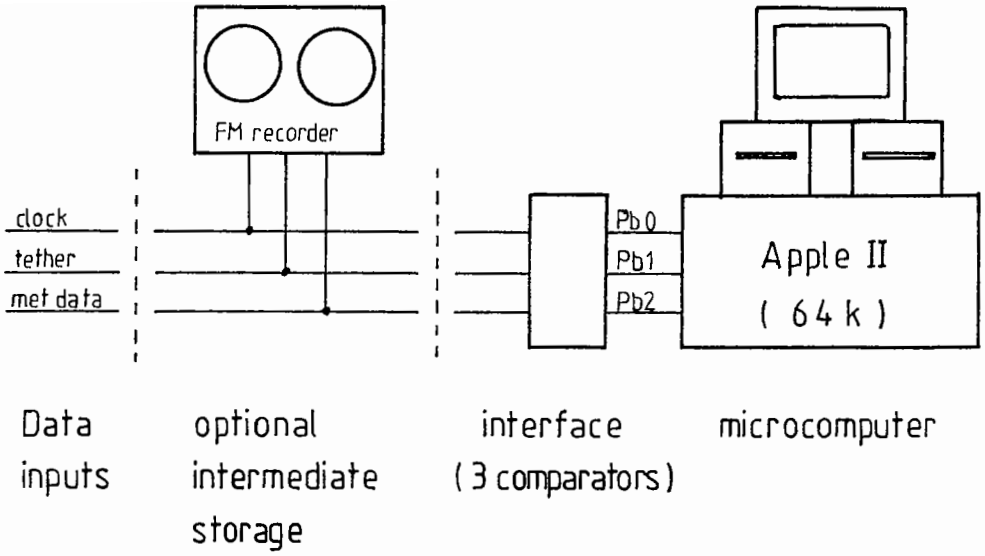

Data Storage and Analysis Equipment

Figure 43

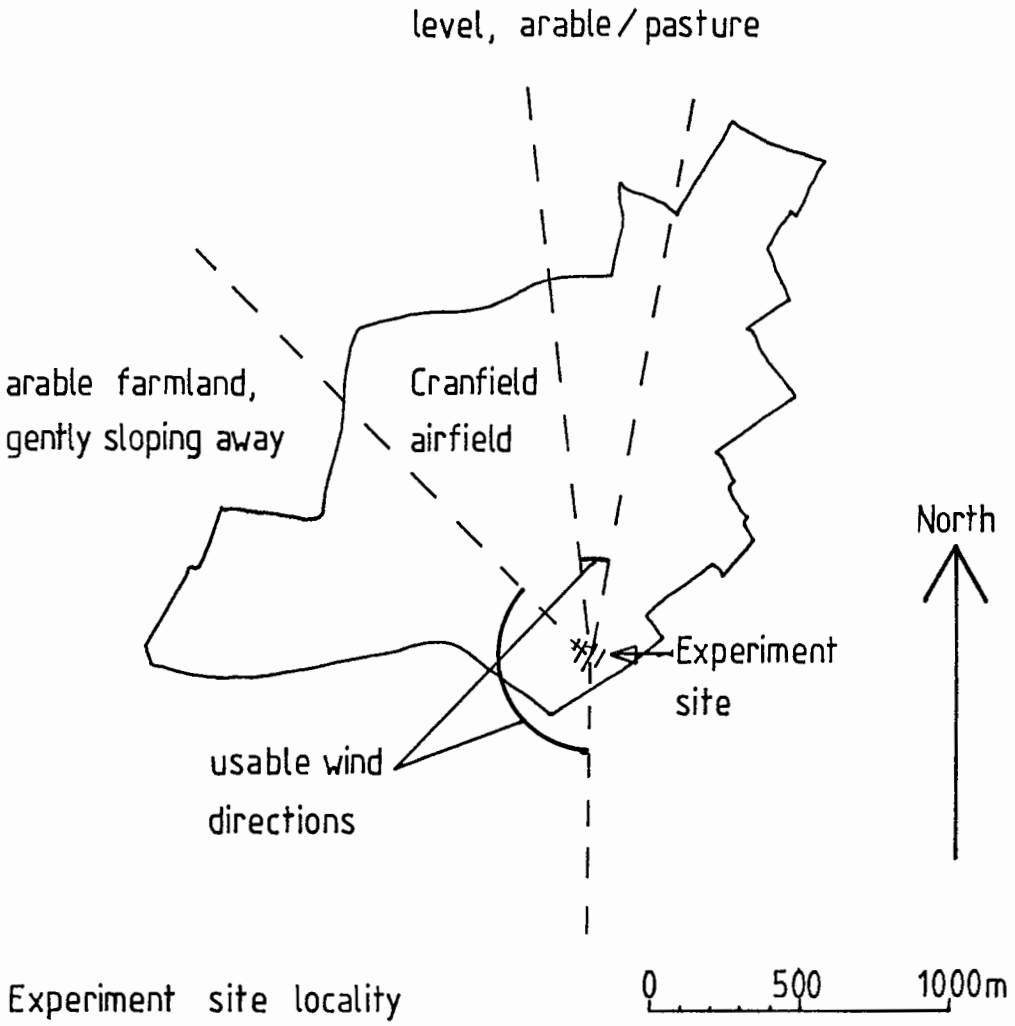

Experiment site locality

Figure 44

Figures 43 and 44

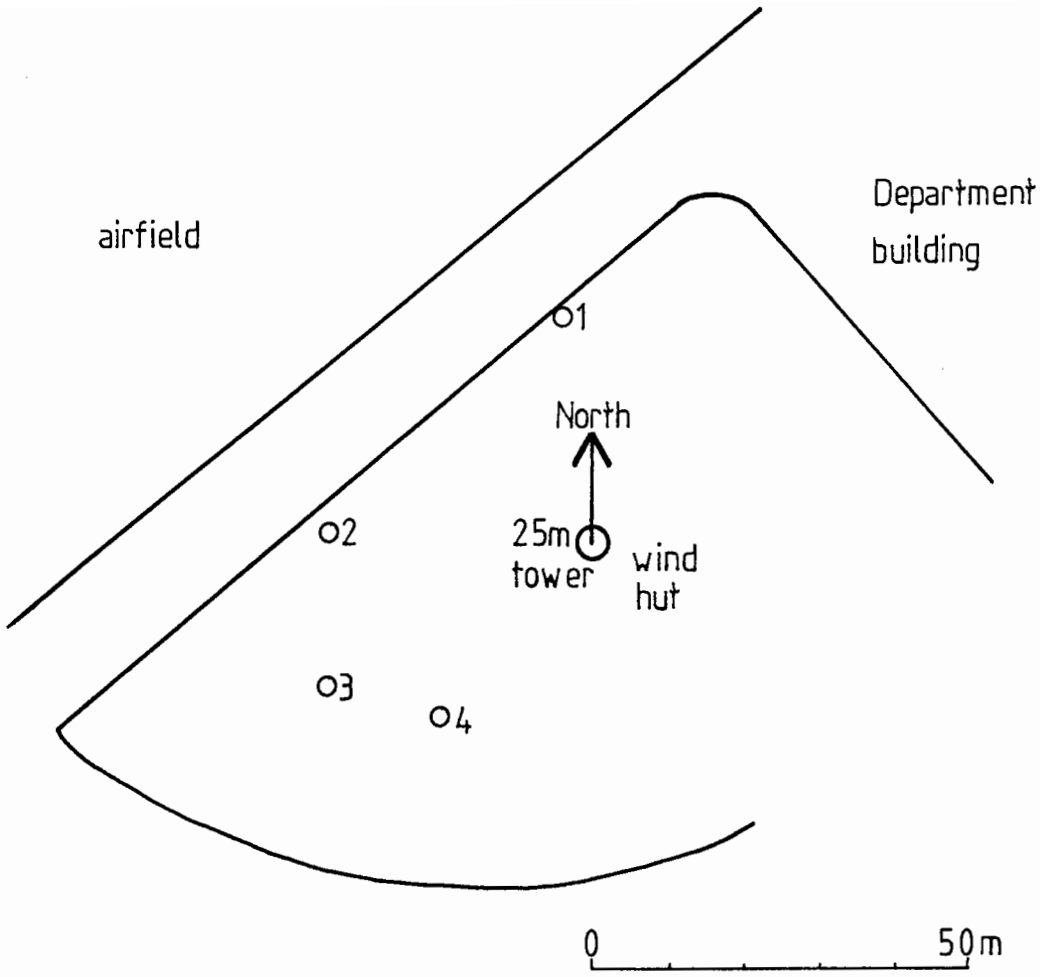

Detailed Plan of Experiment Site

Position	Distance from anemometers	Bearing of anemometers (°mag)
1	32 m	180
2	35 m	100
3	40 m	71
4	30 m	49

Figure 45

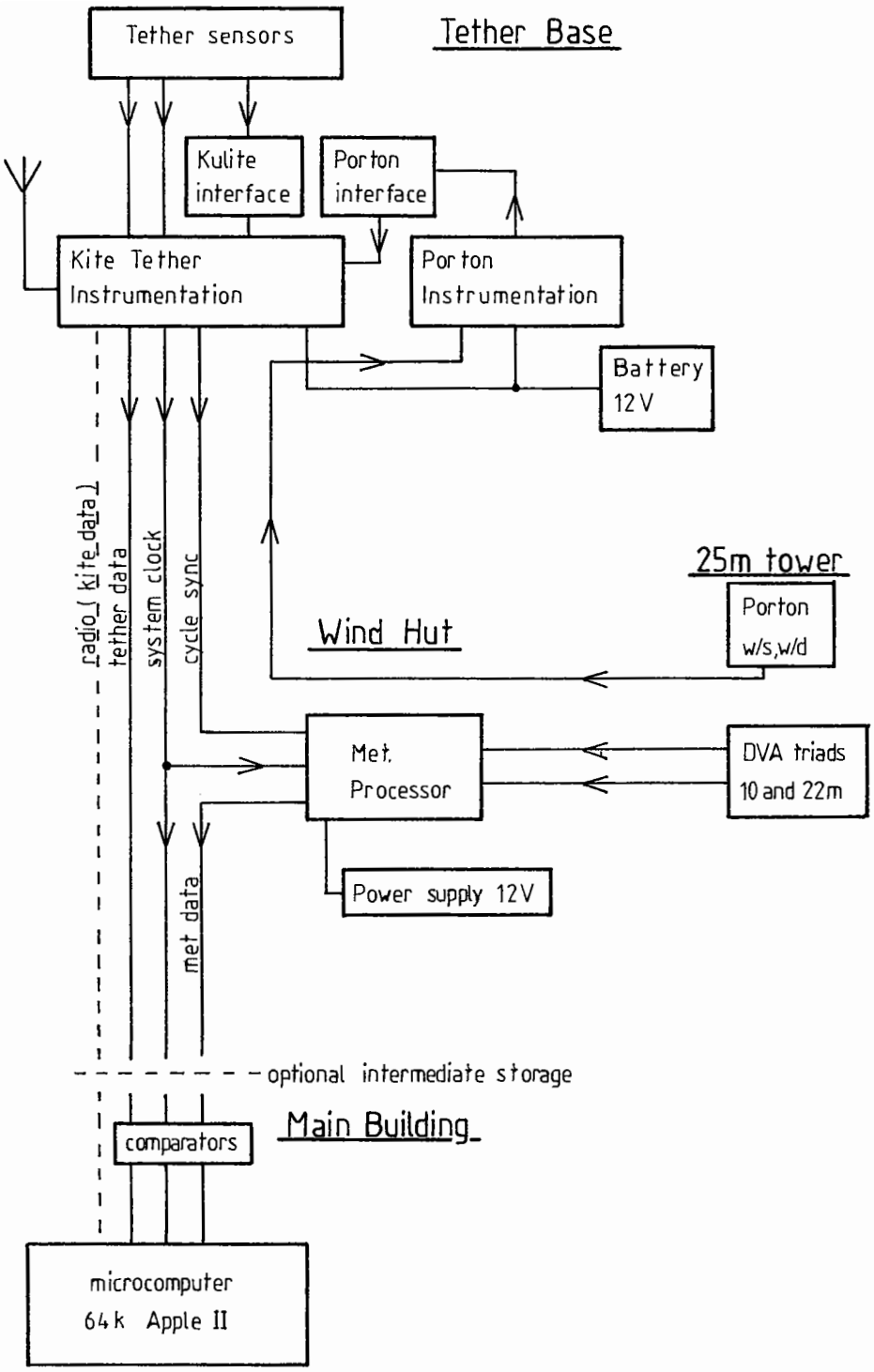

Experiment Equipment Interconnections

Figure 46

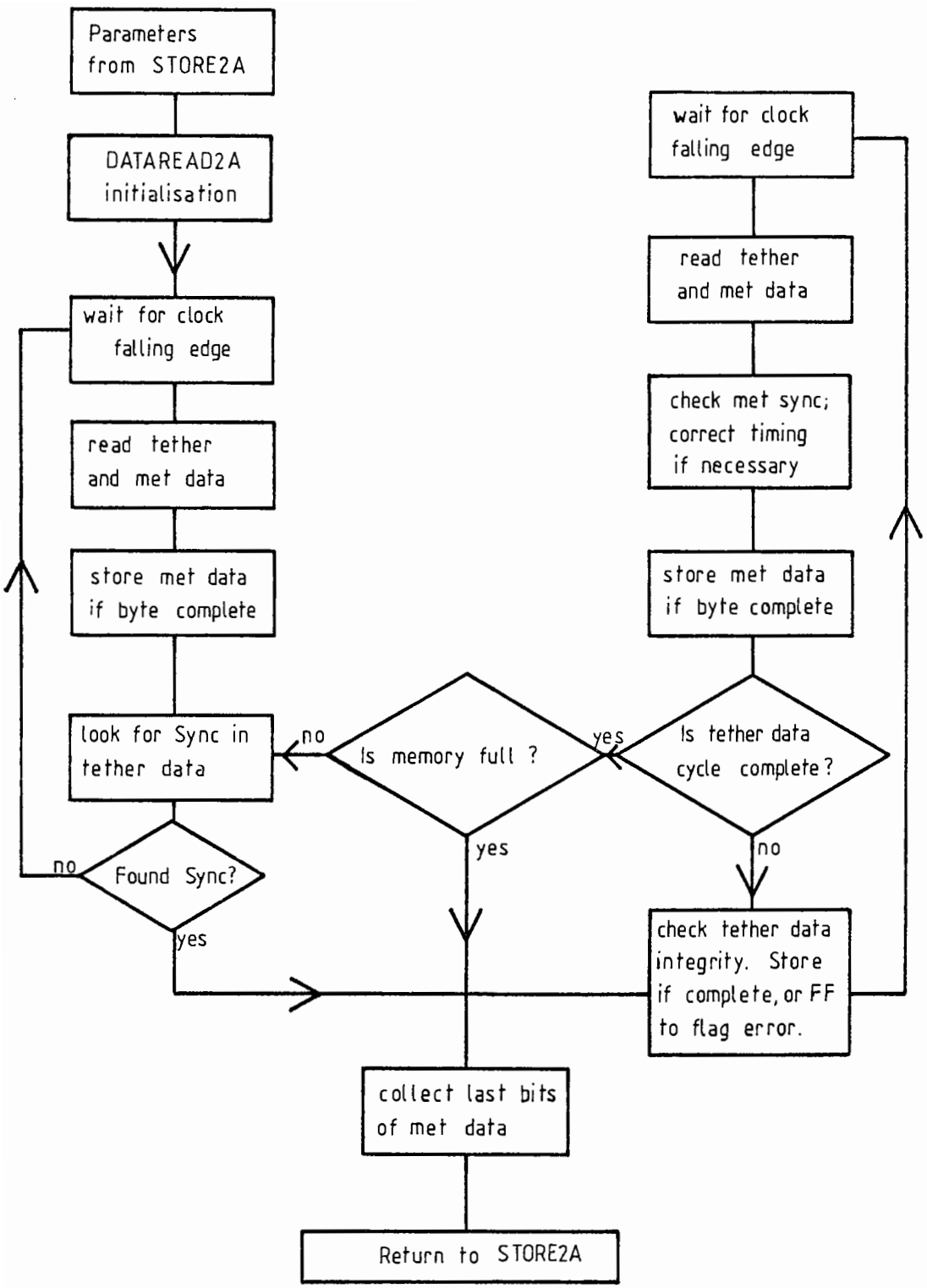

Outline of procedure DATAREAD2A's functions

Figure 47

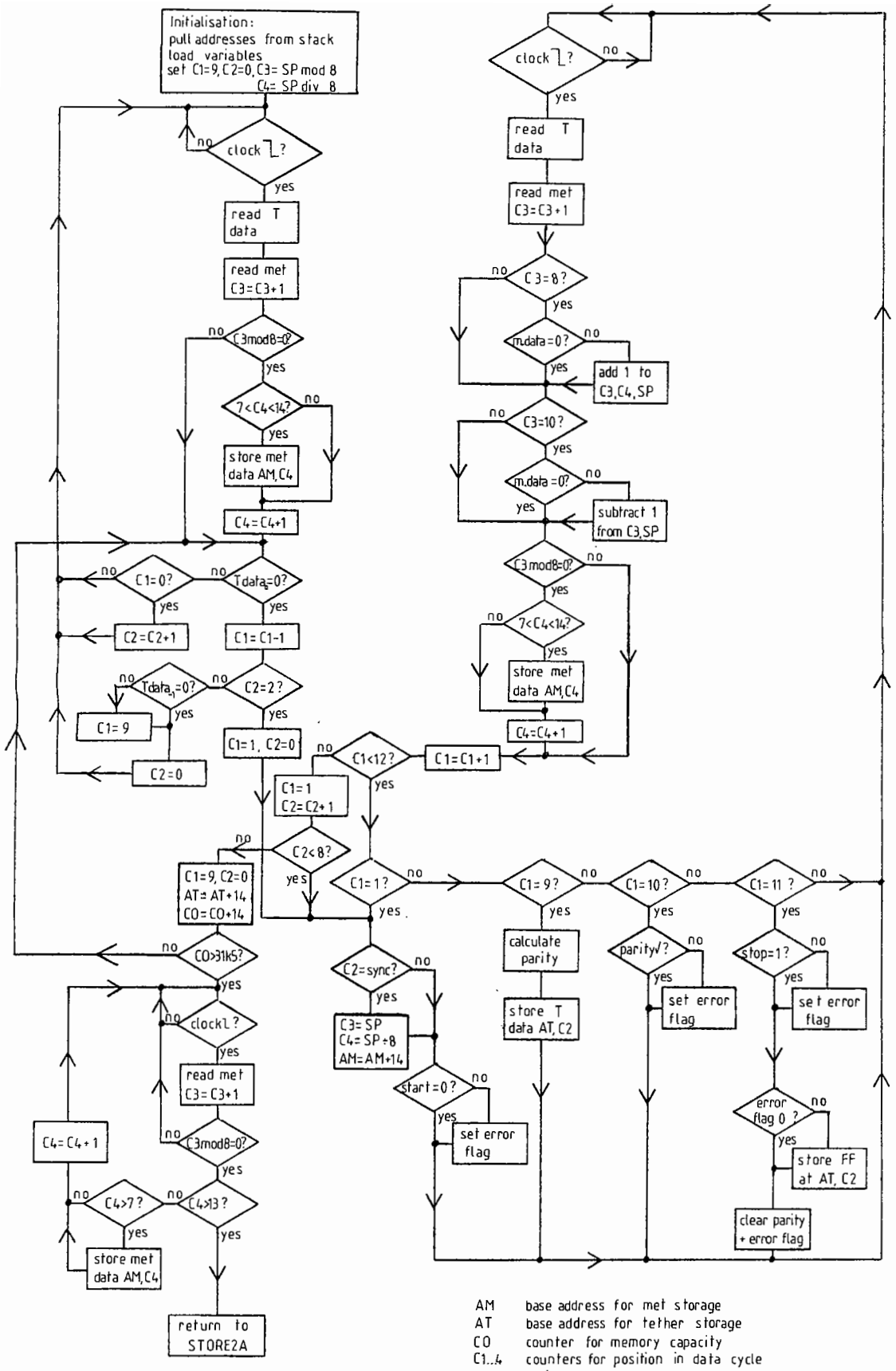

AM base address for met storage
AT base address for tether storage
CO counter for memory capacity
C1..4 counters for position in data cycle
m met
SP, sync variables controlling tether + met phasing
T tether

Flow chart for DATAREAD2A (detailed)

Figure 48

Original raw data :

DATA FILE : SEH12B:TM10DEC4.DATA
=========

R.NO.	CH 1	CH 2	CH 3	CH 4	CH 5	CH 6	CH 7	CH 8	CH 9	CH10	CH11	CH12	CH13	CH14
1217	103	152	0	0	48	154	0	222	136	137	138	144	140	142
1218	104	152	0	0	46	154	0	223	135	137	139	144	139	141
1219	105	152	0	0	48	154	0	224	136	137	139	145	140	141
1220	105	152	0	0	47	154	0	225	135	137	139	145	139	142
1221	101	152	0	0	49	154	0	226	136	2	139	144	139	142
1222	107	152	0	0	47	154	0	227	135	137	139	144	140	141
1223	107	152	0	0	49	154	0	228	135	138	139	145	139	141
1224	104	152	0	0	46	154	0	229	136	137	139	144	139	142
1225	106	153	0	0	48	154	0	230	135	138	139	144	139	142

Data corrected by FLAGFIND :

DATA FILE : SEH12B:TM10DEC4.DATA
=========

R.NO.	CH 1	CH 2	CH 3	CH 4	CH 5	CH 6	CH 7	CH 8	CH 9	CH10	CH11	CH12	CH13	CH14
1217	103	152	0	0	48	154	0	222	136	137	138	144	140	142
1218	104	152	0	0	46	154	0	223	135	137	139	144	139	141
1219	105	152	0	0	48	154	0	224	136	137	139	145	140	141
1220	105	152	0	0	47	154	0	225	135	137	139	145	139	142
1221	101	152	0	0	49	154	0	226	136	137	139	144	139	142
1222	107	152	0	0	47	154	0	227	135	137	139	144	140	141
1223	107	152	0	0	49	154	0	228	135	138	139	145	139	141
1224	104	152	0	0	46	154	0	229	136	137	139	144	139	142
1225	106	153	0	0	48	154	0	230	135	138	139	144	139	142

Example of FLAGFIND error correction

Figure 49

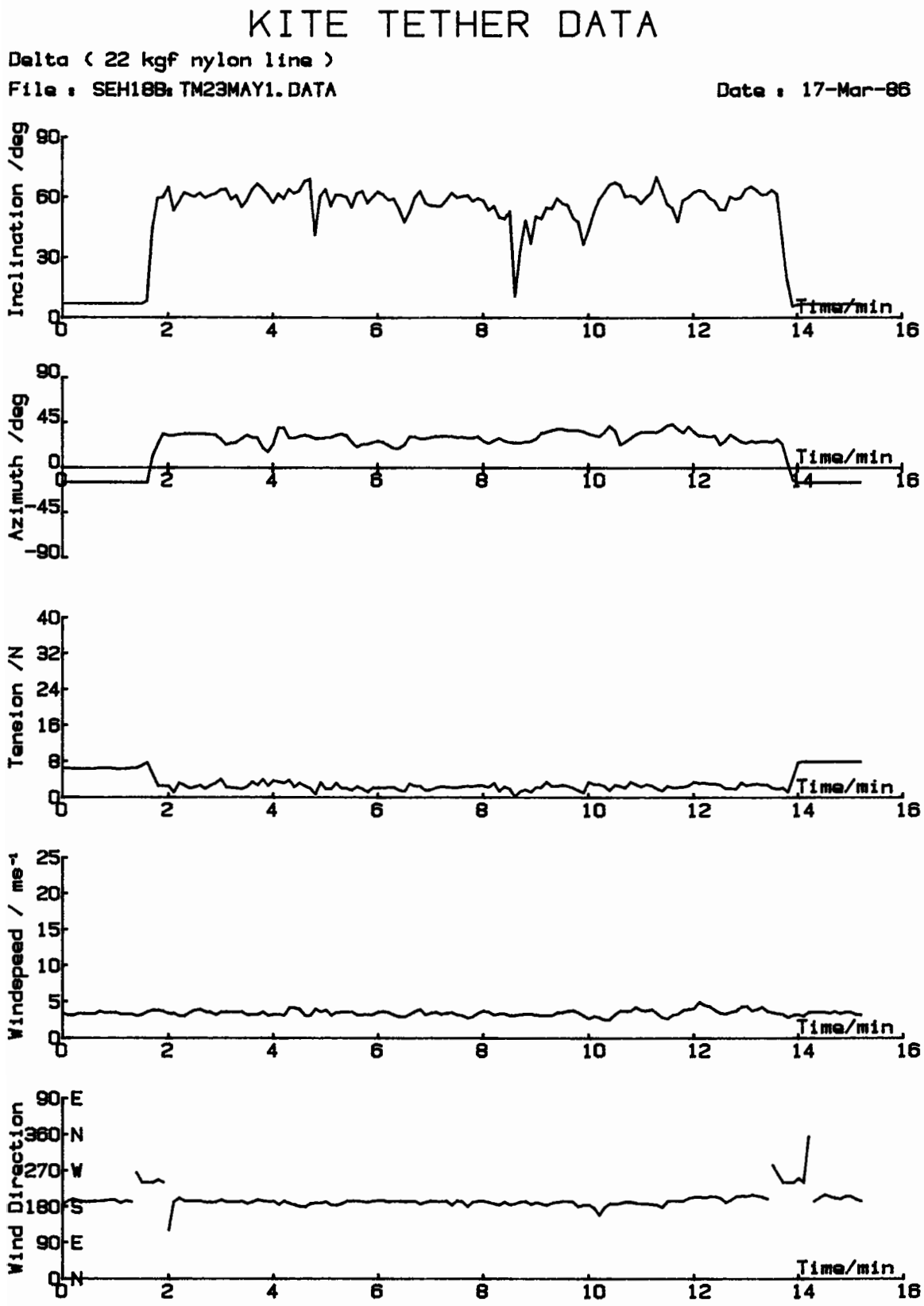

Example of DATALOG/TM's display

Figure 50

DAT[i,j] : Array [1..8,1..16] of real;

j=	1	2	3	4	5	6	7	8
i=1	Mean of Raw Data, channel j							
2	Standard Deviation of Raw Data, channel j							
3	Slope			to convert raw data to				
4	Intercept			dimensional quantities				
5							kite area / m^2	□ X / m
6							kite mass / kg	□ Y / m
7							bridle angle	□ Z / m
8								lag / s

j=	9	10	11	12	13	14	15	16
i=1	Mean of Raw Data, channel j						first record	tension channel number
2	Standard Deviation of Raw Data, channel j						last record	kiteline length/m
3	V_1	V_2	V_3	V_1	V_2	V_3	T full scale / kgf	n_x 0.0243
4	Wind rotation matrix for 10 m DVA triad $W_{0i} = LAB_{ij} V_j$			Wind rotation matrix for 22 m DVA triad $W_{0i} = LAB_{ij} V_j$			sampling rate n_s / Hz	0.0994
5							□ Ra / m	kiteline mass / kgm^{-1}
6							□ ψ_r / rad	kiteline diameter / m
7	W_{01}	W_{02}	W_{03}	W_{01}	W_{02}	W_{03}	□ ψ_a / rad	W(friction) / ms^{-1}
8							□ ψ_{ar} / rad	Z(roughness) / m

□ for definitions see figure 52

Data summary file format

Figure 51

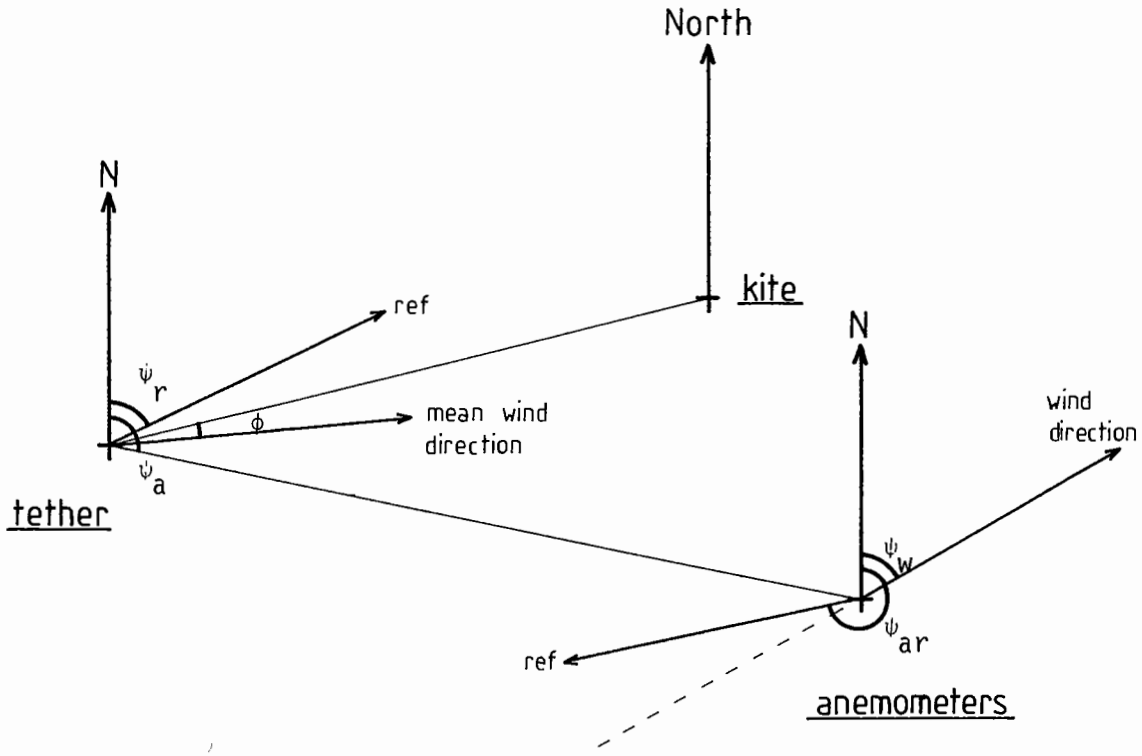

a) definition of angles used to describe the experiments

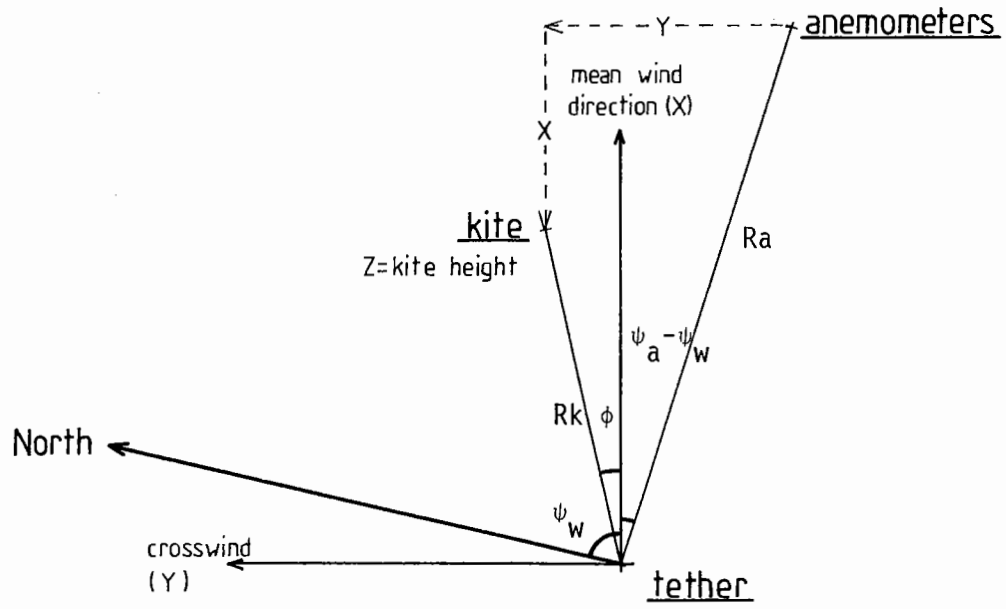

b) kite and anemometer positions relative to the mean wind

Experiment site geometry

Figure 52

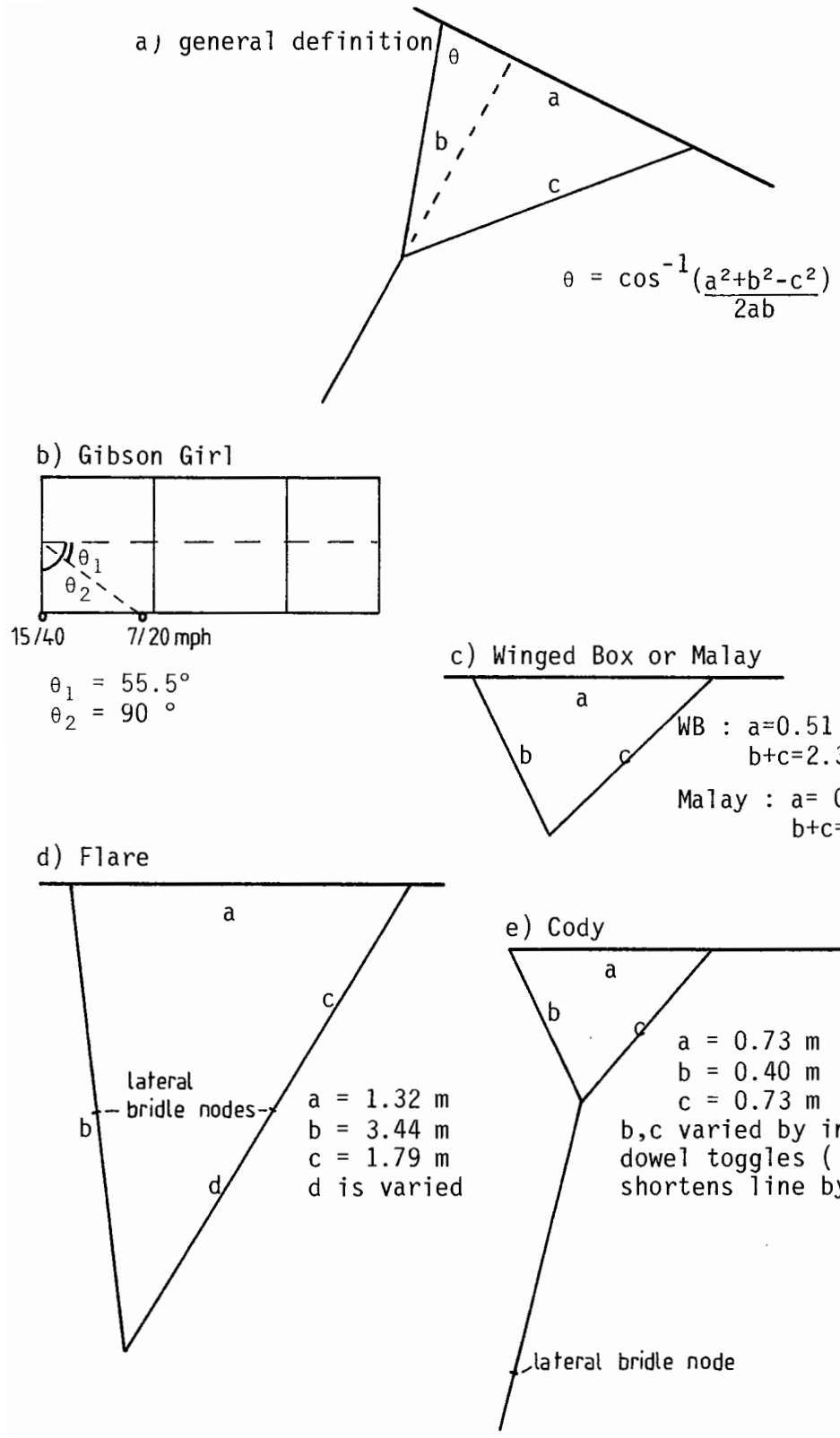

Bridle angle definitions

Figure 53

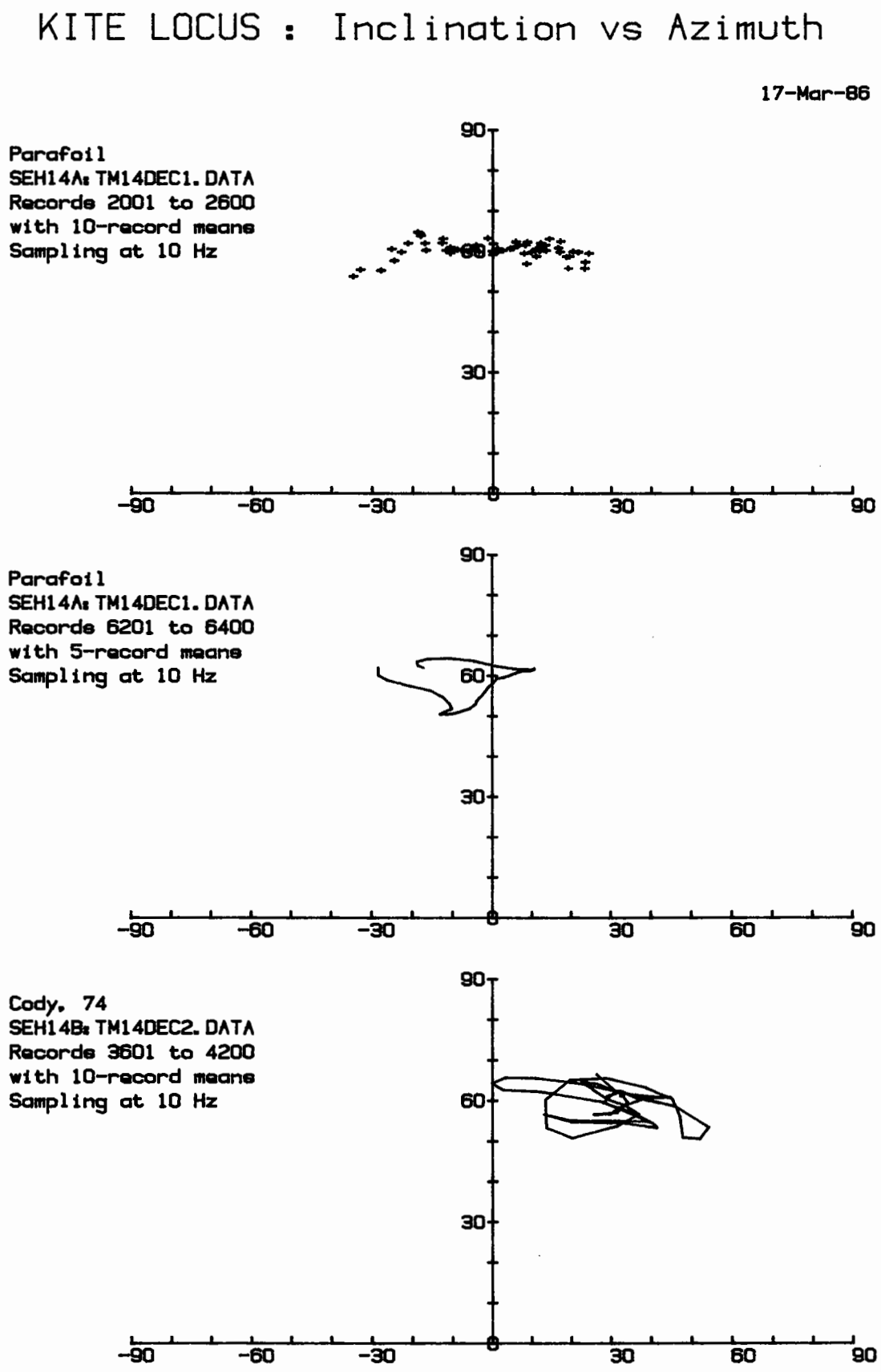

Example of output from ANGLEPLOT

Figure 54

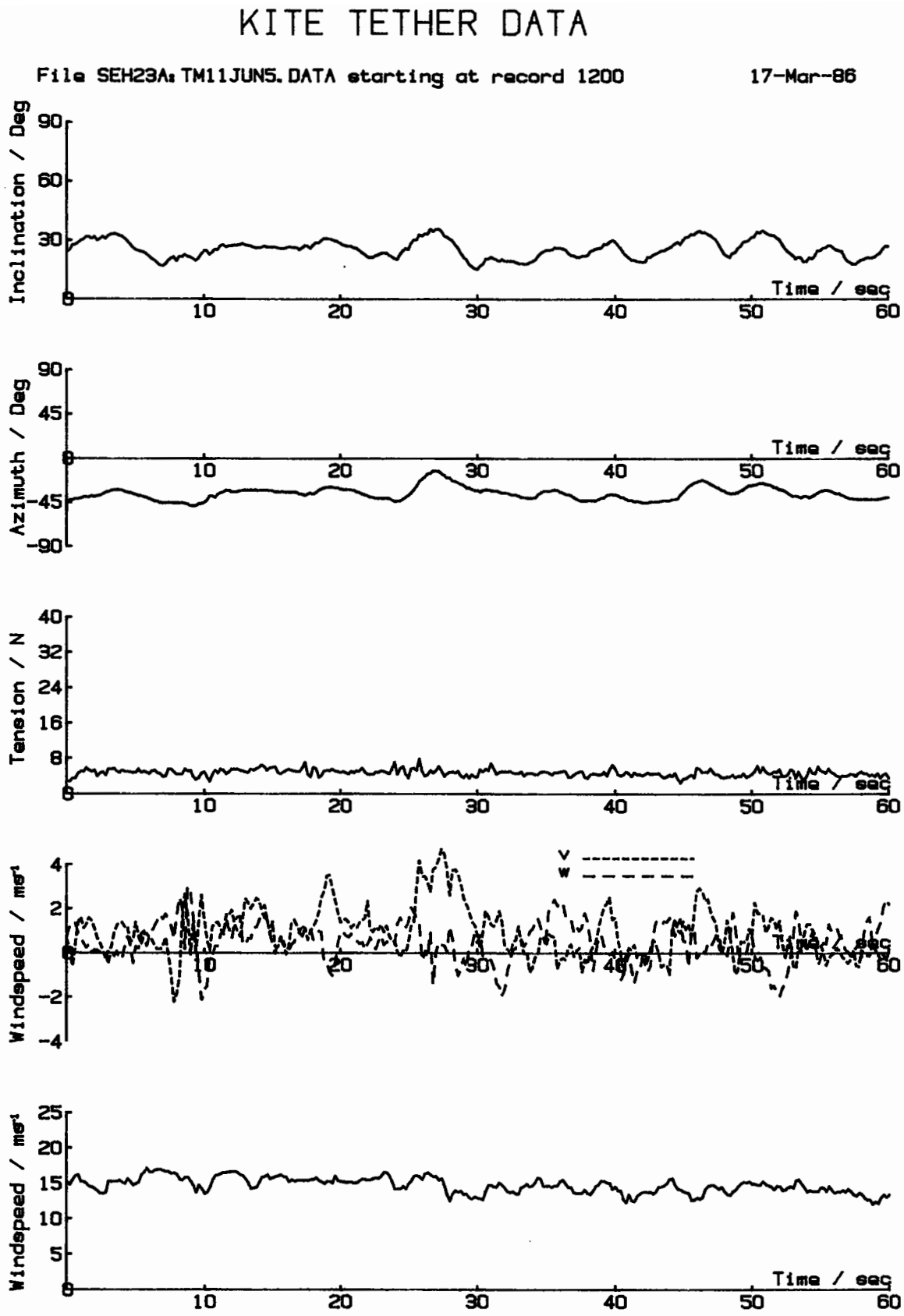

Example of output from DATAPLOTv2

Figure 55

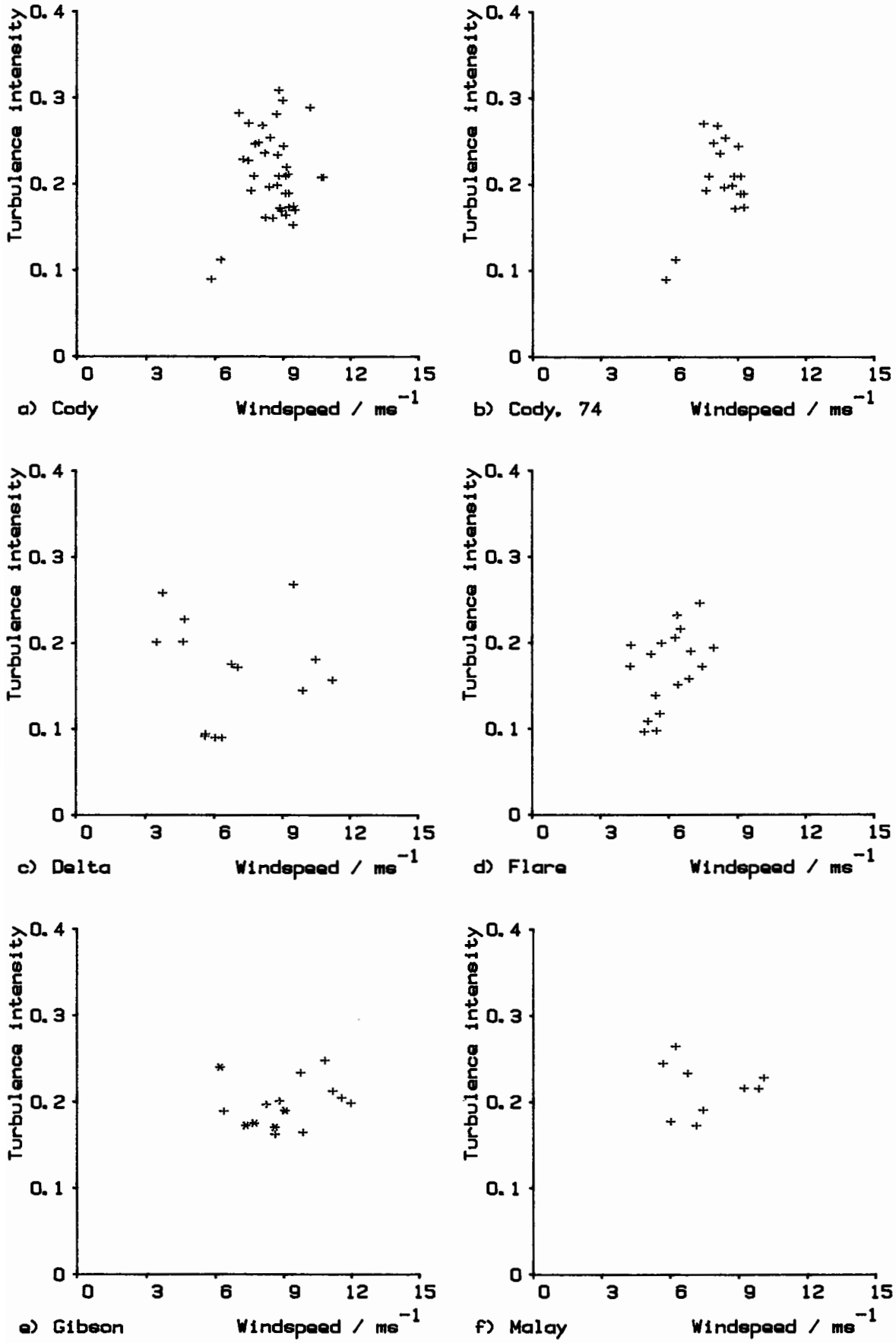

Kite experiments performed

Figure 56

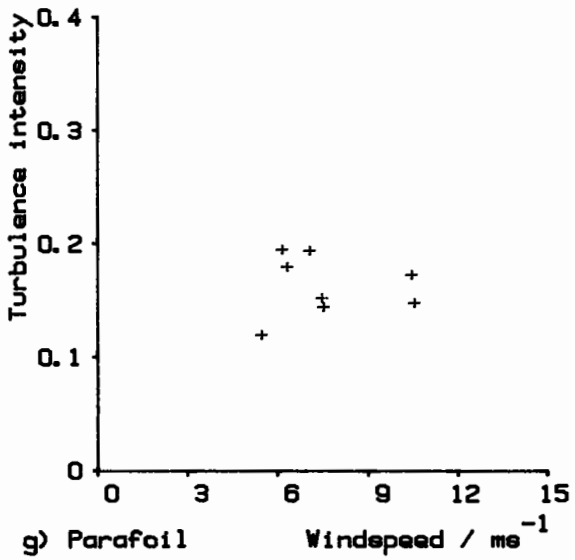

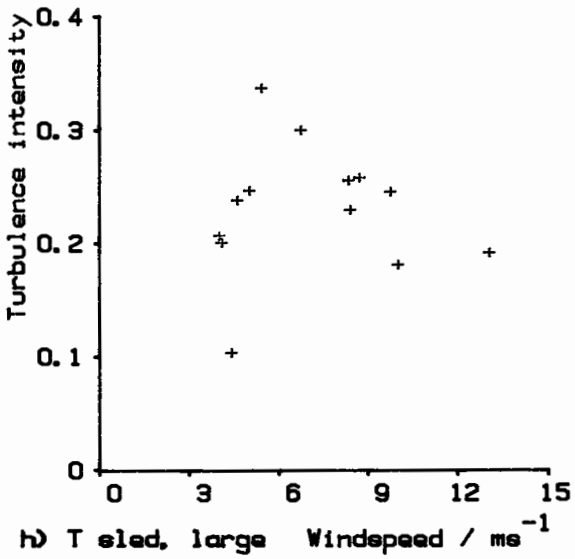

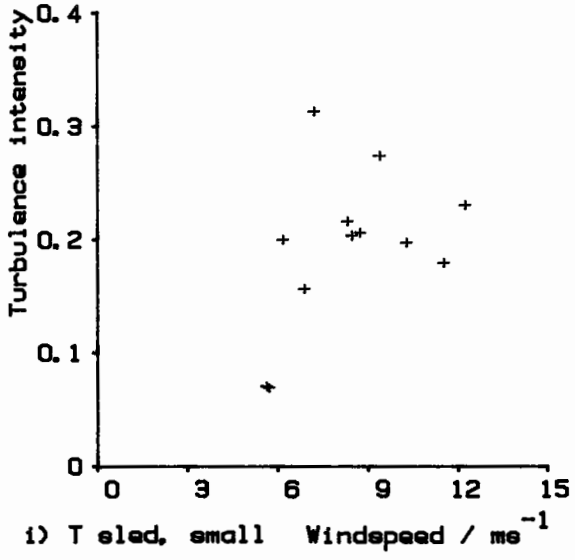

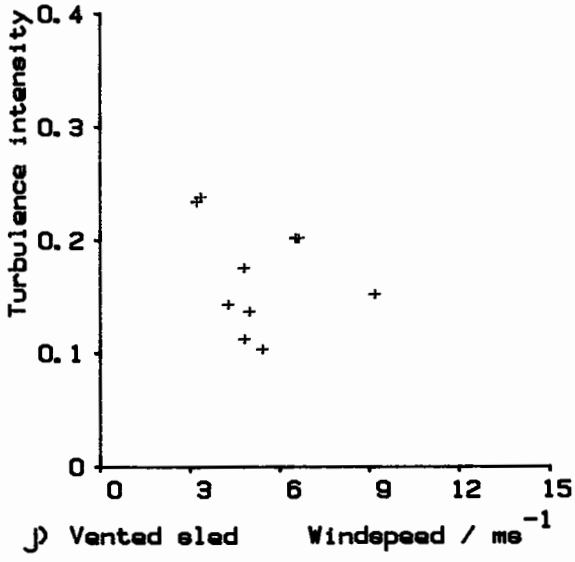

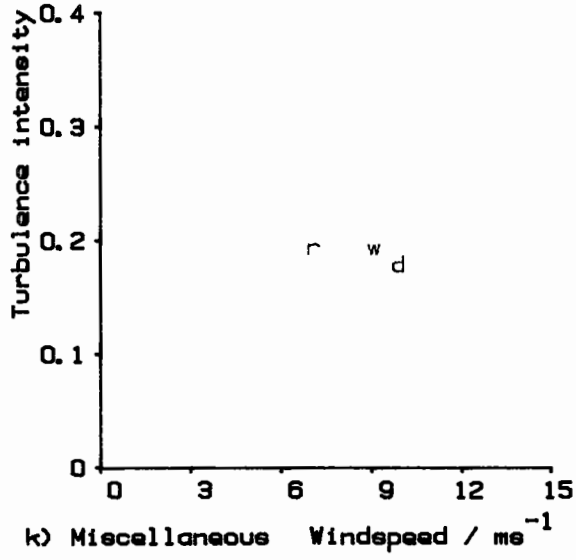

Plot k) of figures 56,61,62,64 to 74 covers the kites : d Dunford Delta
r Rotor
w Winged Box

Kite experiments performed (cont)

Figure 56 cont.

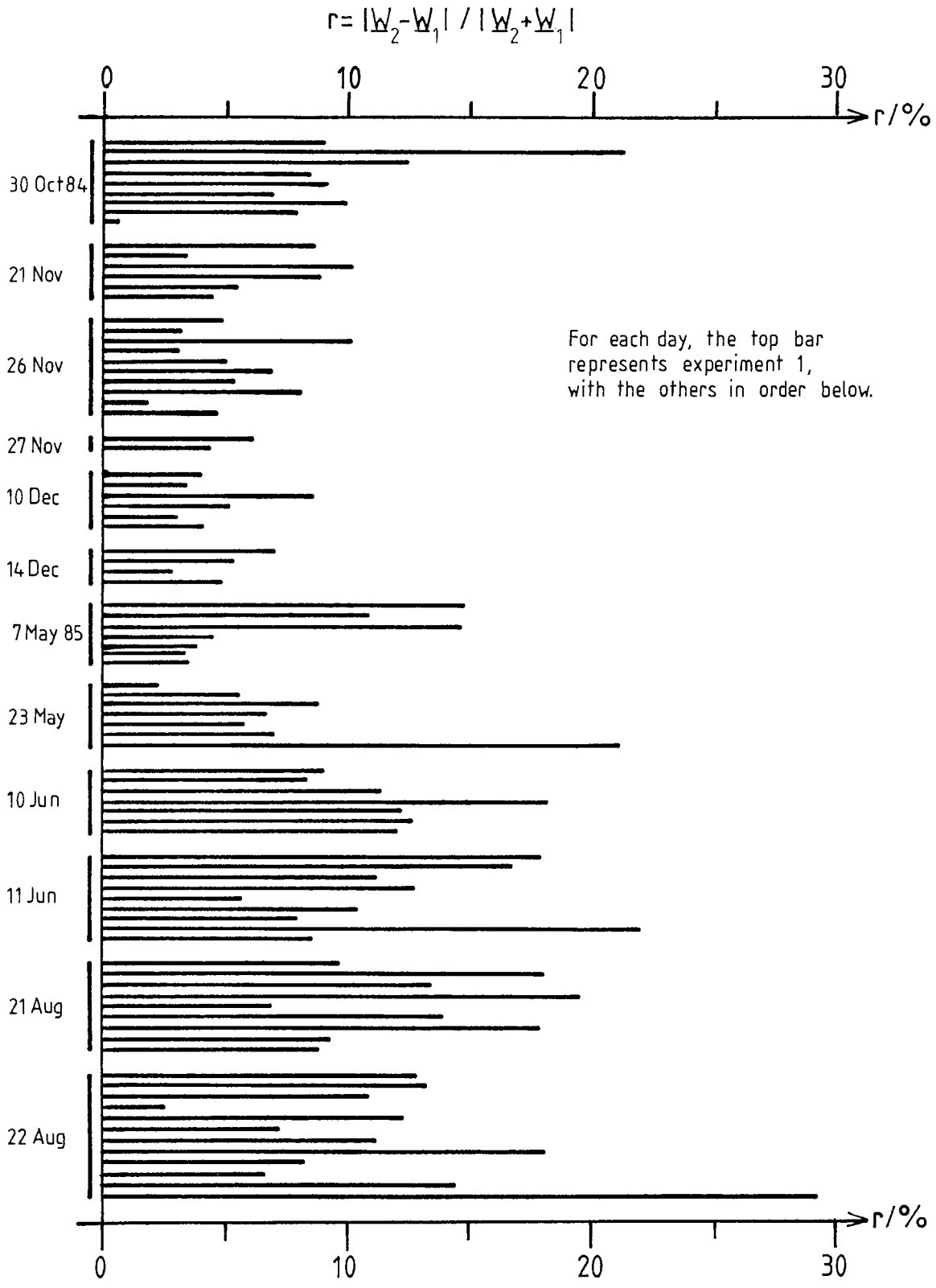

Change in wind velocity during experiment

Figure 57

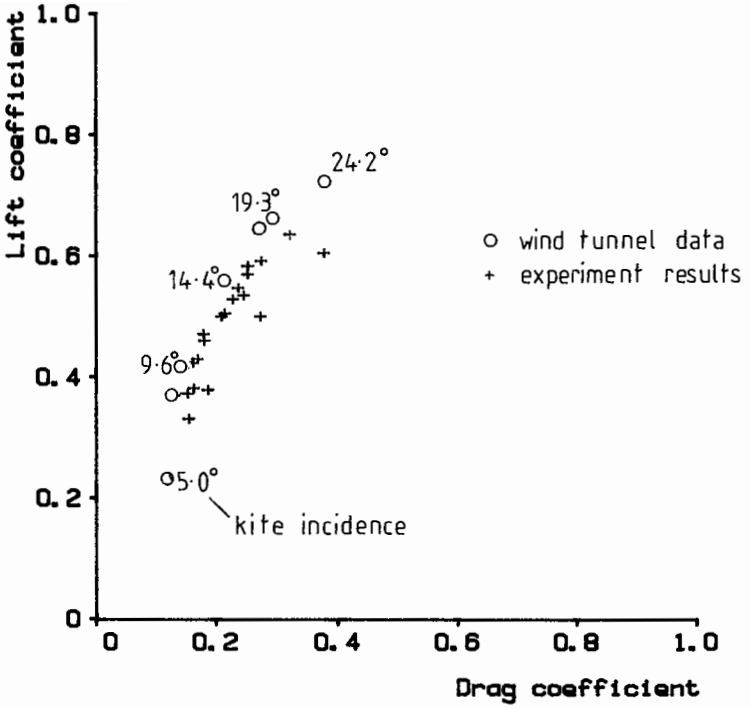

a) Cody kite

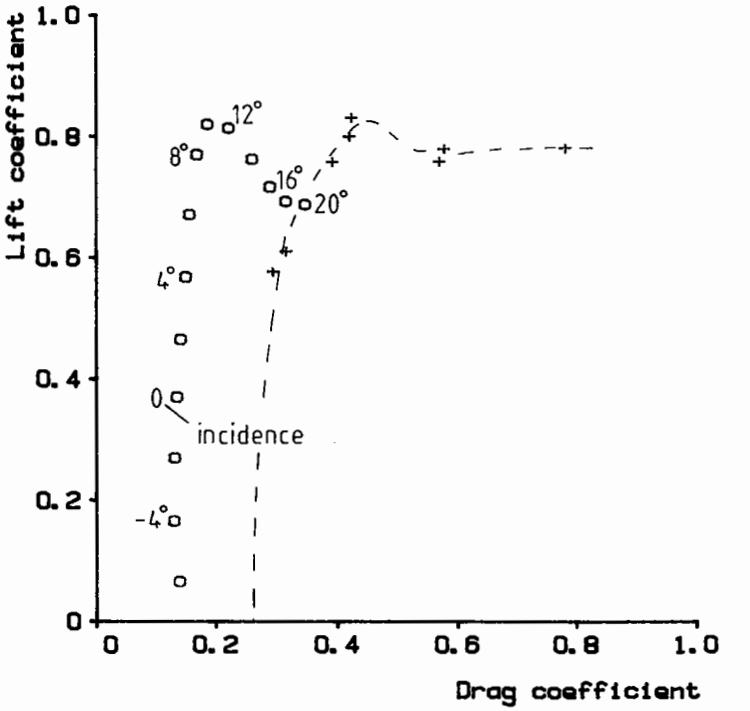

b) Parafoil

Comparison of experiment and wind tunnel measurements

Figure 58

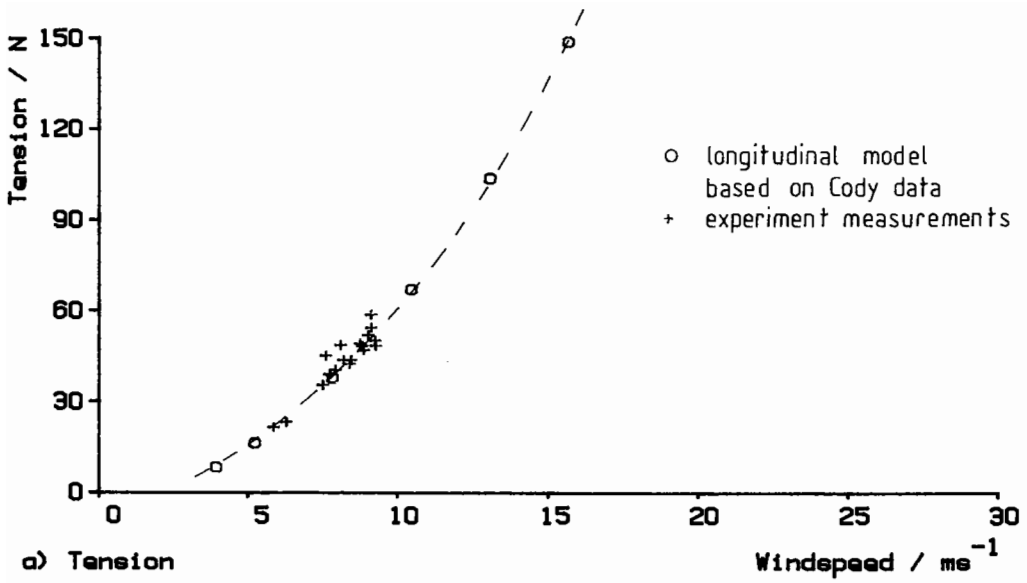

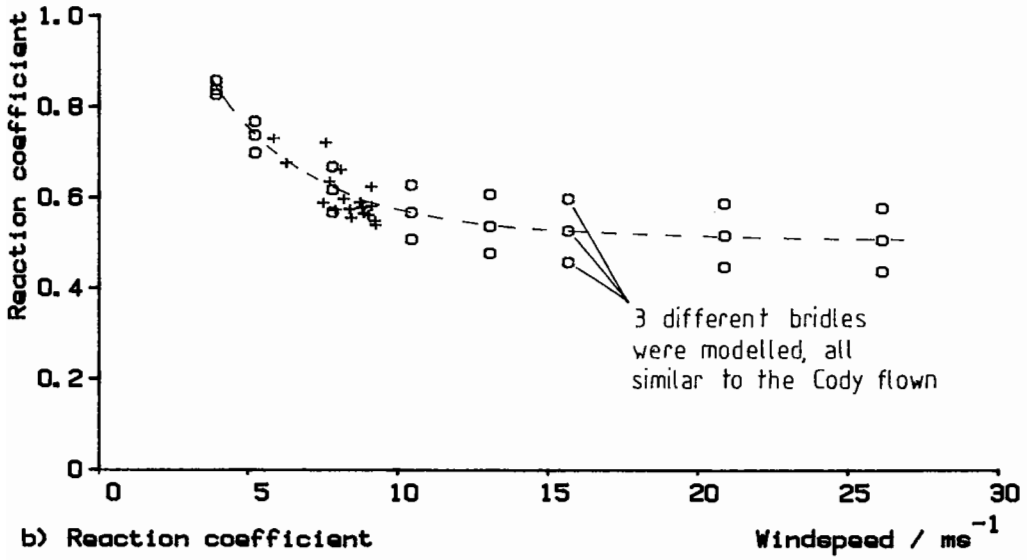

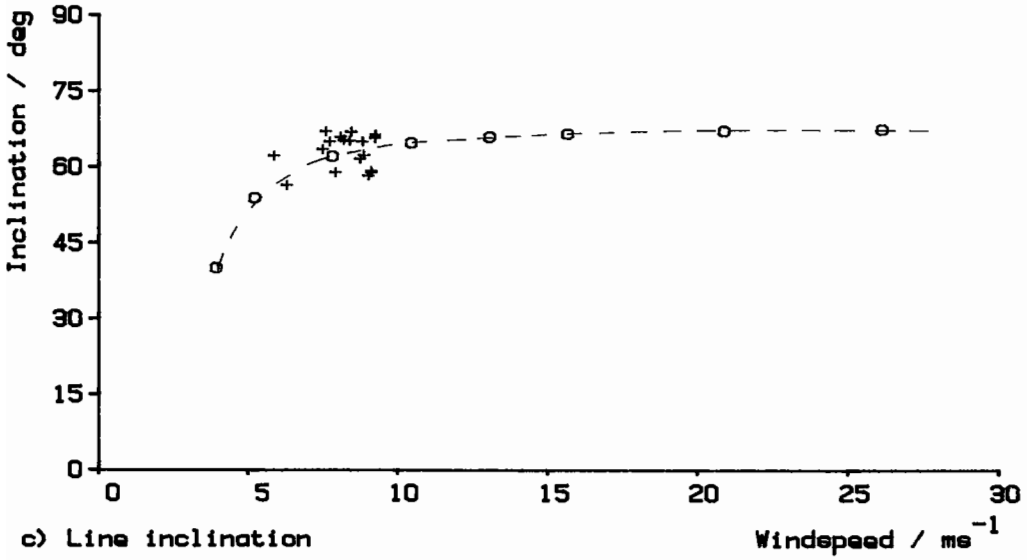

Comparison of experiment and model results for the Cody Figure 59

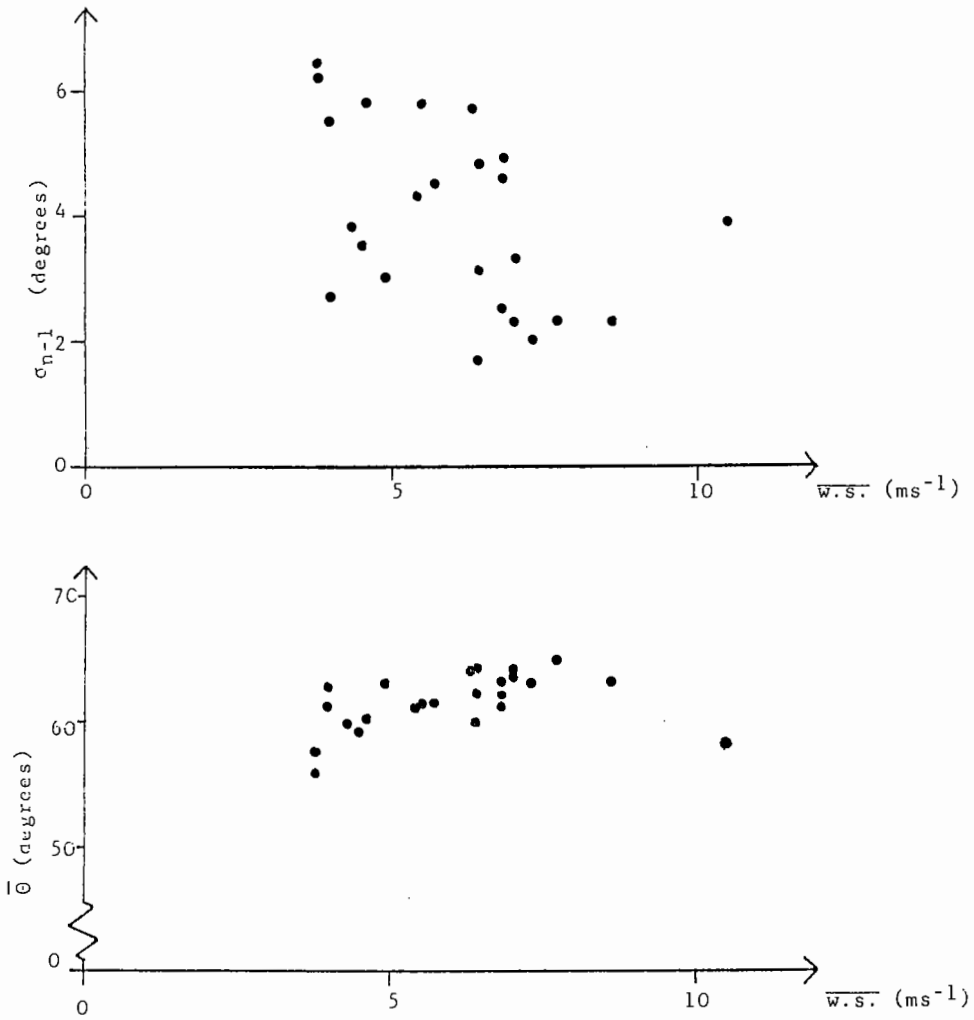

a) Plots of standard deviation and mean angle against mean windspeed for the Red Yellow Delta.
(From Nowell, 1984)

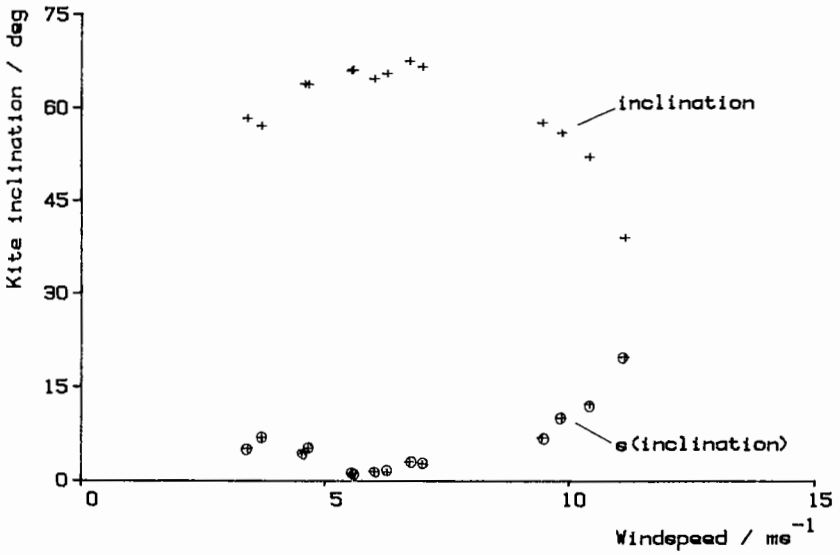

b) Kite inclination vs windspeed for the (Red / Yellow) Delta from the current work.

Comparison of Delta inclination results

Figure 60

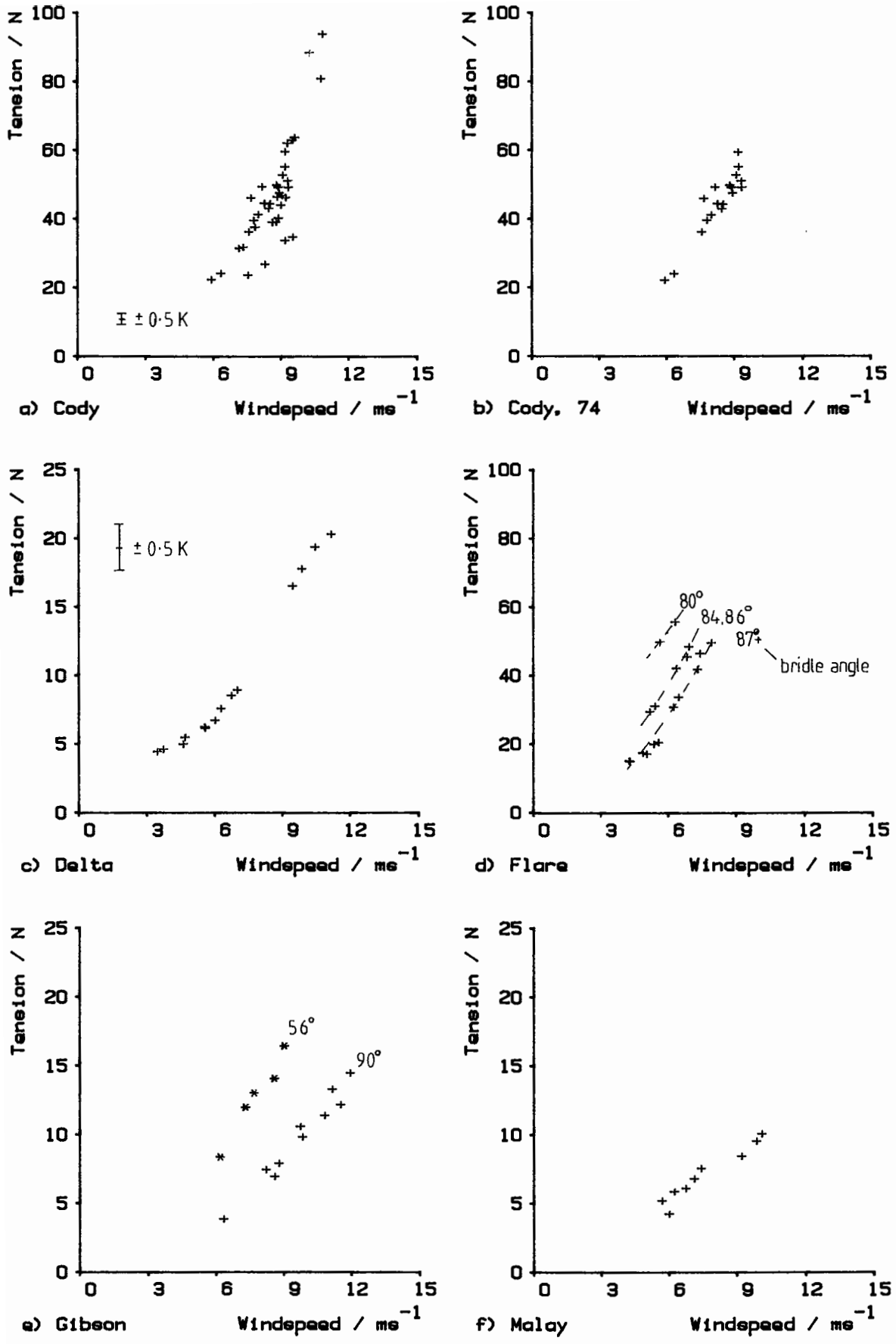

Tension vs windspeed results

Figure 61

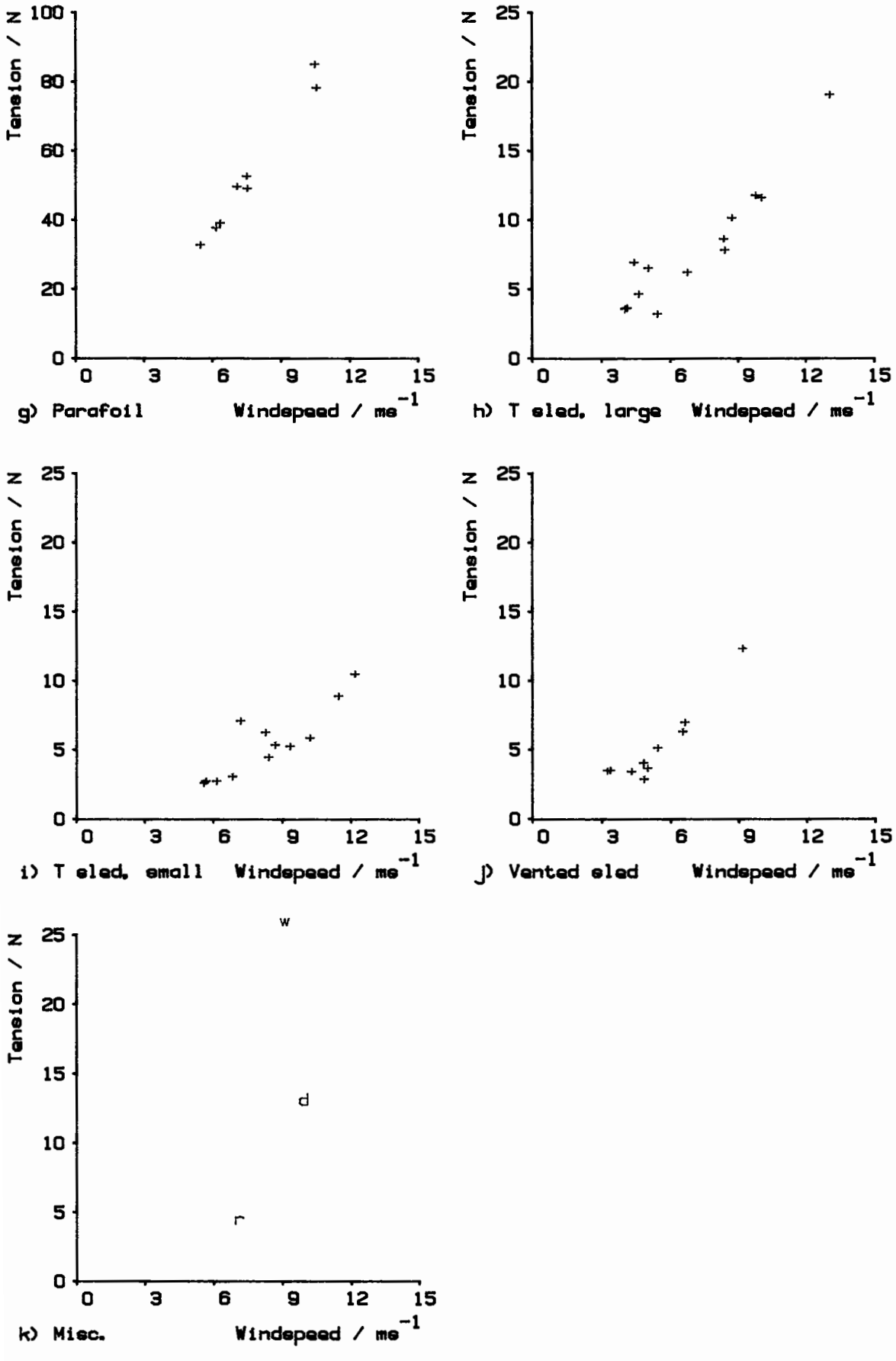

Tension vs windspeed results (cont)

Figure 61 cont.

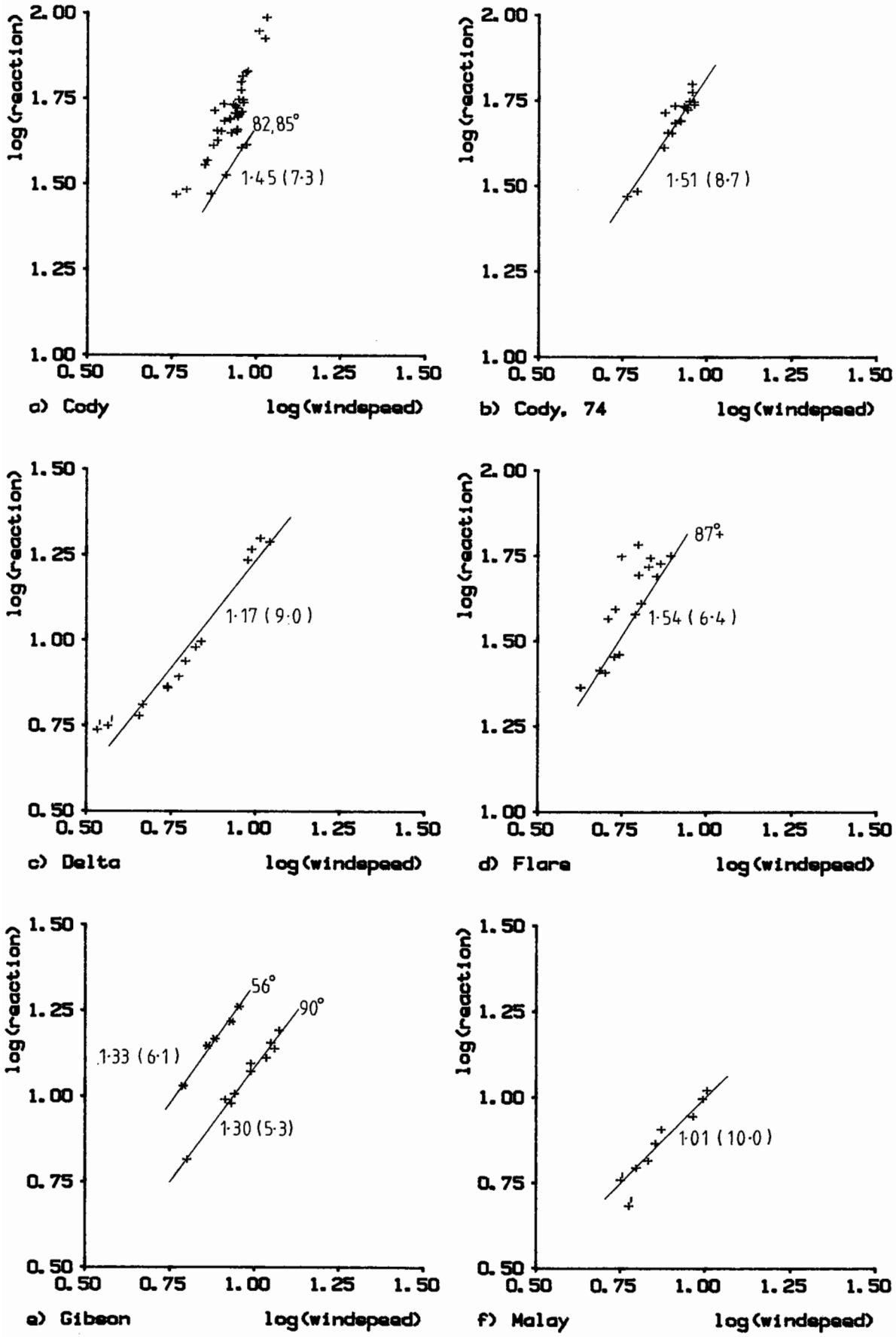

Reaction vs windspeed (log format)

Figure 62

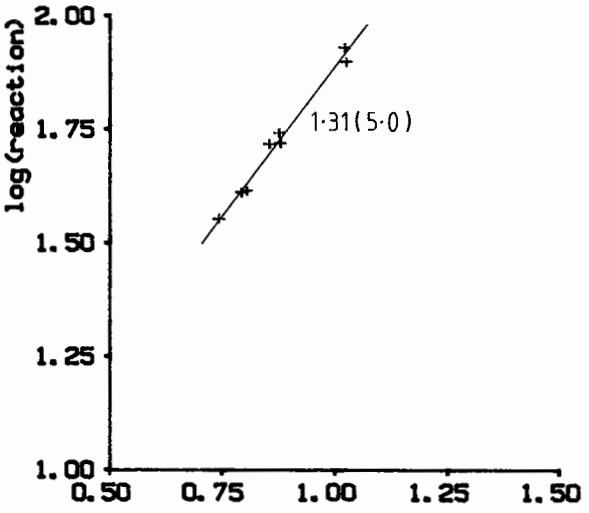

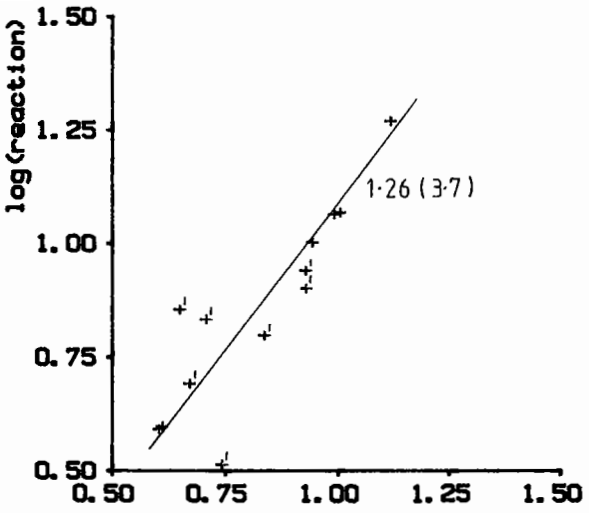

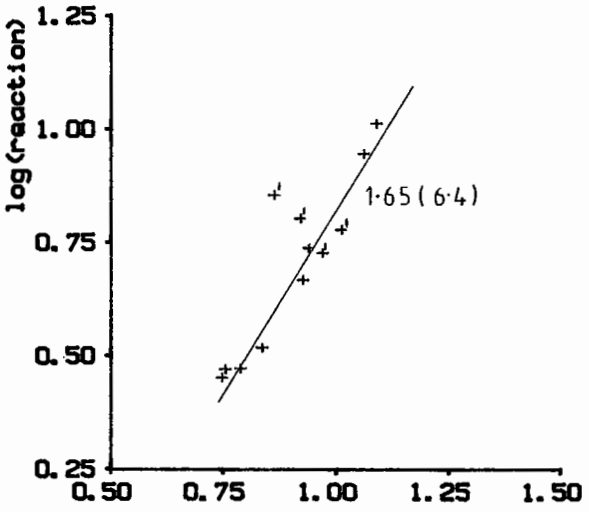

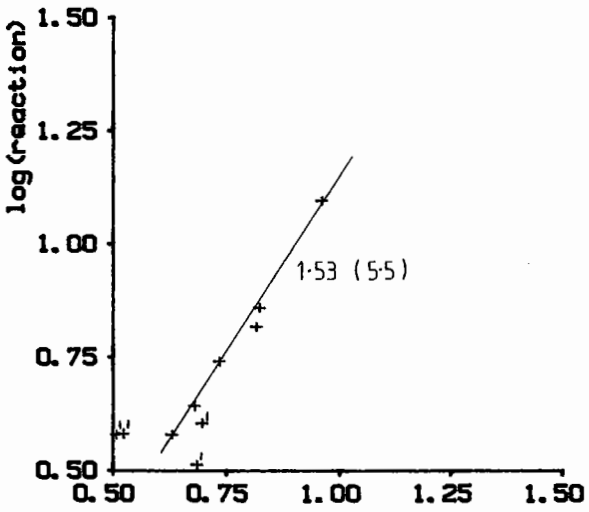

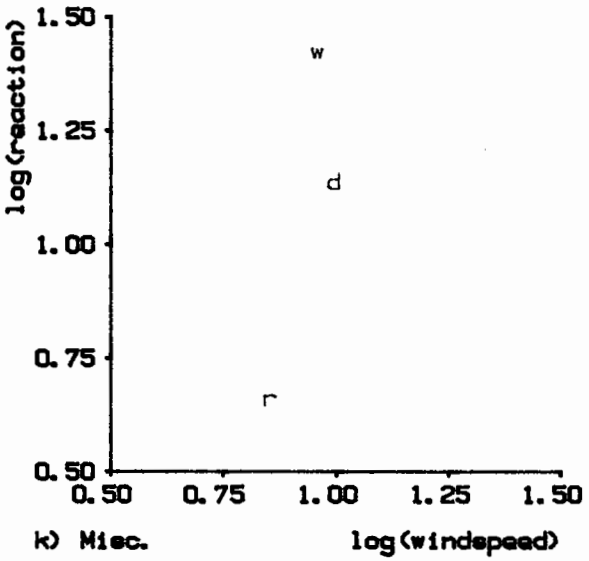

The numbers shown are slope (% standard deviation)

+ : Points omitted from regression

Reaction vs windspeed (log format, cont)

Figure 62 cont.

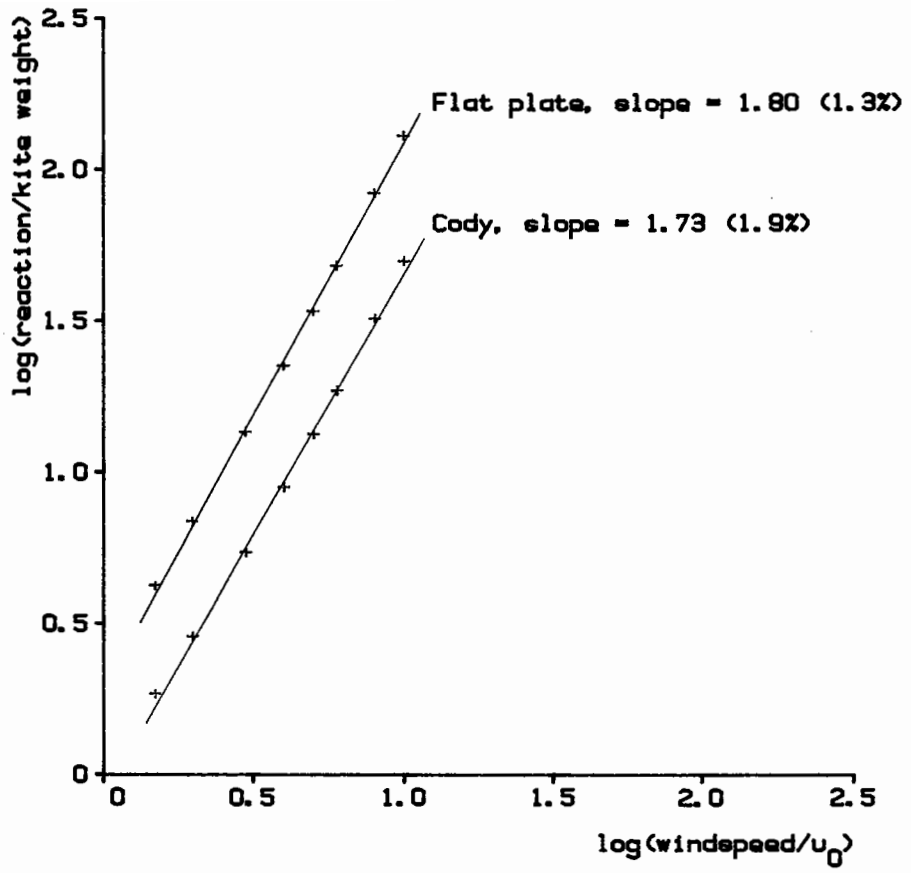

Reaction vs windspeed (log format) for longitudinal kite model

The slope of the linear regression is given for each set of points, with the standard deviation expressed as a percentage in brackets.

Figure 63

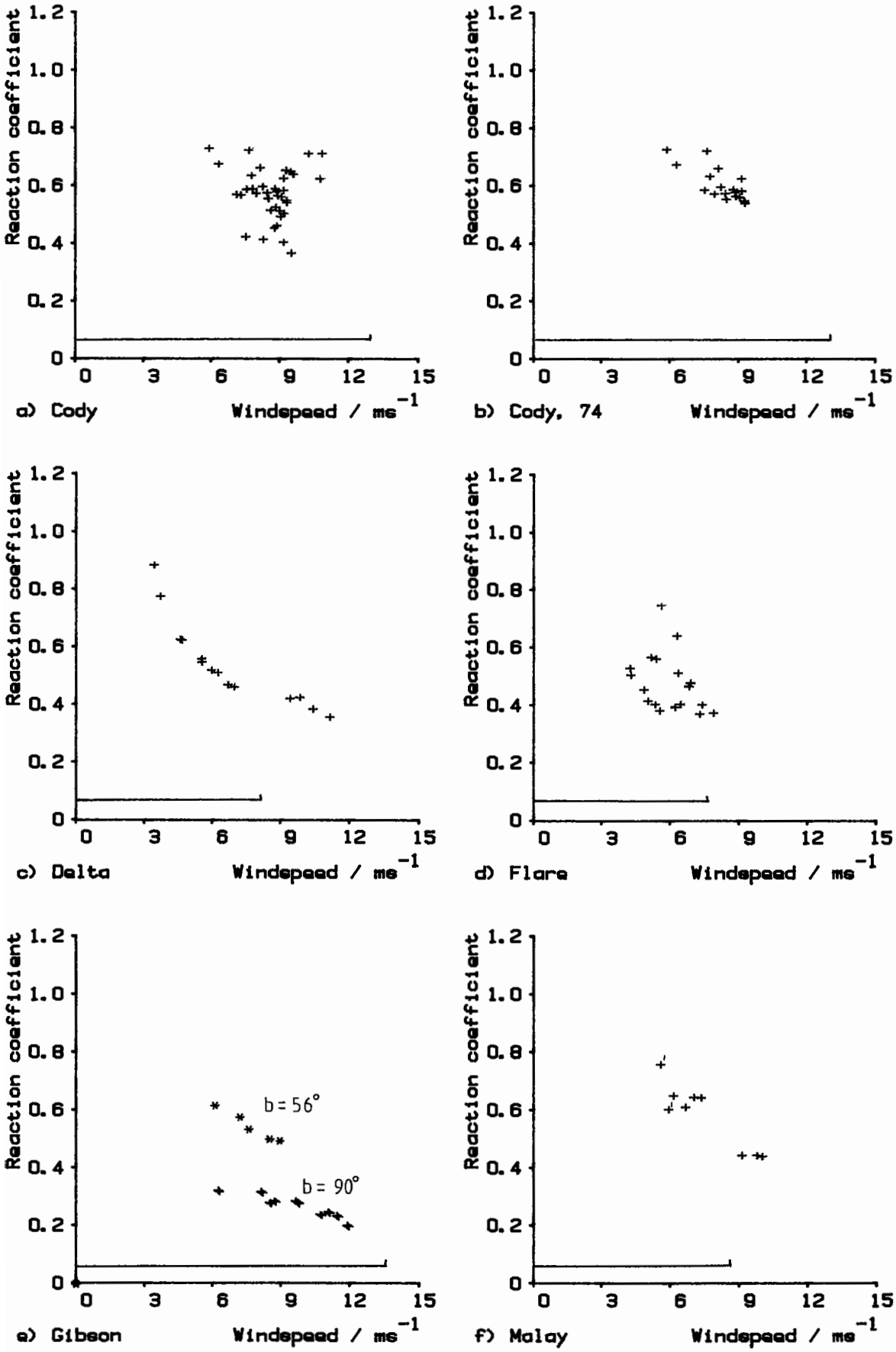

Reaction coefficient vs windspeed results

Figure 64

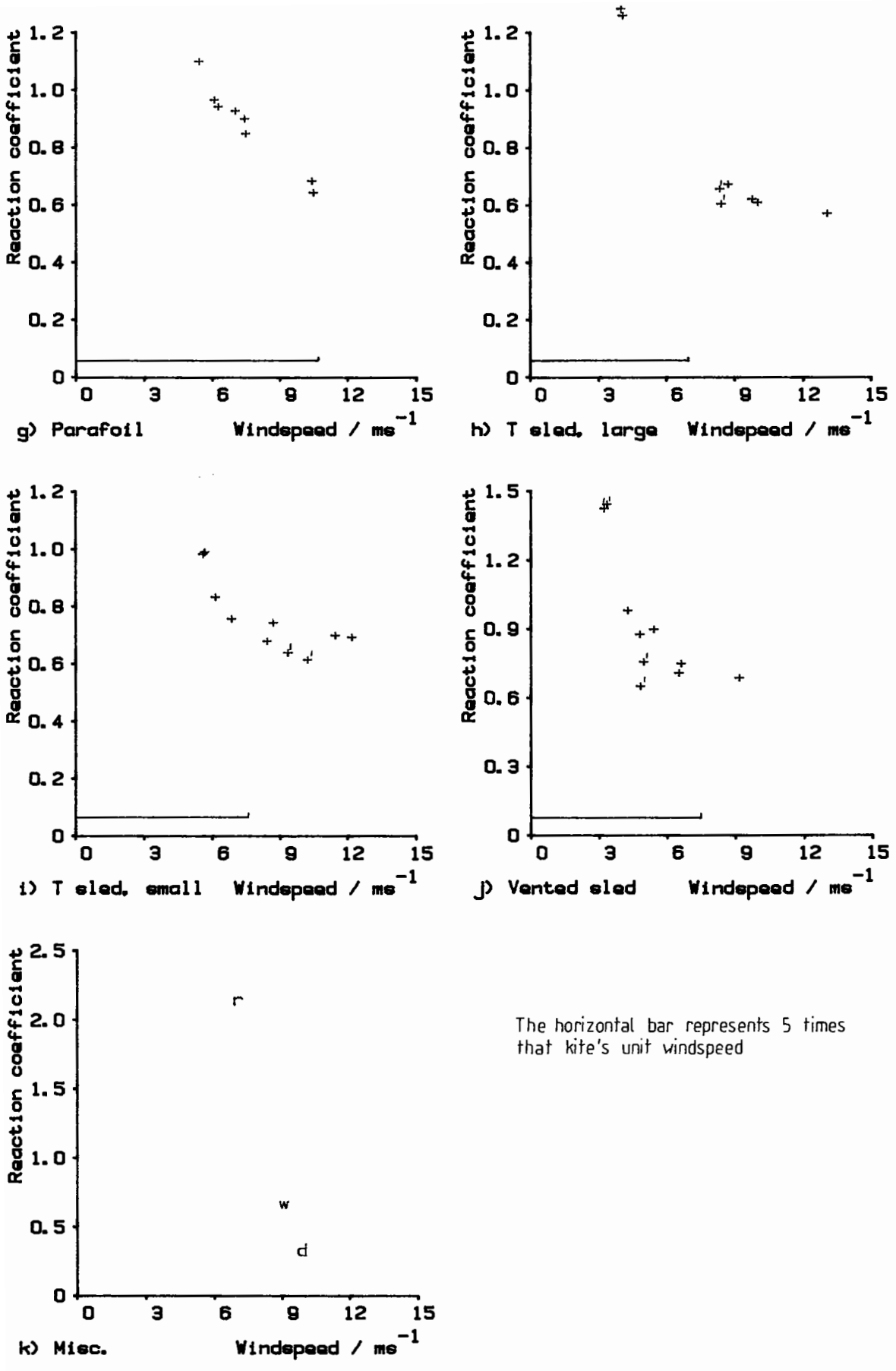

Reaction coefficient vs windspeed results (cont)

Figure 64 cont.

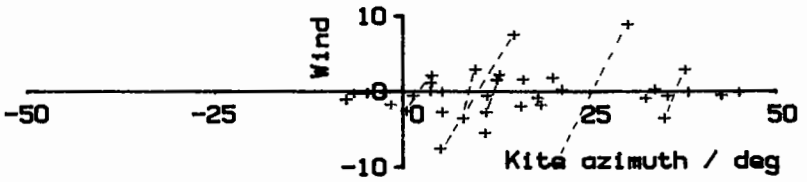

a) Cody

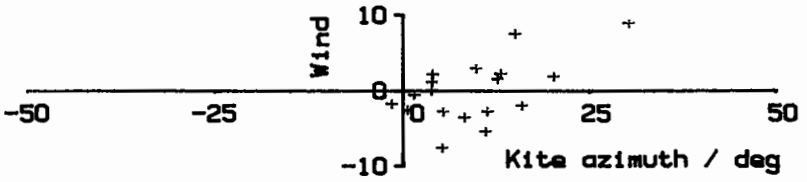

b) Cody, 22-Aug-85

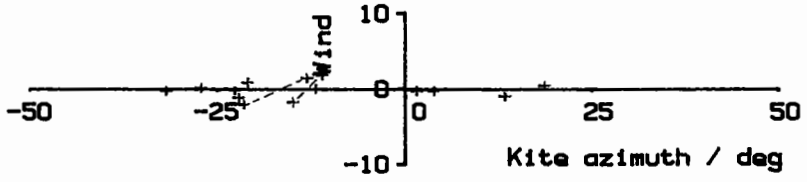

c) Delta

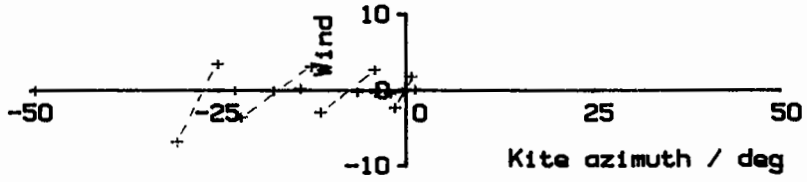

d) Flare

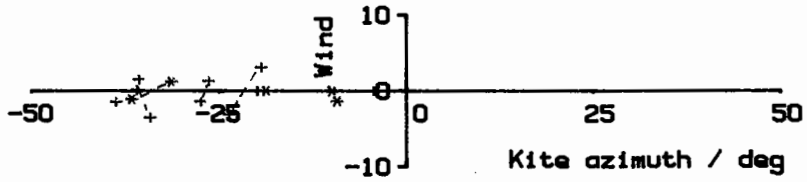

e) Gibeon

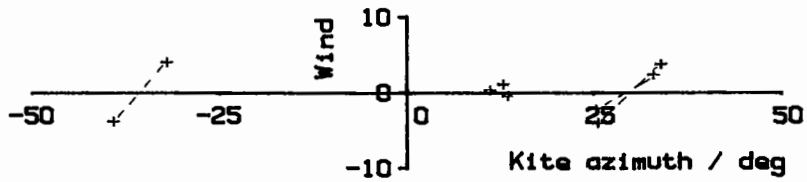

f) Malay

Kite azimuth ve wind azimuth

Figure 65

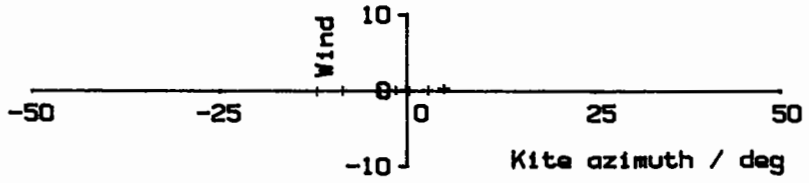

g) Parafoil

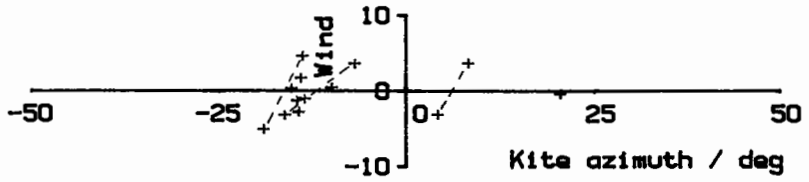

h) T sled, large

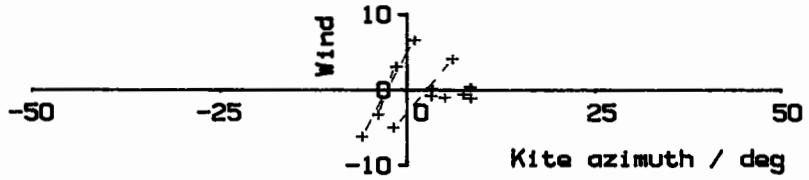

i) T sled, small

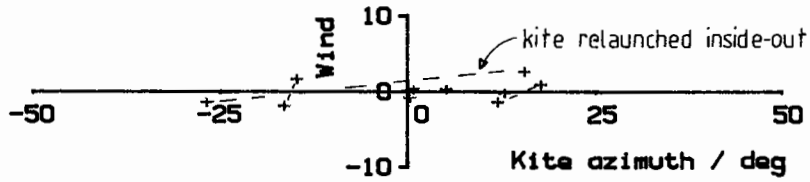

j) Vented sled

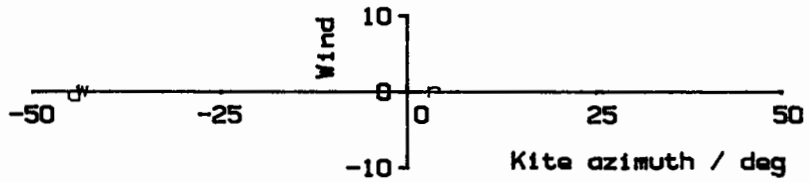

k) Miscellaneous

The dashed lines join points corresponding to the same experiment.

Kite azimuth vs wind azimuth (cont) Figure 65 cont.

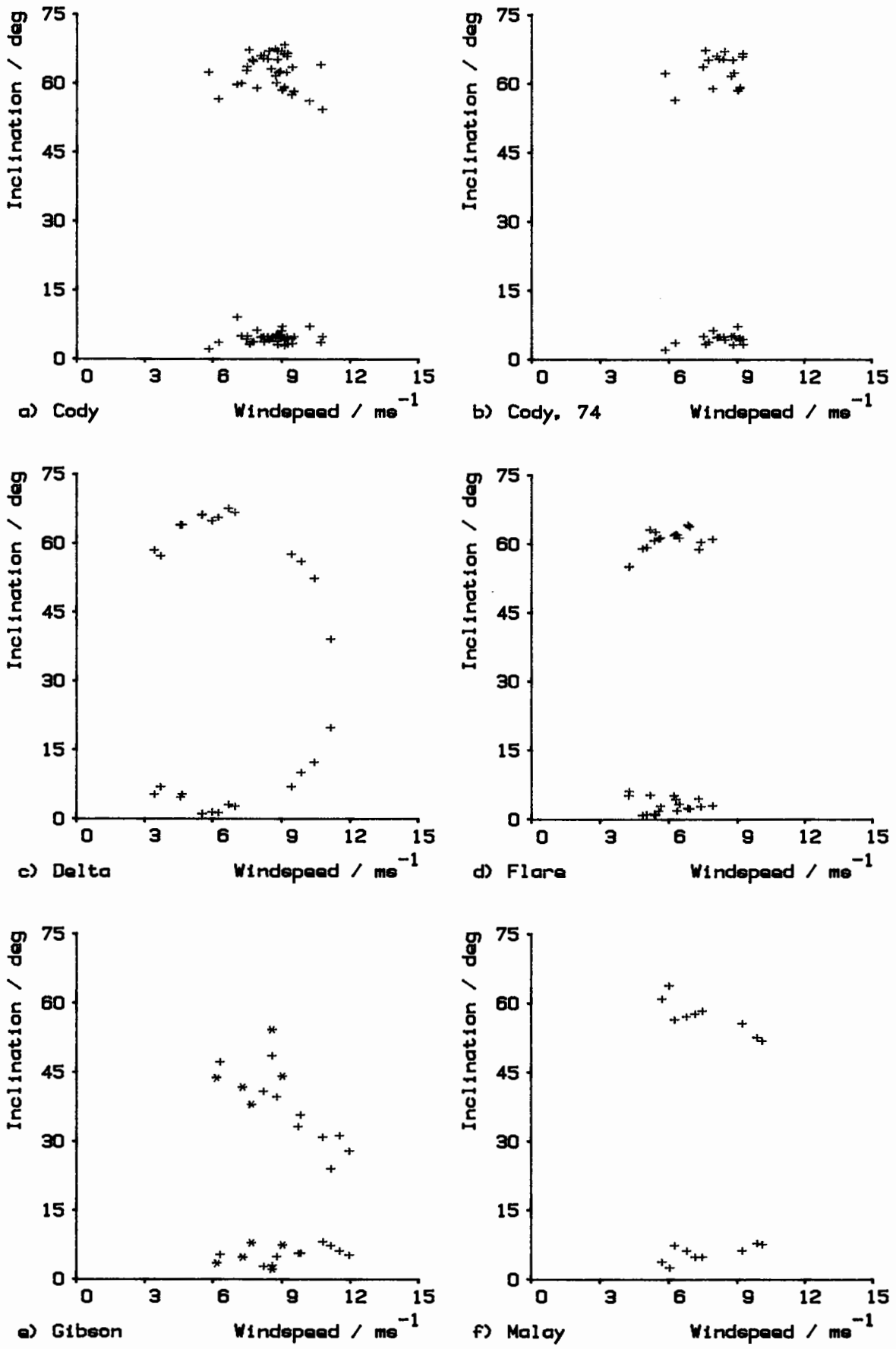

Kite inclination vs windspeed

Figure 66

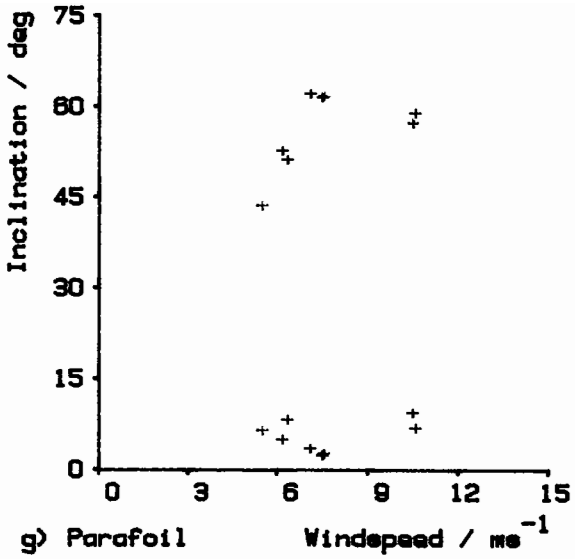

g) Parafoil

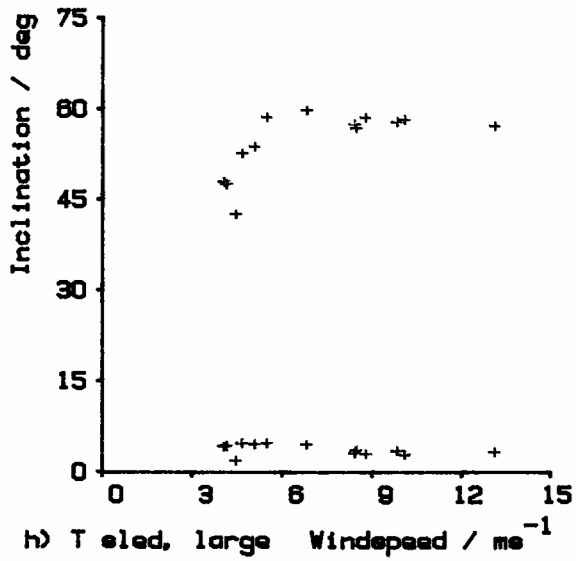

h) T sled, large

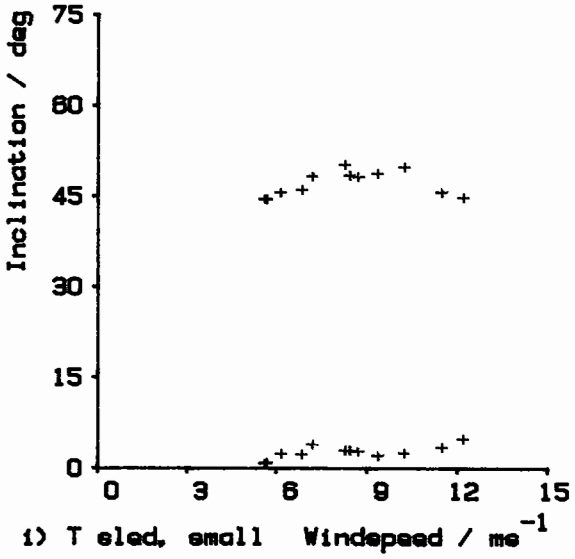

i) T sled, small

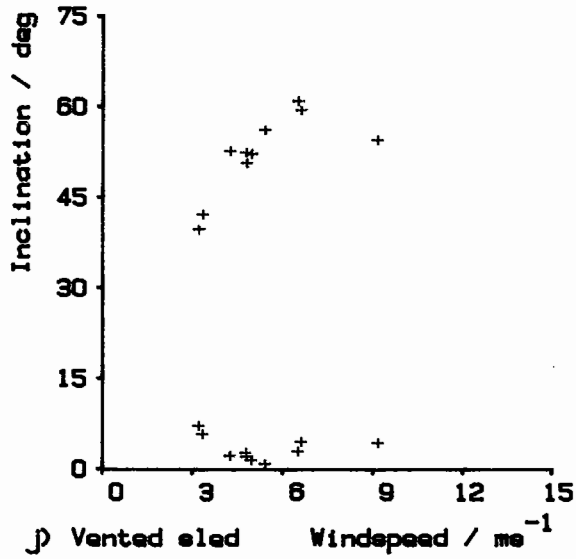

j) Vented sled

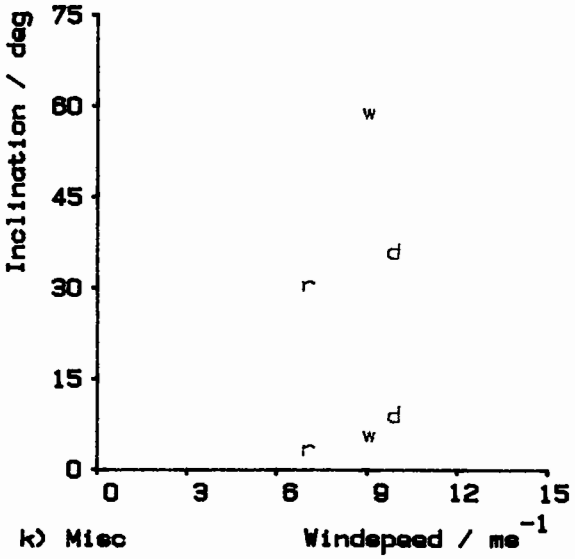

k) Misc

Each plot includes both line inclination and its standard deviation (the lower set of points).

Kite inclination vs windspeed (cont)

Figure 66 cont.

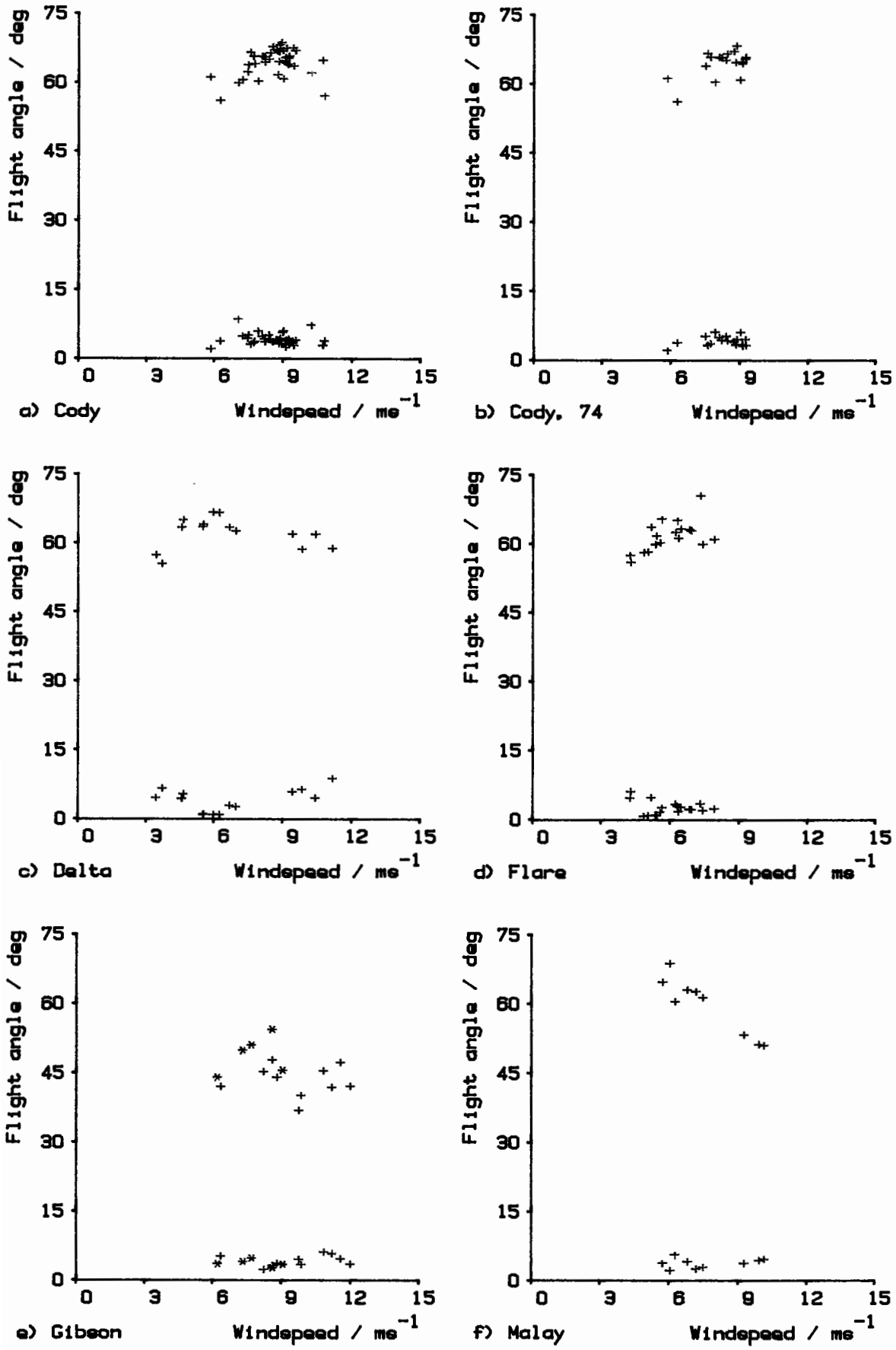

Kite flight angle vs windspeed

Figure 67

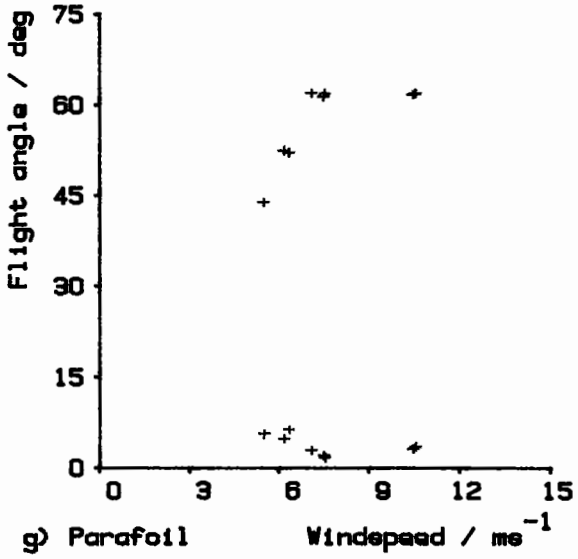

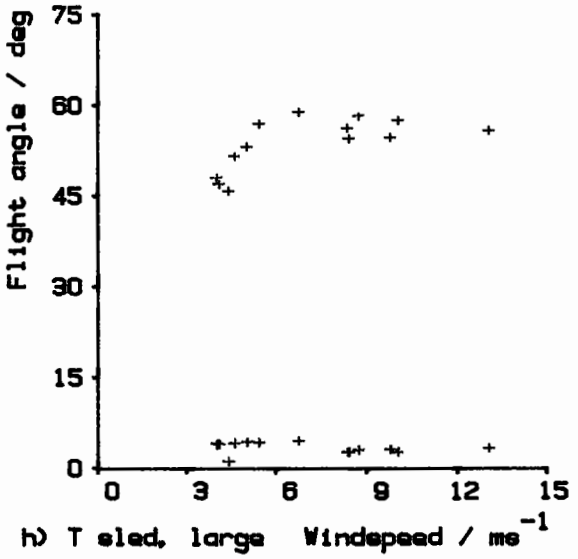

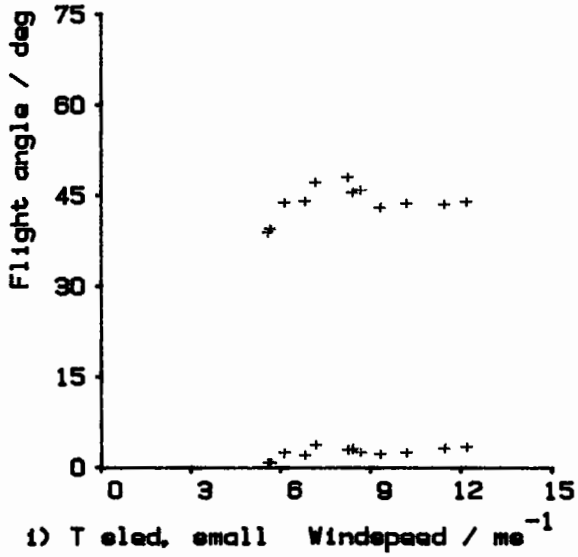

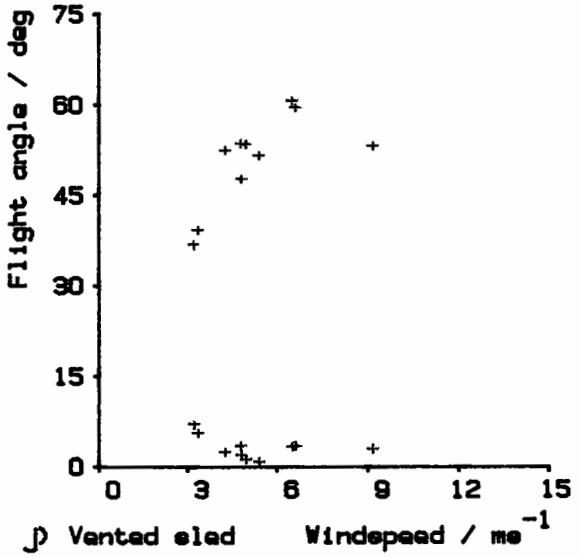

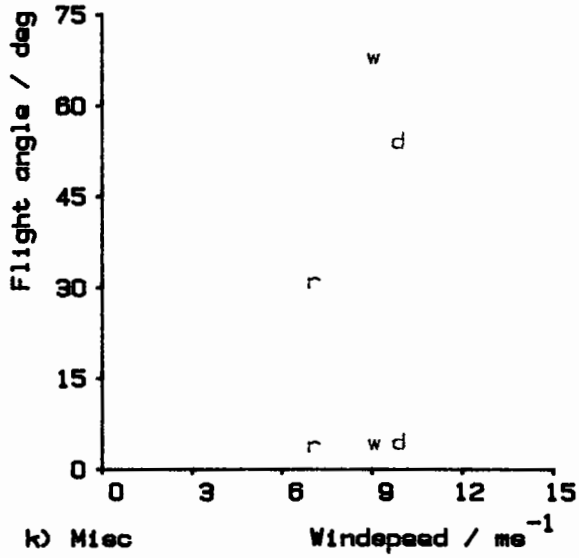

The lower set of points is the flight angle standard deviation.

Kite flight angle vs windspeed (cont)

Figure 67 cont.

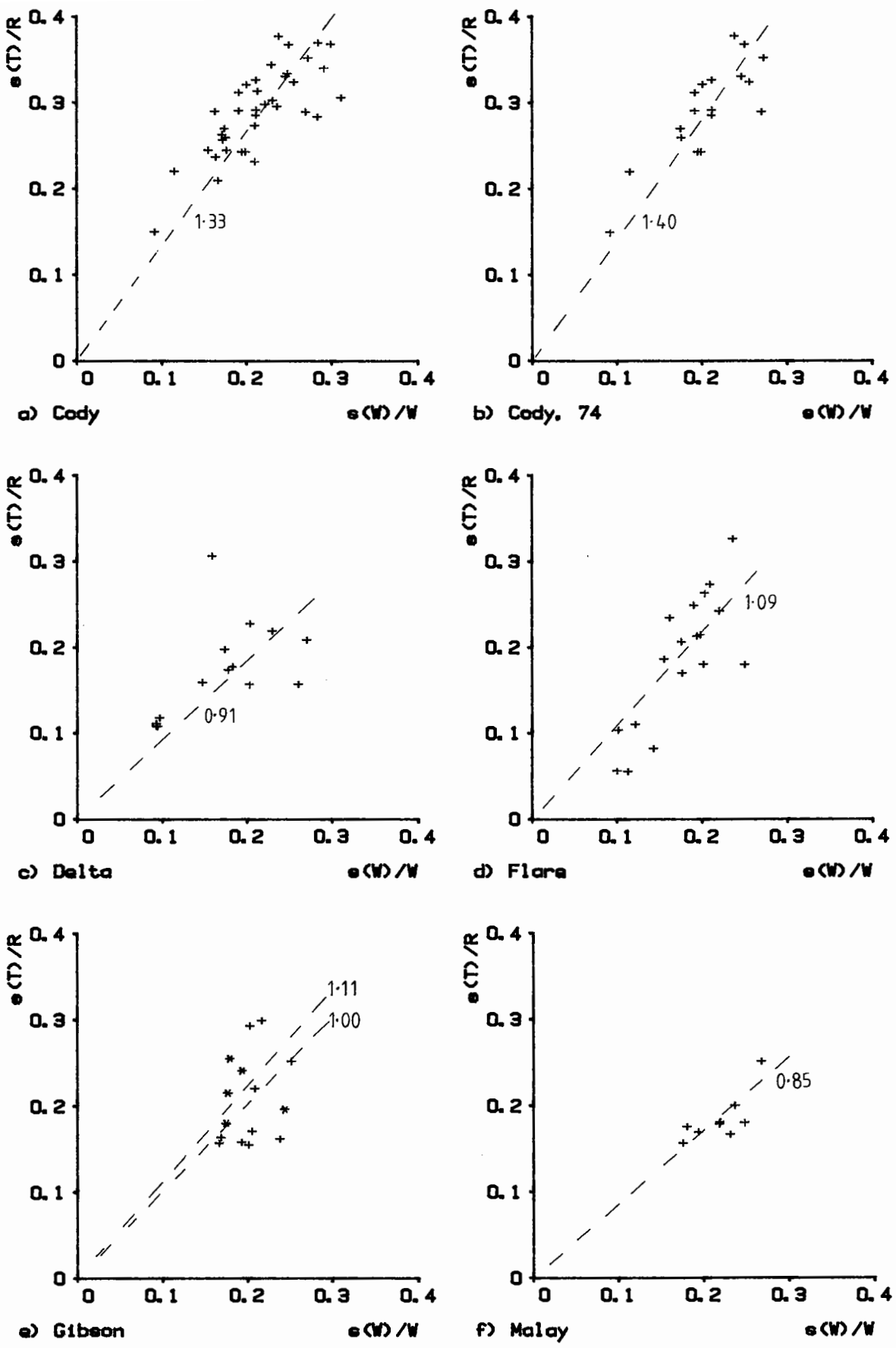

Tension variation vs windspeed variation

Figure 68

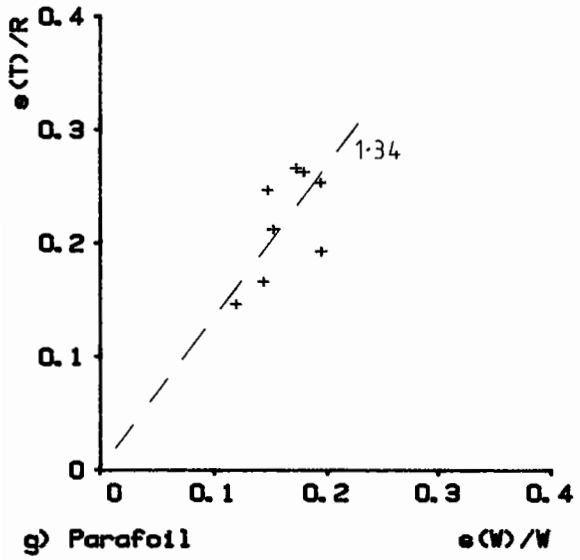

g) Parafoil

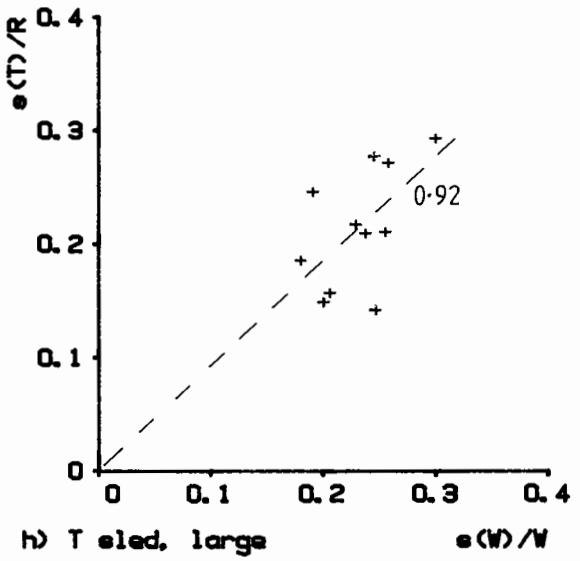

h) T sled, large

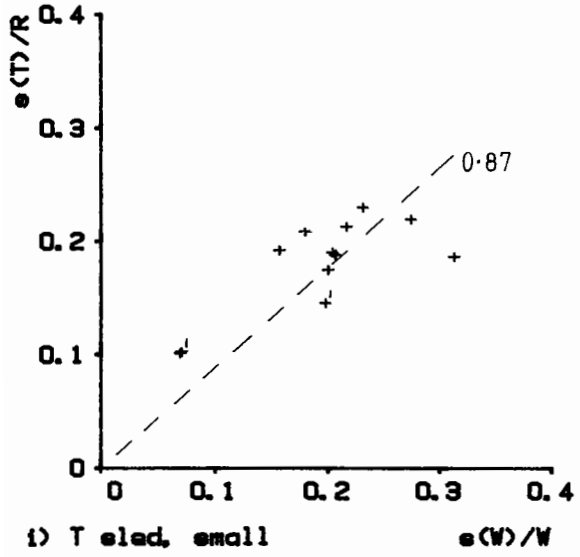

i) T sled, small

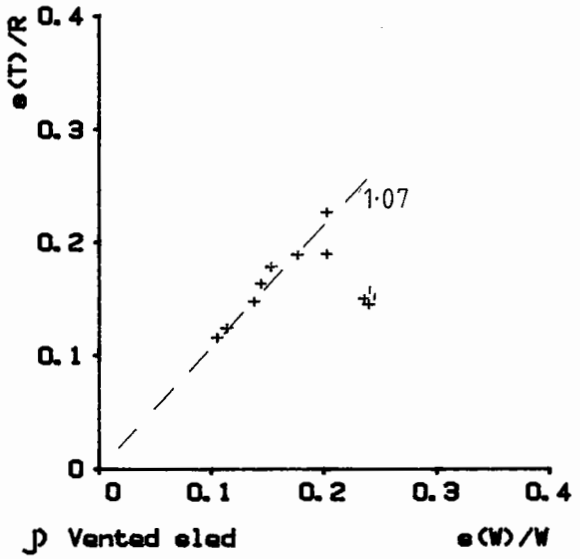

j) Vented sled

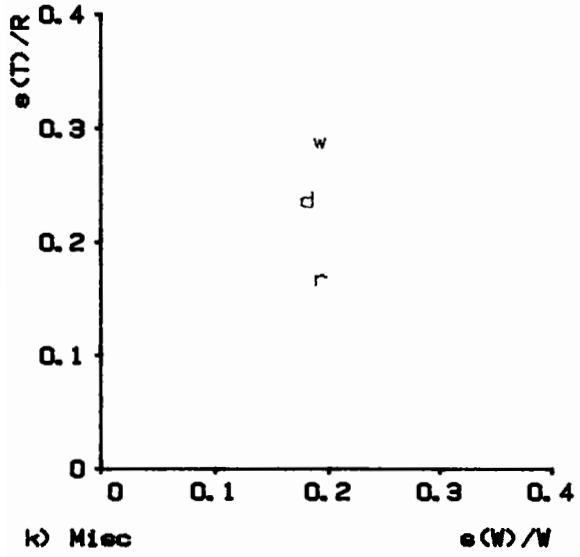

k) Misc

The slope of the regression through the origin is shown for each plot.

Tension variation vs windspeed variation (cont)

Figure 68 cont.

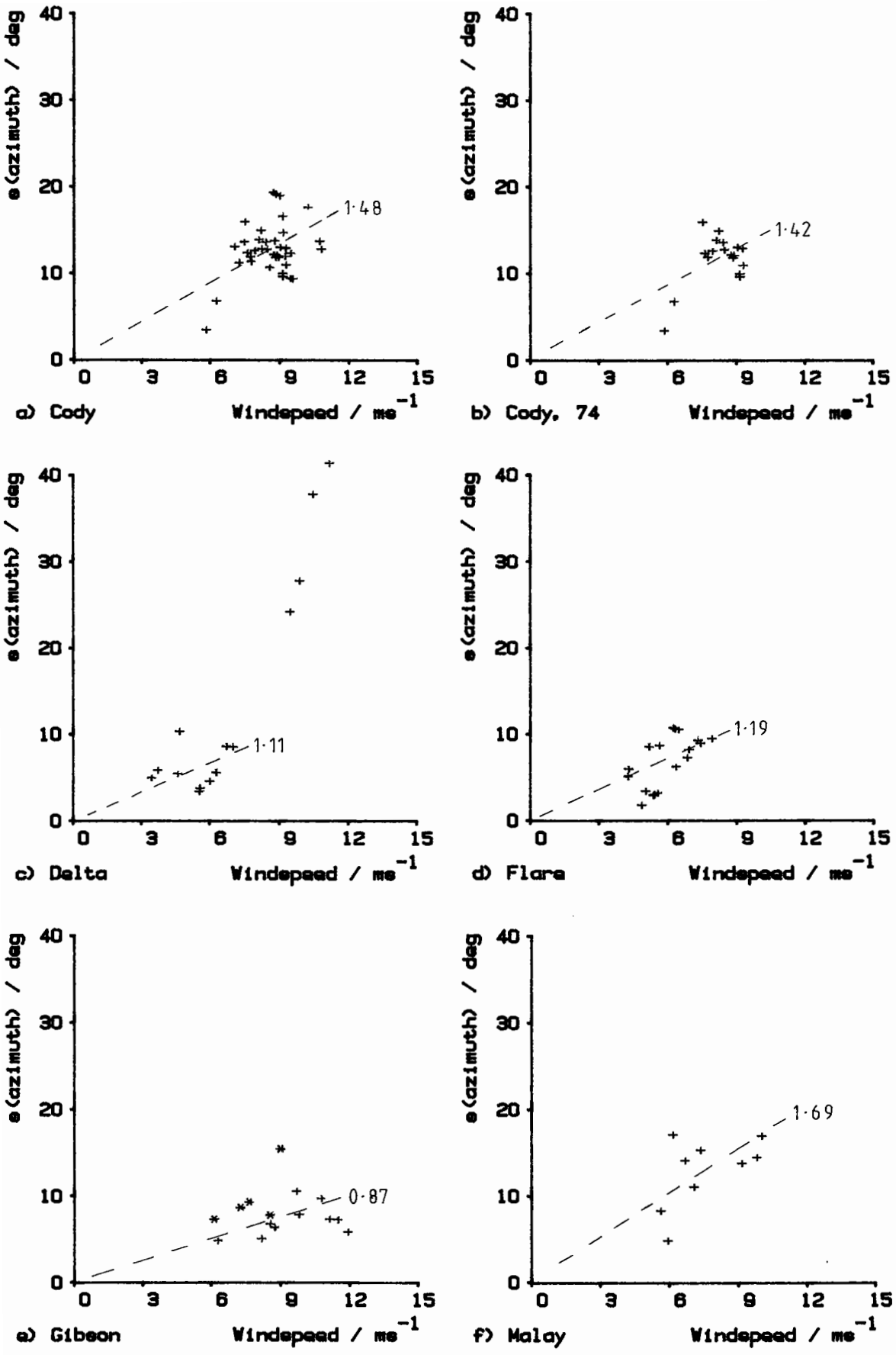

Kite azimuth standard deviation vs windspeed

Figure 69

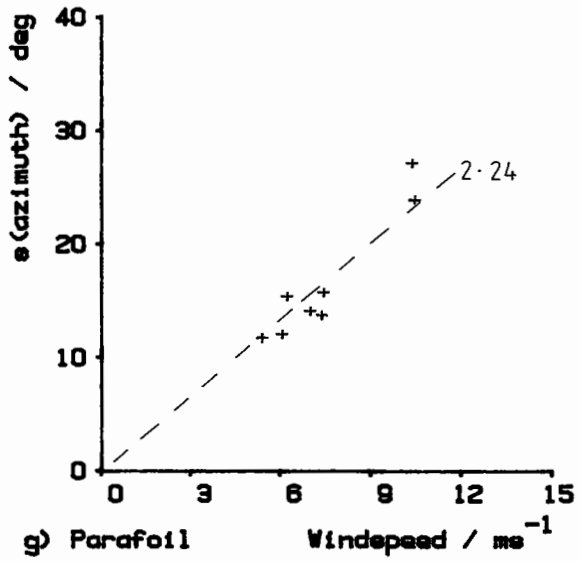

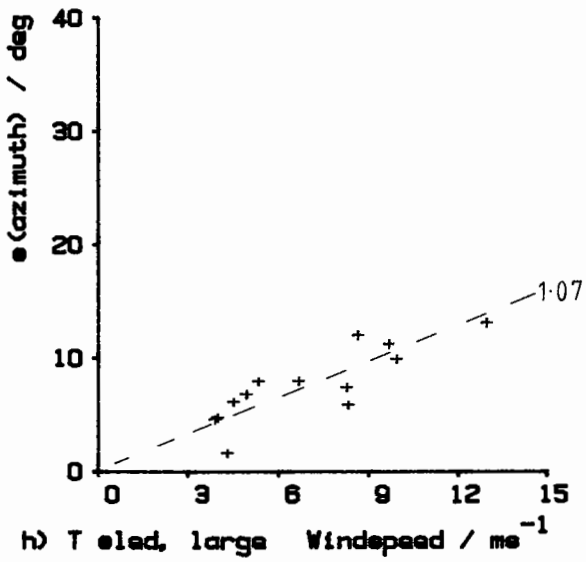

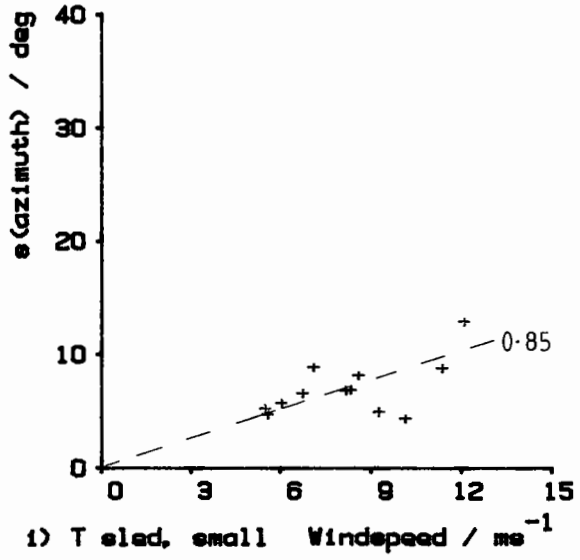

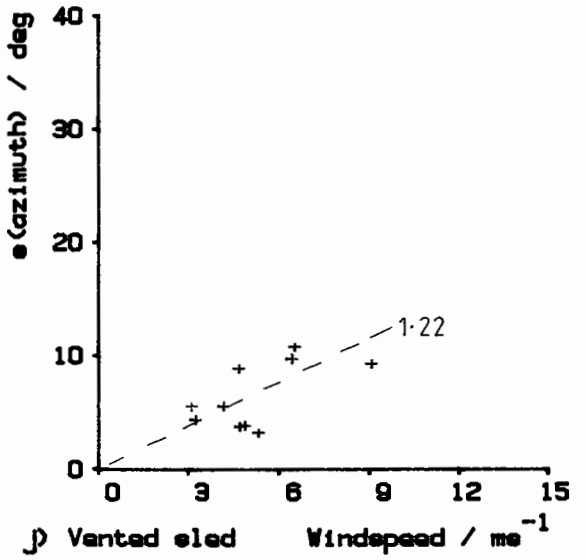

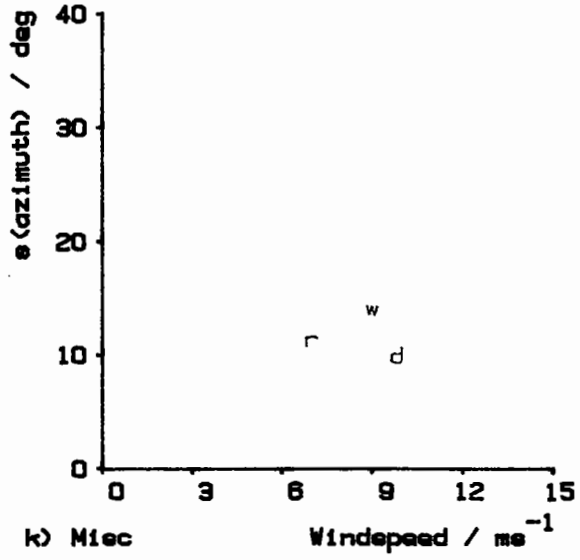

The slope of the regression through the origin is shown / ° per ms^{-1}

Kite azimuth standard deviation vs windspeed (cont)

Figure 69 cont.

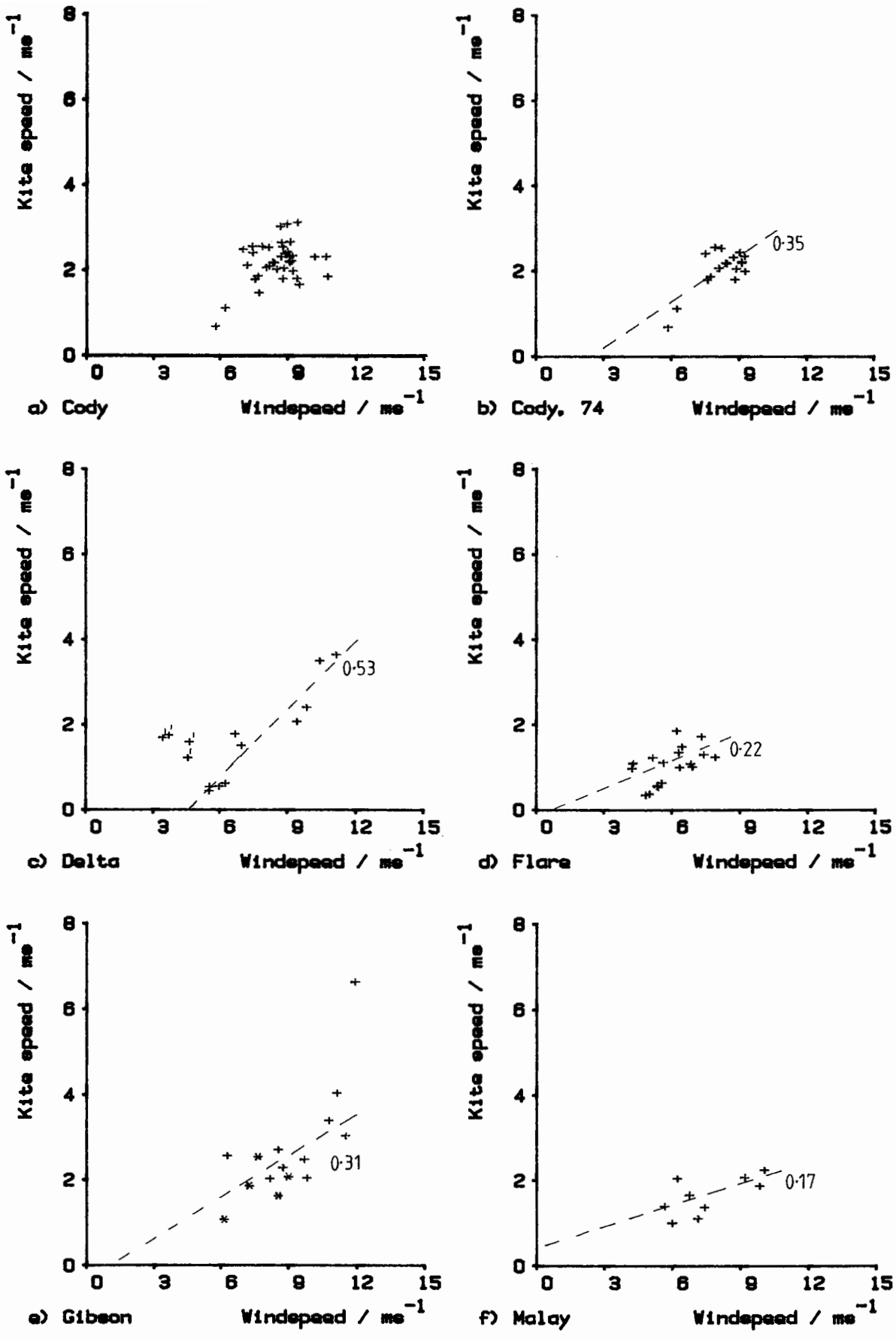

Kite speed vs windspeed

Figure 70

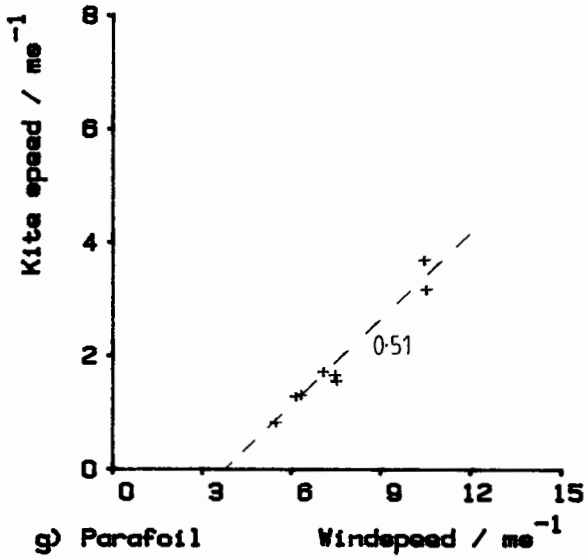

g) Parafoil

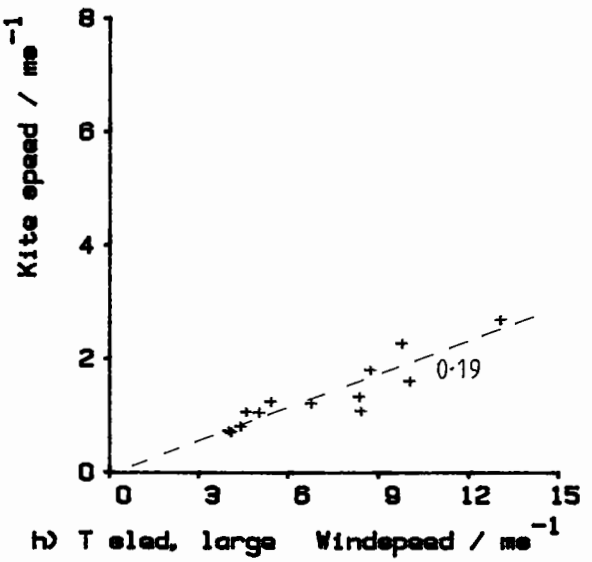

h) T sled, large

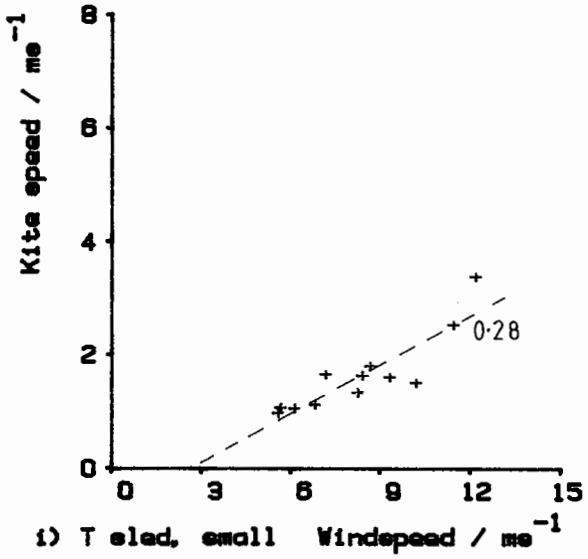

i) T sled, small

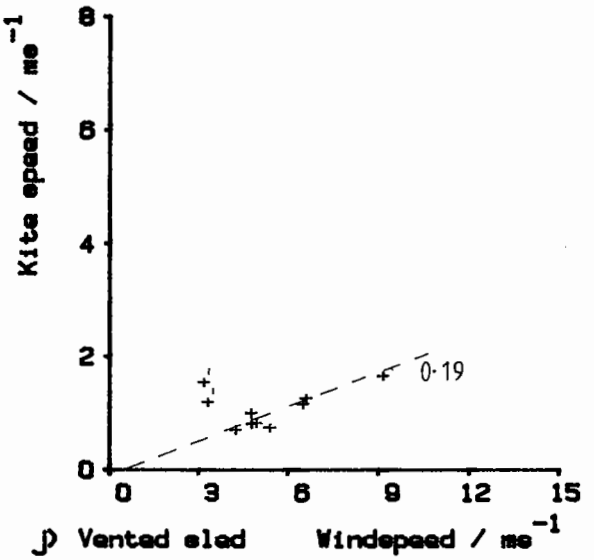

j) Vented sled

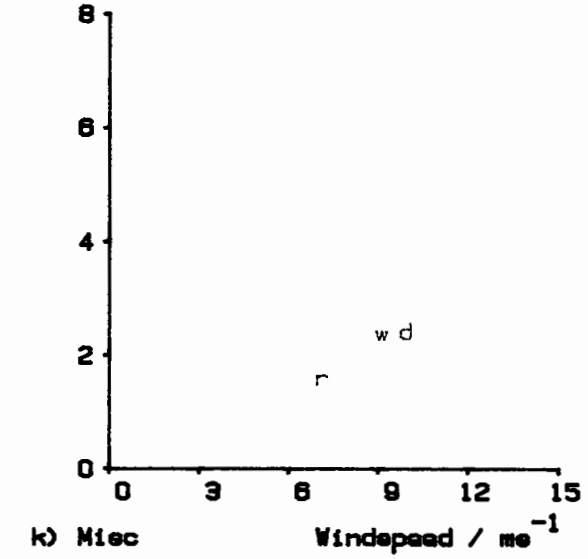

k) Misc

Regression slope is shown for each plot

The primed points in c) and j) are all due to the line motion at low tension, and not the kite's motion.

Kite speed vs windspeed (cont)

Figure 70 cont.

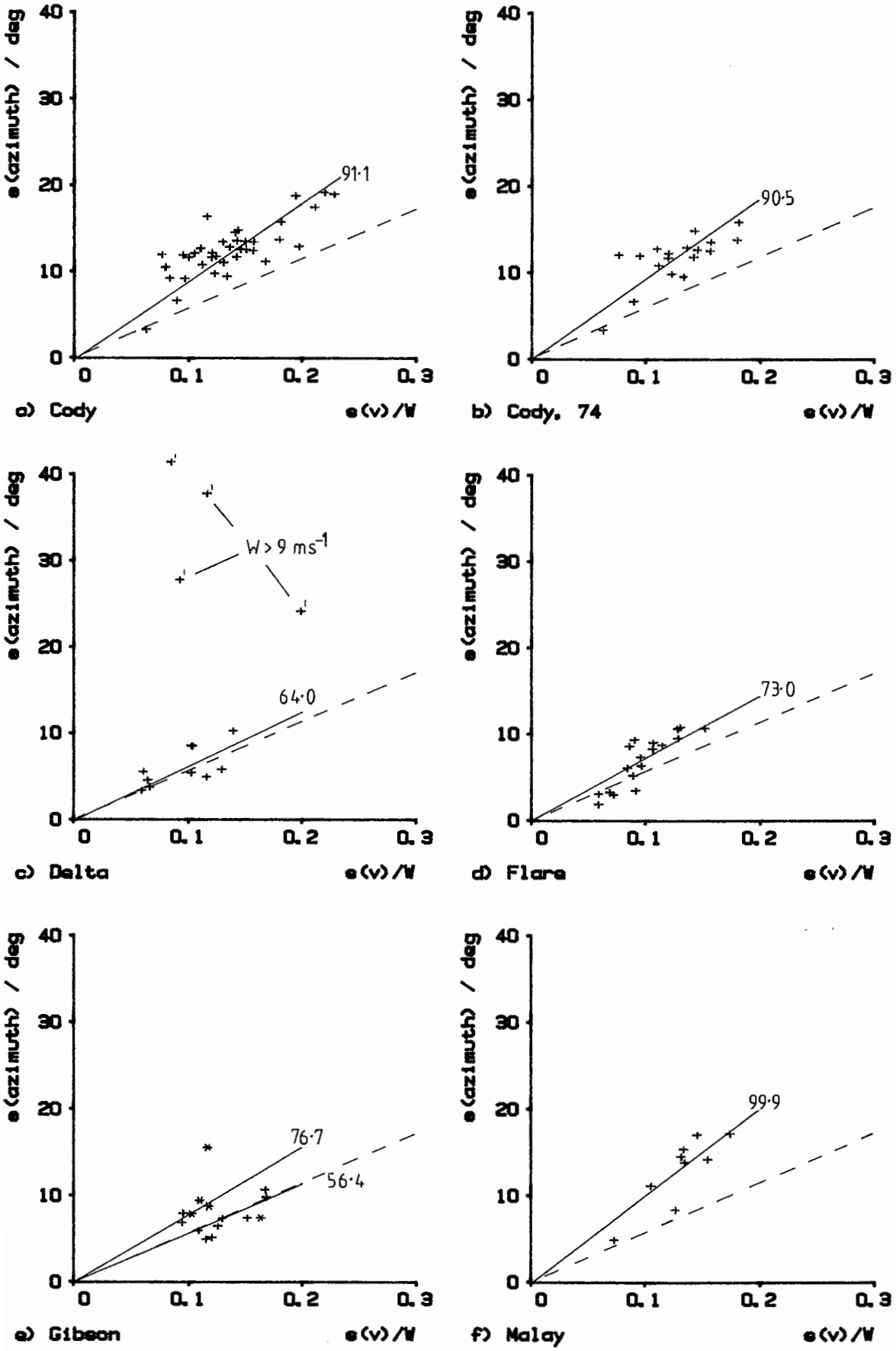

Azimuth : kite variation ve wind variation

Figure 71

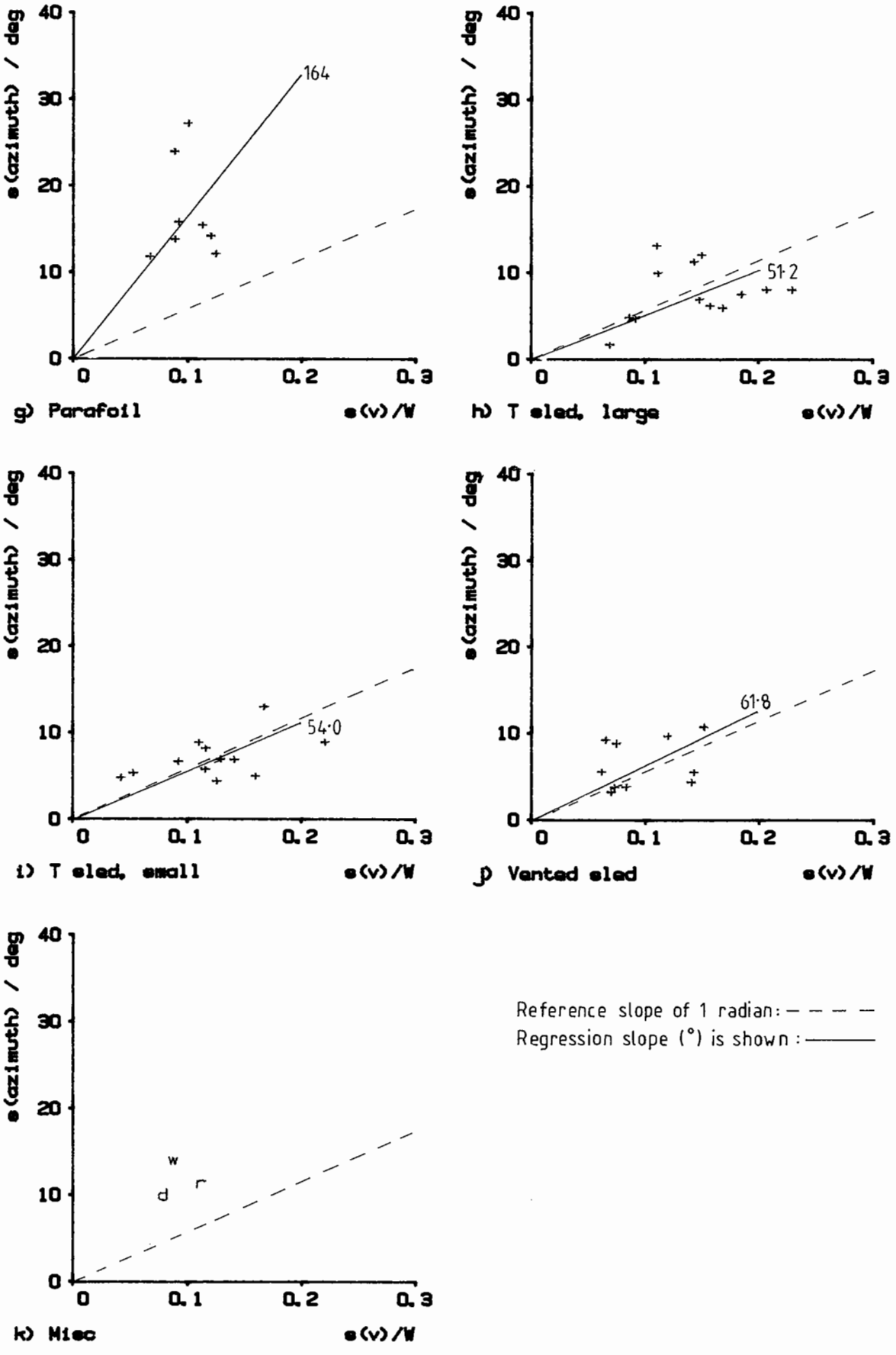

Azimuth : kite variation ve wind variation (cont)

Figure 71 cont.

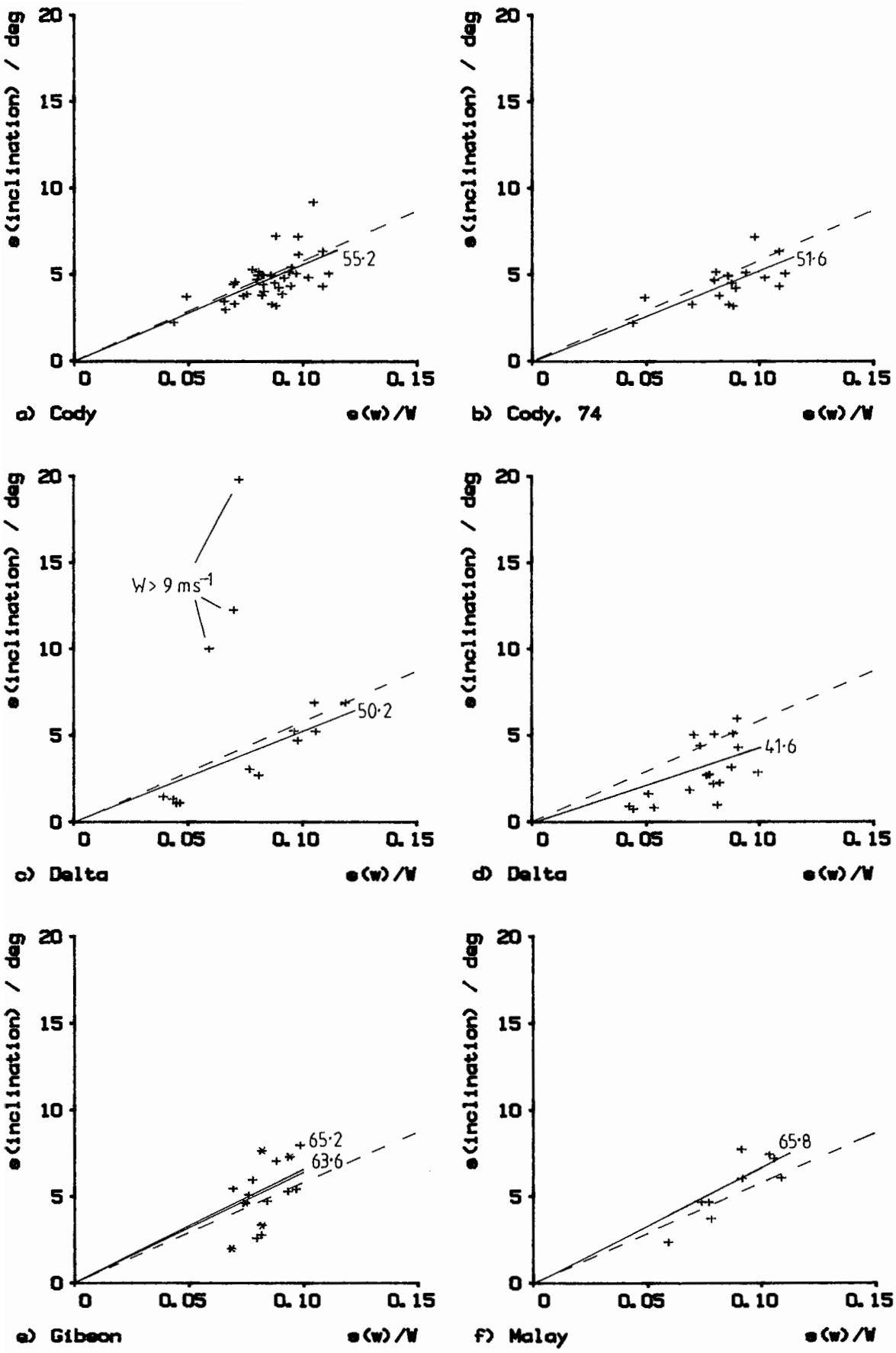

Inclination : kite variation vs wind variation

Figure 72

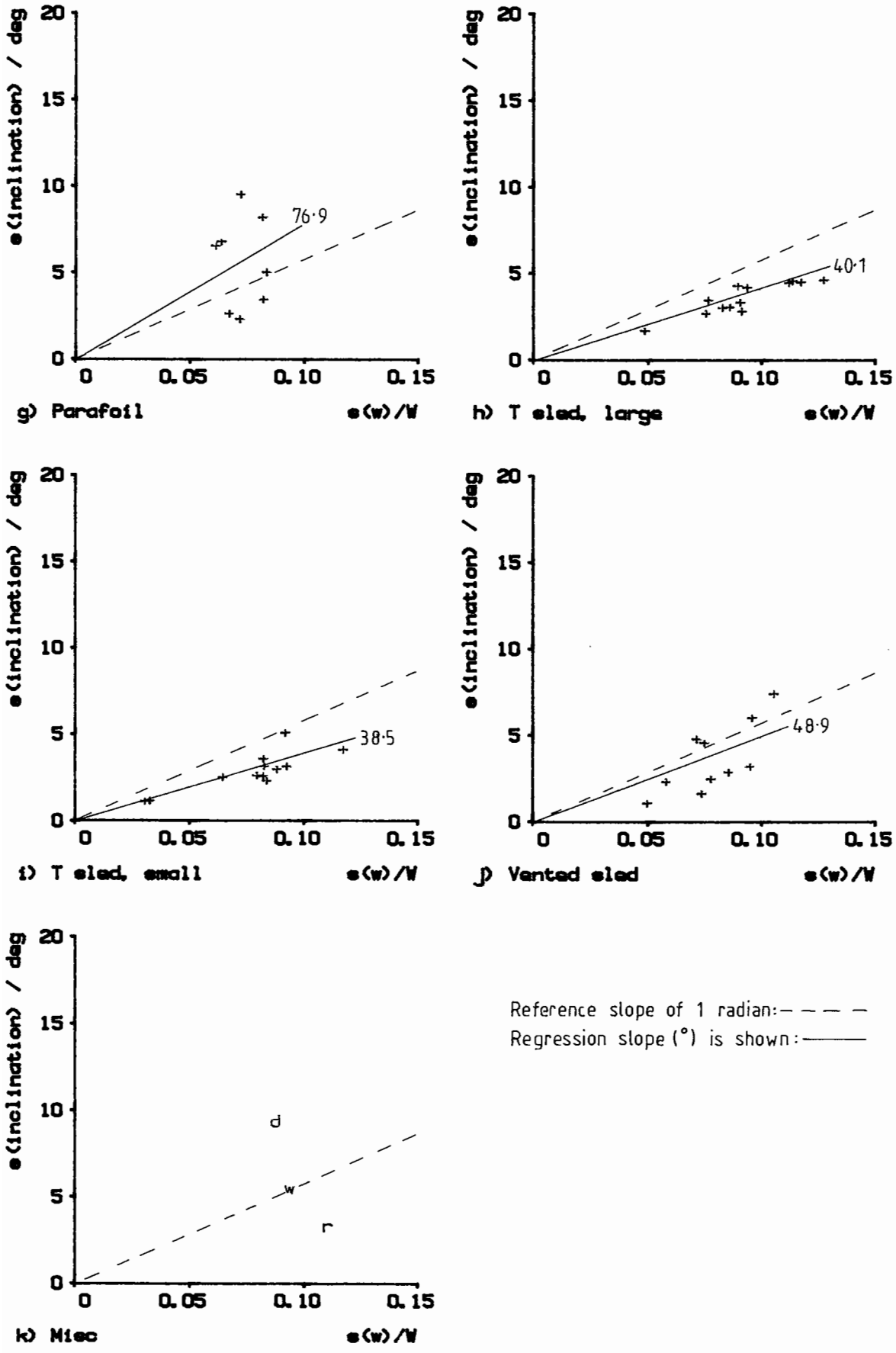

Inclination : kite variation vs wind variation (cont)

Figure 72 cont.

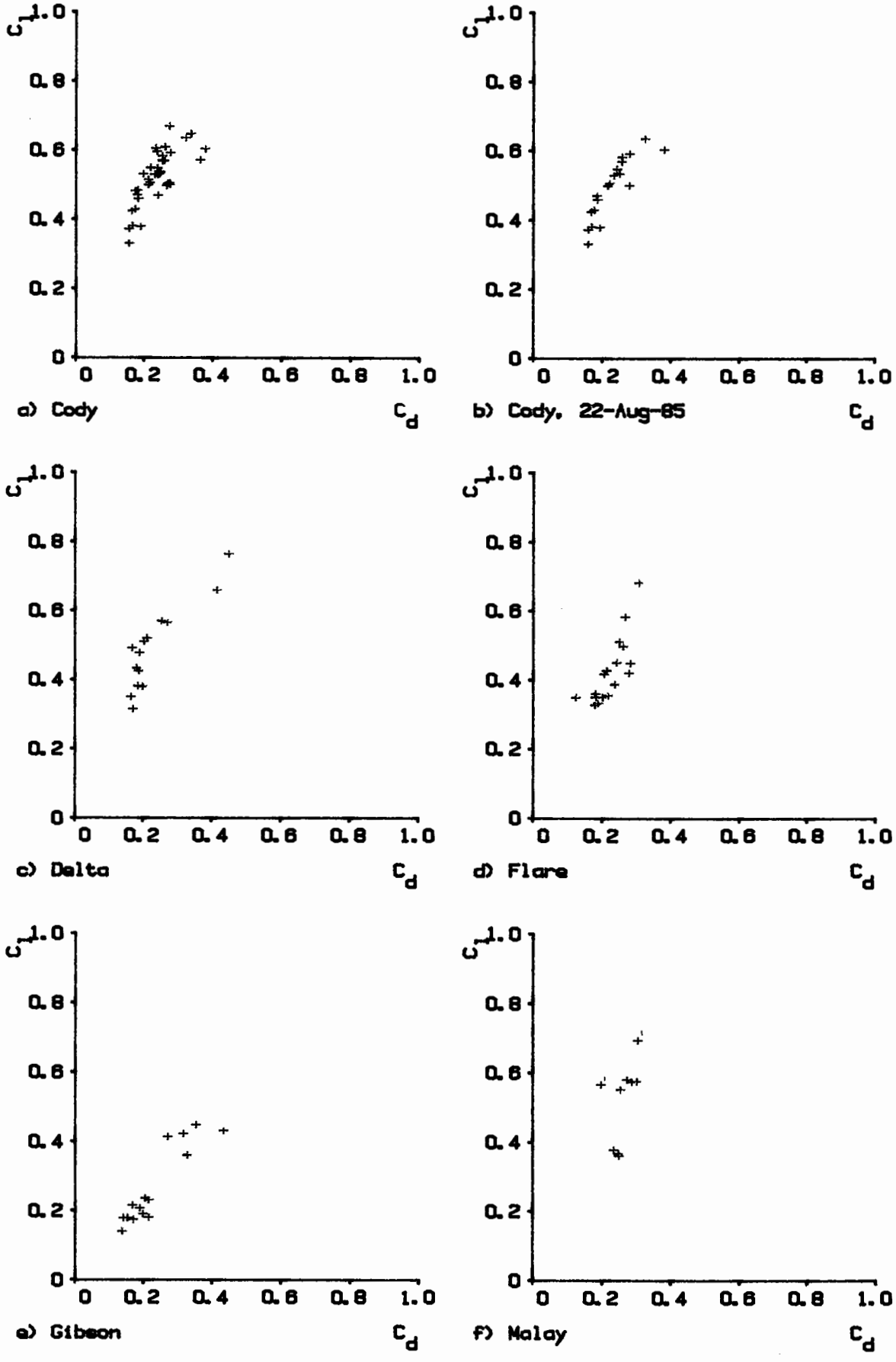

Lift - drag polars from experiments

Figure 73

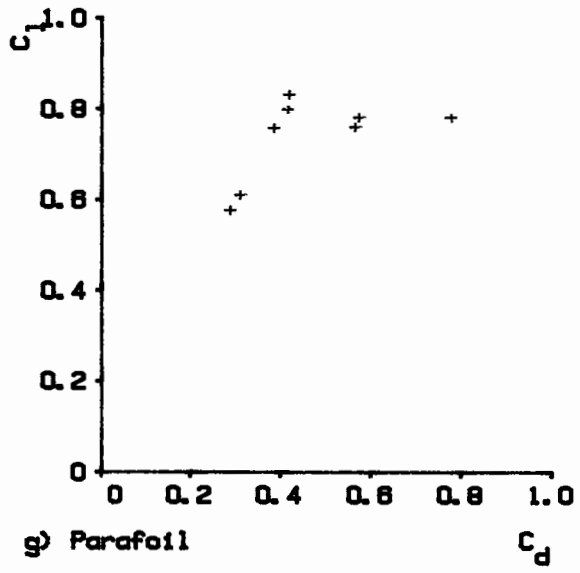

g) Parafoil

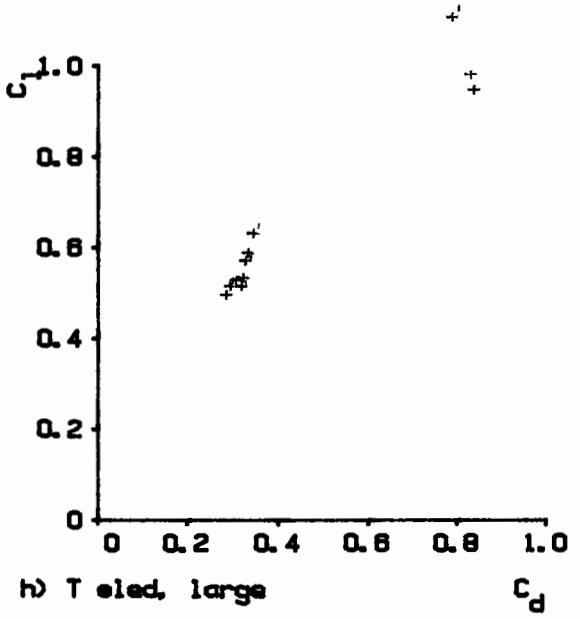

h) T sled, large

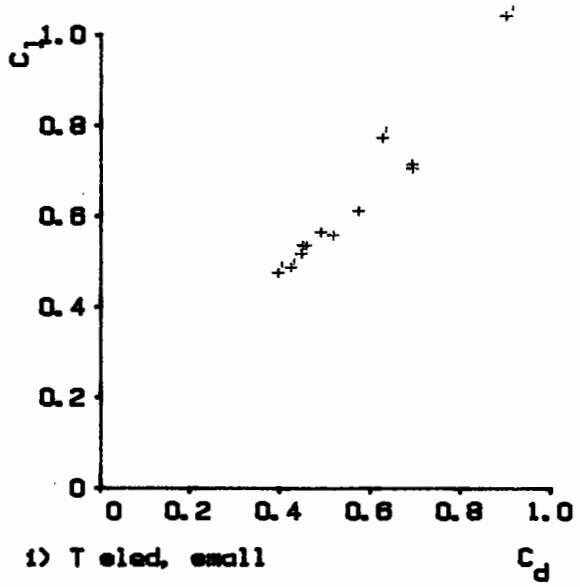

i) T sled, small

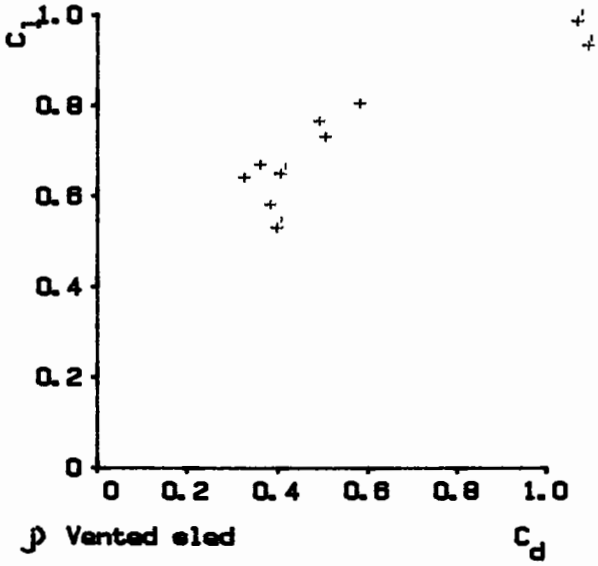

j) Vented sled

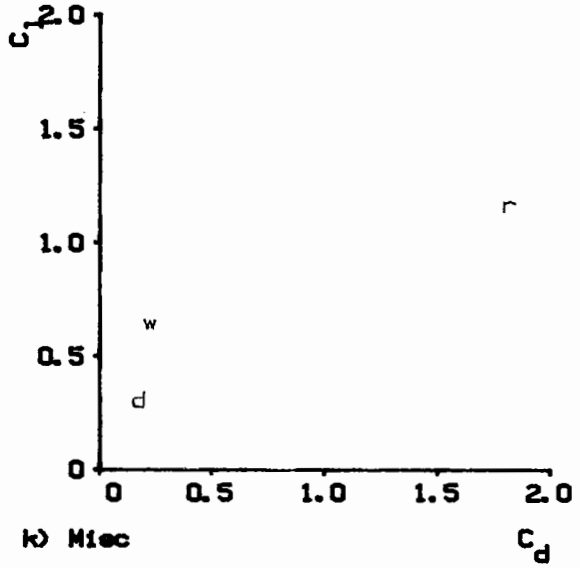

k) Misc

Lift - drag polars from experiments (cont)

Figure 73 cont.

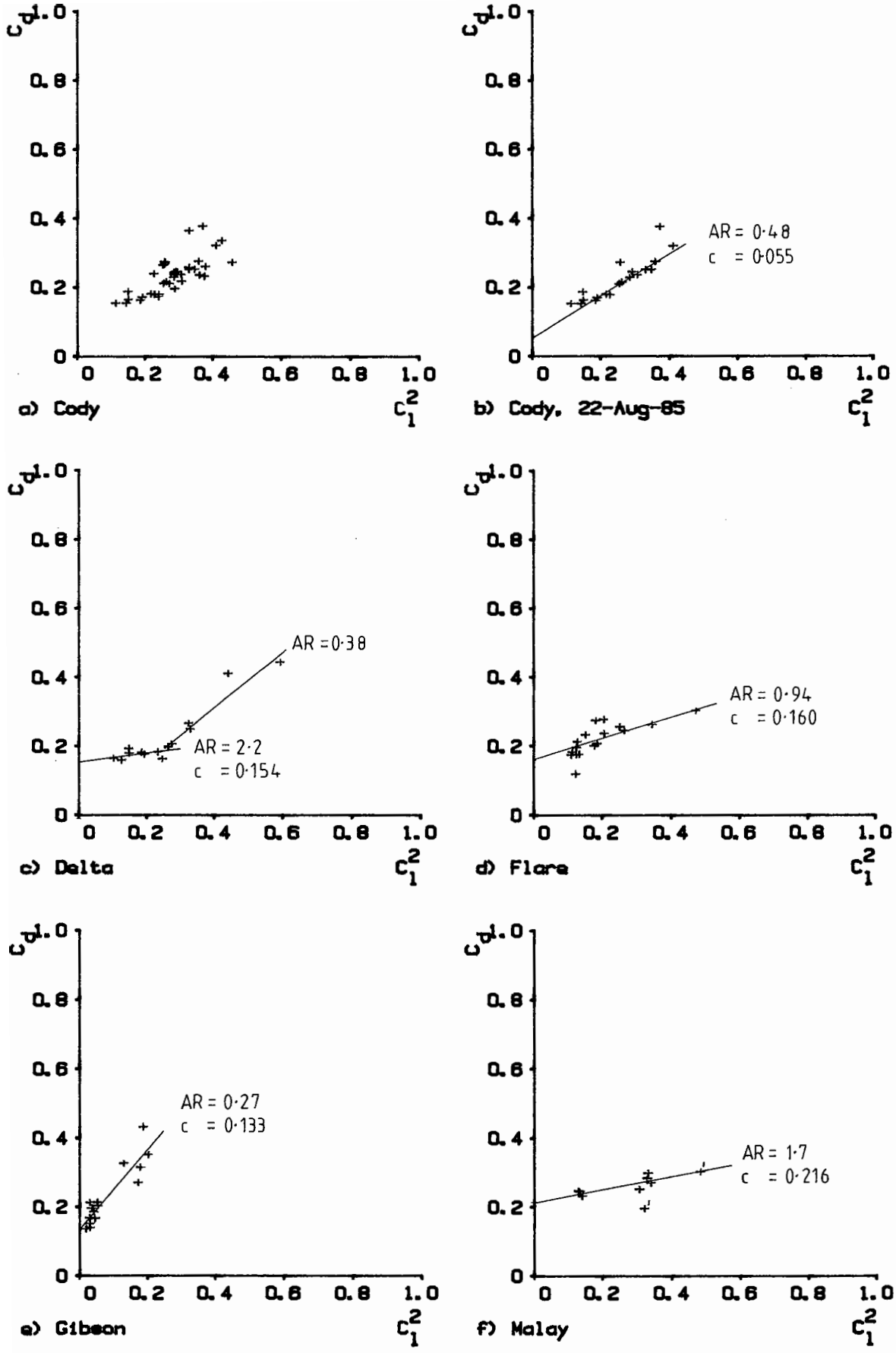

Drag variation with lift

Figure 74

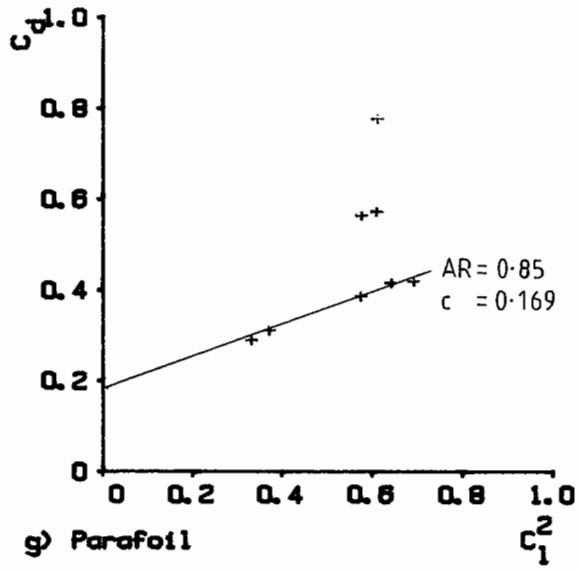

g) Parafoil

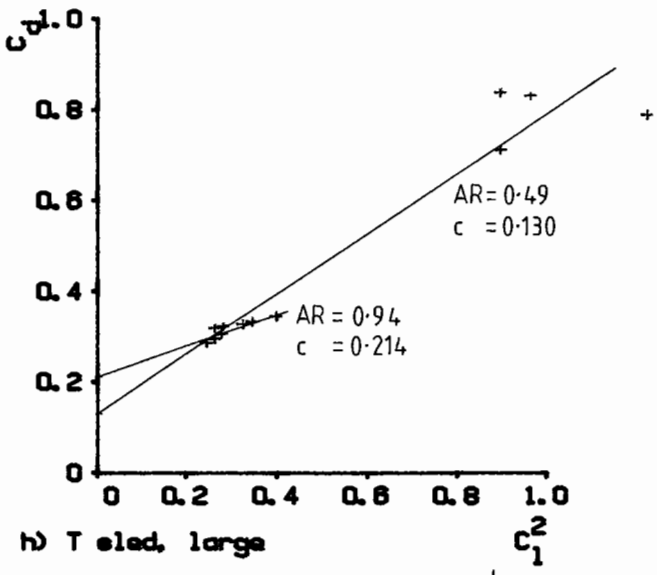

h) T sled, large

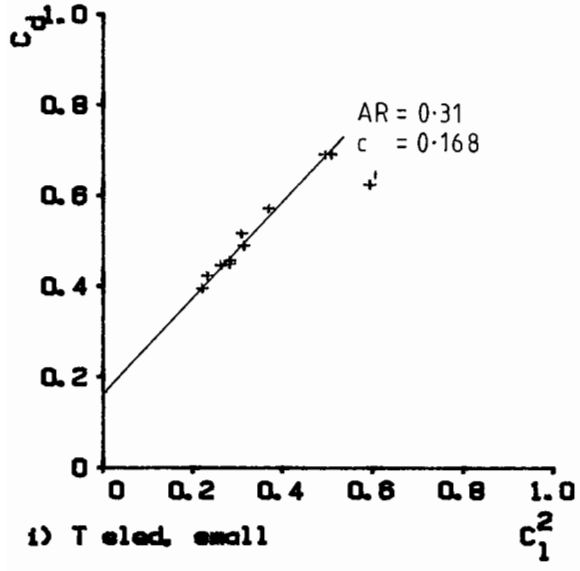

i) T sled, small

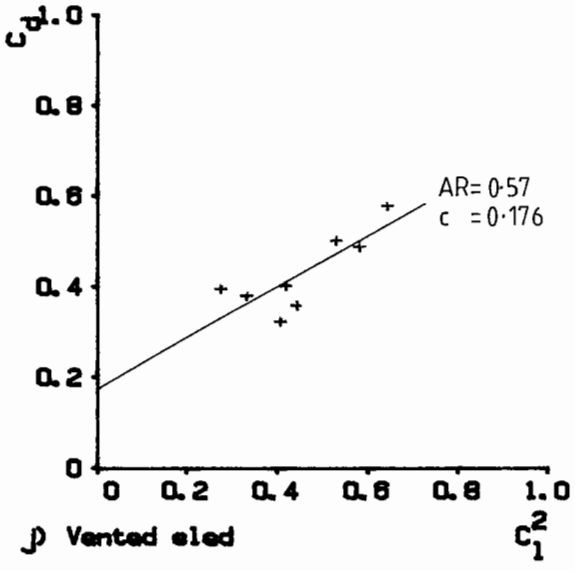

j) Vented sled

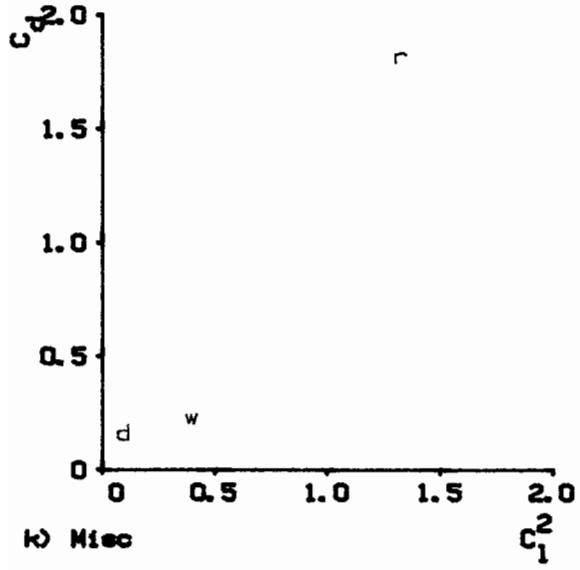

k) Misc

c = drag coefficient at zero lift

Drag variation with lift (cont)

Figure 74 cont.

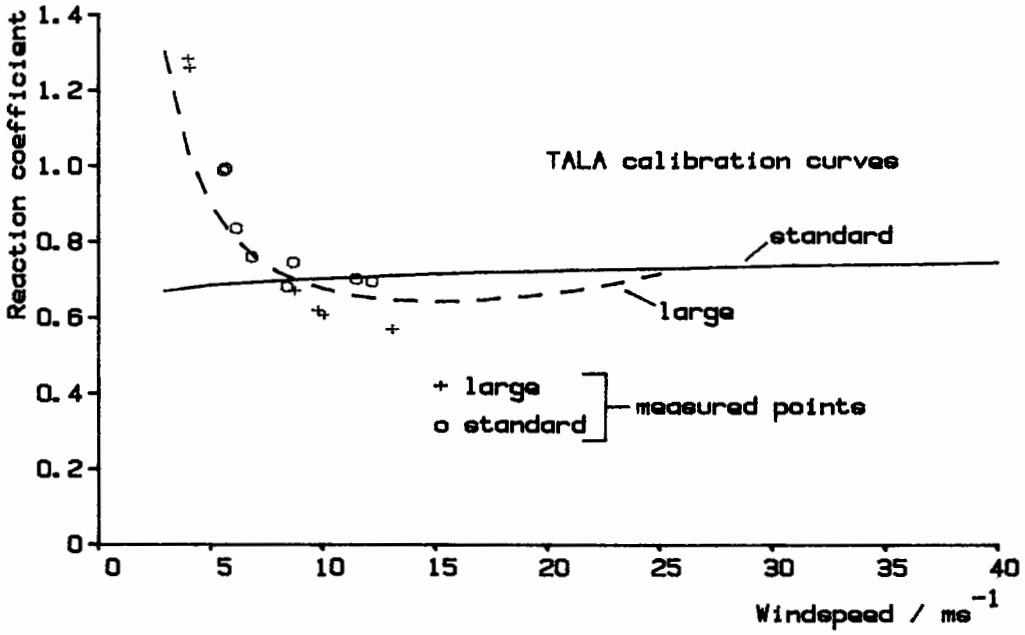

TALA calibration curves compared with measured performance

Figure 75

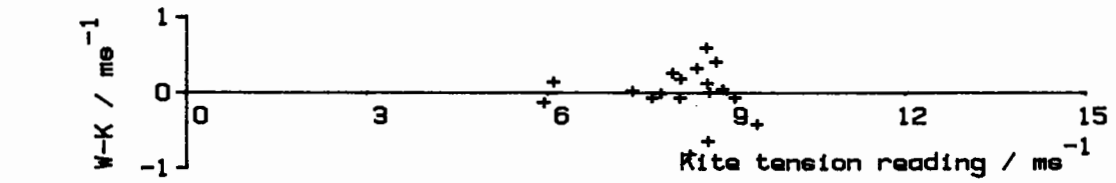

a) Cody, 74

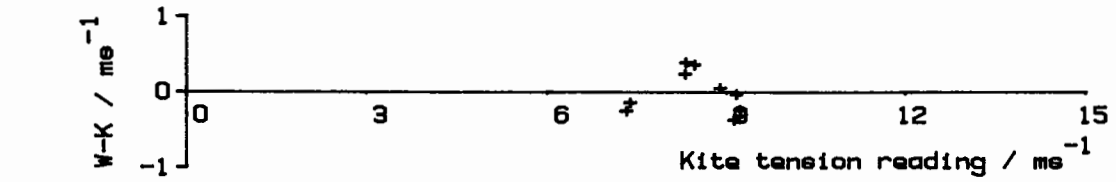

b) Cody, 77,79

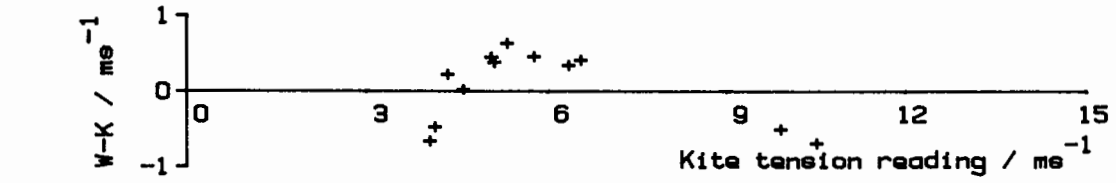

c) Delta

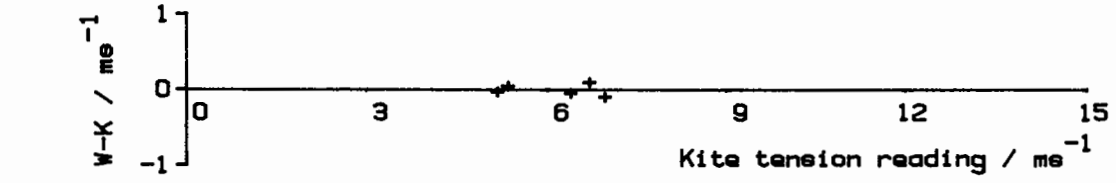

d) Flare, 84,86

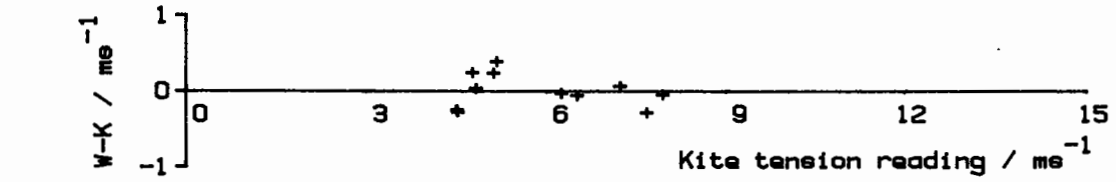

e) Flare, 87+

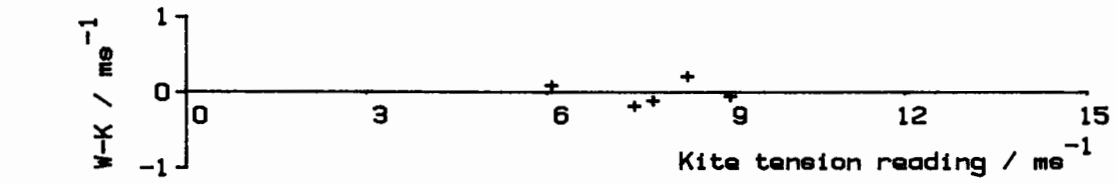

f) Gibson, 56

Kite Anemometer calibration plots

Figure 76

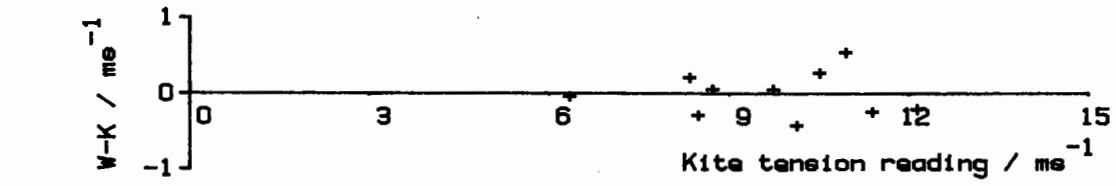

g) Gibson, 90

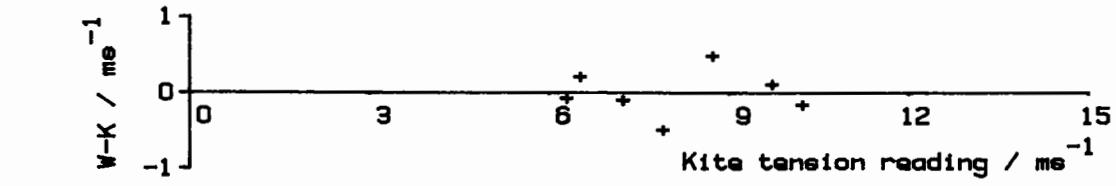

h) Malay

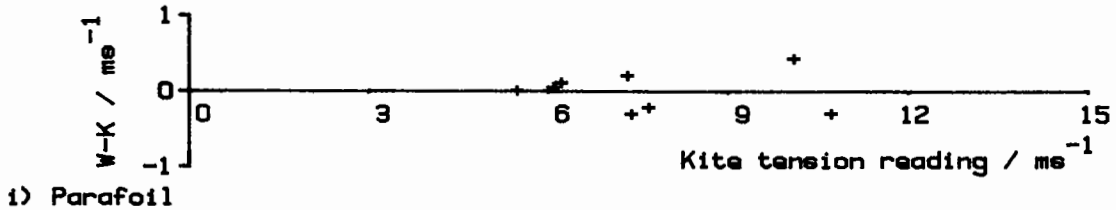

i) Parafoil

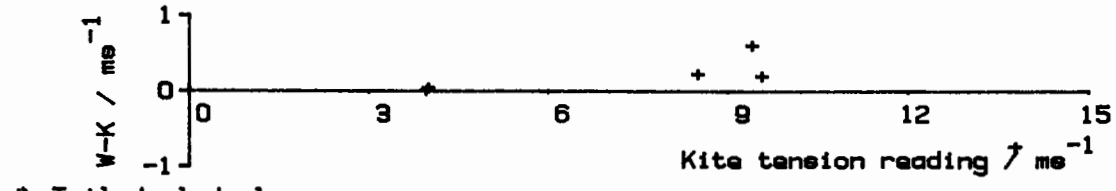

j) Tailed sled, large

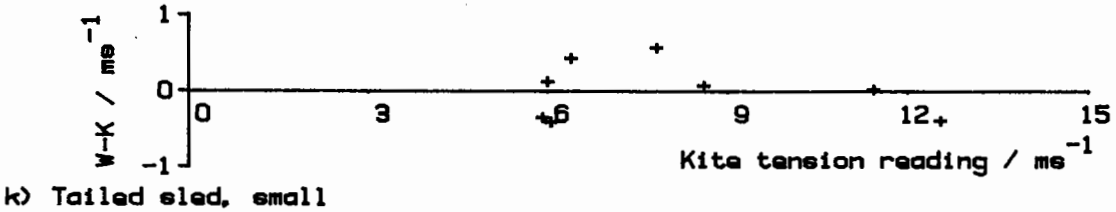

k) Tailed sled, small

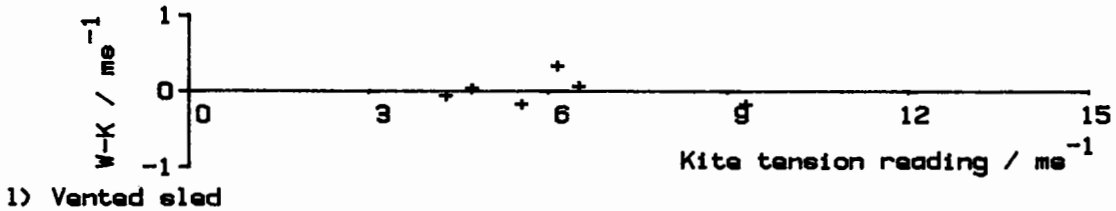

l) Vented sled

Kite Anemometer calibration plots (cont)

Figure 76 cont.

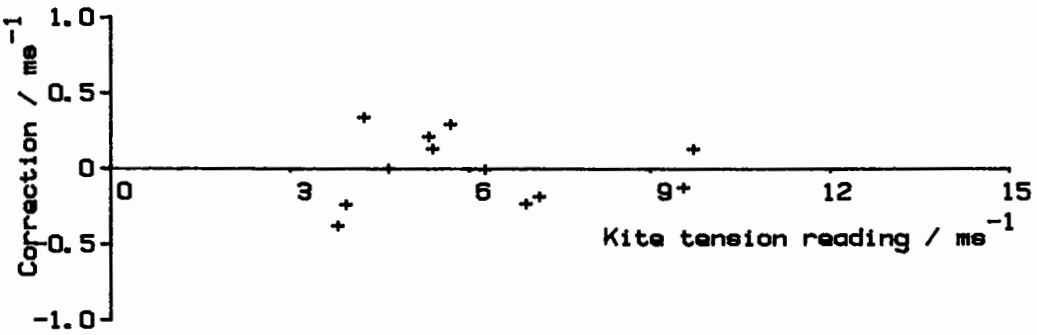

a) Delta

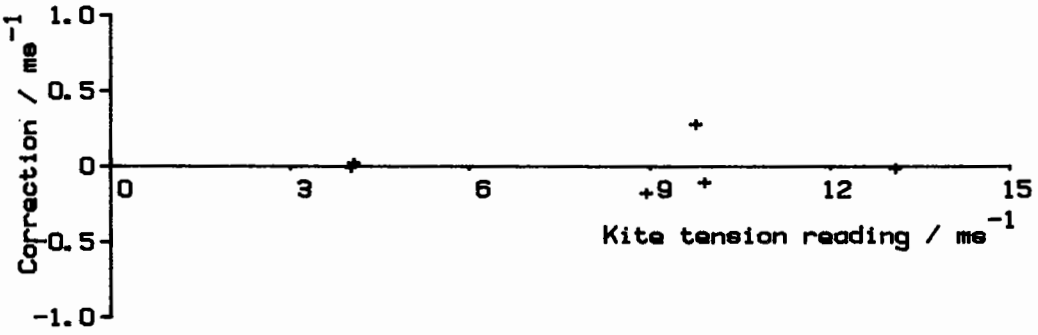

b) Tailed sled, large

Second order Kite Anemometer calibrations

These calibrations include the quadratic correction given at the foot of table 16.

Figure 77

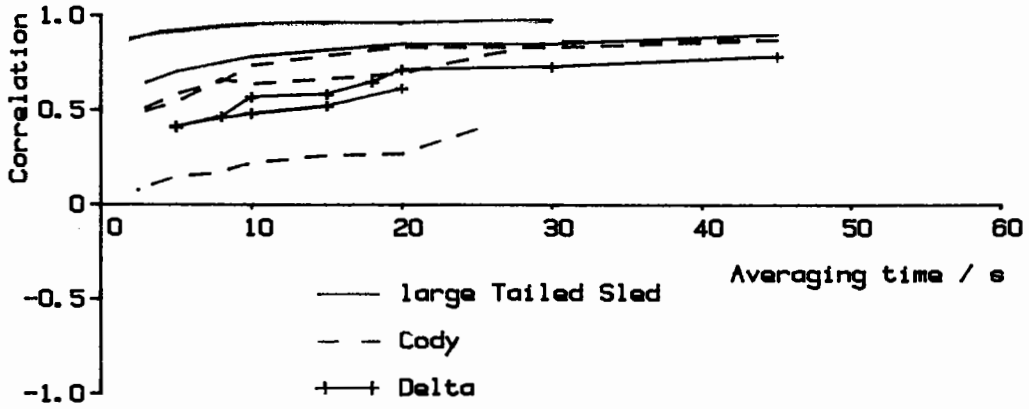

a) large Tailed Sled, Cody and Delta

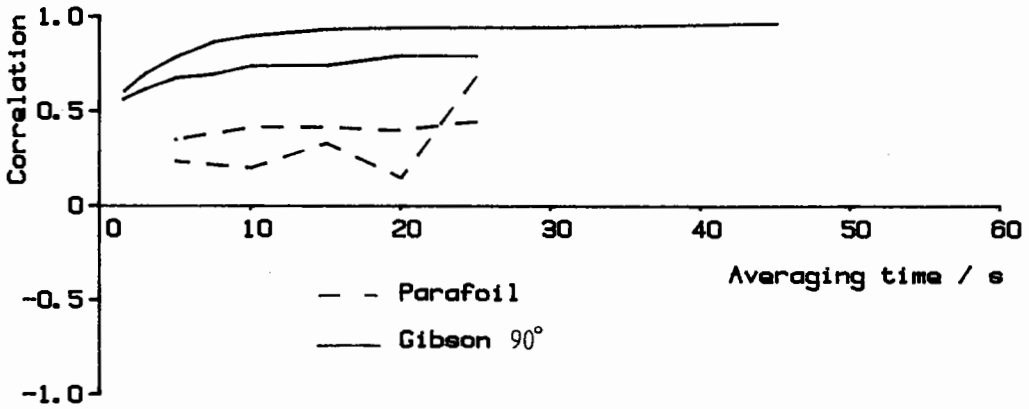

b) Gibson and Parafoil

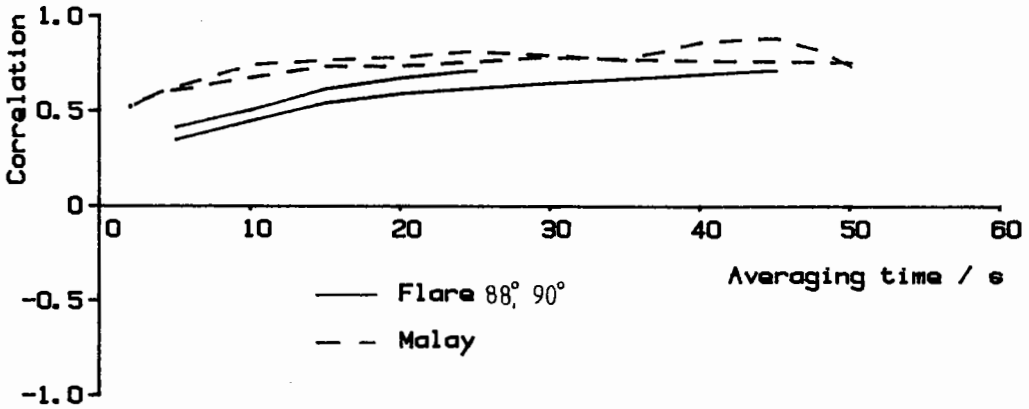

c) Flare and Malay

Correlations between measured windspeed and windspeed estimated from line tension as a function of the averaging period used to define the two mean windspeeds.

Figure 78

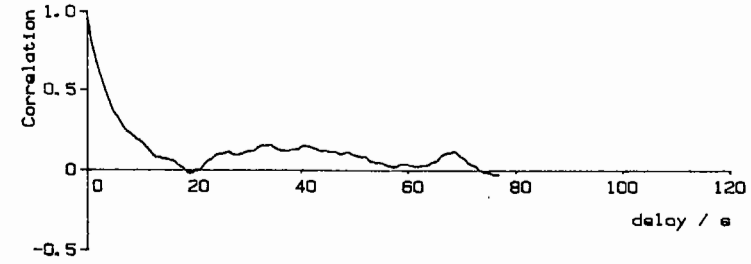

a) Cody 74. Windspeed

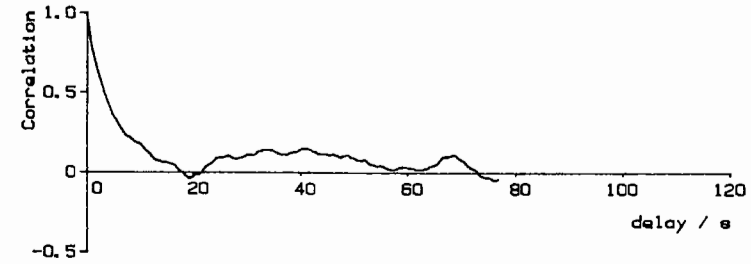

b) Cody 74. longitudinal wind component

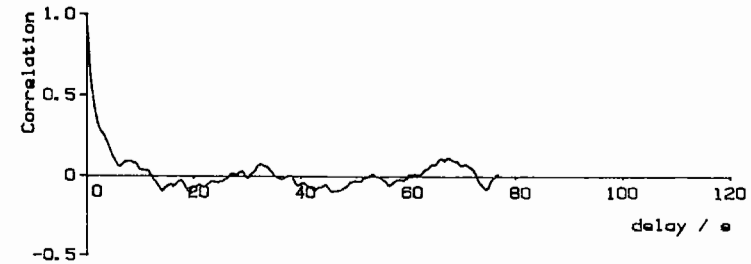

c) Cody 74. lateral wind component

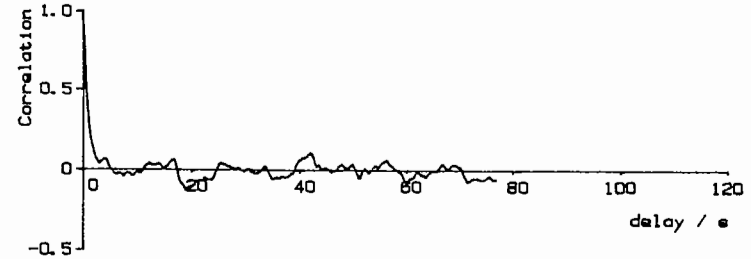

d) Cody 74. vertical wind component

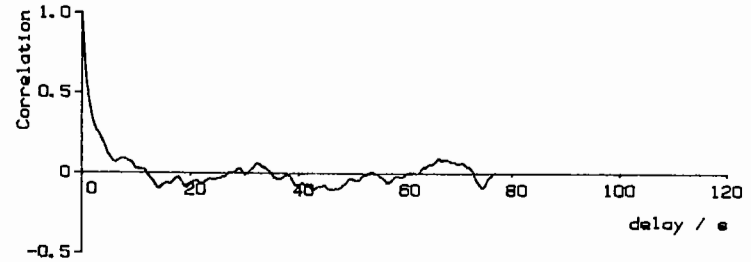

e) Cody 74. Wind azimuth

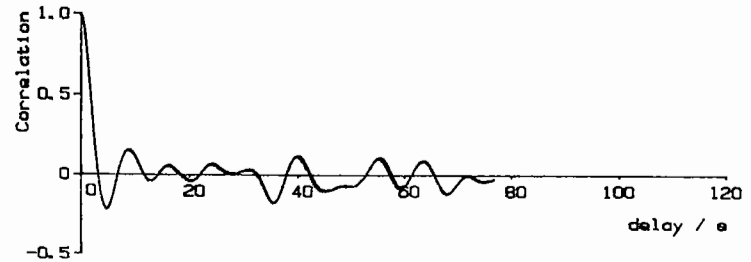

f) Cody 74. Kite azimuth

Figure 79

Examples of kite and wind autocorrelations (table 17 lists the data files used)

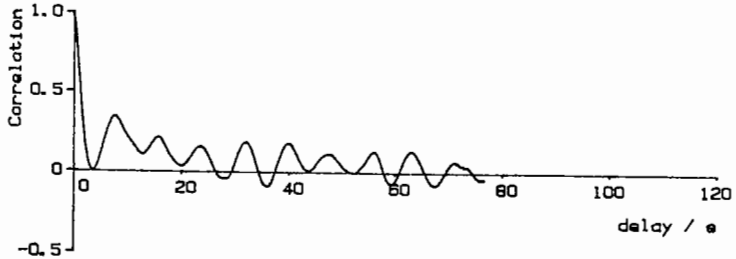

g) Cody 74, Tension

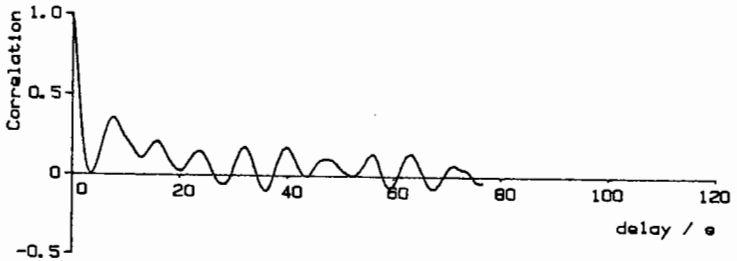

h) Cody 74, windspeed measured from tension

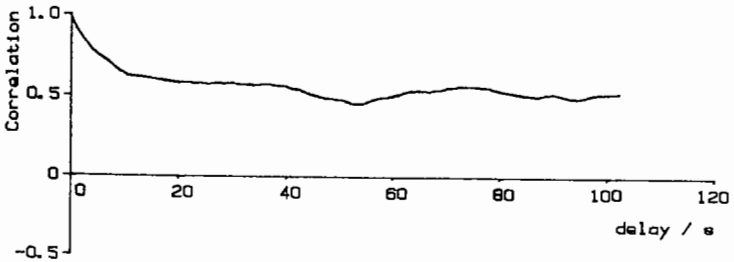

i) Tailed sled, large, windspeed

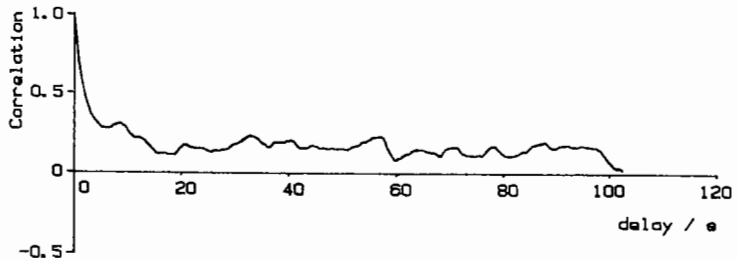

j) Tailed sled, large, wind azimuth

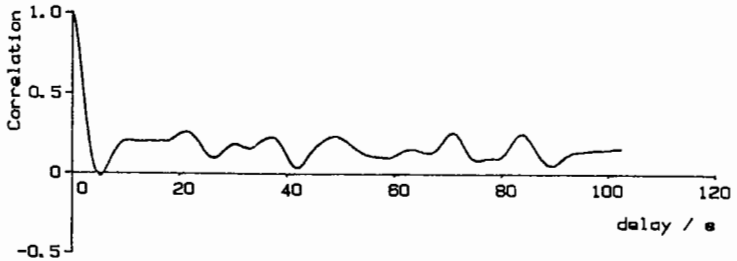

k) Tailed sled, large, kite azimuth

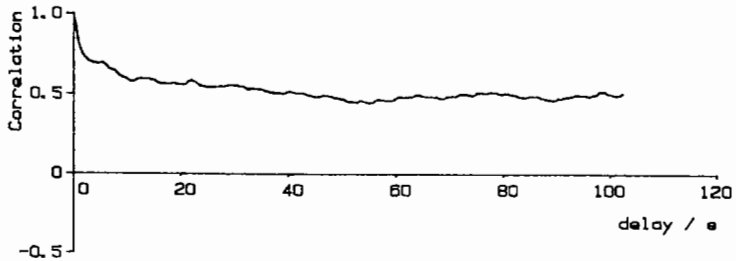

l) Tailed sled, large, windspeed measured from tension

Autocorrelation examples (see table 17 for details of data used to calculate them)

Figure 79 cont.

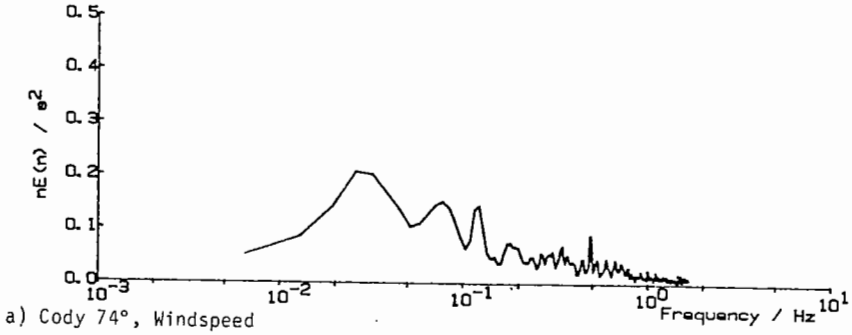

a) Cody 74°, Windspeed

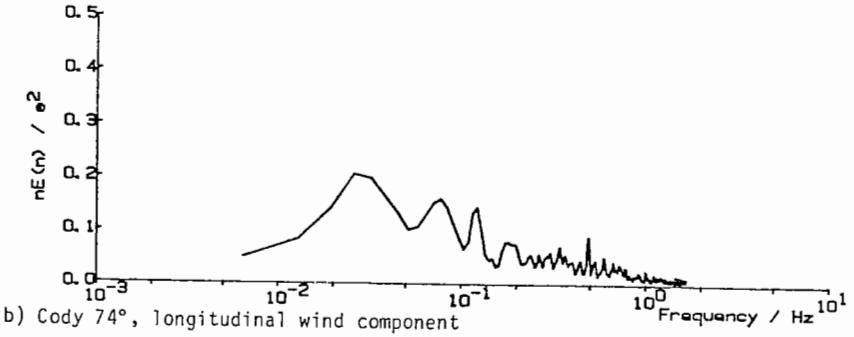

b) Cody 74°, longitudinal wind component

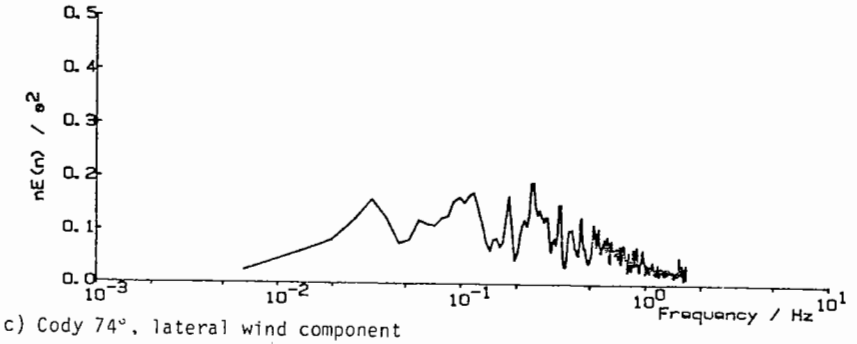

c) Cody 74°, lateral wind component

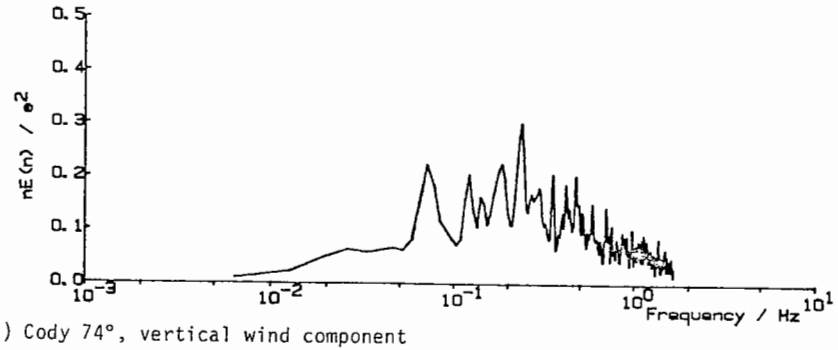

d) Cody 74°, vertical wind component

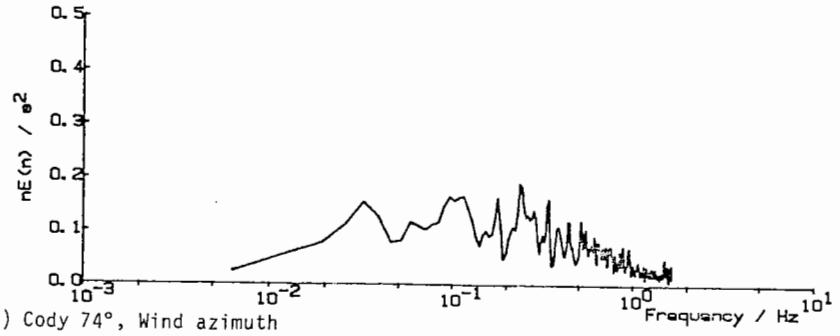

e) Cody 74°, Wind azimuth

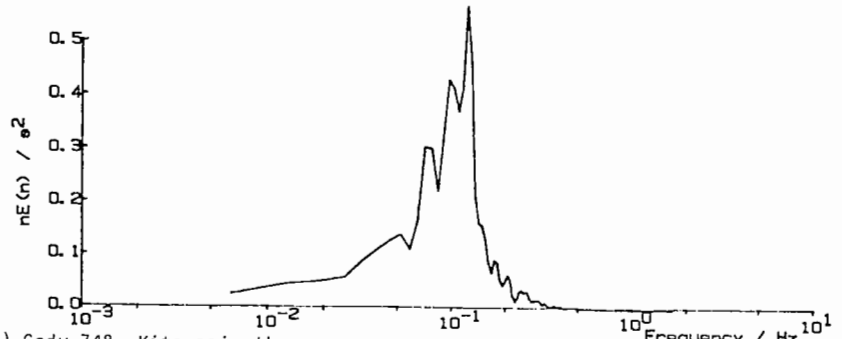

f) Cody 74°, Kite azimuth

Figure 80

Power spectra examples, derived from autocorrelations of figure 79 (see table 17 for details of the original data).

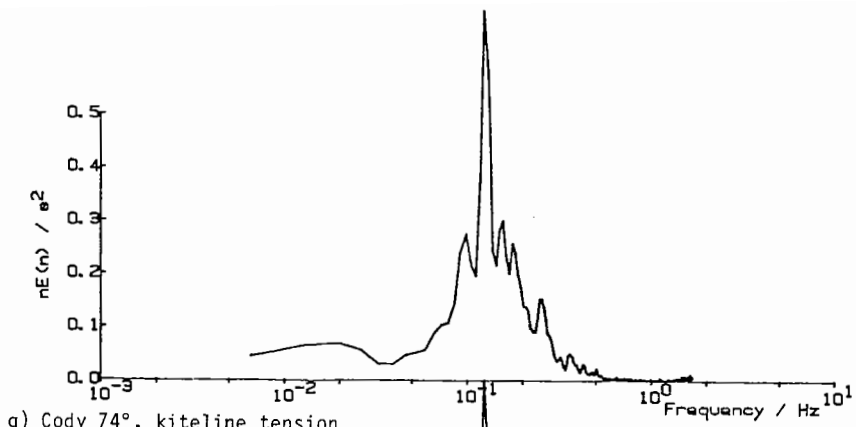

g) Cody 74°, kiteline tension

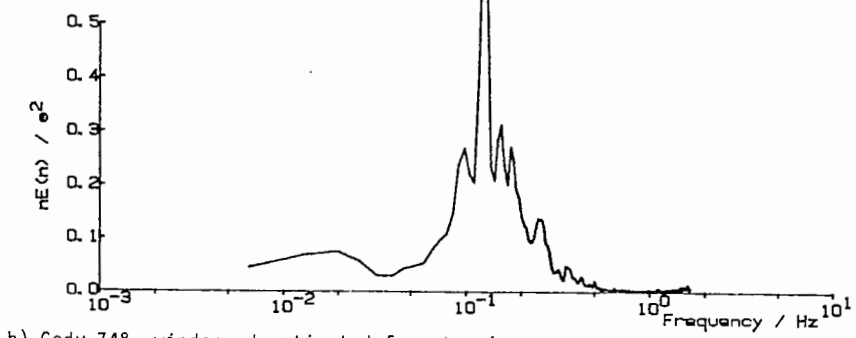

h) Cody 74°, windspeed estimated from tension

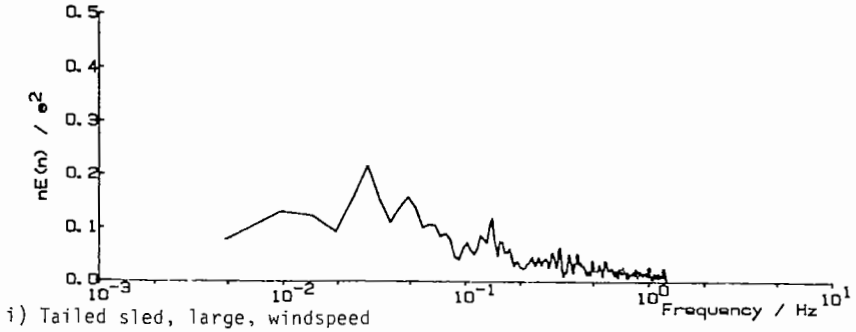

i) Tailed sled, large, windspeed

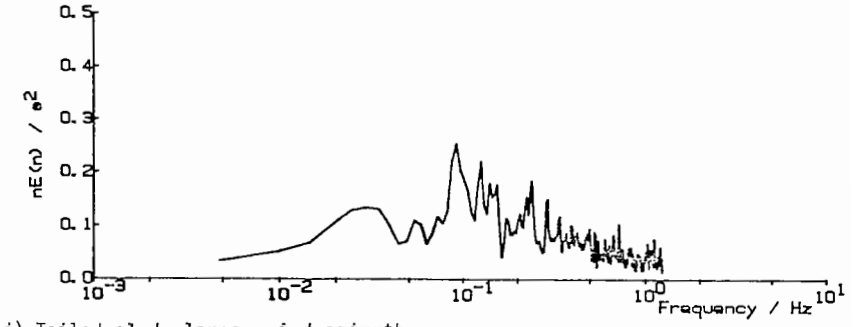

j) Tailed sled, large, wind azimuth

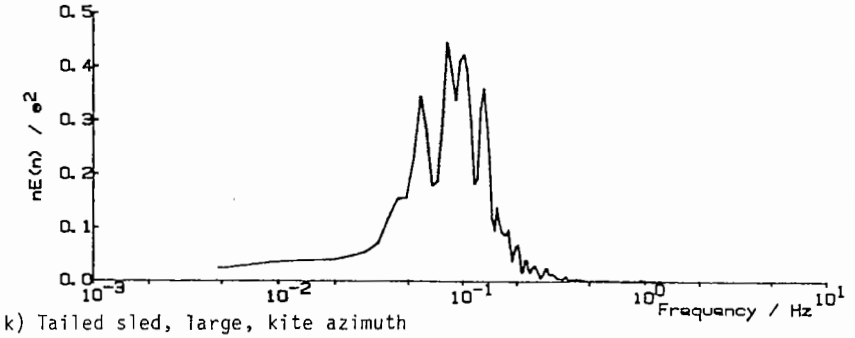

k) Tailed sled, large, kite azimuth

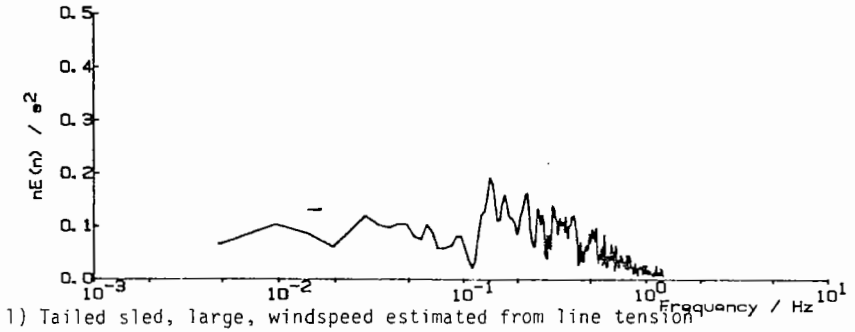

l) Tailed sled, large, windspeed estimated from line tension

Power spectra examples (see table 17 for details of the original data)

Figure 80 cont.

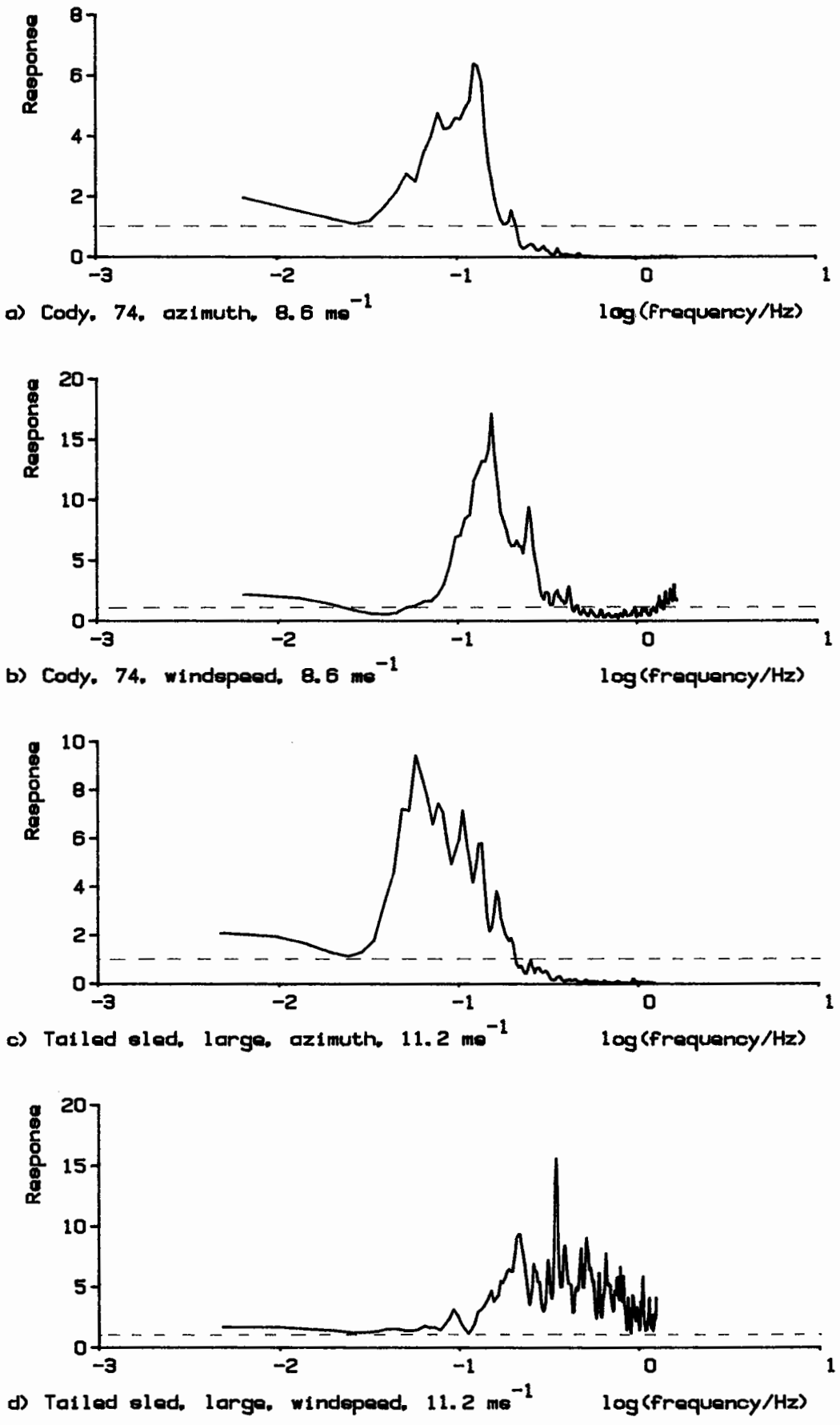

Transfer functions derived from power spectra of figure 80

Figure 81

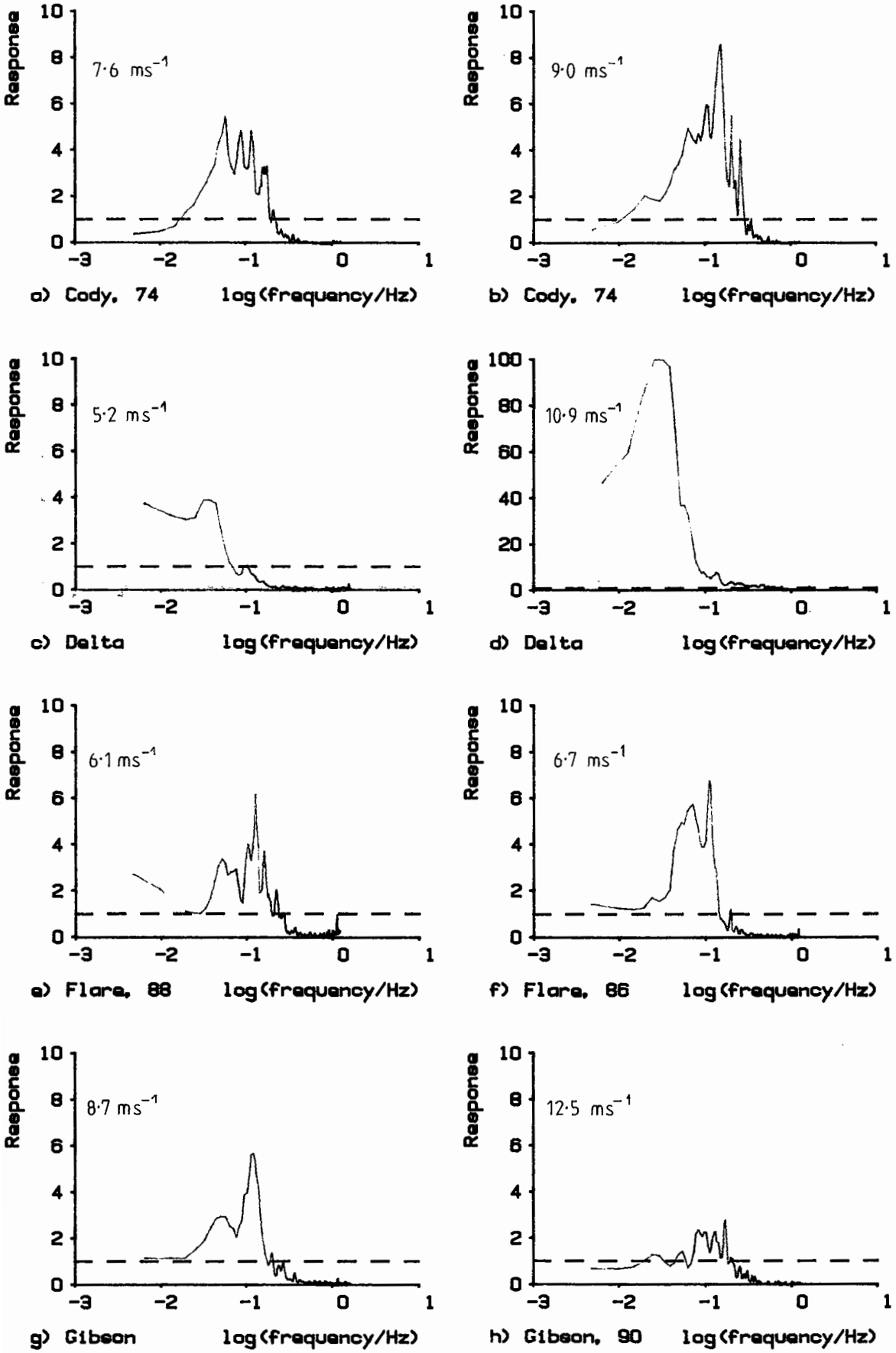

Azimuth transfer functions

Figure 82

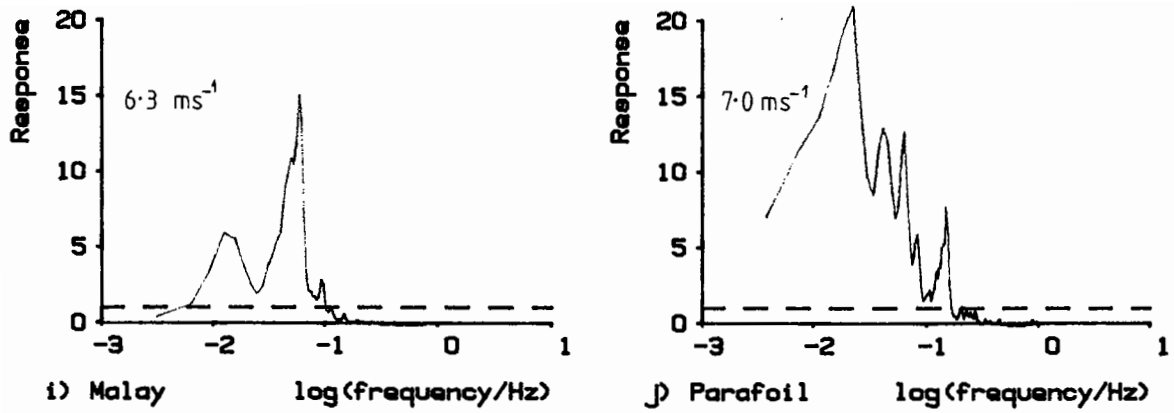

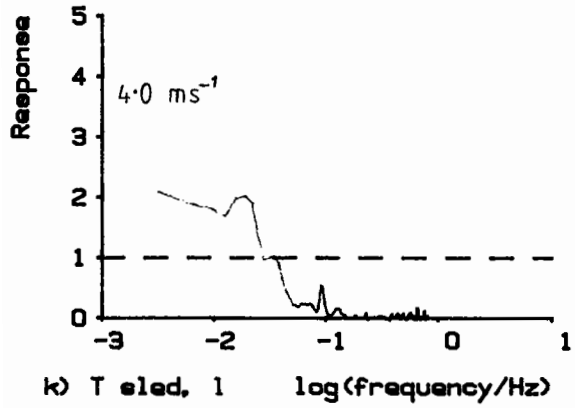

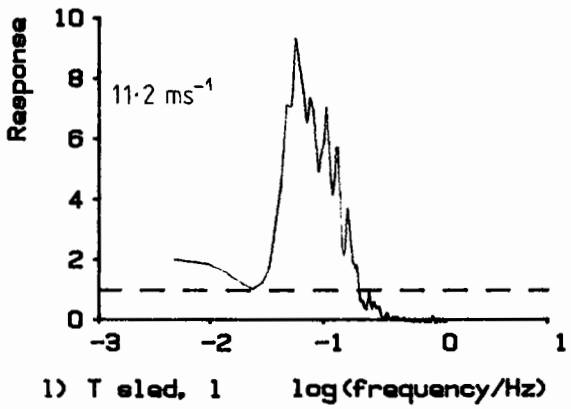

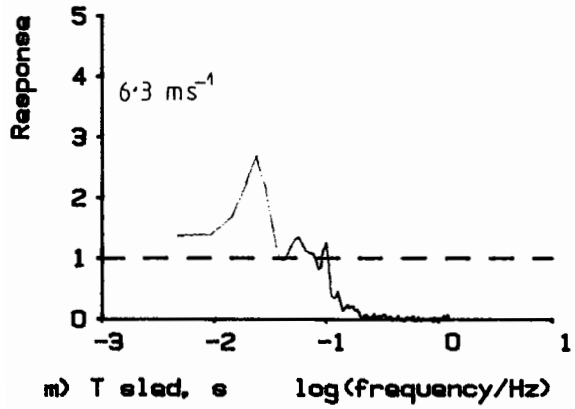

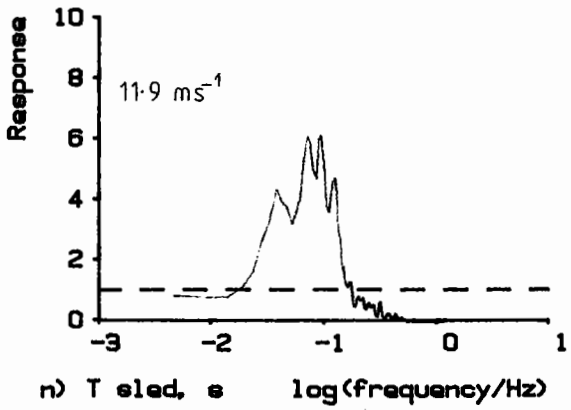

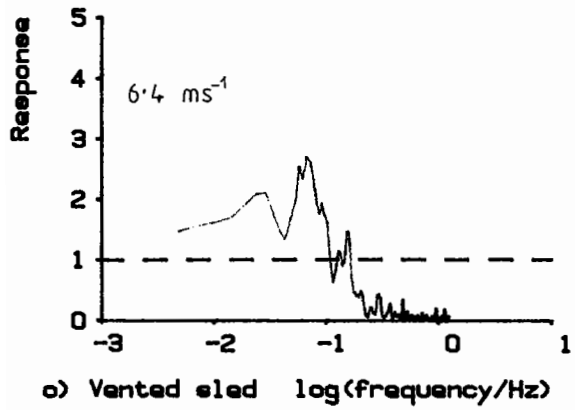

Azimuth transfer functions (cont)

Figure 82 cont.

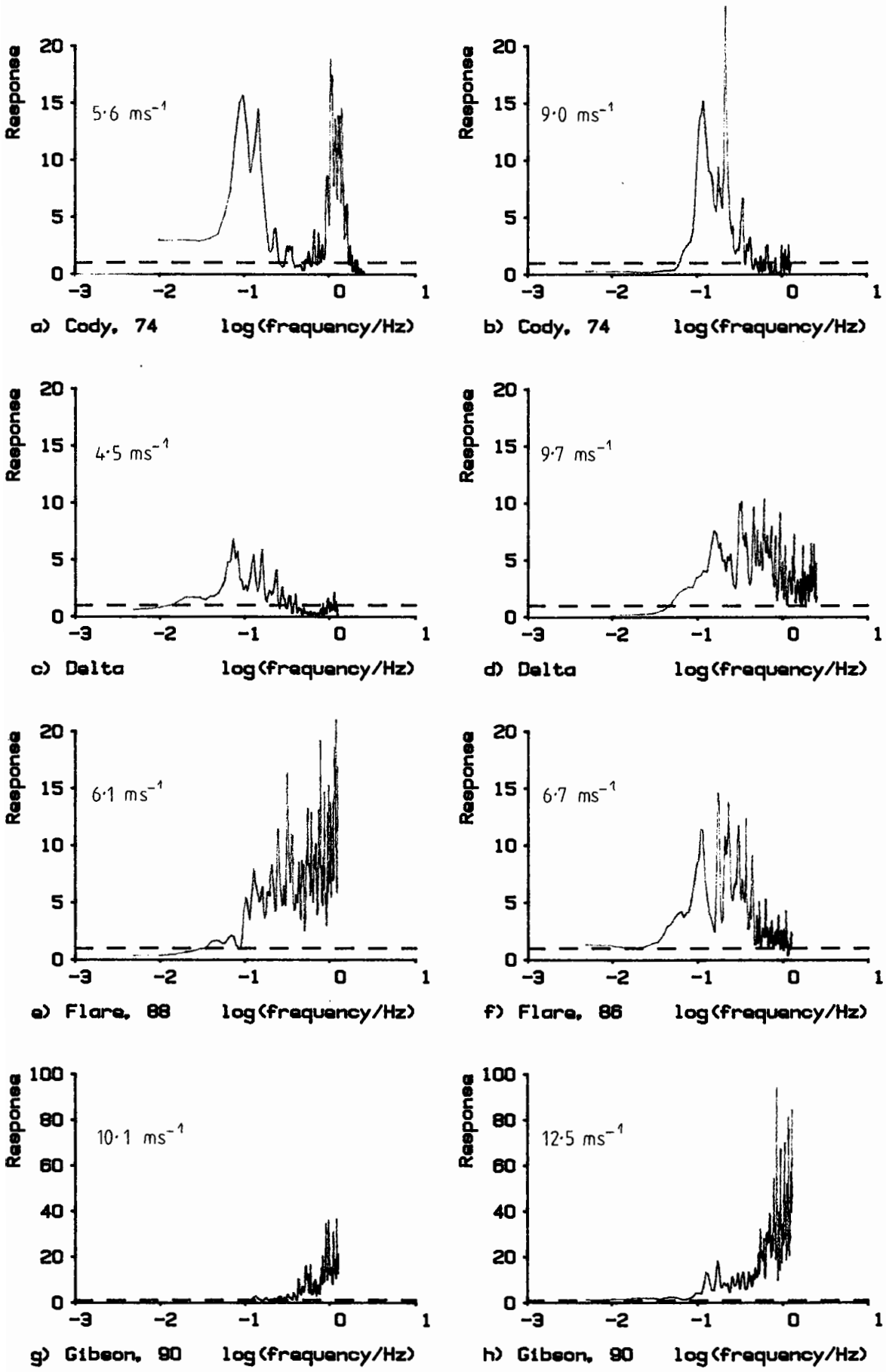

Windspeed transfer functions

Figure 83

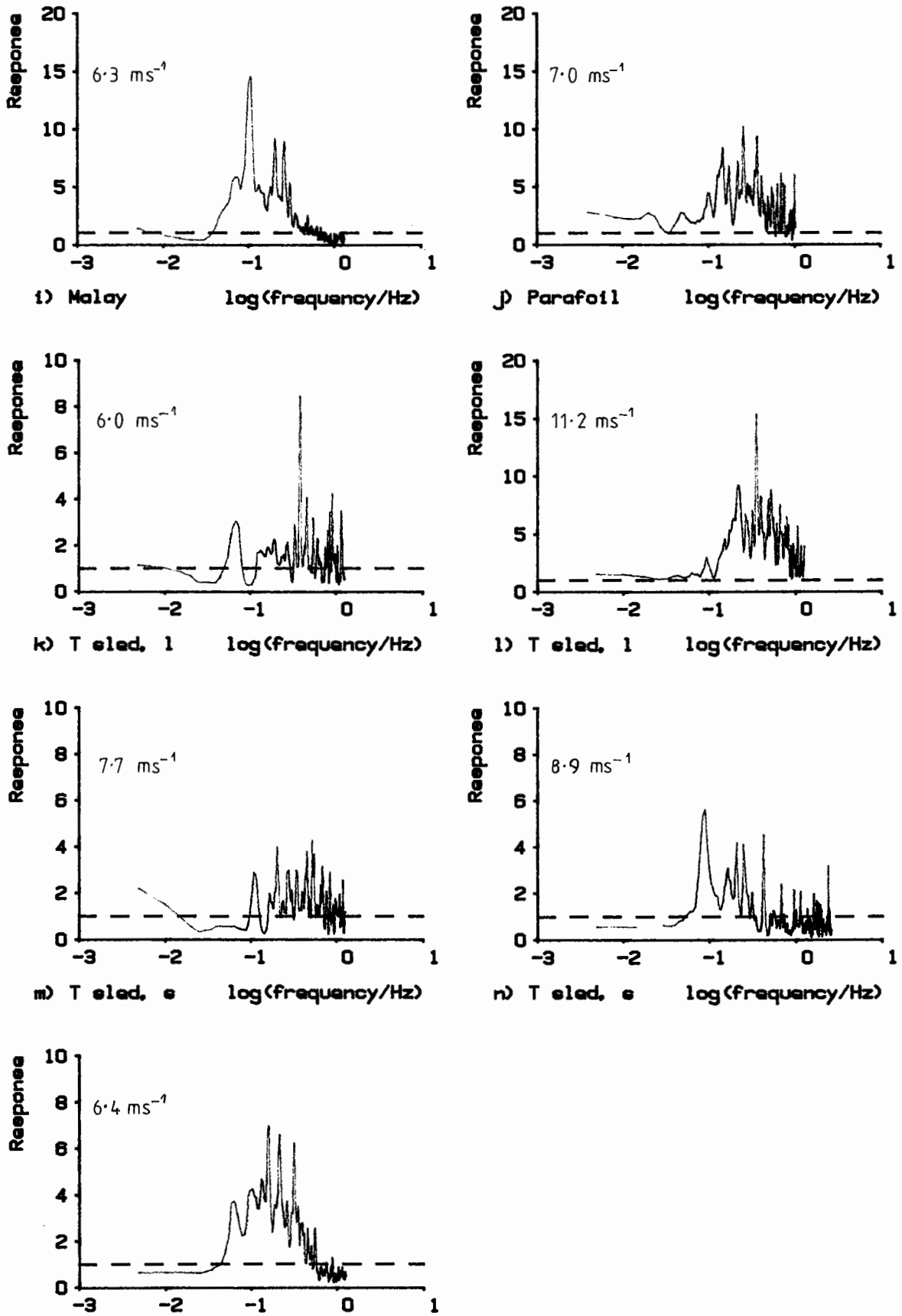

Figure 83 cont.

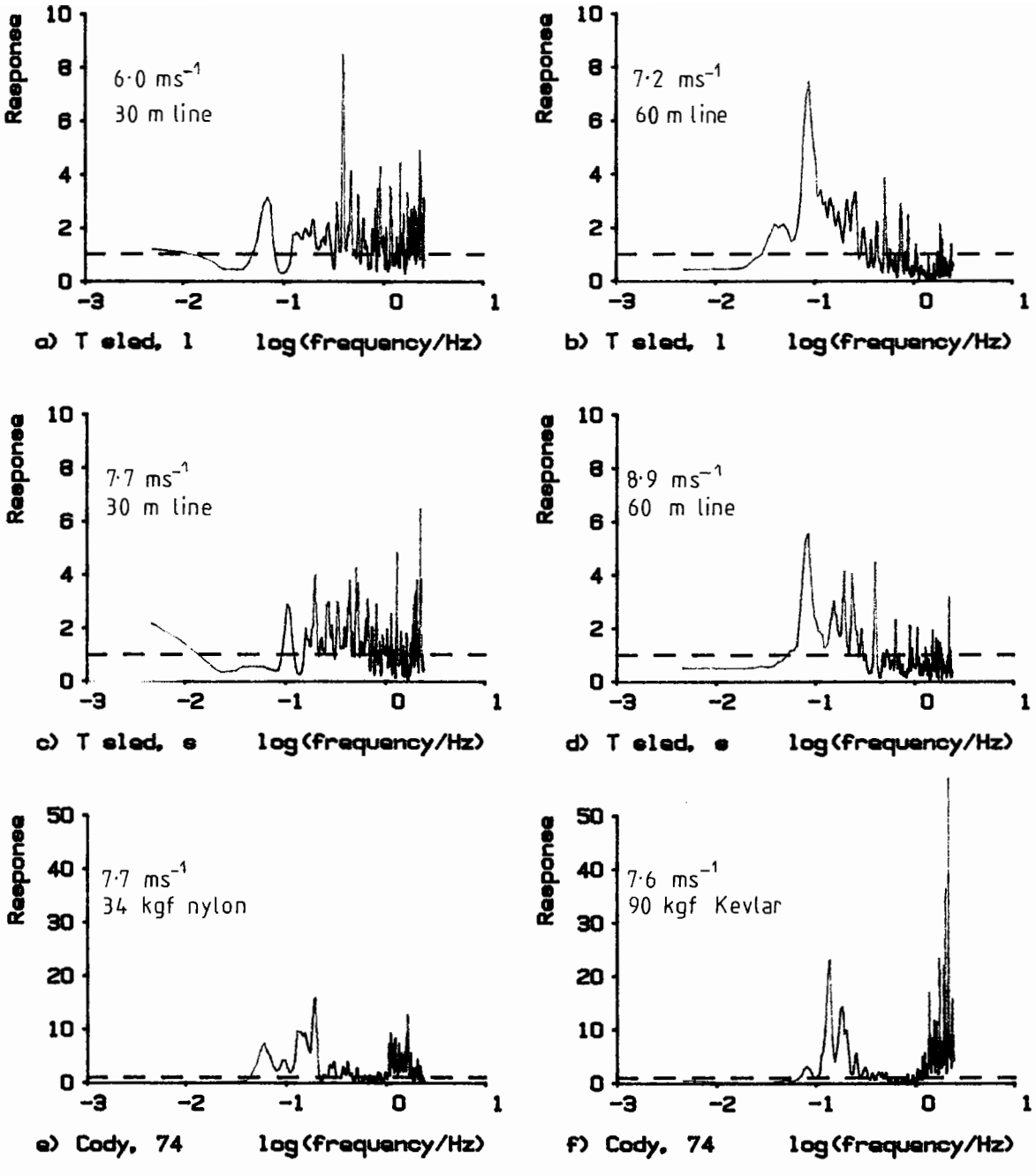

Kiteline comparisons using windspeed transfer functions Figure 84